



저작자표시-비영리-변경금지 2.0 대한민국

이용자는 아래의 조건을 따르는 경우에 한하여 자유롭게

- 이 저작물을 복제, 배포, 전송, 전시, 공연 및 방송할 수 있습니다.

다음과 같은 조건을 따라야 합니다:



저작자표시. 귀하는 원저작자를 표시하여야 합니다.



비영리. 귀하는 이 저작물을 영리 목적으로 이용할 수 없습니다.



변경금지. 귀하는 이 저작물을 개작, 변형 또는 가공할 수 없습니다.

- 귀하는, 이 저작물의 재이용이나 배포의 경우, 이 저작물에 적용된 이용허락조건을 명확하게 나타내어야 합니다.
- 저작권자로부터 별도의 허가를 받으면 이러한 조건들은 적용되지 않습니다.

저작권법에 따른 이용자의 권리는 위의 내용에 의하여 영향을 받지 않습니다.

이것은 [이용허락규약\(Legal Code\)](#)을 이해하기 쉽게 요약한 것입니다.

[Disclaimer](#)

공학박사 학위 논문

불확실성과 외란에 영향을 받는 전기 유압 시스템의 능동 외란 제거
제어에 관한 연구

**ACTIVE DISTURBANCE REJECTION CONTROL OF ELECTRO-
HYDRAULIC SYSTEMS SUBJECT TO UNCERTAINTIES AND
DISTURBANCES**

울산대학교 대학원

기계자동차 공학과

NGUYEN MANH HUNG

**ACTIVE DISTURBANCE REJECTION CONTROL OF ELECTRO-
HYDRAULIC SYSTEMS SUBJECT TO UNCERTAINTIES AND
DISTURBANCES**

Supervisor: Professor Kyoung-Kwan Ahn

A Dissertation

Submitted to
the Graduate School of the University of Ulsan
In partial Fulfillment of the Requirements
for the Degree of

Doctor of Philosophy

by

NGUYEN MANH HUNG

Department of Mechanical and Automotive Engineering
University of Ulsan, Korea

June 2024

불확실성과 외란에 영향을 받는 전기 유압 시스템의 능동 외란 제거
제어에 관한 연구

**ACTIVE DISTURBANCE REJECTION CONTROL OF ELECTRO-
HYDRAULIC SYSTEMS SUBJECT TO UNCERTAINTIES AND
DISTURBANCES**

지도교수 안경관

이 논문을 공학박사 학위 논문으로 제출함


2024 년 06 월

울산대학교 대학원

기계자동차 공학과

ACTIVE DISTURBANCE REJECTION CONTROL OF ELECTRO-HYDRAULIC SYSTEMS SUBJECT TO UNCERTAINTIES AND DISTURBANCES


**This certifies that the dissertation
of NGUYEN MANH HUNG is approved by**



Committee Chair Prof. Byung-Ryong Lee



Committee Member Prof. Kyoung-Kwan Ahn



Committee Member Prof. Cheol-Keun Ha



Committee Member Prof. Gi-Seo Park



Committee Member Prof. Ji-Sung Jang

Department of Mechanical and Automotive Engineering

University of Ulsan

Jun 2024

Acknowledgment

During my four-year Ph.D. program, I had the great opportunity to collaborate with extraordinary people. Their expertise, dedication, and solid support played an important role in the successful completion of this thesis. Without their constant encouragement and kind assistance, this endeavor would not have come to fruition. I am immensely grateful for the invaluable contributions and guidance provided by these remarkable individuals, as their collective efforts significantly enhanced the quality and depth of this research.

Firstly, I would like to express my deepest appreciation to my advisor, Prof. Kyoung-Kwan Ahn, for the continuous support of my Ph.D. study and related research, for his motivation, patience, immense knowledge, and during my study at University of Ulsan. In addition, his dedication, expertise, and unwavering support have played an instrumental role in shaping my academic journey. Besides, his insightful guidance and constructive feedback have helped me refine my critical thinking and analytical skills. I am truly fortunate to have had the privilege of learning from such a distinguished individual, and his mentorship will eternally be cherished and remembered as a significant influence in my academic journey.

Secondly, I would like to express my gratitude to committee members, Prof. Byung-Ryong Lee, Prof. Cheol-Keun Ha, Prof. Gi-Seo Park, and Prof. Ji-Sung Jang, for their comprehensive evaluation and insightful comments and for providing valuable suggestions for improving the quality of this thesis. At the same time, I highly appreciate University of Ulsan as well as the Korean government for their financial support in my research, which helped me to realize my dream of studying abroad.

Furthermore, this endeavor would not have been possible without all members of FPMI Lab. for their encouragement, discussion, and friendship during my research. I extend special thanks to my brother, Dr. Dao Hoang Vu for generously dedicating his precious time to provide substantial assistance and sharing his knowledge and research experience with me.

Finally, I am profoundly grateful to Nguyen Tran Van Anh, my devoted wife of more than 10 years, for her immense sacrifice in single-handedly caring for our beloved children during the time I studied abroad. Their love and encouragement have become an infinite source of strength for me in facing challenges during my time away. Additionally, I also could not have undertaken this journey without the constant encouragement of my parents and in-laws, even from afar.

Ulsan, Korea, June 2024

Nguyen Manh Hung

Contents

Acknowledgment.....	i
Contents	ii
List of Figures.....	iv
List of Tables	vi
ABSTRACT	1
Chapter 1 INTRODUCTION.....	3
1.1 Overview	3
1.2 Research Objectives	5
1.3 Limitations	6
1.4 Thesis Outline	6
Chapter 2 PROBLEM FORMULATION AND PRELIMINARIES.....	8
2.1 Problem Formulation.....	8
2.1.1 Electro-Hydraulic Servo System.....	8
2.1.2 Pump-controlled Hydraulic System	10
2.2 Preliminaries.....	13
2.2.1 Stability Definitions	13
2.2.2 Lyapunov Theory	13
2.2.3 Fundamental Lemmas for Stability Analysis	14
2.2.4 Mathematical Inequalities	14
Chapter 3 DISTURBANCE OBSERVER-BASED CONTROL FOR POSITION TRACKING OF ELECTRO-HYDRAULIC SERVO SYSTEMS	16
3.1 Introduction	16
3.2 Controller Design	17
3.2.1 State Observer Design.....	18
3.2.2 Disturbance Observer Design	19
3.2.3 Backstepping Controller Design	21
3.3 Simulation Results.....	22
3.3.1 Simulation Setup.....	22
3.3.2 Controllers for Comparison.....	23
3.3.3 Numerical Simulation	25
3.4 Conclusion.....	30
Chapter 4 EXTENDED SLIDING MODE OBSERVER-BASED CONTROL FOR ELECTRO- HYDRAULIC ACTUATOR.....	32
4.1 Introduction	32
4.2 Extended Sliding Mode Observer-Based Control Design.....	34
4.2.1 Dual Extended Sliding Mode Observer Design	34
4.2.2 ESMO-based Controller Design.....	38
4.2.3 Closed-loop System Stability Analysis	39
4.3 Numerical Simulation Evaluation	40
4.3.1 The Influence of Observer Bandwidth on Estimation Performance	40
4.3.2 Observer-based Control Performance Evaluation.....	41
4.4 Conclusion.....	46
Chapter 5 ADAPTIVE NEURAL NETWORK-BASED CONTROL FOR ELECTRO- HYDRAULIC SYSTEMS SUFFERING FROM COMPLETELY UNKNOWN DYNAMICS AND EXTERNAL DISTURBANCES.....	48
5.1 Introduction	48

5.2 Adaptive Robust Control Design	49
5.2.1 Robust Control Law Design.....	50
5.2.2 Levant's High-Order Exact Differentiator	52
5.2.3 Unknown Dynamic Estimators	52
5.2.4 Disturbance Observer Design	54
5.3 Stability Analysis	55
5.4 Numerical Simulation	57
5.4.1 Simulation Setup	57
5.4.2 Simulation Results	60
5.5 Conclusions	64
Chapter 6 EXTENDED SLIDING MODE OBSERVER-BASED OUTPUT FEEDBACK CONTROL FOR MOTION TRACKING OF ELECTRO-HYDROSTATIC ACTUATORS	65
6.1 Introduction	65
6.2 Observer-Based Output Feedback Control Design	67
6.2.1 Extended Sliding Mode Observer	67
6.2.2 Observer-Based Control Design.....	70
6.2.3 Closed-Loop Stability Analysis	71
6.3 Experiment Validation	72
6.3.1 Experiment Setup.....	72
6.3.2 Experiment Results	74
6.4 Conclusion.....	79
Chapter 7 OUTPUT FEEDBACK ROBUST CONTROL FOR HYDROSTATIC ACTUATORS WITH MISMATCHED UNCERTAINTIES	80
7.1 Introduction	80
7.2 Control System Design.....	82
7.2.1 Extended State Observer Design.....	82
7.2.2 Mismatched Disturbance Observer	84
7.2.3 Observer-based Control Strategy Design.....	86
7.3 Experiment Verification	89
7.3.1 Experiment Setup.....	89
7.3.2 Experiment Results	90
7.4 Conclusions	94
Chapter 8 CONCLUSIONS AND FUTURE WORKS	95
8.1 Conclusions	95
8.2 Future works.....	95
Published papers	97
References.....	99

List of Figures

Fig. 2-1: The configuration of the studied EHSS	8
Fig. 2-2: The configuration of the pump-controlled hydraulic system	10
Fig. 3-1 The proposed control system based on disturbance observers with backstepping control.....	18
Fig. 3-2: Control design in MATLAB/Simulink environment:.....	23
Fig. 3-3 The tracking errors of the proposed method and other approaches in the presence of matched and mismatched disturbances.....	25
Fig. 3-4 The tracking performance of the proposed method compared with those of other approaches.	25
Fig. 3-5: The estimation error of the angular velocity of the inertial load.	27
Fig. 3-6: The estimation of the mismatched disturbance.	27
Fig. 3-7: The estimation error of the mismatched disturbance.....	28
Fig. 3-8: The estimation of the matched disturbance.	28
Fig. 3-9: The estimation error of the matched disturbance.	29
Fig. 3-10: The control actions of considered controllers.....	30
Fig. 3-11: The load pressures of the actuator corresponding to the control actions.....	30
Fig. 4-1 The proposed control scheme for position tracking of an EHSS with a HRA	34
Fig. 4-2 The velocity, mismatched, and matched disturbance estimation errors of the proposed ESMOs with three distinct observer gains.....	41
Fig. 4-3 The tracking performance in slow-motion desired trajectory.....	43
Fig. 4-4 The velocity estimation performance in slow-motion desired trajectory	43
Fig. 4-5 The matched disturbance estimation performance in slow-motion desired trajectory	44
Fig. 4-6 The mismatched disturbance estimation performance in slow-motion desired trajectory.....	45
Fig. 4-7 The control actions of all controllers in the slow-motion desired trajectory	45
Fig. 4-8 The tracking performance in case of fast-motion desired trajectory	46
Fig. 5-1 The control scheme of the proposed control strategy.....	50
Fig. 5-2 The tracking performance of the proposed strategy compared with other control laws with slow-motion reference trajectory.....	60
Fig. 5-3 The tracking errors of the considered four control strategies with slow-motion reference trajectory.	61
Fig. 5-4 The estimates of the mismatched and matched disturbances of the proposed method.....	61
Fig. 5-5 The weighting values of RFB NNs employed of the proposed method.	62
Fig. 5-6 The control signal of all controllers with slow-motion reference trajectory.	62
Fig. 5-7 The tracking performance of the proposed strategy compared with other control laws in fast-motion reference trajectory.	63
Fig. 5-8 The tracking errors of the four controllers in fast-motion reference trajectory.	63

Fig. 6-1: The control structure of the proposed method.....	67
Fig. 6-2: The experimental platform of the studied electro-hydrostatic actuator.....	72
Fig. 6-3: Tracking performances of the compared controllers with the slow-motion reference trajectory and low-load condition.....	74
Fig. 6-4: Tracking errors of the compared controllers with the slow-motion reference trajectory and low-load condition.....	75
Fig. 6-5: Tracking errors of the compared controllers with the slow-motion reference trajectory and heavy-load condition.....	76
Fig. 6-6: Tracking errors of the compared controllers with the fast-motion reference trajectory and low-load condition.....	77
Fig. 6-7: The angular velocity estimation performance.....	78
Fig. 6-8: The estimation of the load pressure-related term.....	78
Fig. 6-9: Disturbance estimation in the fast-motion reference trajectory.....	78
Fig. 6-10: The control input in the fast-motion reference trajectory and low-load condition.....	79
Fig. 7-1: The control structure of the proposed method.....	82
Fig. 7-2. The experimental platform of the studied pump-controlled electro-hydraulic system.....	89
Fig. 7-3. The output tracking performances of the three controllers under the slow-motion reference trajectory.....	91
Fig. 7-4 The output tracking errors of the three controllers under the slow-motion reference trajectory.....	91
Fig. 7-5. The estimates of the angular velocity and load-pressure-related term under the proposed controller.....	92
Fig. 7-6. The estimates of lumped mismatched and matched uncertainties under the proposed controller.....	92
Fig. 7-7. The output tracking performances of the three controllers under the faster motion reference trajectory.....	93
Fig. 7-8. The output tracking errors of the three controllers under the faster motion reference trajectory.....	93

List of Tables

Table 3-1: The hydraulic system parameters	23
Table 3-2 The maximal absolute values of tracking error in the steady-state phase.....	26
Table 3-3 The average tracking errors in the steady-state phase.....	26
Table 3-4 The standard deviation of tracking errors in the steady-state phase.	26
Table 3-5: The maximal absolute value of estimation errors of mismatched and matched disturbances.	29
Table 4-1 Nominal system parameters.....	40
Table 4-2 Performance indexes in the slow-motion trajectory scenario.	44
Table 4-3 Performance indexes in the fast-motion trajectory scenario.	46
Table 5-1 System parameters of the studied EHSS.....	57
Table 5-2 Nominal system parameters of the EHSS for backstepping control design.....	59
Table 5-3 Performance indexes in slow-motion reference trajectory of all considered controllers.....	61
Table 5-4 Performance indexes in fast-motion reference trajectory of all considered controllers.....	64
Table 6-1 The parameters of the studied EHA.....	73
Table 6-2: Performance indexes in the slow-motion trajectory and low-load condition	75
Table 6-3: Performance indexes in the slow-motion trajectory under heavy-load condition.....	76
Table 6-4: Tracking errors of the compared controllers with the fast-motion reference trajectory and low-load condition.....	77
Table 7-1. The nominal parameter of the studied VSPHS	89
Table 7-2. Performance indexes in the slow-motion reference trajectory case.....	92
Table 7-3. Performance indexes in the faster motion reference trajectory case.....	94

Abbreviations

ADRC	Active Disturbance Rejection Control
EHSS	Electro-Hydraulic Servo System
EHS	Electro-Hydraulic System
HRA	Hydraulic Rotary Actuator
ESO	Extended State Observer
ESMO	Extended Sliding Mode Observer
NN	Neural Network
FLS	Fuzzy Logic System
TP	Trajectory Planner
DOB	Disturbance Observer
DSC	Dynamic Surface Control
CFA	Command Filtered Approach
SMC	Sliding Mode Control
FLC	Feedback Linearization Control
BSC	Backstepping Control
ARC	Adaptive Robust Control
UDE	Uncertainty and Disturbance Estimator

ABSTRACT

By virtue of extremely high force/torque output capability, smooth motion generation, great durability, and less maintenance requirement compared to electrical actuators, hydraulic actuation systems have been widely employed in heavy-duty industrial applications including hydraulic manipulators in manufacturing factories, hydraulic presses, construction machines, and so on in recent years. As one of the control problems for such hydraulic systems, motion tracking control has become an interesting research topic and attracted great attention from the research community in both academia and industry. Nonetheless, achieving high-accuracy tracking performance of hydraulic actuators is still a major concern that requires further consideration due to their high-order dynamics, nonlinear characteristics, model uncertainties, and unknown time-varying payload. Therefore, several attempts to enhance the trajectory-following ability of the electro-hydraulic systems (EHSs) have been made and presented in this thesis.

Firstly, control algorithms based on the nominal system model of the studied EHS, which was offline identified in advance, were proposed. To overcome the problem of velocity measurement shortage, a Levant's differentiator was utilized to precisely attain the angular speed of the actuator based on the position information. Besides, to lower the negative impacts of disturbances resulting from the mismatch between the nominal system model and the actual system dynamics, uncertain nonlinearities, and unknown time-varying payload on the closed-loop system, dual disturbance observers (DOBs) with very few tuning parameters were established. Based on that, improved performance was achieved in comparison with some extended state observer (ESO)-based controllers.

Secondly, as an alternative solution to the well-known ESO design, extended sliding mode observers (ESMOs) were first developed to cope with both the non-existence of measurement mechanisms and disturbances. By using the discontinuous function of the error between the measured signal and its estimate, the constructed ESMOs are able to react better against the fast-changing disturbances and estimate immeasurable system states more accurately compared to the ESOs. The stability of the suggested ESMOs was confirmed by using the Lyapunov theory. Subsequently, an ESMO-based controller was developed based on the traditional backstepping framework for an EHSS. Numerical simulations were conducted to demonstrate the effectiveness of the ESMO-based control approaches in comparison with ESO-based controllers.

Thirdly, to avoid the time-consuming and painstaking identification process, adaptive neural networks (NNs) were developed to approximate unknown dynamics, the so-called unstructured uncertainties, that are functions of system states and control input in the system model. Different from the existing methods in the literature, in which only partial state-dependent model uncertainties were assumed to be unknown, the problem of completely unknown dynamics were considered in this research. To surmount this obstacle, multiple NNs are utilized for tracking control of systems suffering from completely unknown dynamics. In addition, imperfections of NN-based approximations are solved by using disturbance observers. Based on the sliding mode theory, a composite controller was synthesized to not only increase the robustness of the closed-loop system but also avoid the computational complexity of the standard backstepping control. The boundary layer approach was adopted to effectively decrease the chattering that naturally exists when applying conventional sliding mode controllers. The obtained results indicated the effectiveness of the suggested method and unveiled its applicability to real applications subject to completely unknown dynamics.

Finally, in addition to the servo-valve-controlled EHSs, the tracking control for pump-controlled EHSs was also investigated in this study. For the sake of cost-effectiveness, an output feedback robust

control was developed based on an ESMO. To address the computational burden of the traditional back-stepping because of the analytic derivative calculation of a virtual control law at each back-stepping iteration, a dynamic surface control (DSC) technique was adopted. Additionally, compared to the existing method in which only mismatched uncertainties in the pressure dynamics were considered, both total matched and mismatched disturbances were sufficiently estimated by the integration of multiple ESOs then they were compensated by feedforward compensation in the synthesized control laws. Subsequently, the composite control approach was introduced and the stability of the recommended method was confirmed through Lyapunov theory. Numerous comparative experiments were conducted to verify the efficacy of the developed controller in comparison with some reference methods.

Chapter 1

INTRODUCTION

1.1 Overview

By virtue of the various aforementioned advantages, electro-hydraulic systems (EHS) have been broadly employed in numerous industrial and commercial applications in recent decades. For example, in industrial machinery, EHSs were extensively used for material handling, assembly lines, metal forming, and pressing operations [1-3]. For construction machinery [4] such as excavators [5], cranes, loaders, and bulldozers, EHSs were utilized to manipulate heavy loads with accuracy and safety. In addition, EHSs are the main parts of landing support systems and flight control surfaces in aviation and aerospace [6, 7]. Besides, EHSs were integrated into robotic and automation systems for tasks that require precise force and motion control [8]. Nonetheless, due to the high-order dynamics, strong nonlinear behavior, model uncertainties, and external disturbances, it is extremely difficult to achieve high-accuracy tracking performance for such EHSs [9].

It is worth noting that model-free control approaches such as proportional-integral-derivative (PID) [10], and fuzzy logic-based control [11], still are valuable solutions to tracking control problems of EHSs. Among them, PID controllers are preferable since they do not require a complicated identification process, simple implementation, information on internal states, and very few tuning parameters [12]. Research works on PID control design have been reported in the literature [13-15]. Generally, the control parameters, K_p , K_i , K_d , of a conventional PID controller are fixed during operation, hence, the system performance cannot be guaranteed in the case that the system is disturbed by external impacts or changes in the working conditions. Additionally, the determination of PID gains is an ad hoc, meticulous, and tedious process. To overcome this obstacle, gain scheduling algorithms based on Ziegler-Nichols [16], fuzzy logic paradigm [17], auto-tuning mechanism [18], and so on, have been extensively studied. Furthermore, optimal PID controllers for EHSs have been carefully investigated for years. Besides, fractional auto-tuning PID controllers that are able to improve the transient response and steady-state control error of EHSs, were developed [19]. Although various attainments were achieved, some drawbacks of distinct PID designs should be pointed out. Firstly, although PID controllers were verified to be effective for linear systems, the stability of the overall control system by using such controllers for nonlinear EHSs could not be explicitly theoretically proven. Secondly, the control performance when using PID controllers cannot be assured due to changes in working conditions and system parameters. Finally, owing to the lack of compensation mechanisms for system dynamics and external disturbances, PID controllers with high gains must be used to suppress their influences, and the closed-loop system might become unstable at some working points as a consequence [20].

In order to cope with nonlinearities in the system dynamics of EHSs, nonlinear control techniques including feedback linearization, sliding mode control, and backstepping control, were generally utilized. The key idea of the feedback linearization theory is that the original nonlinear system is transformed into a linearized one, then control design techniques for linear systems can be easily adopted. This control methodology has been successfully applied to EHSs [21-24]. Nonetheless, it requires complicated computation steps and cannot be available for all nonlinear systems. Meanwhile, sliding mode theory can be considered as a powerful tool for designing robust controllers that are able to suppress unknown disturbances and model uncertainties in system dynamics of EHSs [25-27] by using high switching gains. However, severe chattering with finite frequency and amplitude can be endured due to unmodeled dynamics and switching time delays. Hence, several techniques [28] have been investigated to reduce this drawback of the traditional sliding mode control method. In addition,

designing control laws by using the sliding mode theory becomes more complicated for high-order nonlinear systems and sliding mode controllers are merely effective against matched uncertainties [29]. Compared to the aforementioned control design methods, backstepping emerged as one of the most effective methods, which is broadly utilized to synthesize control laws for nonlinear systems in various applications [30-33]. The key concept of this technique is that instead of designing a unique control law for the overall system, each control law is separately synthesized for individual first-order subsystems at each design step [34]. By doing this, the actual control input is designed at the final step to stabilize the overall system. Additionally, nonlinearities are completely compensated at each backstepping iteration, and consequently, tracking performance is significantly improved. Nonetheless, the control design by using the backstepping approach becomes extremely complicated due to repeated analytical differentiations. Some techniques have been developed to reduce this computational burden of the traditional backstepping control theory, such as dynamic surface control (DSC) [35, 36] and command filtered approach (CFA) [37, 38]. Various DSC-based and CFA-based backstepping controllers have been successfully constructed in numerous applications [39-47]. However, system states and disturbances information which is not always available, is required to be known when employing the above control techniques.

Intuitively, the observer-based control approach is a valuable and effective solution to not only deal with the shortage of states and disturbances information but also reduce the system cost and complexity of control systems by not using expensive and additional sensors. In addition, some signals are impractical to measure and/or influenced by inevitable noise from the working environment [48]. Observers are constructed by combining sensed signals and knowledge of the system model, observed signals can be produced as a result [49]. It is worth noting that these estimated signals may be more accurate, less expensive to produce, and more reliable than directly observed signals. The full-order observer was originally introduced in 1964 by D.G. Luenberger, an American mathematician [50, 51] and further developed in [52] for linear time-invariant systems. However, these concepts cannot be applied to nonlinear systems. Therefore, an extended Luenberger observer design [53] and extended Kalman Filter (EKF) [54-56] have been introduced for estimating missing states of single-input single-output nonlinear systems. In addition, in [57], observers for a class of nonlinear systems were developed. Moreover, based on the concept of sliding mode and equivalent control theories [58] proposed by Utkin, sliding mode observers [59-61] have been constructed to robustly estimate system states by using switching terms in the existence of unknown inputs and model uncertainties. In practice, an exact model of a dynamical system could not be attained since system parameters or system behaviors may change under different operation conditions. Furthermore, external disturbances naturally exist in many engineering systems and deteriorate the system performance. The concept of disturbance observer [62] was first discussed by Kouhei Ohnishi in 1983 [63] and it has been successfully applied to various applications such as robotic manipulators [64], marine vehicles [65], direct drive motors [66, 67], electro-hydraulic systems [68-70], and so on to deal with model uncertainties and external disturbances due to its simplicity and efficacy [71]. The integration of state observers and disturbance observers provides a complete solution to address the shortage of system information and attenuate the effects of model uncertainties and disturbances on control systems [72]. Besides, active disturbance rejection control (ADRC) [73] has been initiated by Jingqing Han, and is also an alternative way for solving problems of model imperfections and external disturbances. The core component of this control approach is an extended state observer (ESO) that is able to observe not only system states but also lumped uncertainties caused by model uncertainties and external disturbances in system dynamics. Hence, ESOs have been adopted in many practical applications [74-77]. Nonetheless, the disadvantages of ESOs including peaking phenomenon when using high gains and slow convergence of estimation restrict their applications in practice. Development of advanced

observers for both state and disturbance estimation and observer-based control strategies is still open research problems that need to be further studied.

Another control problem which is how to achieve high-accuracy tracking performance for systems subject to unstructured uncertainties has become an intriguing research question in recent years. By the capability of self-learning and online weight update, radial basis function neural networks (RBFNN) [78] have been successfully employed in numerous applications including space flexible manipulator [79], robot manipulators [80-83], underwater vehicles [84], active suspension systems [85], servo motor systems [86, 87], and so on [88, 89]. For tracking control problems of EHSs, RBFNNs were widely used to approximate unknown dynamical functions. For example, in [8], model uncertainties and load disturbances of an EHS were approximated and compensated using RBFNNs. Multilayer neural networks [90] were developed to deal with the residual mismatched disturbance, and consequently, improved tracking accuracy was achieved. Nevertheless, it should be pointed out that in the previous studies, only partial system dynamics were assumed to be unknown, dealing with nonlinear systems suffering from fully unknown dynamical functions remains a challenging control problem.

1.2 Research Objectives

This thesis investigates the tracking control problem for valve-controlled and pump-controlled hydraulic systems suffering from parametric uncertainties, unknown dynamics, and external load. These difficulties make the control design challenging. The nominal controllers are first designed by using the backstepping control technique and sliding mode control theory, in which uncertainties and disturbances in the mechanical subsystem and pressure dynamics are lumped into total mismatched and matched disturbances, respectively. To reduce the influences of such disturbances on the overall control system, control algorithms based on Levant's differentiator-based disturbance observers and extended sliding mode observers are developed. Subsequently, these disturbances are compensated by feedforward compensation mechanisms in the control laws. In addition, adaptive neural network control is also adopted to approximate unstructured uncertainties in the system dynamics, and consequently, the tracking performance is significantly improved. The stability of recommended control algorithms is analyzed through the Lyapunov theory. Finally, numerical simulations and experiments are conducted to validate the superiority of the proposed methods over some existing control approaches.

In detail, the objectives of the thesis are discussed as follows:

- To obtain the immeasurable speed of the actuator based on the position signal, a Levant's differentiator is adopted. Subsequently, dual disturbance observers (DOB) are presented to online estimate both lumped matched and mismatched uncertainties. Finally, a DOB-based backstepping controller is constructed to improve the control accuracy for the motion tracking problem of the considered EHSS.
- To avoid the complexity of the control structure due to the combination of a state observer and DOBs for dealing with the shortage of internal system states and the influences of the model uncertainties and external load, dual extended sliding mode observers (ESMO) are introduced. Based on this, a composite controller is constructed accordingly. Compared to some well-known ESO-based control algorithms, significantly improved tracking performance for EHSS is achieved.
- It should be admitted that the identification process of a system model for a real system is always a time-consuming and painstaking task. With the help of adaptive NN-based approximators, unknown dynamical functions in the system dynamics can be online approximated. To cope with the adverse effects of not only the approximation imperfections

but also external disturbances, DOBs are employed. In addition, to effectively mitigate the computational complexity of the standard backstepping due to the analytic derivative calculation of the virtual control law at each backstepping iteration, sliding mode control theory is used to design the actual control input for stabilizing the closed-loop system. Hence, the tracking error is considerably reduced as a result.

- Owing to the high energy efficiency and cost-effectiveness, tracking control for pump-controlled hydraulic systems besides the valve-controlled hydraulic actuation systems has also been a trendy research topic in recent years. To avoid measurement noise and reduce the overall system cost, output feedback motion tracking control is considered. Firstly, an ESMO is developed to estimate immeasurable states and lumped-matched disturbances in the system dynamics. The control algorithm is then synthesized by employing the traditional backstepping control framework and dynamic surface control technique. The stability of the closed-loop system is verified by using Lyapunov theory and the superiority effectiveness of the proposed method is illustrated by comparative experiments.
- With the same control objective as above, multiple-ESO configuration is employed, in which an ESO is utilized for observation of immeasurable states, i.e., angular speed and load pressure-relating term, and lumped matched disturbances. In light of this, another ESO works as a DOB for estimating the lumped mismatched disturbance. The dynamic surface control (DSC) approach is adopted to remarkably diminish the “explosion of complexity” of the conventional backstepping control technique. Accordingly, an improved tracking performance is attained.

For each proposed control method, the Lyapunov theory is utilized to theoretically analyze the stability of not only constructed observers but also the overall closed-loop system. Simulation and experiment results are given to demonstrate the effectiveness of the proposed methods in comparison with several well-known reference control algorithms reported in the literature.

1.3 Limitations

In this thesis, several advanced control approaches for enhancing the tracking performance of electro-hydraulic systems subject to model uncertainties and external disturbances are constructed. The stability of the closed-loop system is theoretically proven using the Lyapunov theory. The advantage of each control algorithm is confirmed by both comparative simulation examples and experiment studies. However, some limitations of the dissertation are remaining as follows:

- The dynamics of servo valves and bidirectional pumps have not been considered in the control design process.
- The derivatives of lumped uncertainties and disturbances are assumed to be bounded.
- In most research works, the nominal system models are assumed to be available.
- The relationship between the desired performance and the input saturation problem has not been explicitly pointed out.
- Control algorithms for servo valve-controlled hydraulic systems are merely verified by numerical simulations. Due to the lack of a real test bench, the influences of measurement noises on the measured signals have not been considered.

1.4 Thesis Outline

The dissertation is organized as follows:

- Chapter 1 shows the research motivations, goals, limitations, and the outline of the thesis.
- Chapter 2 presents the construction of a system model of studied electro-hydraulic systems and some mathematical notations and Lyapunov stability theory.

- Chapter 3 investigates an active disturbance rejection framework by using disturbance observers.
- Chapter 4 discusses the extended sliding mode observer for enhancing the reference trajectory tracking qualification.
- Chapter 5 gives an adaptive neural network control for electro-hydraulic servo systems subject to completely unknown dynamics and external disturbances.
- Chapter 6 presents an extended sliding mode observer-based output feedback control for tracking problems of an electro-hydrostatic actuator.
- Chapter 7 provides output feedback robust control based on multiple ESOs configuration for the motion tracking problem of an electro-hydrostatic actuator considering lumped mismatched uncertainties.
- Chapter 8 concludes the thesis and gives a discussion about future works.

PROBLEM FORMULATION AND PRELIMINARIES

2.1 Problem Formulation

2.1.1 Electro-Hydraulic Servo System

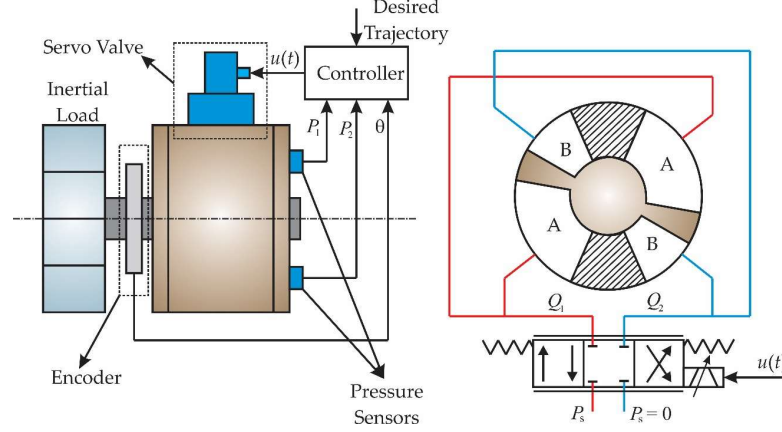


Fig. 2-1: The configuration of the studied EHSS

The schematic of the studied EHSS is illustrated in Fig. 2-1. On the basis of the second Newton's law, the motion dynamic of the actuator is given by

$$J\ddot{\theta} = D_m P_L - \tau_f - \tau_d \quad (2.1)$$

where J and θ are the inertial moment and the angular position of the actuator shaft, respectively; D_m denotes the radian displacement of the HRA; $P_L = P_1 - P_2$ represents the load pressure with P_1 and P_2 reflex the pressures in the forward chamber and reverse chamber of the HRA; $\tau_f = B\dot{\theta}$ is the frictional torque with B as the viscous friction coefficient; and τ_d signifies the torque disturbances caused by unmodeled dynamics, parameter deviations, and unknown external load.

The load pressure dynamics in the HRA are given by [91]

$$\frac{V_t}{4\beta_e} \dot{P}_L = -D_m \dot{\theta} - Q_i + Q_L + q(t) \quad (2.2)$$

where V_t is the total control volume of the HRA, β_e denotes the effective buck modulus of the hydraulic oil, $Q_i = C_i P_L$ represents the internal leakage caused by the pressure deviation between two chambers of the actuator with C_i is the internal leakage coefficient, Q_L signifies the load flow, and $q(t)$ reflects the modeling uncertainties.

Based on the flow through an orifice formula, the load flow through the servo valve is determined by [92]

$$Q_L = C_d w x_v \sqrt{\frac{1}{\rho} (P_s - \text{sign}(x_v) P_L)} \quad (2.3)$$

where C_d denotes the discharge coefficient, w is the spool valve area gradient, ρ represents the oil density, x_v is the displacement of the servo valve's main spool, and P_s is the supply pressure.

In previous works, scholars have pointed out that the tracking performance is only negligibly improved when considering the servo valve dynamics [76, 93, 94]. In addition, due to the extremely high bandwidth of the servo valve compared to the dynamics of the other hydraulic components and

for the sake of simplicity in designing the controller, the valve dynamics can be ignored. The simplified servo valve model is employed as [91, 93, 95]

$$x_v = k_v u \quad (2.4)$$

where k_v is the servo valve coefficient and u denotes the control voltage.

Substituting (2.4) into (2.3) yields

$$Q_L = k_t u \sqrt{(P_s - \text{sign}(x_v) P_L)} \quad (2.5)$$

where $k_t = C_d w k_v \sqrt{l/\rho}$ represents the overall load flow coefficient. The function $\text{sign}(\cdot)$ stands for the standard signum function which is defined by

$$\text{sign}(u) = \begin{cases} 1, & \text{if } u > 0 \\ 0, & \text{if } u = 0 \\ -1, & \text{if } u < 0 \end{cases}$$

Defining $\mathbf{x} \triangleq [x_1, x_2, x_3]^T = [\theta, \dot{\theta}, D_m P_L / J]^T$ as the state vector, the whole system dynamics are represented as

$$\begin{cases} \dot{x}_1 = x_2 \\ \dot{x}_2 = x_3 + f_1(x_2) + d_1(t) \\ \dot{x}_3 = f_2(x_2, x_3) + g_2(x_3, u)u + d_2(t) \end{cases} \quad (2.6)$$

where the dynamical functions and lumped disturbances are determined by

$$\begin{aligned} f_1(x_2) &= -\frac{\tau_f}{J}; d_1(t) = -\frac{\tau_d}{J}; f_2(x_2, x_3) = -\frac{4D_m^2 \beta_e}{J V_t} x_2 - \frac{4\beta_e C_t}{V_t} x_3; \\ g_2(x_3, u) &= \frac{4D_m \beta_e k_t}{J V_t} \sqrt{P_s - \text{sign}(u) \frac{J}{D_m} x_3}; \text{ and } d_2(t) = \frac{4\beta_e D_m}{J V_t} q(t). \end{aligned}$$

For convenience, some reasonable assumptions are made as follows [76, 95]:

Assumption 2-1. The desired reference trajectory is smooth and bounded up to the second-order derivative, i.e., $x_{1d} \in C^3$, and the absolute value of load pressure $|P_L|$, is adequately smaller than the supply pressure P_s to guarantee that the dynamical function $g_2(x_2, x_3)$ is far away from zero.

Assumption 2-2. The dynamical function $f_1(x_2)$ is Lipschitz with respect to x_2 in its operational range and $f_2(x_2, x_3)$ is globally Lipschitz with respect to x_2 and x_3 .

Hence, there exist positive constants c_{f_1} and c_{f_2} such that the following inequalities hold

$$|f_1(x_2) - f_1(\bar{x}_2)| \leq c_{f_1} |x_2 - \bar{x}_2| \quad (2.7)$$

$$|f_2(x_2, x_3) - f_2(\bar{x}_2, x_3)| \leq c_{f_2} |x_2 - \bar{x}_2| \quad (2.8)$$

Assumption 2-3. The internal uncertainties and external disturbances in the system dynamics of the studied EHSS are grouped into two lumped disturbance terms $d_1(t)$ and $d_2(t)$ which are assumed to be differentiable. In addition, the first-order derivatives $\dot{d}_1(t)$ and $\dot{d}_2(t)$ are supposed to be bounded but their bounds are unknown, i.e., $|\dot{d}_1(t)| \leq \gamma_1$ and $|\dot{d}_2(t)| \leq \gamma_2$.

Remark 2-1. In practice, the load capacity of hydraulic systems is restricted by their kinematic and dynamic constraints such as maximal velocity, acceleration, and torque/force being able to be generated. Hence, the system performance cannot be guaranteed or some unexpected problems with the system may occur in the conditions in which these constraints are violated. For example, under the heavy-load condition and exceedingly fast-changing reference trajectory, the control input will be saturated in its range, whereas the system output still cannot follow the desired trajectory as closely as expected. The system performance will deteriorate as a result. The same phenomenon will happen in the existence of excessive internal and external leakages in the case of the aged actuator. Therefore, from the practical perspective, the lumped uncertainties $d_1(t)$ and $d_2(t)$ are bounded by positive constants which are determined by system parameters. Due to the limited scope, the problem of the heavy-load condition and the aging actuator is not considered in this research.

The principal control objective is to design robust controllers that are capable of attaining a high-accuracy tracking performance for positioning control of the above EHSS without angular velocity measurement under the presence of lumped mismatched and matched disturbances in the system dynamics of the EHSS. In this regard, several advanced control approaches are presented in Chapter 3 and Chapter 4. To avoid the complicated system identification process, i.e., dynamical functions are assumed to be unknown, a neural network control based on disturbance observer is constructed in Chapter 5 to achieve a high control accuracy.

2.1.2 Pump-controlled Hydraulic System

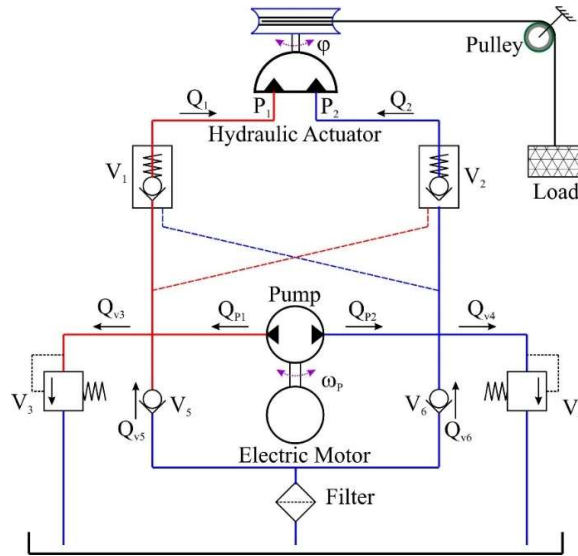


Fig. 2-2: The configuration of the pump-controlled hydraulic system

The schematic of the considered pump-controlled hydraulic system is illustrated in Fig. 2-2. A bidirectional hydraulic pump controlled by an electric motor was used to manipulate the motion of the hydraulic rotary actuator (HRA). To ensure that the system pressure does not surmount the maximal predefined pressure, two relief valves V_3 and V_4 were utilized. The two pilot-operated check valves V_1 and V_2 were employed to regulate the flow of the hydraulic oil into and out of the actuator. Meanwhile, the general check valves V_5 and V_6 guaranteed that there was no flow from the system to the tank. A gravitational load rigidly connected to the actuator shaft through a drum and pulley system was intentionally added to evaluate the system's performance.

Remark 2-2. According to the schematic of the studied EHS, it should be pointed out that, in the normal working condition, the pilot-operated check valves V_1 and V_2 allow the flow from the hydraulic pump to a chamber of the HRA and from the remaining chamber to the suction of the

hydraulic pump for lifting or lowering the gravitational load. In the non-working state, i.e., the hydraulic pump does not run, no flow is supplied by the pump to the hydraulic components; therefore, the pilot-operated check valves V1 and V2 are completely blocked to securely lock the load at the current position and guarantee that there is no adverse impact on the hydraulic pump.

According to Newton's second law, the motion dynamics of the hydraulic actuator are derived by

$$J_A \ddot{\varphi} = D_A (P_1 - P_2) - B\dot{\varphi} - A_f S_f(\dot{\varphi}) - \tau_l \quad (2.9)$$

where J_A denotes the total inertial moment of the actuator shaft; $\dot{\varphi}$ and $\ddot{\varphi}$ are the angular speed and acceleration of the hydraulic actuator, respectively; D_A signifies the displacement of the actuator; B signifies the total viscous friction coefficient; A_f presents the Coulomb friction coefficient; $S_f(\dot{\varphi})$ denotes the continuous approximation of the standard signum function; P_1 and P_2 are the pressures in the left and the right chambers of the actuator; τ_l reflects the total torque disturbance caused by the modeling errors and unknown external load.

The pressure dynamics of the two chambers of the hydraulic actuator were determined in the following equations:

$$\begin{aligned} \dot{P}_1 &= \frac{\beta_e}{V_{01} + D_A \varphi} (Q_1 - D_A \dot{\varphi} - C_{At} (P_1 - P_2)) \\ \dot{P}_2 &= \frac{\beta_e}{V_{02} - D_A \varphi} (Q_2 + D_A \dot{\varphi} + C_{At} (P_1 - P_2)) \end{aligned} \quad (2.10)$$

where β_e is the bulk modulus of the hydraulic oil, V_{01} and V_{02} denote the initial volumes of the two chambers of the actuator including the volume of the pipeline, φ is the angular position of the actuator shaft, C_{At} is the leakage coefficient of the actuator, and Q_1 and Q_2 are the flow rates into the hydraulic actuator chambers, which are determined by

$$\begin{cases} Q_1 = Q_{P1} + Q_{v5} - Q_{v3} \\ Q_2 = Q_{P2} + Q_{v6} - Q_{v4} \end{cases} \quad (2.11)$$

The flow rates supplied to the chambers of the hydraulic actuator are presented as

$$\begin{cases} Q_{P1} = D_p \omega_p - C_{Pt} (P_1 - P_2) \\ Q_{P2} = -D_p \omega_p + C_{Pt} (P_1 - P_2) \end{cases} \quad (2.12)$$

where D_p is the pump displacement, ω_p denotes the speed of the pump, and C_{Pt} signifies the total leakage coefficient of the pump.

Assuming that the system pressure does not surmount the setting pressure of the relief valve, hence, we have

$$Q_{v3} = 0; Q_{v4} = 0 \quad (2.13)$$

Combining (2.10), (2.11), (2.12), and (2.13) yields

$$\begin{aligned} \dot{P}_1 &= \frac{\beta_e}{V_{01} + D_A \varphi} (D_p \omega_p - C_t (P_1 - P_2) + Q_{v5} - D_A \dot{\varphi}) \\ \dot{P}_2 &= \frac{\beta_e}{V_{02} - D_A \varphi} (-D_p \omega_p + C_t (P_1 - P_2) + Q_{v6} + D_A \dot{\varphi}) \end{aligned} \quad (2.14)$$

where $C_t = C_{At} + C_{Pt}$ is the total equivalent leakage coefficient.

Remark 2-3. Since the system parameters J_A , D_A , B , A_f , β_e , V_{01} , V_{02} , D_P , and C_t cannot be exactly known, their nominal values \bar{J}_A , \bar{D}_A , \bar{B} , \bar{A}_f , $\bar{\beta}_e$, \bar{V}_{01} , \bar{V}_{02} , \bar{D}_P , and \bar{C}_t , respectively, were experimentally identified, which were adopted to design the observers and control law in the following sections. The effects of parameter deviations, external load, and unmodeled dynamics were lumped into total mismatched and matched disturbances.

Defining $\mathbf{x} = [x_1, x_2, x_3]^T = [\varphi, \dot{\varphi}, \bar{D}_A / \bar{J}_A (P_1 - P_2)]^T$, according to (2.9) and (2.14), the overall system dynamics can be derived in the strict feedback form as

$$\begin{aligned}\dot{x}_1 &= x_2 \\ \dot{x}_2 &= x_3 + f_2(x_2) + d_1(t) \\ \dot{x}_3 &= g_3(x_1)u + f_3(x_2, x_3) + d_2(t)\end{aligned}\tag{2.15}$$

where $u = \omega_p$ is the control input, and the dynamical functions are given by

$$\begin{aligned}f_2(x_2) &= -\frac{\bar{B}}{\bar{J}_A}x_2 - \frac{\bar{A}_f S_f(x_2)}{\bar{J}_A}; d_1(t) = -\frac{\tau_l}{\bar{J}_A} + \Delta f_2(x_2) \\ f_3(x_2, x_3) &= -\left(\frac{\bar{\beta}_e}{\bar{V}_{01} + \bar{D}_A x_1} + \frac{\bar{\beta}_e}{\bar{V}_{02} - \bar{D}_A x_1}\right)\left(\bar{C}_t x_3 + \frac{\bar{D}_A^2}{\bar{J}_A} x_2\right) \\ g_3(x_1) &= \left(\frac{\bar{\beta}_e}{\bar{V}_{01} + \bar{D}_A x_1} + \frac{\bar{\beta}_e}{\bar{V}_{02} - \bar{D}_A x_1}\right)\frac{\bar{D}_A \bar{D}_P}{\bar{J}_A} \\ d_2(t) &= \left(\frac{\bar{\beta}_e}{\bar{V}_{01} + \bar{D}_A x_1} Q_{v5} - \frac{\bar{\beta}_e}{\bar{V}_{02} - \bar{D}_A x_1} Q_{v6}\right)\frac{\bar{D}_A}{\bar{J}_A} + \Delta g_3(x_1)u + \Delta f_3(x_2, x_3)\end{aligned}\tag{2.16}$$

where $\Delta f_2(x_2)$, $\Delta f_3(x_2, x_3)$, and $\Delta g_3(x_1)$ are uncertain functions due to the parameter perturbation and modeling errors.

Remark 2-4: Considering the system dynamics (2.15), since the nominal system parameters were assumed to be known, the dynamical functions $f_2(x_2)$, $f_3(x_2, x_3)$, and $g_3(x_1)$ can be defined according to system states. The influences of parametric uncertainties, unmodeled dynamics, and external disturbances on the mechanical and pressure dynamics were treated as the lumped terms $d_1(t)$ and $d_2(t)$, the so-called lumped mismatched and matched disturbances, respectively, which were to be online estimated and then adequately compensated in the control laws.

Model-based control strategies that guarantee the system output x_1 tracks the desired trajectory x_{1d} as closely as possible in the case that only the angular position of the actuator is measurable and in the presence of both mismatched and matched uncertainties, are provided in Chapter 6 and Chapter 7. To facilitate the control design, some practical assumptions are made as follows:

Assumption 2-4: The desired position trajectory x_{1d} is sufficiently smooth up to the third-order derivative, that is $x_{1d} \in C^3$.

Assumption 2-5: The function $f_2(x_2)$ is globally Lipschitz with respect to x_2 and $f_3(x_2, x_3)$ is Lipschitz with respect to x_2 and x_3 .

Assumption 2-6: The lumped disturbances $d_1(t)$ and $d_2(t)$ were assumed to be differentiable, and their first-order derivatives $h_1(t)$ and $h_2(t)$, respectively, were bounded by unknown positive

constants, i.e., $|h_1(t)| \leq \bar{h}_1$ and $|h_2(t)| \leq \bar{h}_2$. In addition, the lumped mismatched disturbance $d_1(t)$ is also supposed to be bounded by an unknown nonnegative constant, that is $|d_1(t)| \leq \bar{d}_1$.

Remark 2-5: It should be admitted that the torque generation ability of a hydraulic system is restricted in a specific range because of the maximal working pressure that the pumping system can provide and the safety constraints. The load-carrying capacity of it is limited as a result. Hence, the assumption that the lumped mismatched uncertainty is bounded is practically reasonable.

2.2 Preliminaries

2.2.1 Stability Definitions

Consider a nonlinear time-invariant system $\dot{x} = f(x)$, where $f: R^n \rightarrow R^n$, a point $x_e \in R^n$ is an equilibrium point of the system if $f(x_e) = 0$.

Definition 2-1. The system is globally asymptotically stable if, for every trajectory $x(t)$, we have $x(t) \rightarrow x_e$ as $t \rightarrow \infty$.

Definition 2-2. The system is locally asymptotically stable near or at x_e if there is an $\gamma > 0$ such that $\|x(0) - x_e\| < \gamma$, we have $x(t) \rightarrow x_e$ as $t \rightarrow \infty$.

2.2.2 Lyapunov Theory

a) Lyapunov function definition

A function $V: R^n \rightarrow R$ is positive definite if

- $V(z) \geq 0$ for all $z \in R^n$
- $V(z) = 0$ if and only if $z = 0$
- $V(z) \rightarrow \infty$ as $z \rightarrow \infty$

A function $V = x^T P x$ is positive definite if and only if P is a positive definite matrix.

Suppose there is a positive definite function V that satisfies

- $V(z) \rightarrow \infty$ as $z \rightarrow \infty$
- $\dot{V}(z) \leq 0$ for all z

then, all trajectories are bounded, i.e., for each trajectory x , there is a positive constant λ such that $\|x\| \leq \lambda$ for all $t \geq 0$. In this case, V is called a Lyapunov function that proves the trajectories are bounded.

b) Globally Asymptotic Stability

Suppose there is a function V such that

- V is positive definite
- $\dot{V}(z) < 0$ for all $z \neq 0$
- $\dot{V}(0) = 0$

then, every trajectory of $\dot{x} = f(x)$ converges to zero as $t \rightarrow \infty$.

c) **Globally Exponential Stability**

Suppose there is a function V such that

- V is positive definite
- $\dot{V}(z) < -\alpha V(z)$ for all z

then, there is an M such that every trajectory $\dot{x} = f(x)$ satisfies $\|x(t)\| \leq Me^{-\alpha t/2} \|x(0)\|$.

2.2.3 Fundamental Lemmas for Stability Analysis

Lemma 2-1 [96]. Consider a positive definite function $V_1(t)$ satisfying the following inequality

$$\dot{V}_1(t) \leq -kV_1^\alpha(t) \quad (2.17)$$

where $k > 0$ and $0 < \alpha < 1$.

The function $V_1(t)$ converges to zero in finite time t_f given by

$$t_f = \frac{V_1(0)^{1-\alpha}}{k(1-\alpha)} \quad (2.18)$$

Lemma 2-2 [97]. Consider the following Lyapunov function $V_2(t)$ satisfying

$$\dot{V}_2(t) \leq -aV_2(t) + b \quad (2.19)$$

where a and b are adjustable parameters.

According to (2.19), the function $V_2(t)$ is bounded by

$$V_2(t) \leq V_2(0)e^{-at} + \frac{b}{a}(1 - e^{-at}) \quad (2.20)$$

It can be observed that the function $V_2(t)$ reaches the region prescribed by b/a as time goes to infinity. The bound of this region depends on the selection of parameters a and b .

Lemma 2-3. Consider a positive function $V_3(t)$ that satisfies the following inequality

$$\dot{V}_3(t) \leq -\varpi V_3(t) + \sigma \quad (2.21)$$

where ϖ and σ are positive adjustable parameters.

This function approaches the vicinity of the region bounded by σ / ϖ in finite time.

Proof of Lemma 2-3: In the circumstance that at the initial time $t = 0$, if $V_3(0)$ lies in the region defined by σ / ϖ , because of the dynamics (2.21), $V_3(t)$ is eternally constrained in this region.

Assuming that at the beginning, $V_3(0)$ is far from this region. According to (2.20), for all $\varepsilon > 0$, $V_3(t)$ reaches the region bounded by $\varepsilon + \sigma / \varpi$ in finite time t_r determined by

$$t_r \leq -\frac{1}{\varpi} \ln \left[\frac{\varepsilon}{V_3(0) - \sigma / \varpi} \right] \quad (2.22)$$

This completes Proof of Lemma 2.3.

2.2.4 Mathematical Inequalities

Lemma 2-4 [98]: For $(a, b) \in R^2$, Young's inequality holds as follows:

$$ab \leq \frac{va^p}{p} + \frac{b^q}{vq}$$

where $p, q \in [1, \infty)$; $1/p + 1/q = 1$, and $v \in R^+$.

Lemma 2-5 [99]: For any $p \in [1, \infty)$ and $a_i \in R^+$, the following inequality holds

$$(a_1 + \cdots + a_n)^p \leq n^{p-1} (a_1^p + \cdots + a_n^p)$$

DISTURBANCE OBSERVER-BASED CONTROL FOR POSITION TRACKING OF ELECTRO-HYDRAULIC SERVO SYSTEMS**3.1 Introduction**

Electro-hydraulic servo systems (EHSSs) have been widely employed for years in a wide range of industrial applications such as load simulators [100], robot manipulators [101-105], vehicle active suspension [106, 107], and hydraulic press [108] due to their advantages of high produced force/torque, high stiffness, high power-to-weight ratio, high load efficiency, and fast and smooth response [95]. However, high-accuracy position tracking control of electro-hydraulic systems is still challenging owing to highly nonlinear characteristics [109], parametric uncertainties (i.e., significant changes in effective bulk modulus and viscosity with temperature, etc.), unmodeled uncertainties, and external disturbances.

To deal with the nonlinearities of the electro-hydraulic systems, feedback linearization methods such as full-state feedback linearization [110], input-output feedback linearization [22], and partial input feedback linearization [111] were investigated under the assumption that the exact model information is available. In [112], a modified feedback linearization-based position control with supply pressure uncertainty was introduced to improve the tracking performance; however, the parametric uncertainties have not been fully considered in this work. In addition, the feedback linearization controller [113] was proven to not be robust in modeling uncertainty and sensor noise due to the high-order derivative terms in control inputs. Hence, to overcome the challenge of modeling uncertainty, nonlinear robust control, such as sliding mode control (SMC), is proposed in several studies [76, 114, 115]. The main advantage of SMC is that it is well established, simple, and widely applicable [26] to hydraulic servo systems. It has proven to be robust in modeling inaccuracies that satisfied matching conditions. If the chosen switching gains of SMC are bigger than the upper bound on the uncertainties, robust stabilization can be achieved [116]. However, in practice, the upper bound is partly known or even completely unknown, so the switching gains must be sufficiently large to suppress the influence of the uncertainties. The adoption of high-gain feedback control and the sign function in the control law cause chattering problems [117], resulting in insufficient control accuracy, high heat losses in electrical power circuits, and high wear of moving mechanical parts [34]. Therefore, some modifications of the SMC approach [118-121] were introduced to reduce these chattering effects, but there is a tradeoff between tracking accuracy and chattering. Overall, the parametric uncertainties have not been effectively treated in these works. To cope with the parametric uncertainties, the methodology of adaptive control, which utilizes the adaptive mechanism to update the system parameters in the control design, has been studied for the past decades [122, 123]. Based on this adaptation technique, the gains of the controller can be significantly reduced. By merging adaptive control and robust control, nonlinear adaptive robust control (ARC) approaches [124, 125] have been introduced to obtain better performance. In these studies, only bounded tracking performance can be achieved in the presence of mismatched and/or matched disturbances. To obtain an asymptotic tracking performance, a robust integral of the sign of the error (RISE)-based adaptive control [123] has been investigated where unknown parameters are estimated via adaptive technique and all unmodeled uncertainties are compensated by the RISE feedback. However, in this study, the disturbances are assumed to be bounded up to the second-order derivative, therefore this assumption might be restricted in some real applications. Generally, in the above-mentioned works, although model uncertainties have been carefully considered, the influence of external disturbances, i.e., torque/force while interacting with the environment, have not been fully addressed. Therefore, to enhance the tracking performance these disturbances need to be estimated and compensated in the control system design.

To deal with the effects of external disturbances on the control system, disturbance observers (DOs) have been investigated for years with the assumption that their derivatives are bounded [126]. Typically, disturbance observers are broadened to estimate not only the external disturbances but also the model uncertainties. Disturbance and uncertainty are lumped in a generalized term, which is called lumped uncertainties/disturbances. Active disturbance rejection control (ADRC) approaches have been introduced in recent years with various structures to improve the system performance in the presence of disturbances and unmodeled uncertainties such as high-gain disturbance observer [127, 128], sliding perturbation observer [129], uncertainty and disturbance estimator (UDE) [130, 131], sliding mode observer (SMO) for state and disturbance estimation [132], extended disturbance observer [108], adaptive high gain observer [133], and high-order disturbance observer (DOB) [134]. Among them, extended state observers (ESOs) have been widely used in many works [76, 95, 109, 135-138] in recent years because they can estimate not only the unmeasurable system states but also the external disturbances. For example, in [76], an extended state observer (ESO)-based control for a hydraulic rotary actuator originated from [73] was proposed to approximate angular velocity and matched disturbance by using an extended state. In this paper, the mismatched disturbance was only attenuated by using a high-gain ESO. The modification of ESO [76] was introduced in [95] by separating the original system into two subsystems to obtain better performance in which the matched and mismatched disturbances are simultaneously estimated. An integral sliding mode backstepping controller based on ESO for the asymmetric electro-hydraulic actuator was introduced in [138]. However, from the design of the ESO, one can observe that the disturbance estimation performance depends on not only the physical disturbance in the real system but also the unmeasurable state estimation which currently is estimated by the ESO. In contrast, the state estimation of ESO is essentially based on the Luenberger observer, which can be improved by exact differentiators [139, 140]. Hence, combining DOs and exact differentiators is potential to produce a better disturbance estimation compared to the ESO.

Inspired by the aforementioned discussion, this chapter proposes a novel active disturbance rejection control to improve the tracking performance of a hydraulic servo system. In this study, a highly accurate and robust Levant's differentiator [141] is applied to exactly calculate the angular velocity of the actuator. Based on that, two disturbance observers (DOs) with the linear structure are proposed to estimate the matched and mismatched disturbances in the subsystems then the estimated disturbances are fed back into the control law. The DOs-based backstepping controller is proposed to attenuate the influence of the disturbances, unmodeled uncertainties caused by weak modeling, and parameter perturbations as well. The stability of the closed-loop system is proven using the Lyapunov theory. Simulations are conducted in comparison with other control approaches to show the superiorities of the proposed control algorithm.

The remainder of this chapter is organized as follows: The entire control system design including state observers, disturbance observers, and backstepping control, and the system stability analysis are introduced in Section 3.2. Section 3.3 contains the simulation results. The conclusion is provided in Section 3.4.

3.2 Controller Design

The proposed control scheme is designed to improve the tracking performance and robustness with respect to the uncertainties of the hydraulic system. In this stage, nominal system parameters are used to design the observers and the controller. The modeling errors are lumped to the unmodeled terms d_1 and d_2 in the second and third equations of (2.6). The proposed control system is demonstrated in Fig. 3-1 The proposed control system based on disturbance observers with backstepping control.

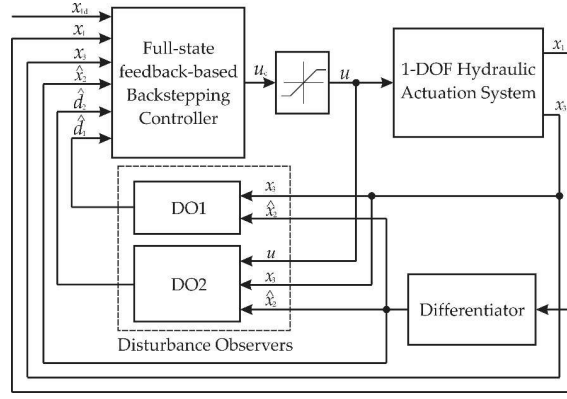


Fig. 3-1 The proposed control system based on disturbance observers with backstepping control.

In this control system, the state observer based on the Levant's differentiator is designed to accurately approximate the angular velocity of the inertial load. The output of this observer is fed back to the controller and two disturbance observers as well. The disturbance observers are constructed to estimate the lumped uncertainties d_1 and d_2 , then they are integrated into the control design step to compensate for their effects on the closed-loop control system. The controller is synthesized by using the backstepping method, which utilizes the measured states (the angular position and the pressures of chambers of the actuator), the estimated state (angular velocity) produced by the state observer, and the estimation of unmodeled uncertainties generated by the disturbance observers. This control algorithm guarantees globally bounded tracking performance in the presence of modeling errors and unmodeled uncertainties.

3.2.1 State Observer Design

The state observer is designed to estimate the angular velocity of the inertial load based on the information from the position sensor. In this research, a second-order Levant's differentiator [139] is employed to estimate exactly and in a finite time the first-order derivative of the position of the inertial load $x_1(t)$.

The second-order Levant's differentiator is mathematically formulated as follows:

$$\begin{cases} \dot{y}_1 = v_1; v_1 = -\lambda_1 |y_1 - x_1|^{2/3} \text{sign}(y_1 - x_1) + y_2 \\ \dot{y}_2 = v_2; v_2 = -\lambda_2 |y_2 - v_1|^{1/2} \text{sign}(y_2 - v_1) + y_3 \\ \dot{y}_3 = -\lambda_3 |y_3 - v_2| \text{sign}(y_3 - v_2) \end{cases} \quad (3.1)$$

where $\lambda_1, \lambda_2, \lambda_3$ are the parameters of the differentiator that are positive constants. The trade-off is as follows: the larger parameters, the faster convergence, and the higher sensitivity to input noise and the sampling step. The estimated angular velocity is defined as

$$\hat{x}_2 = y_2 \quad (3.2)$$

The stability of this differentiator has been proven in previous works [141]. In the steady-state condition, the estimation error $\tilde{x}_2 = x_2 - \hat{x}_2$ of the angular velocity and its derivative satisfy the following equations:

$$|\tilde{x}_2| \leq \alpha; |\dot{\tilde{x}}_2| \leq \beta \quad (3.3)$$

where α is the arbitrarily small positive constant depending on the selection of differentiator parameters and β is a bounded constant that is defined as

$$\beta \leq \frac{|\tilde{x}_{2\max} - \tilde{x}_{2\min}|}{T} = \frac{2\alpha}{T} \quad (3.4)$$

with T being the sampling time.

3.2.2 Disturbance Observer Design

The disturbance observers are designed to estimate the lumped uncertainties of the mechanical and hydraulic systems. Then, the estimated values are fed back to the control law to compensate for their effects on the control system.

Consider the subsystem that is represented in the second equation of (2.6) as

$$\dot{x}_2 = x_3 + f_1(x_2) + d_1 \quad (3.5)$$

The first disturbance observer is constructed to approximate the mismatched lumped uncertainties in the mechanical system, which is depicted as

$$\begin{cases} \dot{\hat{d}}_1 = z_1 + l_1 \hat{x}_2 \\ \dot{z}_1 = -l_1 \hat{d}_1 - l_1 (x_3 + f_1(\hat{x}_2)) \end{cases} \quad (3.6)$$

where z_1 is an intermediary variable of the observer, l_1 is the observer gain with $l_1 > 0$.

Define the estimation error $e_{d1} = d_1 - \hat{d}_1$, the estimation error dynamics is obtained as follows:

$$\dot{e}_{d1} = -l_1 e_{d1} - l_1 \tilde{f}_1 + l_1 \dot{\hat{x}}_2 + \dot{d}_1 \quad (3.7)$$

where

$$\tilde{f}_1 = f_1(x_2) - f_1(\hat{x}_2) \quad (3.8)$$

Theorem 3-1: Based on Assumptions 2-2 and 2-3, the disturbance observer (3.6) which utilizes the state estimation (3.2) guarantees that the disturbance estimation error in (3.7) can be bounded in an arbitrarily small region based on the selection of the DO gain.

Proof of Theorem 3-1:

A candidate Lyapunov function is chosen as

$$V_{d1} = \frac{1}{2} e_{d1}^2 \quad (3.9)$$

Combining the error dynamics in (3.7) and (2.7), the time derivative of (3.9) can be obtained as

$$\begin{aligned} \dot{V}_{d1} &= -l_1 e_{d1}^2 - l_1 e_{d1} \tilde{f}_1 + l_1 e_{d1} \dot{\hat{x}}_2 + e_{d1} \dot{d}_1 \\ &\leq -\left(l_1 - \frac{l_1 c_{f1}}{2\gamma_1^2} - \frac{l_1}{2\gamma_1^2} - \frac{1}{2} \right) e_{d1}^2 + \frac{1}{2} (l_1 c_{f1} \gamma_1^2 + l_1 \gamma_1^2) \beta^2 + \frac{1}{2} \gamma_1^2 \end{aligned} \quad (3.10)$$

Define a set of known constants as

$$\lambda_1 = l_1 - \frac{l_1 c_{f1}}{2\gamma_1^2} - \frac{l_1}{2\gamma_1^2} - \frac{1}{2}; \xi_1 = \frac{1}{2} (l_1 c_{f1} \gamma_1^2 + l_1 \gamma_1^2) \beta^2 + \frac{1}{2} \gamma_1^2 \quad (3.11)$$

where constants l_1 and γ_1 are chosen such that λ_1 is positive.

Based on Assumption 2-3 and (3.3), (3.10) is transformed into

$$\dot{V}_{d1} \leq -\lambda_1 e_{d1}^2 + \xi_1 \quad (3.12)$$

From (3.9) and (3.12), we obtain

$$\dot{V}_{d1} \leq -2\lambda_1 V_{d1} + \xi_1 \quad (3.13)$$

Based on Lemma 2-2 and (3.13), the function (3.9) is bounded by

$$V_{d1} \leq \frac{\xi_1}{2\lambda_1} \quad (3.14)$$

It is clearly seen that the larger observer gain l_1 is, the smaller estimation error e_{d1} will be. Hence, Theorem 3-1 is completely proven.

Similarly, we consider the second subsystem to be defined as

$$\dot{x}_3 = f_2(x_2, x_3) + g_2(x_3, u)u + d_2(x, t) \quad (3.15)$$

The second disturbance observer is designed to estimate the lumped uncertainties of the subsystem defined as follows

$$\begin{cases} \hat{d}_2 = z_2 + l_2 x_3 \\ \dot{z}_2 = -l_2 \hat{d}_2 - l_2 [g_2(u, x_3)u + f_2(\hat{x}_2, x_3)] \end{cases} \quad (3.16)$$

where l_2 is the disturbance observer gain chosen such that $l_2 > 0$.

Define the estimation error $e_{d2} = d_2 - \hat{d}_2$, the estimation error dynamics is computed as follows:

$$\dot{e}_{d2} = -l_2 e_{d2} - l_2 \tilde{f}_2 + \dot{d}_2 \quad (3.17)$$

where

$$\tilde{f}_2 = f_2(x_2, x_3) - f_2(\hat{x}_2, x_3) \quad (3.18)$$

Theorem 3-2: The disturbance observer (3.16) based on Assumptions 2-1 and 2-3, which utilizes the state estimation (3.2), guarantees that the disturbance estimation error in (3.17) can be bounded in an arbitrarily small region based on the selection of the DO gain.

Proof of Theorem 3-2:

Select a candidate Lyapunov function as

$$V_{d2} = \frac{1}{2} e_{d2}^2 \quad (3.19)$$

Taking the time derivative of it and combining it with (3.17), one obtains

$$\begin{aligned} \dot{V}_{d2} &= -l_2 e_{d2}^2 - l_2 e_{d2} \tilde{f}_2 + e_{d2} \dot{d}_2 \\ &\leq -\left(l_2 - \frac{l_2 c_{f2}}{2\gamma_2^2} - \frac{1}{2}\right) e_{d2}^2 + \frac{1}{2} l_2 c_{f2} \gamma_2^2 \tilde{x}_2^2 + \frac{1}{2} \gamma_2^2 \end{aligned} \quad (3.20)$$

Define a set of known constants as

$$\lambda_2 = l_2 - \frac{l_2 c_{f2}}{2\gamma_2^2} - \frac{1}{2}; \xi_2 = \frac{1}{2} l_2 c_{f2} \gamma_2^2 \tilde{x}_2^2 + \frac{1}{2} \gamma_2^2 \quad (3.21)$$

where l_2 and γ_2 are chosen such that $\lambda_2 > 0$.

Based on Assumptions 2-3 and (3.3), (3.20) is transformed into

$$\dot{V}_{d2} \leq -\lambda_2 e_{d2}^2 + \xi_2 \quad (3.22)$$

Combining (3.22) and (3.19), we obtain

$$\dot{V}_{d2} \leq -2\lambda_2 V_{d2} + \xi_2 \quad (3.23)$$

Based on Lemma 2-2 and (3.23), V_{d2} is bounded by

$$V_{d2} \leq \frac{\xi_2}{2\lambda_2} \quad (3.24)$$

It is clearly seen that the larger the observer gain l_2 is, the smaller the estimation error e_{d2} will be. Hence, Theorem 3-2 is completely proven.

Remark 3-1: The proposed DOBs are able to compensate for not only the external disturbances but also model uncertainties caused by large parameter variations and weak modeling as long as Assumption 1 is satisfied.

3.2.3 Backstepping Controller Design

The proposed controller is synthesized by using the recursive backstepping method based on the measured states, estimated state, and approximated lumped uncertainties. The design procedure is intuitive because the unmatched uncertainty in the second equation and the matched uncertainty in the third equation of (2.6) have been completely estimated in the previous sections.

The state errors e_i ($i=1,2,3$) are defined as

$$e_1 = x_1 - x_{1d}; e_2 = x_2 - x_{2d}; e_3 = x_3 - x_{3d} \quad (3.25)$$

where x_{1d} is the desired position trajectory, x_{2d} and x_{3d} are the virtual control inputs. Based on the estimated state and observed disturbances, the virtual control inputs are designed to stabilize the subsystems as follows:

$$\begin{aligned} x_{2d} &= -k_1 e_1 + \dot{x}_{1d} \\ x_{3d} &= -f_1(\hat{x}_2) - \hat{d}_1 - k_1(\hat{x}_2 - \dot{x}_{1d}) + \ddot{x}_{1d} - k_2(\hat{x}_2 - x_{2d}) \end{aligned} \quad (3.26)$$

where k_1 and k_2 are positive feedback gains. The virtual control function x_{3d} is designed for the virtual control input x_3 , such that the output tracking performance is ensured.

The actual control input u is designed to stabilize the whole system, which is defined as

$$u = \frac{1}{g_2(x_3, u)} \left(-f_2(\hat{x}_2, x_3) - \dot{x}_{3d} - k_3(x_3 - x_{3d}) - \hat{d}_2 \right) \quad (3.27)$$

The state error dynamics of the augmented system are given by

$$\begin{cases} \dot{e}_1 = -k_1 e_1 + e_2 \\ \dot{e}_2 = -k_2 e_2 + e_3 + \tilde{\varphi}_1 + (k_1 + k_2)\tilde{x}_2 + e_{d1} \\ \dot{e}_3 = -k_3 e_3 + \tilde{\varphi}_2 + e_{d2} \end{cases} \quad (3.28)$$

Theorem 3-3: Based on Assumptions 2-1, 2-2, and 2-3, the control laws (3.26) and (3.27), which employ the estimated state in (3.2) and the estimation values of disturbances in (3.6) and (3.16) guarantee the ultimately uniformly bounded tracking performance of the system (2.6) under the presence of uncertain nonlinearities and external disturbances.

Proof of Theorem 3-3:

Controller stability analysis is performed by using the Lyapunov theory with the Lyapunov candidate function as

$$V_c = \frac{1}{2}e_1^2 + \frac{1}{2}e_2^2 + \frac{1}{2}e_3^2 \quad (3.29)$$

Combining with (3.3), (3.7), (3.17), and (3.28), the time derivative of V_c can be obtained as

$$\begin{aligned} \dot{V}_c = & -k_1e_1^2 - k_2e_2^2 - k_3e_3^2 + e_1e_2 + e_2e_3 + e_2\tilde{\varphi}_1 \\ & + (k_1 + k_2)e_2\tilde{x}_2 + e_2e_{d1} + e_3\tilde{\varphi}_2 + e_3e_{d2} \end{aligned} \quad (3.30)$$

Using (2.7), (2.8) in Assumption 2-2 and Assumption 2-3, the time derivative of V_c in (3.30) is bounded by

$$\begin{aligned} \dot{V}_c = & -k_1e_1^2 - k_2e_2^2 - k_3e_3^2 + e_1e_2 + e_2e_3 + e_2\tilde{f}_1 \\ & + (k_1 + k_2)\left(\frac{e_2}{\varepsilon}\right)(\varepsilon\tilde{x}_2) + e_2e_{d1} + e_3\varphi\tilde{f}_2 + e_3e_{d2} \\ \leq & -\left(k_1 - \frac{1}{2}\right)e_1^2 - \left(k_2 - \frac{k_1 + k_2}{2\varepsilon^2} - 2\right)e_2^2 - \left(k_3 - \frac{3}{2}\right)e_3^2 \\ & + \frac{1}{2}\tilde{f}_1^2 + \frac{1}{2}\tilde{f}_2^2 + \frac{(k_1 + k_2)}{2}\varepsilon^2\tilde{x}_2^2 + \frac{1}{2}e_{d1}^2 + \frac{1}{2}e_{d2}^2 \end{aligned} \quad (3.31)$$

The inequality (3.31) can be rewritten in the following form

$$\dot{V}_c \leq -\eta_1e_1^2 - \eta_2e_2^2 - \eta_3e_3^2 + \psi \quad (3.32)$$

where

$$\begin{aligned} \eta_1 = & k_1 - \frac{1}{2}; \eta_2 = k_2 - \frac{k_1 + k_2}{2\varepsilon^2} - 2 \\ \eta_3 = & k_3 - \frac{3}{2}; \psi = \frac{1}{2}\tilde{f}_1^2 + \frac{1}{2}\tilde{f}_2^2 + \frac{(k_1 + k_2)}{2}\varepsilon^2\tilde{x}_2^2 + \frac{1}{2}e_{d1}^2 + \frac{1}{2}e_{d2}^2 \end{aligned} \quad (3.33)$$

From (3.32), Lemma 2-2, Theorem 3-1, and Theorem 3-2, V_c is bounded by

$$V_c(t) \leq V(0)\exp(-\tau t) + \frac{\psi}{\tau}[1 - \exp(-\tau t)] \quad (3.34)$$

where $\tau = 2 \times \min\{\eta_1, \eta_2, \eta_3\}$

When t goes to infinity, V_c will stay in a bounded region defined by $V_c \leq \psi/\tau$. Therefore, bounded tracking performance is achieved as follows:

$$|e_1| \leq \sqrt{\frac{2\psi}{\tau}} \quad (3.35)$$

From (3.33), (3.34), and (3.35), when the control gains k_1 , k_2 , and k_3 increase, the tracking error will decrease. This completes the proof of Theorem 3-3.

3.3 Simulation Results

3.3.1 Simulation Setup

In this section, numerical simulations are conducted to verify the superior effectiveness of the proposed algorithm. The simulations were performed on MATLAB/Simulink 2019b, using a Runge-

Kuta solver with a fixed step size $T = 1ms$ as shown in Fig. 3-2. The system parameters of the hydraulic system [76] are listed in Table 3-1.

Table 3-1: The hydraulic system parameters

Parameter (Unit)	Value	Parameter (Unit)	Value
$J(\text{kg} \cdot \text{m}^2)$	0.2	$B(\text{N} \cdot \text{m} \cdot \text{s} \cdot \text{rad}^{-1})$	90
$D_m(\text{m}^3 \cdot \text{rad}^{-1})$	5.8×10^{-5}	$\beta_e(\text{Pa})$	7×10^8
$C_t(\text{m}^3 \cdot \text{s}^{-1} \cdot \text{Pa}^{-1})$	1×10^{-12}	$k_t(\text{m}^3 \cdot \text{s}^{-1} \cdot \text{V}^{-1} \cdot \text{Pa}^{1/2})$	1.1969×10^{-8}
$P_s(\text{Pa})$	1×10^7	$V_t(\text{m}^3)$	1.16×10^{-4}

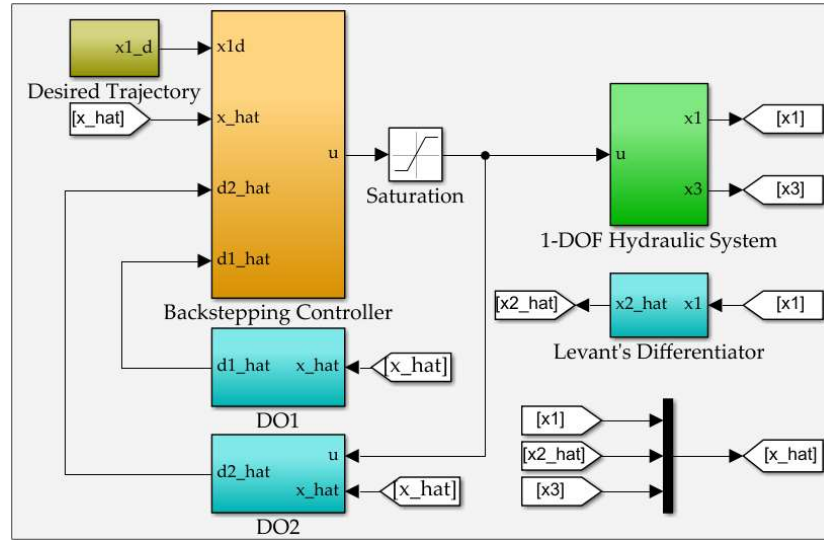


Fig. 3-2: Control design in MATLAB/Simulink environment:

In practice, the output signal of the controller needs to be in a determined range. Generally, the voltage of the input signal u applied to a servo-valve is bounded in a range from $-10V \sim 10V$, therefore, in this case, we have to use a saturation function as follows:

$$u = \begin{cases} u_c & \text{if } -10 \leq u_c \leq 10(\text{V}) \\ -10 & \text{if } u_c < -10(\text{V}) \\ 10 & \text{if } u_c > 10(\text{V}) \end{cases} \quad (3.36)$$

where u_c is the output of the controller.

3.3.2 Controllers for Comparison

To illustrate the superiority of the proposed control law, some controllers are compared as follows:

1) The proposed disturbance observers (3.6) and (3.16) in combination with the exact differentiator (3.1) are employed in the backstepping controller (3.27). The parameters of the two disturbance observers and the state observer are $l_1 = 450$, $l_2 = 450$, $\lambda_1 = 5$, $\lambda_2 = 5$, and $\lambda_3 = 10$, respectively.

2) ESOBC: This is the extended state observer-based backstepping control in [76]. The extended state observer was introduced as

$$\dot{\hat{x}} = A_0 \hat{x} + \Phi(\hat{x}) + G(u, \hat{x})u + H(x_1 - \hat{x}_1) \quad (3.37)$$

in which $H = [4\omega_0, 6\omega_0^2, 4\omega_0^3, \omega_0^4]^T$ is the observer gain matrix with $\omega_0 = 450$.

3) 2-ESOBC: This is the two extended state observer-based backstepping control. The two state observers [95] were investigated as

$$\begin{cases} \dot{\hat{x}}_1 = x_2 + 3\omega_{e1}(x_1 - \hat{x}_1) \\ \dot{\hat{x}}_2 = x_3 + \varphi_1(\hat{x}_2) + \hat{x}_{e1} + 3\omega_{e1}^2(x_1 - \hat{x}_1) \\ \dot{\hat{x}}_{e1} = \omega_{e1}^3(x_1 - \hat{x}_1) \\ \dot{\hat{x}}_3 = g(x_3, u)u + \varphi_2(\hat{x}_2, x_3) + \hat{x}_{e2} + 2\omega_{e2}(x_3 - \hat{x}_3) \\ \dot{\hat{x}}_{e2} = \omega_{e2}^2(x_3 - \hat{x}_3) \end{cases} \quad (3.38)$$

where observer gains are chosen as $\omega_{e1} = 450$ and $\omega_{e2} = 450$.

4) UDEBC: This is the unknown disturbance estimation-based backstepping control. The disturbance observer [142] is designed as follows:

$$\begin{cases} \hat{d}_1 = (\dot{\hat{x}}_2 - x_3 - \varphi_1(\hat{x}_2)) \times q_1 \\ \hat{d}_2 = (\dot{\hat{x}}_3 - g(x_3, u)u - \varphi_2(\hat{x}_2, x_3)) \times q_2 \end{cases} \quad (3.39)$$

where q_1 and q_2 are low-pass filters which are chosen based on the dynamics of the considered system. The structure of these filters is a first-order transfer function as

$$q_i = \frac{1}{T_i s + 1} \quad (i = 1, 2) \quad (3.40)$$

where T_1 and T_2 are manually tuned to achieve the sufficiently accurate estimation of d_1 and d_2 . The larger T_i , the better the noise filtering but the higher lag on the filtered signal and vice versa. The values of T_1 and T_2 are chosen as $T_1 = T_2 = 0.01$.

The controller gains are given by $k_1 = 450$, $k_2 = 350$, and $k_3 = 100$ in all cases.

To measure the effectiveness of each control approach, three performance indexes were employed i.e., the maximum, average, and standard deviation of the tracking errors [76]. These indexes are defined as follows:

(a) Maximal absolute value of tracking errors is used to evaluate the tracking accuracy, which is represented as

$$M_e = \max_{i=1, \dots, N} \{|e_i|\} \quad (3.41)$$

where N is the number of recorded digital signals.

(b) Average tracking error is defined as

$$\mu_e = \frac{1}{N} \sum_{i=1}^N |e_i| \quad (3.42)$$

(c) Standard deviation performance index is defined as

$$\sigma_e = \sqrt{\frac{1}{N} \sum_{i=1}^N [|e_i(i)| - \mu_e]^2} \quad (3.43)$$

3.3.3 Numerical Simulation

In this case study, the desired trajectory of the inertial load and the matched, mismatched disturbances are applied to the system as follows:

$$x_{1d}(t) = 45 \left(1 - \cos\left(\frac{\pi}{2}t\right) \right) (1 - e^{-t}) \quad (\text{degree}) \quad (3.44)$$

$$d_1(t) = \begin{cases} 0 & t < 20s \\ 1500 \sin(\pi(t-20)) & \text{otherwise} \end{cases} \quad (\text{rad} \cdot \text{s}^{-2}) \quad (3.45)$$

$$d_2(t) = \begin{cases} 0 & t < 40s \\ 10^6 \sin(\pi(t-40)) & \text{otherwise} \end{cases} \quad (\text{rad} \cdot \text{s}^{-3}) \quad (3.46)$$

where the magnitudes of $d_1(t)$ and $d_2(t)$ are chosen based on the system specifications and the operation conditions of the real systems. These disturbances are intentionally injected into the considered system to verify the effectiveness of two proposed disturbance observers in improving the tracking performance of the proposed control system.

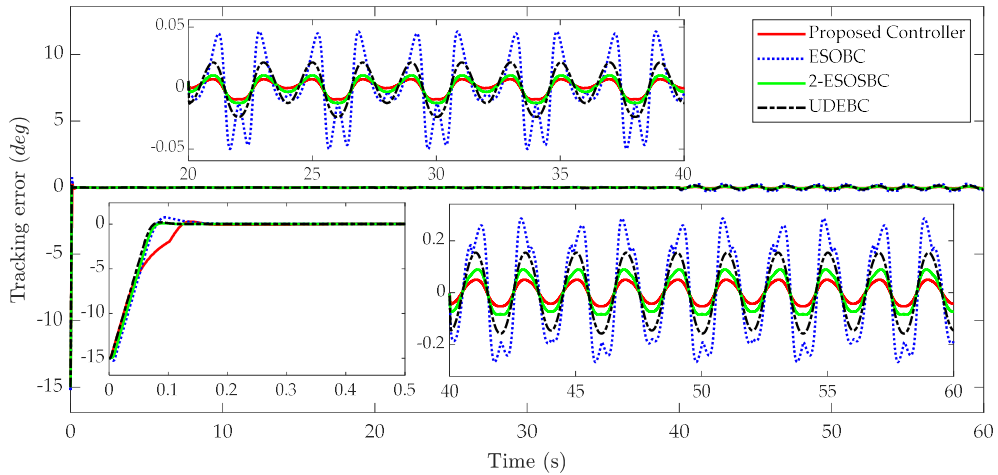


Fig. 3-3 The tracking errors of the proposed method and other approaches in the presence of matched and mismatched disturbances.

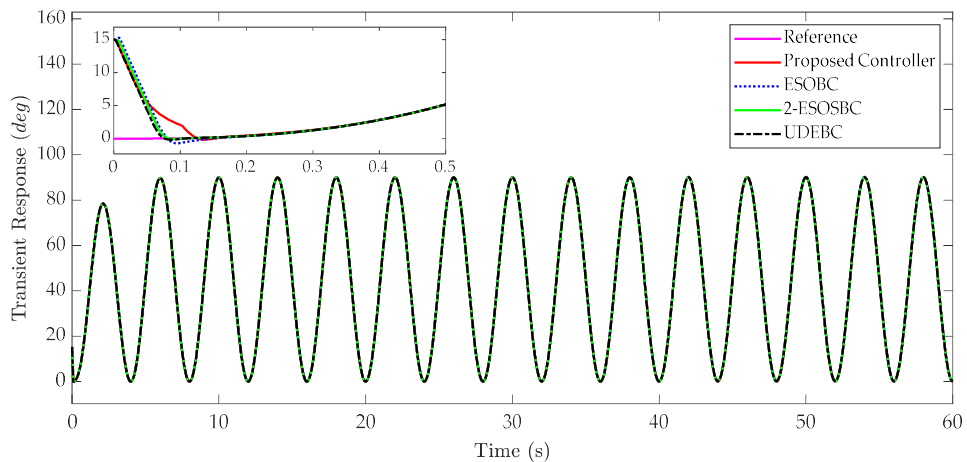


Fig. 3-4 The tracking performance of the proposed method compared with those of other approaches.

The desired trajectory is designed based on the sinusoidal-like function (3.44) to guarantee that it is smooth enough. To compare the tracking performance of the aforementioned control approaches, the mismatched (3.45) and matched disturbance functions (3.46) are injected into the system from the first 20th second and 40th second, respectively.

The tracking errors and tracking performances of four considered controllers are shown in Fig. 3-3 and Fig. 3-4, respectively. The maximum, average, and standard deviations of tracking errors in the steady-state phase are illustrated in Table 3-2, Table 3-3, and Table 3-4 in detail, correspondingly.

Table 3-2 The maximal absolute values of tracking error in the steady-state phase.

Controller	No Disturbance	Mismatched Disturbance	Mismatched/Matched Disturbance
Proposed Controller	0.0045	0.0093	0.0521
ESOBC Controller	0.0045	0.0500	0.2860
2-ESOBC Controller	0.0045	0.0123	0.0895
UDEBC Controller	0.0057	0.0236	0.1572

Table 3-3 The average tracking errors in the steady-state phase.

Controller	No Disturbance	Mismatched Disturbance	Mismatched/Matched Disturbance
Proposed Controller	0.0030	0.0048	0.0331
ESOBC Controller	0.0030	0.0219	0.1728
2-ESOBC Controller	0.0030	0.0065	0.0584
UDEBC Controller	0.0038	0.0131	0.0997

Table 3-4 The standard deviation of tracking errors in the steady-state phase.

Controller	No Disturbance	Mismatched Disturbance	Mismatched/Matched Disturbance
Proposed Controller	0.0014	0.0030	0.0151
ESOBC Controller	0.0014	0.0189	0.1698
2-ESOBC Controller	0.0014	0.0038	0.0254
UDEBC Controller	0.0018	0.0068	0.0469

In the absence of mismatched and matched disturbances in the first 20s, the tracking performance and tracking error plots are roughly similar. The maximal absolute values of tracking errors of the proposed controller, ESOBC, and 2-ESOBC are 0.0045 degrees, whereas that of the UDEDC is slightly bigger with 0.0057 degrees.

In the presence of the mismatched lumped disturbance from the 20 th second, the maximal value of tracking errors of the system with the ESOBC is significantly higher than other controllers with 0.05 degrees, because this mismatched term is only suppressed by using high gain feedback while this disturbance is estimated and compensated in other methods, while that of UDEBC is 0.0236 degrees. It can be seen from Table 3-2 that the tracking errors of the 2-ESOBC and proposed controller are better than the ESOBC and UDEBC, since the angular velocity and matched disturbance are approximated more precisely. In this case, the maximal absolute values of tracking errors of 2-ESOBC and the proposed method are 0.0123 degrees and 0.0093 degrees, respectively. This indicates that the proposed control approach achieves a better tracking performance than other approaches.

In the worst case, i.e., both mismatched and matched disturbances occur in the system from the 40 th second, the tracking performances of all controllers deteriorate considerably. However, similar to the previous situation, it also illustrates the effectiveness of the proposed controller compared to the remaining controllers in the presence of both mismatched/matched uncertainties and external disturbances. In this case, the tracking performance of ESOBC and UDEBC is seriously deteriorated

due to the effects of heavy disturbance with the maximum absolute values of the tracking errors being 0.2860 and 0.1572 degrees, respectively. Meanwhile, the maximal absolute value of tracking errors of 2-ESOBC is 0.08695 degrees, and the proposed controller has the most outstanding feature with this value being 0.0521 degrees under the effects of both mismatched and matched disturbances.

In addition, to evaluate the tracking performance of the compared methods in terms of smooth tracking performance, the average and standard deviation of tracking errors can be used. From Table 3-3 and Table 3-4, it can be observed that the average tracking error and standard deviation indexes of the proposed control algorithm are considerably smaller than other control approaches in the presence of mismatched and matched disturbances. They illustrate that smoother tracking performance is achieved by the proposed method in comparison with others.

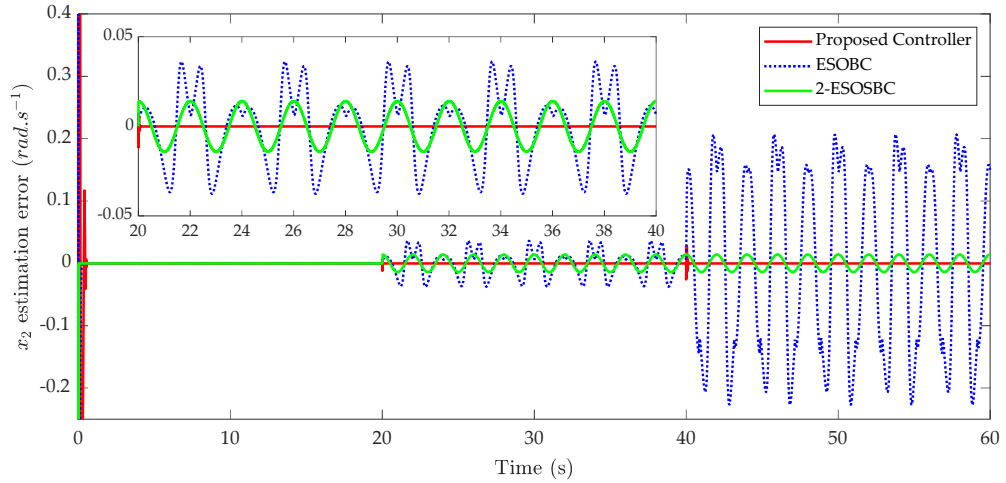


Fig. 3-5: The estimation error of the angular velocity of the inertial load.

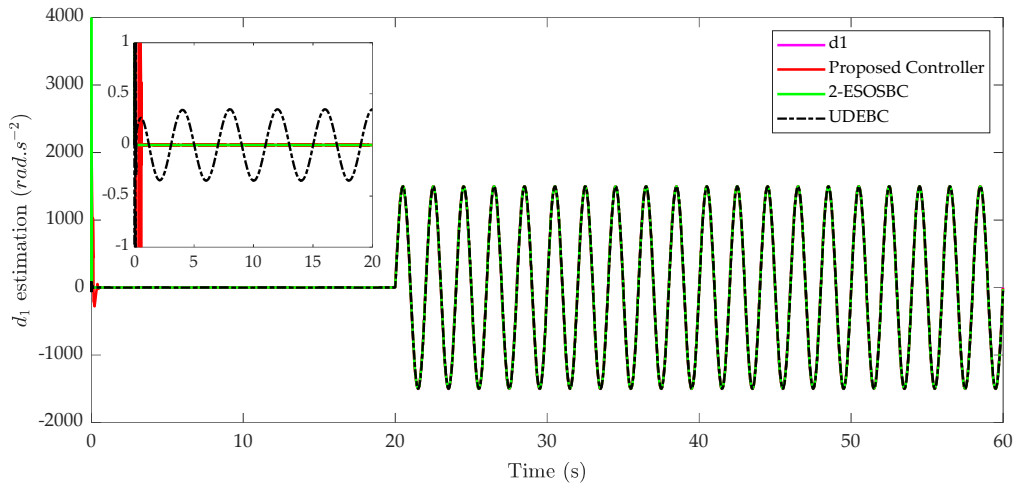


Fig. 3-6: The estimation of the mismatched disturbance.

As above analysis, in the steady-state condition, the proposed controller achieves the best tracking performance in terms of steady-state tracking errors compared with other control methods, since the angular velocity of the actuator is estimated more accurately by employing Levant’s differentiator, and the matched/mismatched disturbances are also approximated then fed back to the controller to compensate for the effects of these disturbances on the control system.

The estimation error of the angular velocity is depicted in Fig. 3-5. It is immediately apparent that the angular velocity of the actuator is approximated by using the Levant’s differentiator much more exactly than using ESO [48]. It also can be seen from this figure, the estimation error of the 2ESOBC

is much better than the ESOBC. In the occurrence of mismatched disturbance from the 20th second to 40th second, the velocity estimation errors of ESOBC and 2-ESOBC increase significantly, whereas that of the proposed controller remains unchanged. This error of ESOBC continues to enlarge dramatically under the influence of the matched disturbance in the last 20 s on the control system. Hence, the tracking performance of ESOBC deteriorates markedly under the presence of matched disturbance. An interesting point is observed that compared to the ESOBC, the angular velocity estimation in the 2-ESOBC is better since the pressure information is measured and fed back to the mismatched ESO which estimates the mismatched disturbance and also cancels its effect on the angular velocity estimation. In addition, based on the Levant's differentiator, the angular velocity estimation in the proposed controller is the best compared to those in the remaining controllers because this estimation is independent of the system model and uncertainties/disturbances. Hence, it contributes to the best tracking performance in the above discussion as well as the best matched and mismatched disturbances estimations in the next section of the proposed controller compared to those of the remaining controllers.

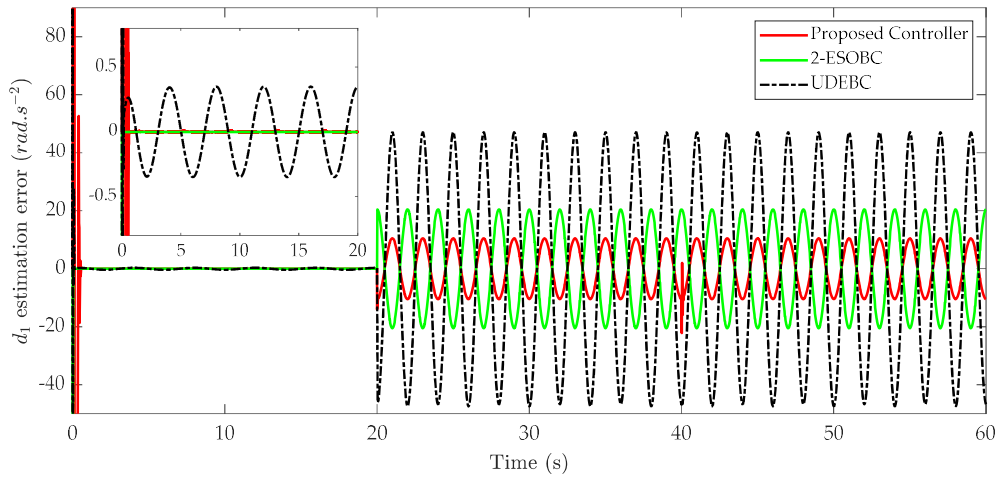


Fig. 3-7: The estimation error of the mismatched disturbance.

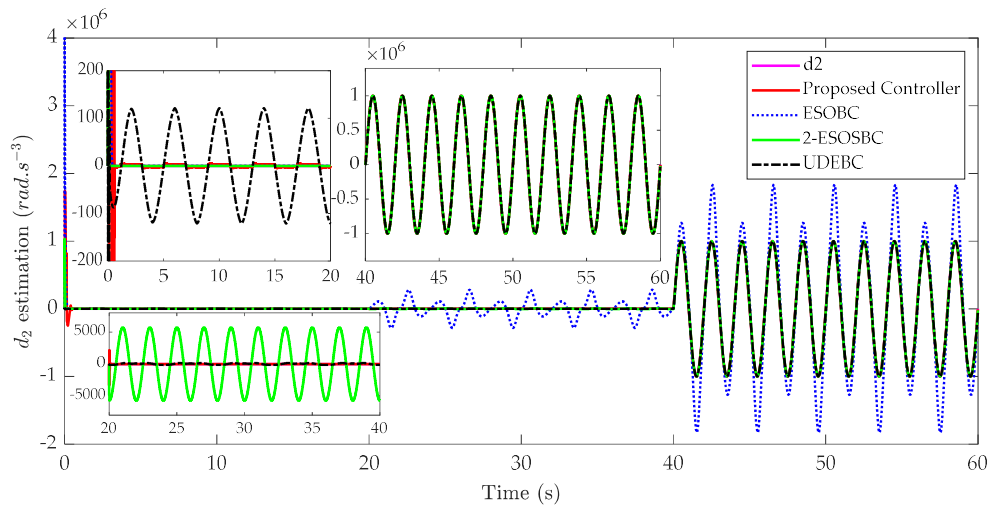


Fig. 3-8: The estimation of the matched disturbance.

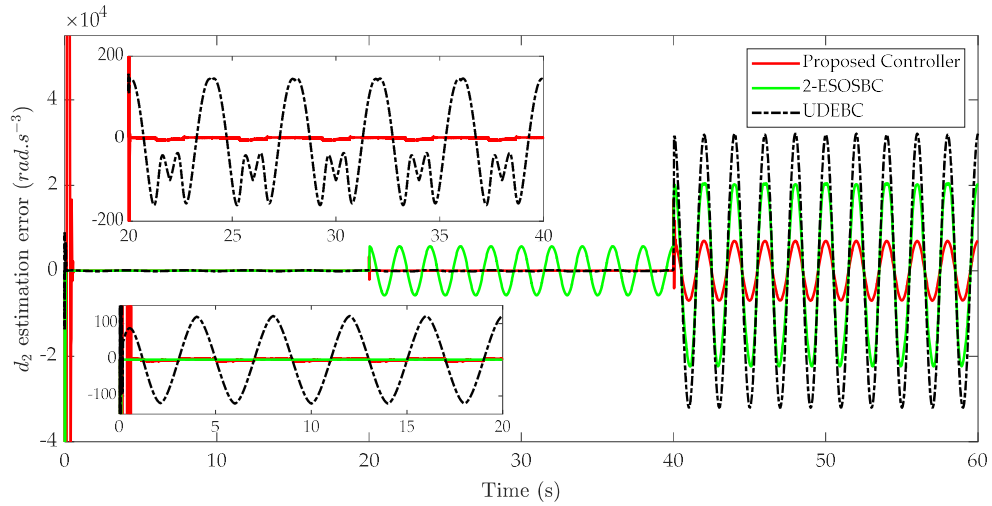


Fig. 3-9: The estimation error of the matched disturbance.

The estimation and estimation errors of mismatched disturbance are illustrated in Fig. 3-6 and Fig. 3-7. As shown in Fig. 3-7, it is clearly seen that although the UDEBC can estimate the mismatched disturbance, the estimation error is considerably bigger than 2-ESOBC and the proposed method. From Table 3-5, it can be observed that while the maximal absolute value of the mismatched disturbance estimation error of UDEBC is $47.2756 \text{ rad}\cdot\text{s}^{-2}$, those of 2-ESOBC and the proposed approach are $20.4977 \text{ rad}\cdot\text{s}^{-2}$ and $16.3231 \text{ rad}\cdot\text{s}^{-2}$, respectively. The results show that the proposed controller is able to estimate the mismatched disturbance the most accurately in comparison with UDEBC and 2-ESOBC.

Table 3-5: The maximal absolute value of estimation errors of mismatched and matched disturbances.

Controller	Maximal Value of Estimation Error	
	Mismatched Disturbance ($\text{rad}\cdot\text{s}^{-2}$)	Matched Disturbance ($\text{rad}\cdot\text{s}^{-3}$)
Proposed Controller	16.3231	1.1843×10^4
ESOBC Controller		8.5159×10^5
2-ESOBC Controller	20.4977	2.1428×10^4
UDEBC Controller	47.2756	3.2072×10^4

The estimation and estimation errors of matched disturbance are illustrated in Fig. 3-8 and Fig. 3-9. In Fig. 3-9, the proposed disturbance observer is able to estimate more accurately the matched disturbance compared with other methods. It is worth noting that the matched disturbance estimation of the ESOBC and 2-ESOBC are affected by the mismatched disturbance due to the coupling problem between state and disturbance estimation. This leads the estimation errors even in the absence of matched disturbances, and hence, they degrade the tracking performance of the control system. Furthermore, the ES-OBC uses high-gain feedback to suppress the matched disturbance, but in the case of heavy disturbance, this method cannot work well.

The maximal absolute values of matched disturbance of the estimation error are illustrated in Table 3-5. As can be seen from this table, the maximal absolute values of estimation error of ESOBC, UDEBC are $8.5159\times 10^5 \text{ rad}\cdot\text{s}^{-3}$ and $3.2072\times 10^4 \text{ rad}\cdot\text{s}^{-3}$, respectively, whereas these values of 2-ESOBC and the proposed method are $2.1428\times 10^4 \text{ rad}\cdot\text{s}^{-3}$ and $1.1843\times 10^4 \text{ rad}\cdot\text{s}^{-3}$, respectively.

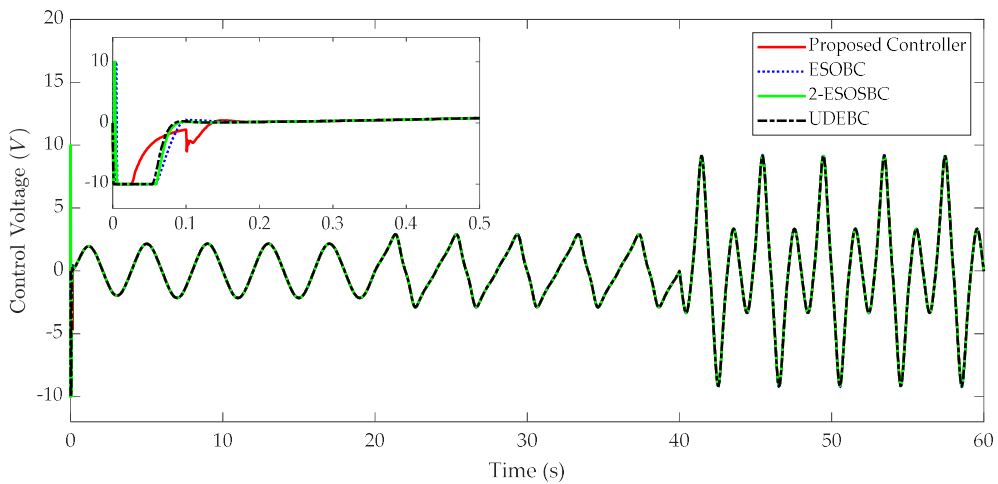


Fig. 3-10: The control actions of considered controllers.

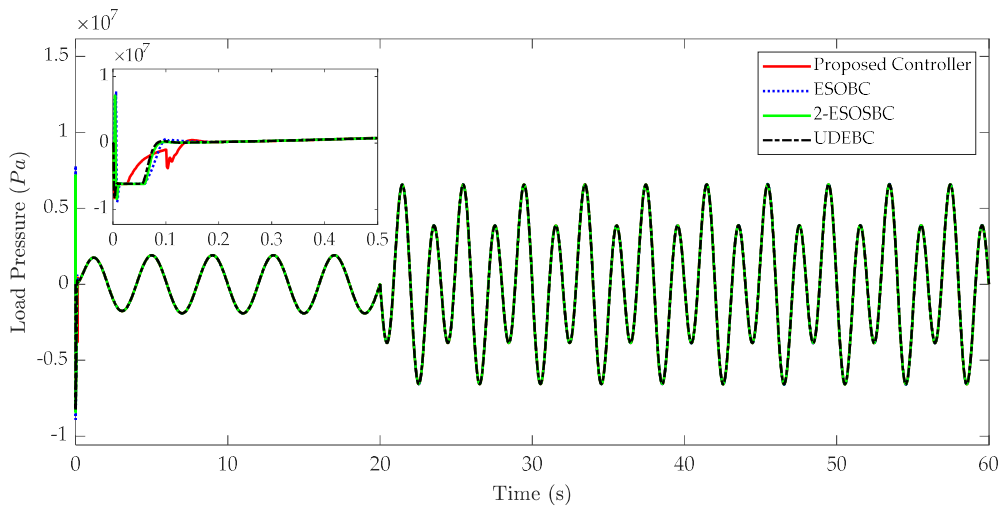


Fig. 3-11: The load pressures of the actuator corresponding to the control actions.

The control action and load pressures are shown in Fig. 3-10 and Fig. 3-11, respectively. Due to the same desired position trajectory and similar tracking performances, all four controllers generate the equivalent profiles of control input. It can be seen that in the presence of matched disturbance in the last 20 s, the value of control input increases significantly to compensate for the effect of this uncertainty. The load pressure also changes to guarantee the tracking performance of the control system in the presence of mismatched and/or matched disturbances, and hence, the shapes of load pressures are also quite similar.

3.4 Conclusion

In this study, a novel backstepping controller based on Levant's differentiator-based disturbance observers has been proposed for a hydraulic servo system. In this work, the angular velocity of the actuator is exactly estimated by employing the exact robust Levant's differentiator. Lumped matched and mismatched disturbances are simultaneously considered and by using new DOs that approximate not only the uncertain nonlinearities but also the external disturbances. Based on that, the novel nonlinear controller is synthesized using the systematic backstepping method. The closed-loop system stability is completely proven using Lyapunov theory, which shows that the proposed controller guarantees a better tracking performance in the presence of time-varying uncertainties and external

disturbances compared with other approaches. Comparative simulation results are attained to demonstrate the effectiveness of the proposed method. Future works include applying advanced nonlinear disturbance observers to improve the tracking performance and experiment validation on the real hydraulic systems

EXTENDED SLIDING MODE OBSERVER-BASED CONTROL FOR ELECTRO-HYDRAULIC ACTUATOR

4.1 Introduction

Owing to excellent characteristics including a small weight-to-power ratio, fast and smooth response, ability to generate tremendous force/torque, and so on [72], electro-hydraulic servo systems (EHSSs) have been broadly adopted as major actuation components for hydraulic robot manipulators [143-145], hydraulic active suspensions [146], hydraulic human power amplifiers [147], and so forth in both industry and academia. Hence, as one of the most popular control problems for such EHSSs, position tracking control has been currently receiving a vast amount of attention in recent years. By virtue of model compensation mechanisms, nonlinear control techniques such as feedback linearization control [21, 112], sliding mode control (SMC) [120, 148], and back-stepping control (BC) [93, 149] are powerful tools to synthesize controllers for highly nonlinear EHSSs. However, the controllers constructed based on the aforementioned control techniques cannot achieve a high-accuracy position tracking performance for EHSSs subject to uncertainties and disturbances arising from parameter deviations, modeling errors, unknown external loads, and so on, since these terms are not fully taken into consideration in the control mechanisms. Therefore, several key techniques are required to be integrated into the above-mentioned control approaches to cope with uncertainties and disturbances existing in the EHSSs, which improve the overall control performance.

Firstly, universal approximators predicated upon radial basis function neural networks (RBF NNs) [90, 150, 151] and fuzzy logic systems (FLSs) [152-154] have been successfully adopted to cope with state-dependence lumped uncertainties in EHSSs. However, due to the heavy computational burden and long convergence time of adaptive laws, their applications to real-life applications are restricted [155]. Compared to such approximators, disturbance observers (DOBs) such as linear disturbance observers (LDOBs) [97], nonlinear disturbance observers (NDOBs) [102], and high-gain disturbance observers (HGDOBs) [127] are effective to cope with not only state-dependence lumped uncertainties but also unknown external disturbances which are not generally easy to be directly quantified by sensors. In Reference [156], Hamid Razmjooei et al. proposed a novel DOB structure for position tracking control of a proportional valve-controlled-based electro-hydraulic system, although some strong assumptions were given, the finite-time convergence property of disturbance estimation was not pointed out explicitly. Therefore, it should be noted that the above-mentioned DOB designs only achieve ultimately uniformly bounded (UUB) estimation performance in the case of time-varying disturbance. Besides, separate state observers are required to realize such DOBs, which may complicate the design and reduce the reliability of the closed-loop system as a consequence. Hence, for the simplification of the control system, inspired by the well-known Luenberger observer [50-52], extended state observer (ESO) which was initially developed by J. Han [157-159], can be regarded as a powerful tool to simultaneously estimate immeasurable state and lumped disturbances in uncertain nonlinear systems. Based on the noticeable features of ESOs such as intuitive concept and simplicity for implementation, they have been broadly applied to EHSSs to actively compensate for the effects of lumped uncertainties and disturbances which are assumed to be differentiable and bounded in changing rate [76] on the control system. For example, an ESO-based output feedback controller for EHSSs [93] was introduced to achieve a high position tracking accuracy, in which only lumped model uncertainties in pressure dynamics were addressed. Besides, an ESO [94] was constructed to estimate not only velocity but also disturbance for the mechanical system of EHSSs, however, only mismatched disturbance was compensated. To adequately address both matched and mismatched disturbances, dual ESOs [95] were established, hence, the tracking performance was significantly enhanced.

Additionally, in References [160, 161], finite-time continuous ESOs with time-varying observer gains were established to improve the convergence rate of the state and disturbance estimation errors in the dynamics of an electro-hydraulic actuation system, and consequently, improved tracking performance was achieved. Generally, the ESO whose stability is guaranteed by terms proportional to the error between the measured and estimated values of a system output, has been considered to be a valuable solution for states and disturbances estimation up to now. However, it is worth noticing for research whether the estimation ability can be improved if a nonlinear switching function of that deviation is adopted for the design of observers.

In the literature, a sliding mode observer (SMO) [162] utilized the standard signum function, that is, the “sign” function, of the estimated-measured output error to drive the estimated states to a sliding surface where there is no difference between the estimated output and the measured output. Additionally, by using the “sign” function, the SMO can rapidly react to fast-changing state variables required to observe and the observer trajectories become insensitive to many forms of noise [163]. Besides, based on the finite-time convergence attribute of SMC, SMOs are expected to achieve a shorter convergence time compared to conventional state observers [164]. As a result of the above-mentioned superiority, the SMO was employed to robustly estimate immeasurable states in previous studies for EHSSs. In Reference [132], an SMO was constructed to estimate the velocities of the load and main spool valve of an EHSS, then the lumped disturbances were algebraically computed based on the system dynamics. As another modification of SMO, an adaptive high-order SMO [165] was introduced in which the derivatives of estimated states were obtained by means of a high-order sliding mode differentiator. In contrast to the state estimation capability of the SMO, sliding mode disturbance observers (SMDOs) based on the equivalent theory were investigated in previous studies [166-171] for disturbance estimation. In particular, an adaptive SMDO [166] was developed for the track-following system of an optical disk with the assumption that the disturbance model is known in advance. A deadbeat predictive current control based on a second-order SMDO [167] for induction machine (IM) drives, was introduced to tackle lumped mismatched disturbance. In Reference [170], a robust tracking control scheme based on an SMDO for omnidirectional mobile robots was proposed to deal with kinematic uncertainties due to incomplete measurement. As an extended version to take the valuable features of the SMO, which inherits the simple structure of ESO designs, ESMOs can be considered as a great solution to estimate both system states and disturbances. In the literature, ESMOs were successfully applied to various applications such as Markovian jump linear systems [172], permanent-magnet synchronous motor (PMSM) [173, 174], descriptor stochastic systems [175], satellites autonomous navigation [176], electro-optical tracking system [177], and so on. However, in these studies, the system models are in linear-time-invariant form and thus there is a gap in adopting ESMOs for nonlinear systems. In Reference [144], an ESMO was introduced to observe joint velocities and contact force with the environment in the mechanical system of hydraulic robots only. It should be mentioned that the employment of ESMO for EHSSs has not been sufficiently considered in the literature. Hence, in this study, dual ESMOs are first constructed to approximate the angular velocity of the actuator and lumped disturbances simultaneously accurately in both the mechanical system and pressure dynamics of the considered EHSS.

Motivated by the above comprehensive analysis, in this chapter, an ESMO-based backstepping controller is proposed to achieve a high-accuracy tracking performance for an EHSS without velocity measurement in the presence of parameter deviations, unmodeled dynamics, and external disturbances in the mechanical part and pressure dynamics, which are lumped into generalized mismatched and matched disturbances, respectively. The main contributions of this study are summarized as follows:

1) For the first time, a novel active disturbance rejection control strategy based on dual ESMOs is developed for EHSSs in the presence of both lumped mismatched and matched uncertainties and disturbances in the mechanical system and hydraulic pressure dynamics, respectively

2) Compared to the well-known ESO designs [76, 95], a better estimation performance with higher accuracy, faster response, and more robustness against uncertainties, can be achieved by employing the proposed ESMOs. The introduction of ESMO could satisfy the fundamental requirement for a new alternative to ESO for both state and disturbance estimation in high-order nonlinear EHSSs.

3) On the strength of the proposed ESMOs, the suggested composite control strategy for the studied EHSS is able to perform better in comparison with the existing ESO-based control approaches in terms of not only position tracking performance but also state and disturbance observation capability.

The remainder of this chapter is organized as follows. The modeling of the studied EHSS is considered in Section 4.2, whereas in Section 4.3, the design of the proposed SMO and control strategy is introduced in detail. Comparative numerical simulation results with several case studies are provided in Section 4.4. Finally, Section 4.5 concludes the chapter.

4.2 Extended Sliding Mode Observer-Based Control Design

The control scheme of the proposed method is illustrated in Fig. 4 2. In this framework, dual ESMOs are established to exactly estimate the immeasurable angular velocity, lumped mismatched and matched disturbances whose observed values are then integrated into the control law synthesized using the backstepping technique to compensate for their effects on the system dynamics. Finally, the control action is restricted to a reasonable range before applying to the control valve of the EHSS.

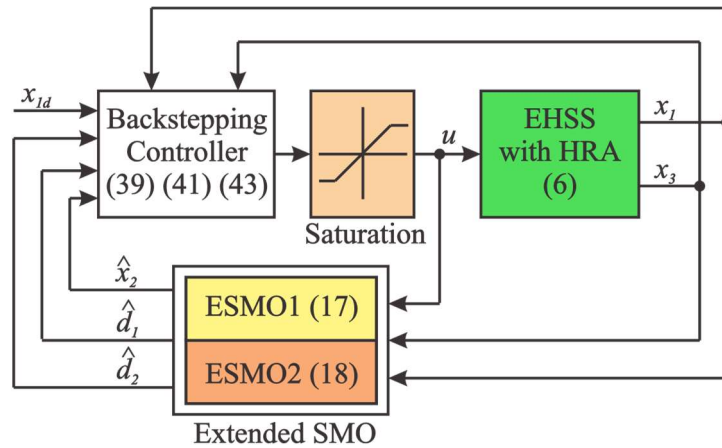


Fig. 4-1 The proposed control scheme for position tracking of an EHSS with a HRA

4.2.1 Dual Extended Sliding Mode Observer Design

The total system dynamics (2.6) are split into two augmented subsystems as follows:

a) Mechanical subsystem dynamics

$$\begin{cases} \dot{x}_1 = x_2 \\ \dot{x}_2 = x_3 + f_1(x_2) + x_{e1} \\ \dot{x}_{e1} = h_1(t) \end{cases} \quad (4.1)$$

where x_{e1} is an extended state which denotes the unmatched lumped disturbance $d_1(t)$ and $h_1(t)$ reflects the first-order derivative of $d_1(t)$.

b) Load pressure dynamics

$$\begin{cases} \dot{x}_3 = f_2(x_2, x_3) + g_2(x_3, u)u + x_{e2} \\ \dot{x}_{e2} = h_2(t) \end{cases} \quad (4.2)$$

where x_{e2} is the second extended state which represents the matched lumped disturbance $d_2(t)$ and $h_2(t)$ signifies the first-order derivative of $d_2(t)$.

For simplicity of expression, the terms comprising $f_1(\hat{x}_2)$, $f_2(\hat{x}_2, x_3)$, and $g_2(x_3, u)$ are abbreviated by \hat{f}_1 , \hat{f}_2 , and g_2 , respectively. To estimate not only the angular velocity of the actuator but also both lumped unmatched and matched disturbances, dual ESMOs are constructed as

$$\begin{cases} \dot{\hat{x}}_1 = \hat{x}_2 + \eta_1 \text{sign}(x_1 - \hat{x}_1) \\ \dot{\hat{x}}_2 = x_3 + \hat{f}_1 + \hat{x}_{e1} + 2\omega_1 \eta_1 \text{sign}(x_1 - \hat{x}_1) \\ \dot{\hat{x}}_{e1} = \omega_1^2 \eta_1 \text{sign}(x_1 - \hat{x}_1) \end{cases} \quad (4.3)$$

$$\begin{cases} \dot{\hat{x}}_3 = \hat{f}_2 + g_2 u + \hat{x}_{e2} + \eta_2 \text{sign}(x_3 - \hat{x}_3) \\ \dot{\hat{x}}_{e2} = 2\omega_2 \eta_2 \text{sign}(x_3 - \hat{x}_3) \end{cases} \quad (4.4)$$

where \hat{x}_i , $i = 1, 2, 3$ denote the estimated values of x_i and $\tilde{x}_i = x_i - \hat{x}_i$ are the estimation errors of the system states; \hat{x}_{ej} , $j = 1, 2$ are the estimates of x_{ej} and $\tilde{x}_{ej} = x_{ej} - \hat{x}_{ej}$ reflect the approximation errors of the lumped mismatched and matched disturbances. η_1 and η_2 are designed positive constants that guarantee the existence of the sliding mode for dual ESMOs; ω_1 and ω_2 are the bandwidths of the two observers, which will be determined later.

Combining (4.1), (4.2), (4.3), and (4.4), the estimation error dynamics of the proposed ESMOs can be derived as

$$\begin{cases} \dot{\tilde{x}}_1 = \tilde{x}_2 - \eta_1 \text{sign}(\tilde{x}_1) \\ \dot{\tilde{x}}_2 = \tilde{f}_1 + \tilde{x}_{e1} - 2\omega_1 \eta_1 \text{sign}(\tilde{x}_1) \\ \dot{\tilde{x}}_{e1} = h_1 - \omega_1^2 \eta_1 \text{sign}(\tilde{x}_1) \end{cases} \quad (4.5)$$

$$\begin{cases} \dot{\tilde{x}}_3 = \tilde{f}_2 + \tilde{x}_{e2} - \eta_2 \text{sign}(\tilde{x}_3) \\ \dot{\tilde{x}}_{e2} = h_2 - 2\omega_2 \eta_2 \text{sign}(\tilde{x}_3) \end{cases} \quad (4.6)$$

where $\tilde{f}_1 = f_1 - \hat{f}_1$, $\tilde{f}_2 = f_2 - \hat{f}_2$.

Moreover, according to Assumption 2-2, we have $|\tilde{f}_1| \leq c_{f_1} |\tilde{x}_2|$ and $|\tilde{f}_2| \leq c_{f_2} |\tilde{x}_2|$.

Theorem 4-1. For subsystems (4.1) and (4.2) with Assumption 2-2, the two recommended ESMOs presented in (4.3) and (4.4) guarantee that the velocity and disturbance estimation errors, i.e., \tilde{x}_2 , \tilde{x}_{e1} , and \tilde{x}_{e2} , converge to arbitrarily small regions depending on the selection of the observer bandwidths ω_1 and ω_2 .

Proof of Theorem 4-1: Consider a candidate Lyapunov function as

$$V_{11} = \frac{1}{2} \tilde{x}_1^2 \quad (4.7)$$

Taking the time derivative of (4.7) and combining with (4.5) yields

$$\begin{aligned}\dot{V}_{11} &= \tilde{x}_1(\tilde{x}_2 - \eta_1 \text{sign}(\tilde{x}_1)) \\ &\leq -(\eta_1 - |\tilde{x}_2|)|\tilde{x}_1|\end{aligned}\quad (4.8)$$

It can be observed that in the region $|\tilde{x}_2| \leq \eta_1 - \eta_0$ with $\eta_0 > 0$, the following inequality holds

$$\dot{V}_{11} \leq -\eta_0 |\tilde{x}_1| = -\sqrt{2}\eta_0 V_{11}^{1/2} \quad (4.9)$$

Based on (4.9) and Lemma 2-1, it can be concluded that the estimation error \tilde{x}_1 converges to zero in finite time t_1 . From $t > t_1$, the equivalent error dynamics of (4.5) are obtained as

$$\begin{cases} \dot{\tilde{x}}_2 = \tilde{f}_1 + \tilde{x}_{e1} - 2\omega_1 \tilde{x}_2 \\ \dot{\tilde{x}}_{e1} = h_1 - \omega_1^2 \tilde{x}_2 \end{cases} \quad (4.10)$$

Defining $\boldsymbol{\varepsilon}_1 = [\varepsilon_{11}, \varepsilon_{12}]^T = [\tilde{x}_2, \tilde{x}_{e1}/\omega_1]^T$ as scaled estimation error vector, the error dynamics (4.10) can be transformed into

$$\dot{\boldsymbol{\varepsilon}}_1 = \omega_1 \mathbf{A}_1 \boldsymbol{\varepsilon}_1 + \mathbf{B}_1 \tilde{f}_1 + \frac{1}{\omega_1} \mathbf{C}_1 h_1 \quad (4.11)$$

where $\mathbf{A}_1 = \begin{bmatrix} -2 & 1 \\ -1 & 0 \end{bmatrix}$; $\mathbf{B}_1 = \begin{bmatrix} 1 \\ 0 \end{bmatrix}$; and $\mathbf{C}_1 = \begin{bmatrix} 0 \\ 1 \end{bmatrix}$.

Since the matrix \mathbf{A}_1 is negative definite, there exists a positive definite matrix \mathbf{P}_1 that satisfies the following Lyapunov equation

$$\mathbf{A}_1^T \mathbf{P}_1 + \mathbf{P}_1 \mathbf{A}_1 = -2\mathbf{I}_{2 \times 2} \quad (4.12)$$

where $\mathbf{I}_{2 \times 2}$ is the identity matrix of size 2×2 .

A candidate Lyapunov function is chosen as

$$V_{\varepsilon_1} = 0.5 \boldsymbol{\varepsilon}_1^T \mathbf{P}_1 \boldsymbol{\varepsilon}_1 \quad (4.13)$$

Taking time derivative, then applying Young's inequality yields

$$\begin{aligned}\dot{V}_{\varepsilon_1} &= -\omega_1 \boldsymbol{\varepsilon}_1^T \boldsymbol{\varepsilon}_1 + \boldsymbol{\varepsilon}_1^T \mathbf{P}_1 \mathbf{B}_1 \tilde{f}_1 + \frac{1}{\omega_1} \boldsymbol{\varepsilon}_1^T \mathbf{P}_1 \mathbf{C}_1 h_1 \\ &\leq -(\omega_1 - 1) \boldsymbol{\varepsilon}_1^T \boldsymbol{\varepsilon}_1 + \frac{1}{2} \mathbf{B}_1^T \mathbf{P}_1^T \mathbf{P}_1 \mathbf{B}_1 \tilde{f}_1^2 + \frac{1}{2\omega_1^2} \mathbf{C}_1^T \mathbf{P}_1^T \mathbf{P}_1 \mathbf{C}_1 h_1^2 \\ &\leq -(\omega_1 - 1) \boldsymbol{\varepsilon}_1^T \boldsymbol{\varepsilon}_1 + \frac{1}{2} \lambda_{\max}(\mathbf{B}_1^T \mathbf{P}_1^T \mathbf{P}_1 \mathbf{B}_1) c_{f_1}^2 \boldsymbol{\varepsilon}_1^T \boldsymbol{\varepsilon}_1 + \frac{1}{2\omega_1^2} \lambda_{\max}(\mathbf{C}_1^T \mathbf{P}_1^T \mathbf{P}_1 \mathbf{C}_1) \gamma_1^2\end{aligned}\quad (4.14)$$

Notation: $\lambda_{\max}(\mathbf{X})$ and $\lambda_{\min}(\mathbf{X})$ are the maximal eigenvalue and minimal eigenvalue of the matrix \mathbf{X} , respectively.

For conciseness, defining $\lambda_1 = \lambda_{\max}(\mathbf{B}_1^T \mathbf{P}_1^T \mathbf{P}_1 \mathbf{B}_1)$ and $\lambda_2 = \lambda_{\max}(\mathbf{C}_1^T \mathbf{P}_1^T \mathbf{P}_1 \mathbf{C}_1)$, (4.14) can be rewritten as

$$\begin{aligned}\dot{V}_{\varepsilon_1} &\leq -\left(\omega_1 - \frac{1}{2} \lambda_1 c_{f_1}^2 - 1\right) \boldsymbol{\varepsilon}_1^T \boldsymbol{\varepsilon}_1 + \frac{1}{2\omega_1^2} \lambda_2 \gamma_1^2 \\ &\leq -\frac{2}{\lambda_{\max}(\mathbf{P}_1)} \left(\omega_1 - \frac{1}{2} \lambda_1 c_{f_1}^2 - 1\right) V_{\varepsilon_1} + \frac{1}{2\omega_1^2} \lambda_2 \gamma_1^2\end{aligned}\quad (4.15)$$

According to Lemma 2-2, the estimation errors \tilde{x}_2 and \tilde{x}_{e1} are bounded by

$$\begin{aligned} |\tilde{x}_2| &\leq \frac{1}{\omega_1^{3/2}} \sqrt{\frac{\lambda_2 \gamma_1^2 \lambda_{\max}(\mathbf{P}_1)}{2 \left(1 - \frac{1}{2\omega_1} \lambda_1 c_{f_1}^2 - \frac{1}{\omega_1}\right) \lambda_{\min}(\mathbf{P}_1)}} \\ |\tilde{x}_{e1}| &\leq \frac{1}{\omega_1^{1/2}} \sqrt{\frac{\lambda_2 \gamma_1^2 \lambda_{\max}(\mathbf{P}_1)}{2 \left(1 - \frac{1}{2\omega_1} \lambda_1 c_{f_1}^2 - \frac{1}{\omega_1}\right) \lambda_{\min}(\mathbf{P}_1)}} \end{aligned} \quad (4.16)$$

A Lyapunov function is chosen as $V_{21} = 0.5\tilde{x}_3^2$. Taking time derivative of it then combining with (4.6), one obtains

$$\dot{V}_{21} = \tilde{x}_3 \dot{\tilde{x}}_3 \leq -(\eta_2 - |\tilde{f}_2| - |\tilde{x}_{e2}|) |\tilde{x}_3| \quad (4.17)$$

In the case that η_2 is chosen such that $\eta_2 > |\tilde{f}_2| + |\tilde{x}_{e2}|$, the estimation error \tilde{x}_3 converges to zero in finite time t_2 . After that, the equivalent error dynamics of (4.6) are given by

$$\dot{\tilde{x}}_{e2} = -2\omega_2 \tilde{x}_{e2} - 2\omega_2 \tilde{f}_2 + h_2 \quad (4.18)$$

Consider a candidate Lyapunov function given by

$$V_{\varepsilon_2} = 0.5\tilde{x}_{x_{e2}}^2 \quad (4.19)$$

Taking a time derivative and then substituting (4.18) into it yields

$$\begin{aligned} \dot{V}_{\varepsilon_2} &= \tilde{x}_{x_{e2}} \dot{\tilde{x}}_{x_{e2}} \\ &\leq -(\omega_2 - 1)\tilde{x}_{e2}^2 + \omega_2 c_{f_2}^2 \tilde{x}_2^2 + \frac{\gamma_2^2}{2} \end{aligned} \quad (4.20)$$

Remark 4-1. According to Lemma 2-3, it can be seen that the velocity estimation error converges to the vicinity of its bound determined in (4.16) finite time and is constrained in this region after that. Without loss of generality and for the sake of simplicity, after the velocity estimation error reaches its bounded region, this bound will be used to specify the bounded region of the lumped matched disturbance estimation error.

According to (4.16), (4.20) can be transformed into

$$\dot{V}_{\varepsilon_2} \leq -(\omega_2 - 1)\tilde{x}_{e2}^2 + \omega_2 c_{f_2}^2 \frac{1}{\omega_1^3} \left(\frac{\lambda_2 \gamma_1^2 \lambda_{\max}(\mathbf{P}_1)}{2 \left(1 - \frac{1}{2\omega_1} \lambda_1 c_{f_1}^2 - \frac{1}{\omega_1}\right) \lambda_{\min}(\mathbf{P}_1)} \right) + \frac{\gamma_2^2}{2} \quad (4.21)$$

To reduce the complexity of the tuning procedure of the designed observers, the observer bandwidth of the second ESMO is chosen as $\omega_2 = \omega_1 = \omega$, (4.21) can be rewritten as

$$\dot{V}_{\varepsilon_2} \leq -(\omega - 1)\tilde{x}_{e2}^2 + c_{f_2}^2 \frac{1}{\omega^2} \left(\frac{\lambda_2 \gamma_1^2 \lambda_{\max}(\mathbf{P}_1)}{2 \left(1 - \frac{1}{2\omega} \lambda_1 c_{f_1}^2 - \frac{1}{\omega}\right) \lambda_{\min}(\mathbf{P}_1)} \right) + \frac{\gamma_2^2}{2} \quad (4.22)$$

Based on Lemma 2-2, when the time goes to infinity, the estimation error \tilde{x}_{e2} is bounded by

$$|\tilde{x}_{e2}| \leq \sqrt{\frac{c_{f_2}^2 \lambda_2 \gamma_1^2 \lambda_{\max}(\mathbf{P}_1)}{2(\omega-1)\omega^2 \left(1 - \frac{1}{2\omega} \lambda_1 c_{f_1}^2 - \frac{1}{\omega}\right) \lambda_{\min}(\mathbf{P}_1)} + \frac{\gamma_2^2}{2(\omega-1)}} \quad (4.23)$$

This completes the proof of Theorem 4-1.

Remark 4-2. From (4.16) and (4.23), it can be observed that the dual ESMOs (4.5) and (4.6) guarantee an ultimate boundedness estimation performance depending on the bandwidths of the observers if the switching gains η_1 and η_2 are selected so that the sliding mode existence conditions are assured. By choosing the same bandwidth, i.e., $\omega_1 = \omega_2 = \omega$, the number of adjusting parameters are reduced. Hence, the complexity of tuning process is reduced.

Remark 4-3. To guarantee a high-accuracy position tracking performance, a state feedback controller is synthesized. Hence, the estimated values which are awaited to be chattering-free, are fed back into both inner and outer control loops, i.e., pressure loop and position loop. For chattering reduction, the hyperbolic tangent function is employed instead of the “sign” function in the ESMO design.

4.2.2 ESMO-based Controller Design

Considering the system dynamics (2.6), it can be observed that the relative degree of each virtual system is one. Hence, the control strategy can be designed by adopting the conventional recursive backstepping method.

Step 1: Defining the actual position tracking error as $z_1 = x_1 - x_{1d}$, then taking the time derivative of it and combining it with the system dynamics (2.6), one obtains

$$\dot{z}_1 = x_2 - \dot{x}_{1d} \quad (4.24)$$

The virtual control law α_1 for ensuring the system output tracks the desired trajectory is designed as

$$\alpha_1 = \dot{x}_{1d} - k_1 z_1 \quad (4.25)$$

where k_1 is a positive feedback gain.

Step 2: Let $z_2 = x_2 - \alpha_1$ as the virtual tracking error for the second step. Differentiating the above virtual tracking error in this step and considering (2.6), one obtains

$$\dot{z}_2 = x_3 + f_1(x_2) + d_1 - \dot{\alpha}_1 \quad (4.26)$$

Since the mismatched disturbance $d_1(t)$ and the angular velocity x_2 are not measurable, the virtual control signal for (4.26) is designed using estimated values \hat{x}_2 and \hat{x}_{e1} as

$$\alpha_2 = -f_1(\hat{x}_2) - \hat{x}_{e1} + \dot{\alpha}_1 - k_2(\hat{x}_2 - \alpha_1) \quad (4.27)$$

where the control gain k_2 is a positive constant.

Step 3: To construct the final control action u , an auxiliary error signal is introduced as $z_3 = x_3 - \alpha_2$. Taking the time derivative of it and noting (2.6) yields

$$\dot{z}_3 = f_2(x_2, x_3) + g_2(x_3, u)u + d_2 - \dot{\alpha}_2 \quad (4.28)$$

To compensate for the effect of matched disturbance $d_2(t)$ on the closed-loop control system, the actual control action is constructed as

$$u = \frac{1}{g_2(x_3, u)} (-f_2(\hat{x}_2, x_3) - \hat{x}_{e2} + \dot{\alpha}_2 - k_3 z_3) \quad (4.29)$$

where k_3 is a positive feedback control gain which is determined later.

4.2.3 Closed-loop System Stability Analysis

Theorem 4-2. The control strategy established by (4.25), (4.27), and (4.29) along with dual ESMOs (4.5) and (4.6) assures the UUB tracking performance of the closed-loop control system under the effects of both lumped matched and mismatched disturbances and unmeasurable angular velocity.

Proof of Theorem 4-2:

Consider the Lyapunov function given by

$$V_c = \frac{1}{2} z_1^2 + \frac{1}{2} z_2^2 + \frac{1}{2} z_3^2 \quad (4.30)$$

Taking time derivative yields

$$\dot{V}_c = z_1 \dot{z}_1 + z_2 \dot{z}_2 + z_3 \dot{z}_3 \quad (4.31)$$

Based on the definition of control errors z_1 , z_2 , and z_3 then combining with (4.24)-(4.29), the derivative of the Lyapunov function can be transformed into

$$\begin{aligned} \dot{V}_c = & -k_1 z_1^2 + z_1 z_2 + z_2 z_3 + z_2 \tilde{f}_1 + z_2 \tilde{x}_{e1} \\ & -k_2 z_2^2 + k_2 z_2 \tilde{x}_2 + z_3 \tilde{f}_2 + z_3 \tilde{x}_{e2} - k_3 z_3^2 \end{aligned} \quad (4.32)$$

Applying Young's inequality, one obtains

$$\dot{V}_c \leq -\left(k_1 - \frac{1}{2}\right) z_1^2 - \left(\frac{k_2}{2} - 2\right) z_2^2 - \left(k_3 - \frac{3}{2}\right) z_3^2 + \left(\frac{c_{f1}^2 + c_{f2}^2 + k_2}{2}\right) \tilde{x}_2^2 + \frac{\tilde{x}_{e1}^2}{2} + \frac{\tilde{x}_{e2}^2}{2} \quad (4.33)$$

From (4.16) and (4.23), we have

$$\begin{aligned} \dot{V}_c \leq & -\left(k_1 - \frac{1}{2}\right) z_1^2 - \left(\frac{k_2}{2} - 2\right) z_2^2 - \left(k_3 - \frac{3}{2}\right) z_3^2 \\ & + \left(\frac{c_{f1}^2 + c_{f2}^2 + k_2}{2}\right) \frac{\delta_{\varepsilon_1}}{\omega^2 \lambda_{\varepsilon_1} \lambda_{\min}(\mathbf{P}_1)} + \frac{\delta_{\varepsilon_1}}{2 \lambda_{\varepsilon_1} \lambda_{\min}(\mathbf{P}_1)} \\ & + \frac{c_{f2}^2 \lambda_2 \gamma_1^2}{2(\omega-1) \omega \lambda_{\varepsilon_1} \lambda_{\min}(\mathbf{P}_1)} + \frac{\gamma_2^2}{4(\omega-1)} \\ = & -\Psi V_c + \Gamma \end{aligned} \quad (4.34)$$

where

$$\begin{aligned} \lambda_{\varepsilon_1} &= \frac{2}{\lambda_{\max}(\mathbf{P}_1)} \left(\omega - \frac{1}{2} \lambda_1 c_{f1}^2 - 1 \right) \\ \Psi &= \min\{2k_1 - 1, k_2 - 4, 2k_3 - 3\} \\ \Gamma &= \left(\frac{c_{f1}^2 + c_{f2}^2 + k_2}{2}\right) \frac{\delta_{\varepsilon_1}}{\omega^2 \lambda_{\varepsilon_1} \lambda_{\min}(\mathbf{P}_1)} + \frac{\delta_{\varepsilon_1}}{2 \lambda_{\varepsilon_1} \lambda_{\min}(\mathbf{P}_1)} + \frac{c_{f2}^2 \lambda_2 \gamma_1^2}{2(\omega-1) \omega \lambda_{\varepsilon_1} \lambda_{\min}(\mathbf{P}_1)} + \frac{\gamma_2^2}{4(\omega-1)} \end{aligned} \quad (4.35)$$

It can be recognized that the Lyapunov function V_c converges to a bounded area $V_c \leq \Gamma/\Psi$ as time goes to infinity. The boundary of this region decreases if the controller gains k_1 , k_2 , and k_3 ; and the bandwidth of observers ω increase.

Remark 4-4: First of all, a simple controller with an open-loop structure is designed and applied to the system such that the system stability is guaranteed. Based on the initial conditions of the system, the constants η_1 and η_2 of the ESMOs must be carefully chosen to be sufficiently large to guarantee that the estimated state tracks the measured state as closely as possible. It is worth noting that if these values are designed excessively, the estimation performance may be degraded due to the occurrence of chattering issues. Then the observer bandwidth is determined to obtain an expected estimation performance without the chattering phenomenon. In the subsequent step, the estimated states and disturbances are integrated into a model-based controller by using nonlinear control design techniques such as a backstepping framework. Finally, the controller gains must also be thoroughly selected so as to achieve the desired tracking performance.

4.3 Numerical Simulation Evaluation

The nominal parameters of the considered EHA with HRA [76] are given in Table 4-1, which are adopted for designing observers the positioning-tracking controllers. Numerical simulations are conducted in MATLAB/Simulink 2019b environment with the fixed step size of 1 ms.

Table 4-1 Nominal system parameters

Symbol	Quantity	Value	Unit
B	Viscous damping coefficient	90	$\text{N} \cdot \text{m} \cdot \text{s} \cdot \text{rad}^{-1}$
J	Inertial moment of the actuator	0.2	$\text{kg} \cdot \text{m}^2$
D_m	Radian displacement	5.8×10^{-5}	$\text{m}^3 \cdot \text{rad}^{-1}$
V_t	Total control volume	1.16×10^{-4}	m^3
C_t	Internal leakage coefficient	1×10^{-12}	$\text{m}^3 \cdot \text{s}^{-1} \cdot \text{Pa}^{-1}$
k_t	Total load flow coefficient	1.1969×10^{-8}	$\text{m}^3 \cdot \text{s}^{-1} \cdot \text{V}^{-1} \cdot \text{Pa}^{-1/2}$
P_s	Supply pressure	1×10^7	Pa or $\text{N} \cdot \text{m}^{-2}$
β_e	Effective bulk modulus	0.7×10^9	$\text{N} \cdot \text{m}^{-2}$

4.3.1 The Influence of Observer Bandwidth on Estimation Performance

In order to examine the influence of the observer bandwidth on the estimation performance of the proposed ESMO, numerical simulations with open-loop structure and different values of observer gain are performed. The system is driven by an external control input signal $u = 5\sin(2\pi t)V$. In addition, the two lumped disturbance terms $d_1(t) = 1500\sin(2\pi t) \text{ rad/s}^2$ and $d_2(t) = 10^6\sin(2\pi t) \text{ rad/s}^3$ are purposely injected into the system dynamics to assess the observation capability of the recommended ESMO. The observer bandwidths are chosen as 350, 400, and 450 for assessing the influence of the observer bandwidth on estimation performance.

The estimation errors of angular velocity, mismatched disturbance, and matched disturbance are given in Fig. 4-2. As shown in this figure, the observer bandwidth has a great influence on the estimation performance of the proposed ESMOs. Specifically, the estimation errors will be considerably decreased if the observer bandwidth increases. For example, the maximal values of velocity estimation errors are 0.0573 rad/s, 0.0657 rad/s, and 0.0778 rad/s corresponding to the observer bandwidths of 450, 400, and 350, respectively. In terms of disturbance estimation capability, the maximal values of disturbance observation errors are 62.8146 rad/s², 73.5998 rad/s², and 88.4152

rad/s² for mismatched disturbance estimation, and 3.0224×10^4 rad/s³, 3.4567×10^4 rad/s³, and 4.0516×10^4 rad/s³ for matched disturbance estimation when the observer bandwidths are selected as 450, 400, and 350, correspondingly. Hence, it can be observed that the results support the conclusion given in Theorem 4-1 in the previous section. In addition, the superior features of the proposed ESMO in comparison with the existing well-known ESO will be analyzed in the following section.

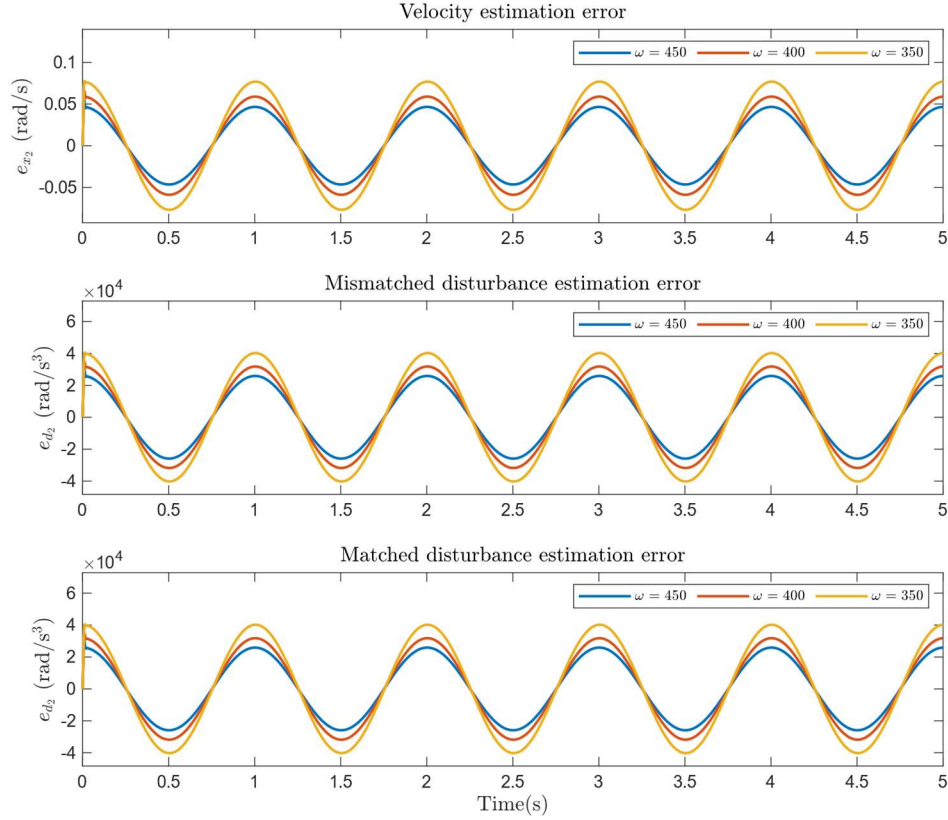


Fig. 4-2 The velocity, mismatched, and matched disturbance estimation errors of the proposed ESMOs with three distinct observer gains.

4.3.2 Observer-based Control Performance Evaluation

a) Performance Evaluation Setup

To demonstrate the preeminence of the recommended ESMO-based controller, control strategies are used for fair comparison as follows:

1) DESMO-BC: The proposed controller with the controller gains being selected as $k_1 = 450$, $k_2 = 350$, and $k_3 = 100$. The parameters of ESMOs (4.5) and (4.6) are $\omega_1 = \omega_2 = 450$; $\eta_1 = 1$; and $\eta_2 = 2 \times 10^4$.

2) DESO-BC: The dual ESO-based backstepping controller [95] with the same control structure and controller parameters as the proposed control approach. The two ESOs are designed as

$$\begin{cases} \dot{\hat{x}}_1 = \hat{x}_2 + 3\omega_{e1}(x_1 - \hat{x}_1) \\ \dot{\hat{x}}_2 = x_3 + \hat{f}_1 + \hat{x}_{e1} + 3\omega_{e1}^2(x_1 - \hat{x}_1) \\ \dot{\hat{x}}_{e1} = \omega_{e1}^3(x_1 - \hat{x}_1) \end{cases} \quad (4.36)$$

$$\begin{cases} \dot{\hat{x}}_3 = \hat{f}_2 + g_2 u + \hat{x}_{e2} + 2\omega_{e2}(x_3 - \hat{x}_3) \\ \dot{\hat{x}}_{e2} = \omega_{e2}^2(x_3 - \hat{x}_3) \end{cases} \quad (4.37)$$

3) SESO-BC: With the assumption that only the angular position of the HRA is measurable, an output feedback controller [76] with similar control architecture and controller gains to the above control strategies. The angular velocity, load pressure, and matched disturbance are estimated by an ESO whose dynamics are mathematically presented as

$$\dot{\hat{\mathbf{x}}} = \mathbf{A}_0 \hat{\mathbf{x}} + \mathbf{F}(\hat{\mathbf{x}}) + \mathbf{G}(\hat{\mathbf{x}}, u)u + \mathbf{H}(x_1 - \hat{x}_1) \quad (4.38)$$

where $\mathbf{x} = [x_1, x_2, x_3, x_4]^T$ with $x_4 = d_2(t)$ and

$$\mathbf{A}_0 = \begin{bmatrix} 0 & 1 & 0 & 0 \\ 0 & 0 & 1 & 0 \\ 0 & 0 & 0 & 1 \\ 0 & 0 & 0 & 0 \end{bmatrix}; \quad \mathbf{F}(\hat{\mathbf{x}}) = \begin{bmatrix} 0 \\ f_1(\hat{x}_2) \\ f_2(\hat{x}_2, \hat{x}_3) \\ 0 \end{bmatrix}; \quad \mathbf{G}(\mathbf{x}, u) = \begin{bmatrix} 0 \\ 0 \\ g_2(\hat{x}_3, u) \\ 0 \end{bmatrix}; \quad \mathbf{H} = \begin{bmatrix} 4\omega_0 \\ 6\omega_0^2 \\ 4\omega_0^3 \\ \omega_0^4 \end{bmatrix}$$

with the observer bandwidth being chosen as $\omega_0 = 450$.

Performance indexes including absolute maximum, average, and standard deviation of the tracking errors [76, 178] are used to statistically evaluate the reference-following ability of the above controllers, which are denoted by M_e , μ_e , and σ_e , respectively.

b) Numerical Simulation Verification

To evaluate the robustness of the considered controllers in both two case studies, the lumped mismatched and matched disturbances which are mathematically formulated, are intentionally inserted into the studied EHSS as

$$\begin{aligned} d_1(t) &= 1500 \sin(2\pi t + \pi/12) \quad (\text{rad/s}^2) \\ d_2(t) &= 10^6 \sin(2\pi t + \pi/16) \quad (\text{rad/s}^3) \end{aligned} \quad (4.39)$$

where the magnitudes of disturbances are chosen based on the system specifications [178].

First of all, a slow-motion reference trajectory $x_{1d}(t) = 45(1 - \cos(\pi t/4))(1 - e^{-t})^\circ$ is utilized to evaluate the tracking performance. In addition, the non-zero initial angular position of the actuator is chosen as 5° for demonstrating both the transient responses and steady-state performances of all controllers. The output tracking performances and tracking errors of all three control approaches under the slow-motion reference trajectory are illustrated in Fig. 4-3.

As shown in the upper part of this figure, in general, the charts constituted by angular positions overlap with the graph of the desired trajectory. This result reflexes that all controllers are able to ensure that the system outputs track the desired reference trajectory tightly despite the existence of both mismatched and matched disturbances and the non-existence of the velocity measurement mechanism. Based on this, it can be concluded that all control algorithms possess anti-disturbance capability at a certain level. The tracking errors are demonstrated in the lower part of Fig. 4-3 where the transient tracking performances and steady-state tracking qualifications of all considered controllers are represented more distinctly. At a glance, compared to the DESO-BC and DESMO-BC controllers, although the SESO-BC controller possesses cost-effectiveness, it performs the worst tracking performance due to the lack of pressure sensors and mismatched disturbance compensation mechanisms.

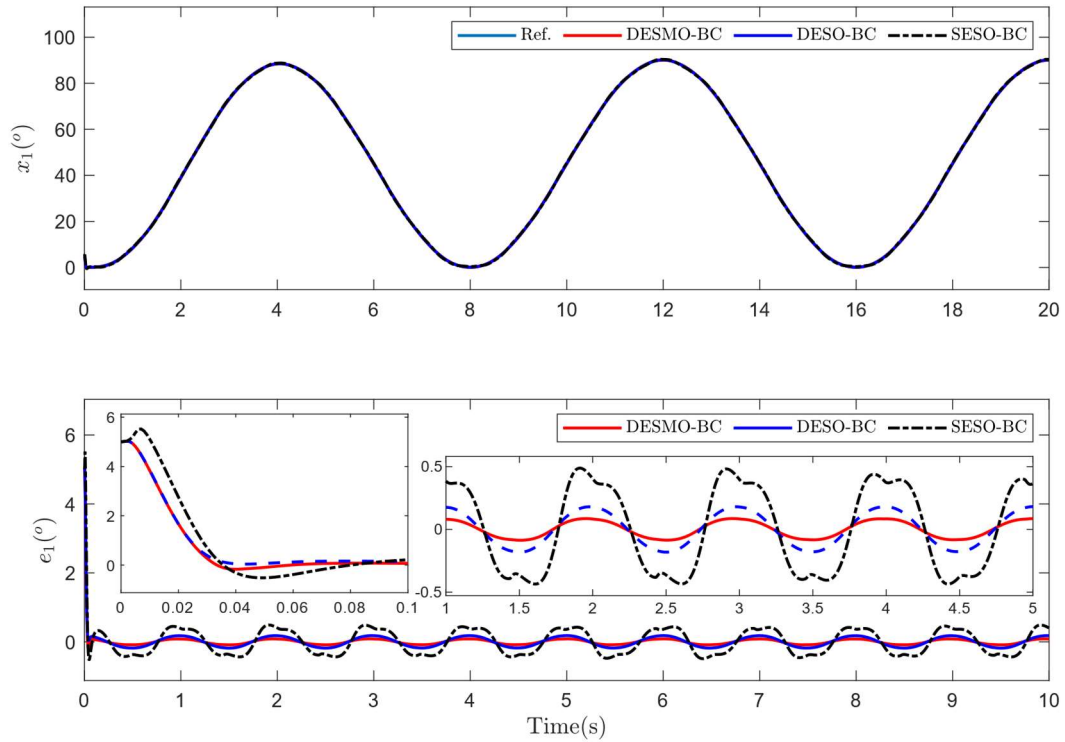


Fig. 4-3 The tracking performance in slow-motion desired trajectory

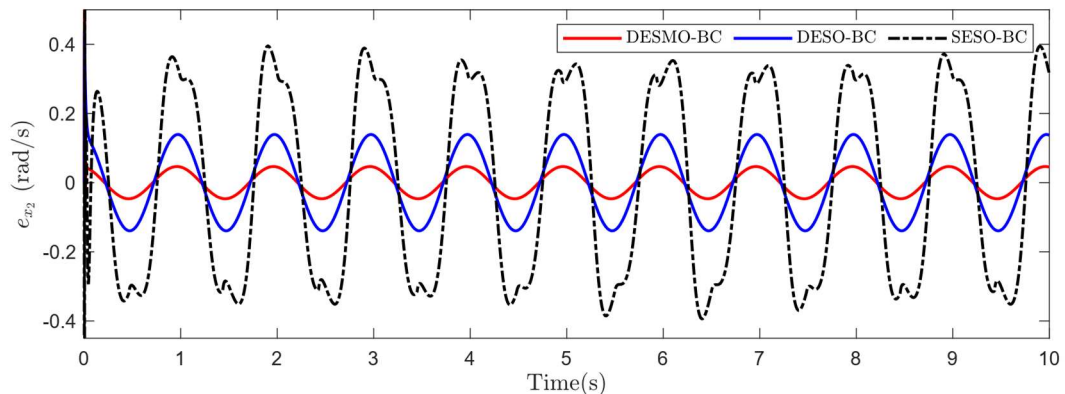


Fig. 4-4 The velocity estimation performance in slow-motion desired trajectory

The tracking performances of all controllers in the transient regime and steady-state regime are illustrated more explicitly in the zoom-in subfigures of the lower part of Fig. 4-3. The left-hand side zoom-in subfigure depicts the transient performances of all control approaches. As shown, the SESO-BC controller has possession of the longest convergence time and largest overshoot in comparison with the remaining controllers. It is worth noting that although the DESMO-BC controller and DESO-BC controller possess a similar transient tracking performance at the beginning, the tracking error curve obtained by the proposed control algorithm reaches the origin faster than the DESO-BC controller. The superiority of the recommended method is revealed more plainly in the right-hand side subfigure which exhibits the tracking errors of all controllers in the steady-state regime. As displayed, the suggested controller outperforms the remaining controllers in terms of tracking error. To quantitatively examine the control performance of the compared three controllers in the steady-state regime, the maximum, average, and standard deviation of the tracking errors are provided in. As indicated in this table, in the steady-state regime, the maximal absolute value of the final tracking error

of the DESMO-BC control approach is only 0.0864° compared to 0.1818° and 0.4877° obtained by DESO-BC and SESO-BC controllers, respectively. In terms of the two remaining performance indices, i.e., average, and standard deviation of the tracking errors, the proposed controller also performs considerably better than the others.

Table 4-2 Performance indexes in the slow-motion trajectory scenario.

Controller	M_e (deg)	μ_e (deg)	σ_e (deg)
DESMO-BC	0.0864	0.0578	0.0255
DESO-BC	0.1818	0.1185	0.0548
SESO-BC	0.4877	0.3188	0.1196

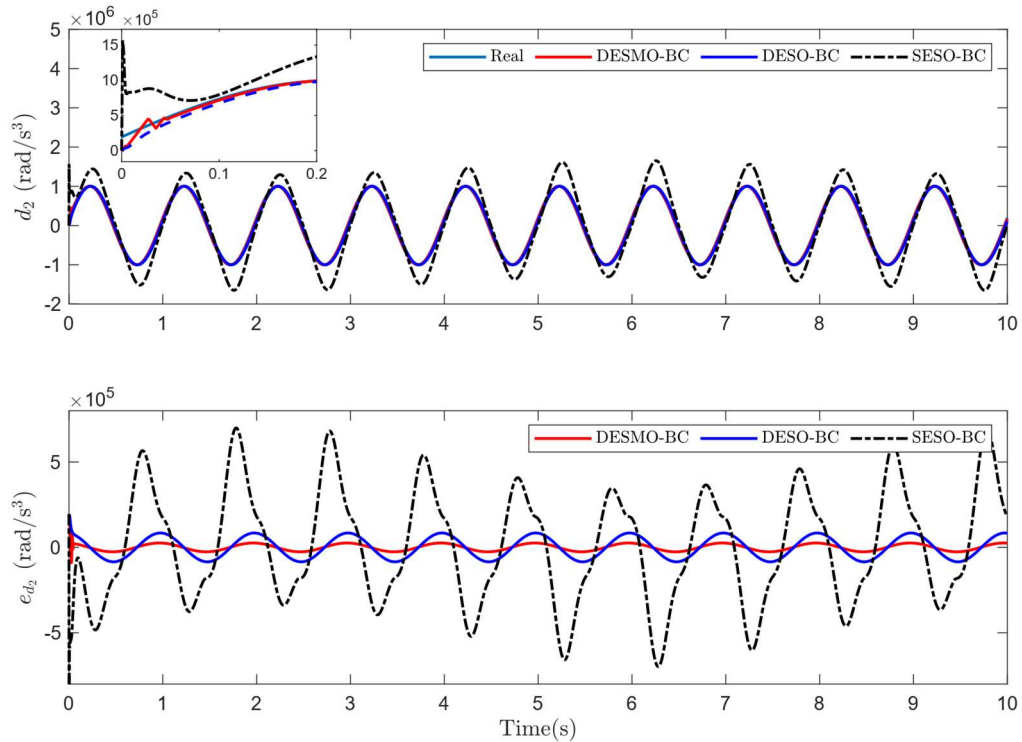


Fig. 4-5 The matched disturbance estimation performance in slow-motion desired trajectory

The angular velocity and lumped matched disturbances estimation performances of the proposed ESMOs in the ESMO-BC control approach and well-known ESOs in SESO-BC and DESO-BC control schemes are illustrated in Fig. 4-4 and Fig. 4-5. Due to the lack of pressure measurement, the SESO-BC control approach uses the measured angular position information only to estimate immeasurable states, i.e., the velocity and load pressure, simultaneously. The estimated velocity and load pressure are then employed to observe the lumped matched disturbances. Therefore, as shown in these figures, the SESO-BC performs the worst performance in terms of both state and disturbance estimation. Meanwhile, the DESO-BC and DESMO-BC control approaches with the existence of position and pressure sensors, the angular velocity and lumped matched disturbances are observed more accurately. The mismatched disturbance estimation performances of the DESO-BC and DESMO-BC control methods are illustrated in Fig. 4-5. From this figure, it is noteworthy that under the same condition, the ESMOs of the suggested control algorithm outperform the ESOs of the DESO-BC controller in terms of both state and disturbance estimation accuracies. In addition, Fig. 4-5 and Fig. 4-6 and their zoom-in subfigures show that the ESMOs of the DESMO-BC controller perform better than the ESOs integrated into the SESO-BC and DESO-BC control algorithms in not only the

steady-state regime but also the transient response. Consequently, better tracking performances are achieved by the proposed controller. More importantly, the smooth estimated values of both state and disturbances are obtained by the proposed ESMOs verifying their applicability in real-life applications.

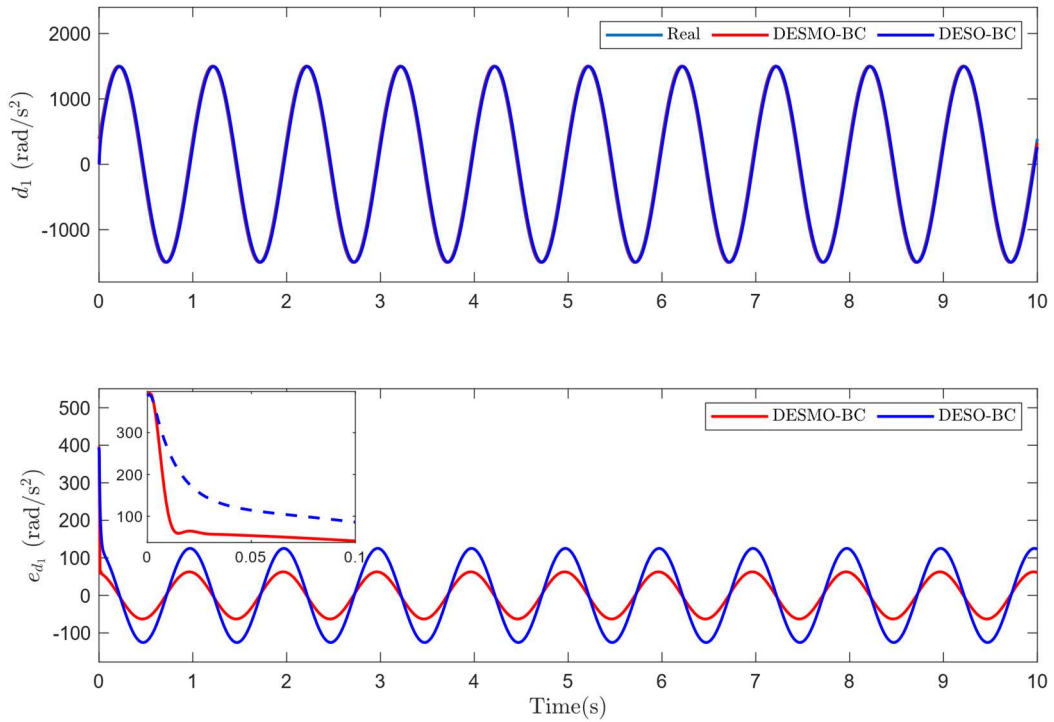


Fig. 4-6 The mismatched disturbance estimation performance in slow-motion desired trajectory

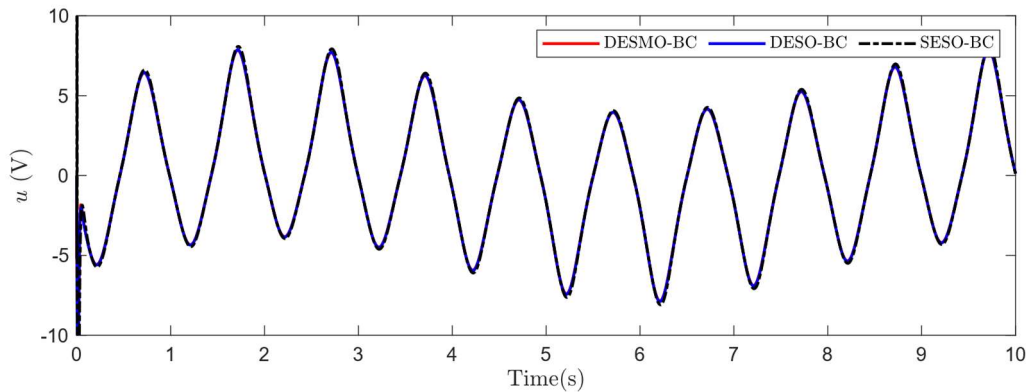


Fig. 4-7 The control actions of all controllers in the slow-motion desired trajectory

Furthermore, control actions in the slow-motion scenario are generated by all three control approaches illustrated in Figure 8. As shown, the continuous and smooth control actions are achieved as a consequence of the chattering-free feature of the state and disturbance estimation. In addition, because the identical reference trajectory is adopted and the close tracking accuracy is attained, these control actions are relatively indistinguishable.

To further examine the contribution of dual ESMOs in exactly estimating fast-changing system states and improving the position tracking performance, a fast-motion reference trajectory $x_{1d}(t) = 10(1 - \cos(3\pi t))(1 - e^{-t})$ is employed. In addition, the lumped disturbances $d_1(t) = 1500\sin(2\pi t)$ rad/s² and $d_2(t) = 10^6\sin(2\pi t)$ rad/s³ are intentionally inserted into the system

dynamics to evaluate the robustness of the closed-loop system. As shown in Fig. 4-8, owing to the non-existence of the pressure measurement mechanism, the lumped mismatched disturbances are not observed and compensated in the SESO-BC approach. Similar to the previous case study, the SESO-BC control approach performs the worst tracking performance and estimation performance. In contrast, the DESO-BC controller and DESMO-BC controller are capable of estimating both lumped mismatched and matched disturbances, therefore, higher accurate tracking accuracies are attained. However, it is worth noting that similar to the slow-motion case, compared to the remaining controllers, the proposed controller is still able to follow the desired trajectory more accurately.

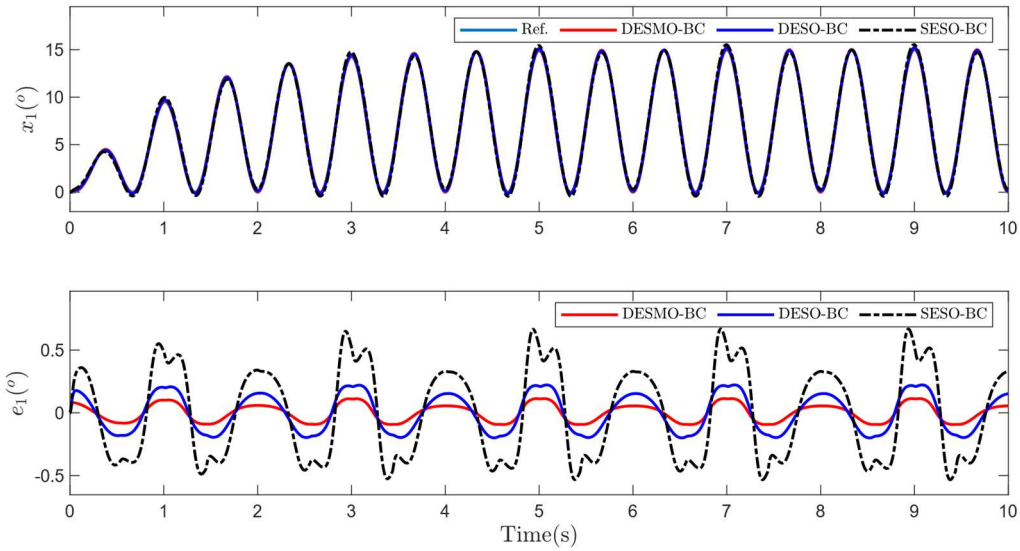


Fig. 4-8 The tracking performance in case of fast-motion desired trajectory

Table 4-3 Performance indexes in the fast-motion trajectory scenario.

Controller	M_e (deg)	μ_e (deg)	σ_e (deg)
DESMO-BC	0.0864	0.0578	0.0255
DESO-BC	0.1818	0.1185	0.0548
SESO-BC	0.4877	0.3188	0.1196

The tracking performance indexes in the steady-state regime are presented in Table 4-3. As shown in this table, the DESMO-BC controller achieves better performance with the maximal tracking error is only 0.1133° compared to 0.2223° and 0.6686° attained by the DESO-BC and SESO-BC controllers, respectively. In terms of the remaining performance indices, the proposed control strategy also performs better than DESO-BC and SESO-BC with significantly smaller values. The obtained comparative results exhibit the superiority and robustness against disturbances of the proposed method in comparison with the remaining control strategies.

4.4 Conclusion

In this chapter, a novel dual ESMO-based control scheme was introduced to achieve a high-accuracy tracking performance for an EHSS with an HRA in the presence of both matched and mismatched disturbances without angular velocity information. By employing the nonlinear switching function instead of the proportional term as in the ESO design, the suggested EMSO is not only robust against uncertainties but also able to strongly react to fast-changing immeasurable system states and disturbances. Then their estimated values are integrated into the control law synthesized via the backstepping technique to compensate for the effects of uncertainties and disturbances on the whole system. The closed-loop system stability was proven using the Lyapunov theory. Finally, comparative

numerical simulations were conducted to validate the effectiveness of the recommended approach in comparison with the existing ESO-based strategies. The results showed that compared to the well-known ESO, a better estimation performance, i.e., higher accuracy and shorter convergence time, was achieved. Based on that, the suggested ESMO-based control approach so-called DESO-BC controller with its simple structure and intuitive concept outperformed the existing ESO-based control algorithms in terms of transient and steady-state performances. Nevertheless, in this work, the effectiveness of the proposed ESMO is only verified via simulation, hence, experimental validation for real EHSSs with valve dynamics and input saturation will be included to demonstrate the advantage of the suggested approach in future works. Moreover, the application of the proposed ESMO to tracking control of general high-order nonlinear systems subject to disturbances and uncertainties will be carefully investigated. In addition, adaptive and finite-time ESMO for attaining an enhanced tracking performance also will be considered in forthcoming studies.

ADAPTIVE NEURAL NETWORK-BASED CONTROL FOR ELECTRO-HYDRAULIC SYSTEMS SUFFERING FROM COMPLETELY UNKNOWN DYNAMICS AND EXTERNAL DISTURBANCES**5.1 Introduction**

Hydraulic servomechanisms have been broadly employed in various industrial applications e.g., hydraulic robot manipulators [179], hydraulic press [108], load simulators [100], vehicle active suspension systems [180], and so on, due to their superiorities such as high power-to-weight ratio, fast and smooth response, high stiffness, and ability to generate a tremendous force/torque [90]. However, the inherent highly nonlinear characteristics, parameter variations, modeling uncertainties, and external disturbances of the EHSS are still the major obstacles to achieving high-accuracy tracking performance. Hence, the position-tracking problem of the EHSS has attracted many studies in recent years.

To control EHSSs, proportional-integral-derivative (PID) control law [181] was initially employed due to its simple structure and easy implementation. However, it is difficult to achieve satisfactory performance since the system dynamics are not compensated in the control law. Alternatively, model-based control strategies for EHSSs such as feedback linearization control (FLC) [112], backstepping control (BC) [93], and adaptive control (ADC) [122] have been widely employed to achieve better tracking performance. Although in these control methods, the system dynamics are taken into account in control design, they are sensitive to the modeling uncertainties and disturbances that naturally exist in EHSSs. In contrast, SMC [34, 162, 182-184] which was originally introduced by Utkin [185], is considered as a powerful candidate to deal with disturbances and uncertainties, satisfying the matching condition in nonlinear systems that are assumed to be bounded. However, it can be seen that all the above model-based control approaches for EHSSs require the system dynamics to be known, which are complicated and difficult to precisely acquire due to high nonlinearities in pressure dynamics and a number of unknown parameters that need to be identified from experimental input-output data [186].

By virtue of the excellent properties of their self-learning capability and online weight adaptive mechanisms, radial basis function (RBF) neural networks (NNs) have been employed in various fields such as robot manipulators [82, 187-189], magnetic levitation systems [89], aircraft [190], hydraulic systems [85, 90, 151, 191, 192], and so on to approximate the unknown dynamic components of control systems. For EHSSs, Z. Yao et al. introduced multilayer RBF NNs to approximate partly mismatched and matched uncertainties [90], and semi-global asymptotic stability was achieved accordingly. In [85], an NN-based estimator was proposed to approximate an unknown term generated in the control design of the hydraulic active suspension systems (ASSs). Besides, an RBF NN-based function approximator [191] was developed to compensate for the effects of the nonlinear friction in EHSSs. In [151], parametric uncertainties and an unknown external load in hydraulic systems were grouped into so-called generalized uncertainties, which were compensated by using RBF NNs. However, in the above-mentioned works, RBF NNs were only exploited to partially approximate model uncertainty in the control system. Hence, the employment of RBF NNs for approximating full model uncertainties is still an open problem.

Besides, although RBF NNs are capable of dealing with model uncertainties, they cannot effectively treat disturbances whose effects on system dynamics are independent of the system states. Hence, the employment of disturbance observers (DOBs) can be considered as an effective way to cope with disturbances in EHSSs. Extended state observers (ESOs) were employed [95, 193] for EHSSs to estimate both unmeasurable system states and matched/mismatched disturbances; therefore,

high-accuracy tracking performances were achieved. In another approach to cope with disturbances, some DOB designs based on exact differentiators [139] have been applied in hydraulic systems. For example, a linear disturbance observer (LDOB) [97] for hydraulic rotary actuator (HRA) control systems and nonlinear disturbance observers (NDOBs) [103, 179] for hydraulic robot manipulators have been successfully employed to actively reject the influence of the grouped disturbances on the tracking performance. It is noted that the above-mentioned DOB designs require the construction of an observer with a careful tuning process of observer gains to achieve highly efficient disturbance compensation. Hence, to simplify the parameter tuning, the unknown disturbance estimator (UDE) [155] has been proposed with only one parameter that needs to be selected. Nevertheless, similar to model-based control approaches, DOB designs require system dynamic information, which inhibits the applications of DOBs. In addition, the employment of RBF-NNs and DOBs to cope with partial uncertainties and disturbances has been studied [194, 195]. However, to the best of the authors' knowledge, the integration of RBF NNs and DOBs into a controller to treat the problem of full model uncertainties and disturbances is still challenging, and this is considered in this study.

Motivated by the above comprehensive analysis, in this chapter, a novel adaptive robust control mechanism for the EHSS with completely unknown dynamics and disturbances is originally proposed. In this framework, high-order sliding mode exact differentiators [141] are adopted to exactly calculate the angular velocity, acceleration, and pressure derivative. Based on that, all unknown dynamic functions in system dynamics are approximated by RBF-NN-based approximators. For the first time, a pair of NN-based DOBs are established to estimate and compensate for the effects of the NN approximation imperfections, unmodeled dynamics, and external load on the control system of the EHSS simultaneously. Finally, the full-state feedback robust control law is synthesized to ensure the high-accuracy tracking performance in the presence of completely unknown dynamic functions and both matched/mismatched lumped disturbances. The overall system stability is proven by utilizing the Lyapunov theory. Several simulations are conducted to verify the effectiveness of the proposed control strategy.

The main contributions of this research are summarized as follows:

- 1) The RBF NN-based function approximators with adaptive mechanisms are designed to online approximate all unknown dynamic functions in the dynamics of the EHSS.
- 2) A pair of DOBs based on the HOSM differentiators along with NNs are first developed to effectively estimate and actively compensate for not only the effects of both mismatched and matched disturbances but also the imperfections of the function approximation of RBF NNs.
- 3) A robust control law based on the RBF NNs and DOBs is synthesized to guarantee the high-accuracy tracking performance of the EHSS control system under the impacts of large model uncertainties and disturbances.
- 4) The combination of RBF NNs and DOBs in order to take all their advantages is originally introduced to efficiently treat both full model uncertainties and disturbances in the dynamics of EHSSs.

The remainder of the chapter is organized as follows. The high-order differentiator, neural network-based system dynamic approximators, disturbance observers, and control strategy are developed in Section 5.2. The total system stability is analyzed in Section 5.3 and comparative numerical simulations are conducted in Section 5.4. Finally, Section 5.5 concludes this chapter.

5.2 Adaptive Robust Control Design

The control scheme of the proposed method is depicted in Fig. 5-1. In this configuration, the angular velocity, angular acceleration, and the first-order derivative of the load pressure are

determined by employing Levant's high-order exact differentiators. Then, the unknown dynamic functions caused by unknown system parameters are approximated based on RBF NN-based approximators. A pair of NN-based DOBs are designed to estimate not only mismatched/matched lumped disturbances but also approximation errors of RBF NNs. Finally, a control law is synthesized to guarantee the stability of the overall system and achieve high-accuracy tracking performance.

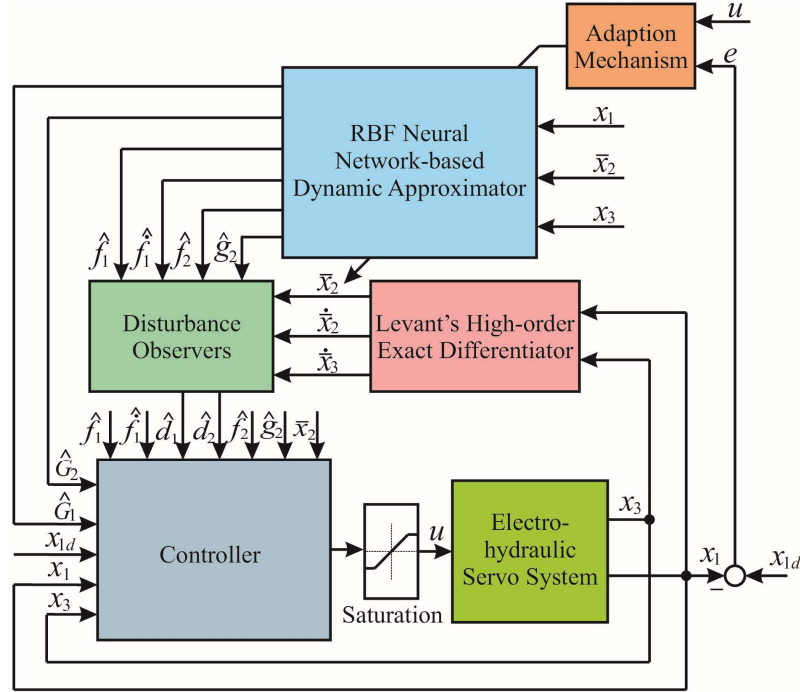


Fig. 5-1 The control scheme of the proposed control strategy.

5.2.1 Robust Control Law Design

To facilitate the controller design, it is assumed that the system dynamic functions $f_1(x_2)$, $f_2(x_2, x_3)$, and $g_2(x_3, u)$ in (2.6) which will be approximated later, are completely known. In addition, the mismatched/matched lumped disturbances and angular velocity of the inertial load are measurable. The control objective is to design a robust control law that ensures high-accuracy tracking performance.

The tracking errors are defined as follows:

$$\begin{cases} e_1 = x_1 - x_{1d} \\ e_2 = x_2 - \dot{x}_{1d} \end{cases} \quad (5.1)$$

where x_{1d} and \dot{x}_{1d} are desired angular position and velocity.

The sliding surface for the actual tracking error is constructed by

$$s = e_2 + \lambda e_1 \quad (5.2)$$

where λ is a positive constant.

To guarantee the convergence for the sliding variable (5.2), an auxiliary sliding surface is designed as

$$\sigma = \dot{s} + ks \quad (5.3)$$

where k is a positive constant.

The time derivative of the auxiliary sliding surface σ defined in (5.3) can be derived as

$$\dot{\sigma} = \dot{s} + k\dot{s} \quad (5.4)$$

For the sake of simplicity, we will use f_1 , \dot{f}_1 , f_2 , and g_2 instead of $f_1(x_2)$, $\dot{f}_1(x_2)$, $f_2(x_2, x_3)$, and $g_2(x_3, u)$. Taking the first and second-order derivatives of the sliding variable (5.4) and combining them with the system dynamics and combining them with the system dynamics (2.6), one obtains

$$\begin{cases} \dot{s} = x_3 + f_1 + d_1 - \ddot{x}_{1d} + \lambda e_2 \\ \ddot{s} = f_2 + g_2 u + d_2 + \dot{f}_1 + \dot{d}_1 - x_{1d}^{(3)} + \lambda(x_3 + f_1 + d_1 - \ddot{x}_{1d}) \end{cases} \quad (5.5)$$

Substituting (5.5) into (5.4), the derivative of σ is given by

$$\begin{aligned} \dot{\sigma} &= f_2 + d_2 + g_2 u + \dot{f}_1 + \dot{d}_1 - x_{1d}^{(3)} + k\lambda(x_2 - \dot{x}_{1d}) \\ &\quad + (\lambda + k)(x_3 + f_1 + d_1 - \ddot{x}_{1d}) \end{aligned} \quad (5.6)$$

Based on this, the equivalent control is synthesized as

$$u_{eq} = \frac{1}{g_2} \begin{pmatrix} -f_2 - d_2 - \dot{f}_1 - \dot{d}_1 + x_{1d}^{(3d)} \\ -(\lambda + k)(x_3 + f_1 + d_1 - \ddot{x}_{1d}) - k\lambda(x_2 - \dot{x}_{1d}) \end{pmatrix} \quad (5.7)$$

The switching control term is designed as

$$u_{sw} = -\frac{1}{g_2} (\eta_1 \text{sgn}(\sigma) + \eta_2 \sigma) \quad (5.8)$$

where η_1 and η_2 are positive constants that will be determined later.

Based on (5.7) and (5.8), the complete control law is derived as

$$u = u_{eq} + u_{sw} \quad (5.9)$$

Theorem 5-1: The control laws (5.7), (5.8), and (5.9) guarantee the finite-time convergence of the auxiliary sliding variable without singularity. Based on that the tracking error asymptotically converges to zero in the case that the functions $f_1(x_2)$, $f_2(x_2, x_3)$, and $g_2(x_3, u)$ are known and the angular velocity along with lumped disturbances d_1 and d_2 are measurable.

Proof of Theorem 5-1: Consider the candidate Lyapunov function as

$$V_c = \frac{1}{2} \sigma^2 \quad (5.10)$$

Taking time derivative of (5.10), one obtains

$$\dot{V}_c = \sigma \dot{\sigma} \quad (5.11)$$

Substituting (5.7), (5.8), and (5.9) into (5.11), we derive

$$\dot{V}_c \leq -\eta_1 |\sigma| \quad (5.12)$$

Combining with (5.11), (5.12) can be rewritten as

$$\dot{V}_c \leq -\eta_1 \sqrt{2V_c} \quad (5.13)$$

It can be observed from (5.13), V_c converges to zero in finite time with convergence time computed as

$$t_r \leq \frac{\sqrt{2}}{\eta} V_c^{1/2}(0) \quad (5.14)$$

Based on this, it can be concluded that by using the control laws (5.7), (5.8), and (5.9), the auxiliary sliding variable converges to zero in finite time, hence, the control system is asymptotically stable.

This completes the proof of Theorem 5-1.

5.2.2 Levant's High-Order Exact Differentiator

To exactly compute the angular velocity and the angular acceleration of the inertial load, the first Levant's differentiator [139] is designed as

$$\begin{cases} \bar{x}_1 = z_1; \dot{z}_1 = -\varsigma_1 |z_1 - x_1|^{3/4} \text{sgn}(z_1 - x_1) + z_2 \\ \bar{x}_2 = z_2; \dot{z}_2 = -\varsigma_2 |z_2 - \dot{z}_1|^{2/3} \text{sgn}(z_2 - \dot{z}_1) + z_3 \\ \bar{x}_3 = z_3; \dot{z}_3 = -\varsigma_3 |z_3 - \dot{z}_2|^{1/2} \text{sgn}(z_3 - \dot{z}_2) + z_4 \\ \dot{z}_4 = -\varsigma_4 \text{sgn}(z_4 - \dot{z}_3) \end{cases} \quad (5.15)$$

where ς_1 , ς_2 , ς_3 , and ς_4 are positive constants and \bar{x}_1 , \bar{x}_2 , and \bar{x}_3 denote the estimated position, velocity, and acceleration, respectively.

Similarly, the second Levant's differentiator to calculate the first-order derivative of load pressure is determined by

$$\begin{cases} \bar{x}_3 = v_1; \dot{v}_1 = -\xi_1 |v_1 - x_3|^{2/3} \text{sgn}(v_1 - x_3) + v_2 \\ \bar{x}_3 = v_2; \dot{v}_2 = -\xi_2 |v_2 - \dot{v}_1|^{1/2} \text{sgn}(v_2 - \dot{v}_1) + v_3 \\ \dot{v}_3 = -\xi_3 \text{sgn}(v_3 - \dot{v}_2) \end{cases} \quad (5.16)$$

where ξ_1 , ξ_2 , and ξ_3 are positive constants; \bar{x}_3 and \bar{x}_3 denote estimates of load pressure and its first-order derivative.

Remark 5-1: The angular velocity and acceleration of the load and the derivative of load pressure of the HRA are computed based on the well-known Levant's exact differentiator [139] with negligible calculation error. The differentiation term of (\bullet) is denoted by $(\dot{\bullet})$. For the sake of condensation, the dynamics of this differentiator are not presented in this study.

5.2.3 Unknown Dynamic Estimators

Consider an arbitrary unknown smooth multivariate function $f(\mathbf{x})$ with \mathbf{x} is the input vector. This function can be represented in RBF NN form as [196]

$$f(\mathbf{x}) = \mathbf{W}_f^T \mathbf{h}_f(\mathbf{x}) + \varepsilon_f \quad (5.17)$$

where \mathbf{W}_f is the ideal neural network weights, $\mathbf{h}_f = [h_j]^T$ with h_j represents the radial-basis function output of the j^{th} node in the hidden layer, and ε_f denotes the function approximation error.

Assumption 5-1: The weight value and the approximation error of NN are bounded as $\|\mathbf{W}_f\| \leq W_{fM}$ and $|\varepsilon_f| \leq \varepsilon_{fM}$ where W_{fM} and ε_{fM} are positive constants.

The radial-basis function is usually chosen as the Gaussian function which has the form [197]

$$h_j = \exp\left(-\frac{\|\mathbf{x} - \mathbf{c}_j\|^2}{2b_j^2}\right) \quad (5.18)$$

where \mathbf{c}_j is the center vector of the j^{th} node in the hidden layer, which has the same dimension as the input vector \mathbf{x} , $\|\bullet\|$ represents the Euclid distance of a vector.

The estimation of the function $f(\mathbf{x})$ denoted by $\hat{f}(\mathbf{x})$.which is the output of RBF NN as

$$\hat{f}(\mathbf{x}) = \hat{\mathbf{W}}_f^T \mathbf{h}_f(\mathbf{x}) \quad (5.19)$$

In (5.7), since the system parameters are unknown, therefore, the functions f_1 , \dot{f}_1 , f_2 , and g_2 are unknown smooth functions which are approximated by employing RBF NN-based approximators as

$$\begin{cases} f_1 = \mathbf{W}_{f_1}^T \mathbf{h}_{f_1}(\mathbf{x}) + \varepsilon_{f_1} \\ \dot{f}_1 = \mathbf{W}_{df_1}^T \mathbf{h}_{df_1}(\mathbf{x}) + \varepsilon_{df_1} \\ f_2 = \mathbf{W}_{f_2}^T \mathbf{h}_{f_2}(\mathbf{x}) + \varepsilon_{f_2} \\ g_2 = \mathbf{W}_{g_2}^T \mathbf{h}_{g_2}(\boldsymbol{\chi}) + \varepsilon_{g_2} \end{cases} \quad (5.20)$$

where the weight values $\|\mathbf{W}_{f_1}\|$, $\|\mathbf{W}_{df_1}\|$, $\|\mathbf{W}_{f_2}\|$, $\|\mathbf{W}_{g_2}\|$ and approximation errors ε_{f_1} , ε_{df_1} , ε_{f_2} , ε_{g_2} are bounded by W_{f_1M} , W_{df_1M} , W_{f_2M} , W_{g_2M} and ε_{f_1M} , ε_{df_1M} , ε_{f_2M} , ε_{g_2M} , respectively; and the input vector $\boldsymbol{\chi} = [x_1, \bar{x}_2, x_3, u]^T$.

The estimates of f_1 , \dot{f}_1 , f_2 , and g_2 are determined as

$$\begin{cases} \hat{f}_1 = \hat{\mathbf{W}}_{f_1}^T \mathbf{h}_{f_1}(\mathbf{x}) \\ \hat{\dot{f}}_1 = \hat{\mathbf{W}}_{df_1}^T \mathbf{h}_{df_1}(\mathbf{x}) \\ \hat{f}_2 = \hat{\mathbf{W}}_{f_2}^T \mathbf{h}_{f_2}(\mathbf{x}) \\ \hat{g}_2 = \hat{\mathbf{W}}_{g_2}^T \mathbf{h}_{g_2}(\boldsymbol{\chi}) \end{cases} \quad (5.21)$$

The approximation errors are determined by

$$\begin{cases} \tilde{f}_1 \triangleq f_1 - \hat{f}_1 = \tilde{\mathbf{W}}_{f_1}^T \mathbf{h}_{f_1} + \varepsilon_{f_1} \\ \tilde{\dot{f}}_1 \triangleq \dot{f}_1 - \hat{\dot{f}}_1 = \tilde{\mathbf{W}}_{df_1}^T \mathbf{h}_{df_1} + \varepsilon_{df_1} \\ \tilde{f}_2 \triangleq f_2 - \hat{f}_2 = \tilde{\mathbf{W}}_{f_2}^T \mathbf{h}_{f_2} + \varepsilon_{f_2} \\ \tilde{g}_2 \triangleq g_2 - \hat{g}_2 = \tilde{\mathbf{W}}_{g_2}^T \mathbf{h}_{g_2} + \varepsilon_{g_2} \end{cases} \quad (5.22)$$

where

$$\begin{cases} \tilde{\mathbf{W}}_{f_1} = \mathbf{W}_{f_1} - \hat{\mathbf{W}}_{f_1} \\ \tilde{\mathbf{W}}_{df_1} = \mathbf{W}_{df_1} - \hat{\mathbf{W}}_{df_1} \\ \tilde{\mathbf{W}}_{f_2} = \mathbf{W}_{f_2} - \hat{\mathbf{W}}_{f_2} \\ \tilde{\mathbf{W}}_{g_2} = \mathbf{W}_{g_2} - \hat{\mathbf{W}}_{g_2} \end{cases} \quad (5.23)$$

The adaption mechanisms are determined as

$$\begin{cases} \dot{\hat{\mathbf{W}}}_{f_1} = \gamma_{f_1} \left(\lambda + k - \frac{1}{\kappa_1} \right) \sigma \mathbf{h}_{f_1} - \Gamma_{f_1} \hat{\mathbf{W}}_{f_1} \\ \dot{\hat{\mathbf{W}}}_{d_{f_1}} = \gamma_{d_{f_1}} \sigma \mathbf{h}_{d_{f_1}} - \Gamma_{d_{f_1}} \hat{\mathbf{W}}_{d_{f_1}} \\ \dot{\hat{\mathbf{W}}}_{f_2} = \gamma_{f_2} \sigma \mathbf{h}_{f_2} - \Gamma_{f_2} \hat{\mathbf{W}}_{f_2} \\ \dot{\hat{\mathbf{W}}}_{g_2} = \gamma_{g_2} \sigma u \mathbf{h}_{g_2} - \Gamma_{g_2} \hat{\mathbf{W}}_{g_2} \end{cases} \quad (5.24)$$

where γ_{f_1} , $\gamma_{d_{f_1}}$, γ_{f_2} , and γ_{g_2} are learning rates of the neural networks, σ is the auxiliary sliding variable defined in (5.3), u is the control input, Γ_{f_1} , $\Gamma_{d_{f_1}}$, Γ_{f_2} , and Γ_{g_2} are positive constants, and κ_1 is the time constant of a disturbance observer, which will be designed later.

5.2.4 Disturbance Observer Design

To actively compensate for the effect of unmodeled disturbances, uncertain nonlinearities, external load, and the imperfection in approximating unknown continuous functions in system dynamics (2.6) on the control system, a pair of NN-based disturbance observers are proposed as

$$\begin{aligned} \dot{\hat{d}}_1 &= \frac{1}{\kappa_1} (\bar{x}_2 - x_3 - \hat{f}_1 - \hat{d}_1) \\ \dot{\hat{d}}_2 &= \frac{1}{\kappa_2} (\bar{x}_3 - \hat{f}_2 - \hat{g}_2 u - \hat{G}_1 - \hat{d}_2) \end{aligned} \quad (5.25)$$

where κ_1 and κ_2 are small positive constants, \hat{d}_1 and \hat{d}_2 are estimates of d_1 and d_2 , respectively. \hat{G}_1 is the NN-based approximation of $G_1 = \tilde{g}_2 u$ which is generated by the NN weighting approximation error of g_2 . The function G_1 is represented by RBF NN as

$$G_1 = \mathbf{W}_{G_1}^T \mathbf{h}_{G_1}(\boldsymbol{\chi}) + \varepsilon_{G_1} \quad (5.26)$$

where the weight value $\|\mathbf{W}_{G_1}\|$ and approximation error ε_{G_1} are bounded by positive constants, i.e., $\|\mathbf{W}_{G_1}\| \leq W_{G_1M}$, $|\varepsilon_{G_1}| \leq \varepsilon_{G_1M}$.

From (5.26), approximated value \hat{G}_1 and the approximation error \tilde{G}_1 are given by

$$\begin{cases} \hat{G}_1 = \hat{\mathbf{W}}_{G_1}^T \mathbf{h}_{G_1} \\ \tilde{G}_1 = \tilde{\mathbf{W}}_{G_1}^T \mathbf{h}_{G_1} + \varepsilon_{G_1} \end{cases} \quad (5.27)$$

where $\tilde{\mathbf{W}}_{G_1} = \mathbf{W}_{G_1} - \hat{\mathbf{W}}_{G_1}$ and the weight is updated according to the following law

$$\dot{\hat{\mathbf{W}}}_{G_1} = 0.5 \gamma_{G_1} \sigma \mathbf{h}_{G_1} - \Gamma_{G_1} \hat{\mathbf{W}}_{G_1} \quad (5.28)$$

where γ_{G_1} and Γ_{G_1} are positive constants.

The disturbance estimation errors are defined by

$$\begin{cases} \tilde{d}_1 = d_1 - \hat{d}_1 \\ \tilde{d}_2 = d_2 - \hat{d}_2 \end{cases} \quad (5.29)$$

Assuming that the state derivatives are perfectly calculated, based on (2.6) and (5.25), the disturbance estimation error dynamics are obtained as

$$\begin{cases} \dot{\hat{d}}_1 = -\frac{1}{\kappa_1}(\tilde{f}_1 + \tilde{d}_1) + \dot{d}_1 \\ \dot{\hat{d}}_2 = -\frac{1}{\kappa_2}(\tilde{f}_2 + \tilde{G}_1 + \tilde{d}_2) + \dot{d}_2 \end{cases} \quad (5.30)$$

Remark 6-2: With the help of the exact high-order differentiators (5.15) and (5.16), and the system dynamics are assumed to be known, i.e., $\tilde{f}_1=0$, $\tilde{f}_2=0$, and $\tilde{g}_2=0$, the disturbance observers (5.25) guarantee the uniformly asymptotic stability under the constant disturbances and boundedness stability under the time-varying disturbances

Based on (5.7), (5.8), (5.9), (5.15), (5.16), (5.21), and (5.25), the control law is redesigned as

$$\begin{aligned} u_{eq} &= \frac{1}{\hat{g}_2} \begin{pmatrix} -\hat{f}_2 - \frac{1}{2}\hat{G}_1 - \frac{1}{2}\hat{G}_2 - \hat{d}_2 - \hat{f}_1 + \hat{d}_1 + x_{1d}^{(3)} \\ -(\lambda + k)(x_3 + \hat{f}_1 + \hat{d}_1 - \dot{x}_{1d}) - k\lambda(\bar{x}_2 - \dot{x}_{1d}) \end{pmatrix} \\ u_{sw} &= -\frac{1}{\hat{g}_2} [\eta_1 \text{sgn}(\sigma) + \eta_2 \sigma] \\ u &= u_{eq} + u_{sw} \end{aligned} \quad (5.31)$$

where

$$e_1 = x_1 - x_{1d}; e_2 = \bar{x}_2 - \dot{x}_{1d}; s = e_2 + \lambda e_1; \sigma = \dot{s} + k\dot{s} \quad (5.32)$$

and the function $G_2 = \varepsilon_{g_2} u$ is approximated by adopting RBF NN as

$$G_2 = \mathbf{W}_{G_2}^T \mathbf{h}_{G_2}(\boldsymbol{\chi}) + \varepsilon_{G_2} \quad (5.33)$$

with $\|\mathbf{W}_{G_2}\| \leq W_{G_2M}$ and $|\varepsilon_{G_2}| \leq \varepsilon_{G_2M}$.

The approximation value of G_2 is determined by

$$\hat{G}_2 = \hat{\mathbf{W}}_{G_2}^T \mathbf{h}_{G_2} \quad (5.34)$$

The weight update law is designed as

$$\dot{\hat{\mathbf{W}}}_{G_2} = 0.5\gamma_{G_2} \sigma \mathbf{h}_{G_2} - \Gamma_{G_2} \hat{\mathbf{W}}_{G_2} \quad (5.35)$$

where γ_{G_2} and Γ_{G_2} are positive constants.

5.3 Stability Analysis

Theorem 5-2: For system (2.6) by using the control laws (5.31) with unknown function approximators (5.21), (5.27) and (5.34), the pair of disturbance observers (5.25), adaptive mechanisms (5.24), (5.28), and (5.35), and differentiators (5.15) and (5.16), the ultimately uniformly bounded tracking performance is ensured in the presence of unknown dynamics and both mismatched and matched disturbances.

Proof of Theorem 5-2: Consider the candidate Lyapunov function as

$$\begin{aligned} V &= \frac{1}{2}\sigma^2 + \frac{1}{2\gamma_{f_1}} \tilde{\mathbf{W}}_{f_1}^T \tilde{\mathbf{W}}_{f_1} + \frac{1}{2\gamma_{df_1}} \tilde{\mathbf{W}}_{df_1}^T \tilde{\mathbf{W}}_{df_1} + \frac{1}{2\gamma_{G_1}} \tilde{\mathbf{W}}_{G_1}^T \tilde{\mathbf{W}}_{G_1} + \frac{1}{2\gamma_{G_2}} \tilde{\mathbf{W}}_{G_2}^T \tilde{\mathbf{W}}_{G_2} \\ &\quad + \frac{1}{2\gamma_{f_2}} \tilde{\mathbf{W}}_{f_2}^T \tilde{\mathbf{W}}_{f_2} + \frac{1}{2\gamma_{g_2}} \tilde{\mathbf{W}}_{g_2}^T \tilde{\mathbf{W}}_{g_2} + \frac{1}{2}\tilde{d}_1^2 + \frac{1}{2}\tilde{d}_2^2 \end{aligned} \quad (5.36)$$

Taking time derivative of (5.36), one obtains

$$\begin{aligned} \dot{V} = & \sigma \dot{\sigma} + \frac{1}{\gamma_{f_1}} \tilde{\mathbf{W}}_{f_1}^T \dot{\tilde{\mathbf{W}}}_{f_1} + \frac{1}{\gamma_{df_1}} \tilde{\mathbf{W}}_{df_1}^T \dot{\tilde{\mathbf{W}}}_{df_1} + \frac{1}{\gamma_{G_1}} \tilde{\mathbf{W}}_{G_1}^T \dot{\tilde{\mathbf{W}}}_{G_1} + \frac{1}{\gamma_{G_2}} \tilde{\mathbf{W}}_{G_2}^T \dot{\tilde{\mathbf{W}}}_{G_2} \\ & + \frac{1}{\gamma_{f_2}} \tilde{\mathbf{W}}_{f_2}^T \dot{\tilde{\mathbf{W}}}_{f_2} + \frac{1}{\gamma_{g_2}} \tilde{\mathbf{W}}_{g_2}^T \dot{\tilde{\mathbf{W}}}_{g_2} + \tilde{d}_1 \dot{\tilde{d}}_1 + \tilde{d}_2 \dot{\tilde{d}}_2 \end{aligned} \quad (5.37)$$

Based on (5.6), (5.30), and (5.31), (5.37) can be transformed into

$$\begin{aligned} \dot{V} = & \sigma \left(\tilde{f}_2 + \frac{1}{2} \tilde{\mathbf{W}}_{g_2}^T \mathbf{h}_{g_2} u + \frac{1}{2} \tilde{G}_1 + \frac{1}{2} \tilde{G}_2 + \tilde{d}_2 + \tilde{f}_1 + \dot{d}_1 \right) \\ & + \left(\lambda + k - \frac{1}{\kappa_1} \right) (\tilde{f}_1 + \tilde{d}_1) - \eta_1 \text{sgn}(\sigma) - \eta_2 \sigma \\ & - \frac{1}{\gamma_{f_1}} \tilde{\mathbf{W}}_{f_1}^T \dot{\tilde{\mathbf{W}}}_{f_1} - \frac{1}{\gamma_{df_1}} \tilde{\mathbf{W}}_{df_1}^T \dot{\tilde{\mathbf{W}}}_{df_1} - \frac{1}{\gamma_{f_2}} \tilde{\mathbf{W}}_{f_2}^T \dot{\tilde{\mathbf{W}}}_{f_2} - \frac{1}{\gamma_{g_2}} \tilde{\mathbf{W}}_{g_2}^T \dot{\tilde{\mathbf{W}}}_{g_2} - \frac{1}{\gamma_{G_1}} \tilde{\mathbf{W}}_{G_1}^T \dot{\tilde{\mathbf{W}}}_{G_1} \\ & - \frac{1}{\gamma_{G_2}} \tilde{\mathbf{W}}_{G_2}^T \dot{\tilde{\mathbf{W}}}_{G_2} + \tilde{d}_1 \left(-\frac{1}{\kappa_1} (\tilde{f}_1 + \tilde{d}_1) + \dot{d}_1 \right) + \tilde{d}_2 \left(-\frac{1}{\kappa_2} (\tilde{f}_2 + \tilde{G}_1 + \tilde{d}_2) + \dot{d}_2 \right) \end{aligned} \quad (5.38)$$

Applying adaptation mechanisms (5.24), (5.28), and (5.35), (5.38) becomes

$$\begin{aligned} \dot{V} = & \frac{\Gamma_{f_1}}{\gamma_{f_1}} \tilde{\mathbf{W}}_{f_1}^T \hat{\mathbf{W}}_{f_1} + \frac{\Gamma_{df_1}}{\gamma_{df_1}} \tilde{\mathbf{W}}_{df_1}^T \hat{\mathbf{W}}_{df_1} + \frac{\Gamma_{f_2}}{\gamma_{f_2}} \tilde{\mathbf{W}}_{f_2}^T \hat{\mathbf{W}}_{f_2} + \frac{\Gamma_{g_2}}{\gamma_{g_2}} \tilde{\mathbf{W}}_{g_2}^T \hat{\mathbf{W}}_{g_2} + \frac{\Gamma_{G_1}}{\gamma_{G_1}} \tilde{\mathbf{W}}_{G_1}^T \hat{\mathbf{W}}_{G_1} \\ & + \frac{\Gamma_{G_2}}{\gamma_{G_2}} \tilde{\mathbf{W}}_{G_2}^T \hat{\mathbf{W}}_{G_2} + \left(\lambda + k - \frac{1}{\kappa_1} \right) \sigma \varepsilon_{f_1} + \sigma \varepsilon_{df_1} + \sigma \varepsilon_{f_2} + \frac{1}{2} \sigma \varepsilon_{G_1} + \frac{1}{2} \sigma \varepsilon_{G_2} \\ & + \left(\lambda + k - \frac{1}{\kappa_1} \right) \sigma \tilde{d}_1 + \sigma \dot{d}_1 + \sigma \tilde{d}_2 - \eta_1 |\sigma| - \eta_2 \sigma^2 - \frac{1}{\kappa_1} \tilde{d}_1 \tilde{\mathbf{W}}_{f_1}^T \mathbf{h}_{f_1} - \frac{1}{\kappa_1} \tilde{d}_1 \varepsilon_{f_1} \\ & - \frac{1}{\kappa_1} \tilde{d}_1^2 + \tilde{d}_1 \dot{d}_1 - \frac{1}{\kappa_2} \tilde{d}_2 \tilde{\mathbf{W}}_{f_2}^T \mathbf{h}_{f_2} - \frac{1}{\kappa_2} \tilde{d}_2 \varepsilon_{f_2} - \frac{1}{\kappa_2} \tilde{d}_2 \tilde{\mathbf{W}}_{G_1}^T \mathbf{h}_{G_1} - \frac{1}{\kappa_2} \tilde{d}_2 \varepsilon_{G_1} - \frac{1}{\kappa_2} \tilde{d}_2^2 + \tilde{d}_2 \dot{d}_2 \end{aligned} \quad (5.39)$$

Based on the Cauchy-Schwarz inequality, the following inequality holds

$$(\mathbf{W}^T \mathbf{h})^2 \leq (\mathbf{W}^T \mathbf{W})(\mathbf{h}^T \mathbf{h}) \quad (5.40)$$

Applying Young's inequality and (5.40), (5.39) can be transformed into

$$\begin{aligned} \dot{V} \leq & - \left(\eta_2 - \frac{5\lambda}{2} - \frac{5k}{2} + \frac{5}{2\kappa_1} - 4 \right) \sigma^2 - \left(\frac{\Gamma_{f_1}}{2\gamma_{f_1}} - \frac{2\lambda_{f_1}}{\kappa_1} \right) \tilde{\mathbf{W}}_{f_1}^T \tilde{\mathbf{W}}_{f_1} - \frac{\Gamma_{df_1}}{2\gamma_{df_1}} \tilde{\mathbf{W}}_{df_1}^T \tilde{\mathbf{W}}_{df_1} \\ & - \left(\frac{\Gamma_{f_2}}{2\gamma_{f_2}} - \frac{2\lambda_{f_2}}{\kappa_2} \right) \tilde{\mathbf{W}}_{f_2}^T \tilde{\mathbf{W}}_{f_2} - \frac{\Gamma_{g_2}}{2\gamma_{g_2}} \tilde{\mathbf{W}}_{g_2}^T \tilde{\mathbf{W}}_{g_2} - \left(\frac{\Gamma_{G_1}}{2\gamma_{G_1}} - \frac{2\lambda_{G_1}}{\kappa_2} \right) \tilde{\mathbf{W}}_{G_1}^T \tilde{\mathbf{W}}_{G_1} - \frac{\Gamma_{G_2}}{2\gamma_{G_2}} \tilde{\mathbf{W}}_{G_2}^T \tilde{\mathbf{W}}_{G_2} \\ & - \left(\frac{7}{8\kappa_1} - \frac{\lambda}{8} - \frac{k}{8} - \frac{1}{2} \right) \tilde{d}_1^2 - \left(\frac{1}{2\kappa_2} - \frac{5}{8} \right) \tilde{d}_2^2 + \frac{\Gamma_{f_1}}{2\gamma_{f_1}} W_{f_1M}^2 + \frac{\Gamma_{df_1}}{2\gamma_{df_1}} W_{df_1M}^2 + \frac{\Gamma_{f_2}}{2\gamma_{f_2}} W_{f_2M}^2 \\ & + \frac{\Gamma_{g_2}}{2\gamma_{g_2}} W_{g_2M}^2 + \frac{\Gamma_{G_1}}{2\gamma_{G_1}} W_{G_1M}^2 + \frac{\Gamma_{G_2}}{2\gamma_{G_2}} W_{G_2M}^2 + \left(\frac{\lambda}{2} + \frac{k}{2} + \frac{3}{2\kappa_1} \right) \varepsilon_{f_1M}^2 + \frac{\varepsilon_{df_1M}^2}{2} + \left(\frac{1}{2} + \frac{2}{\kappa_2} \right) \varepsilon_{f_2M}^2 \\ & + \left(\frac{1}{4} + \frac{2}{\kappa_2} \right) \varepsilon_{G_1M}^2 + \frac{1}{4} \varepsilon_{G_2M}^2 + \delta_1^2 + \frac{\delta_2^2}{2} \end{aligned} \quad (5.41)$$

where λ_{f_1} , λ_{f_2} , and λ_{G_1} are the number of nodes in the hidden layers of NNs for approximating f_1 , f_2 , and G_1 , respectively; control gains, disturbance observer parameters, and NN parameters are chosen such that

$$\begin{aligned} \lambda + k - \frac{1}{\kappa_1} > 0; \eta_2 - \frac{5\lambda}{2} - \frac{5k}{2} + \frac{5}{2\kappa_1} - 4 > 0; \frac{\Gamma_{f_1}}{2\gamma_{f_1}} - \frac{2\lambda_{f_1}}{\kappa_1} > 0; \\ \frac{\Gamma_{f_2}}{2\gamma_{f_2}} - \frac{2\lambda_{f_2}}{\kappa_2} > 0; \frac{\Gamma_{G_1}}{2\gamma_{G_1}} - \frac{2\lambda_{G_1}}{\kappa_2} > 0; \frac{7}{8\kappa_1} - \frac{\lambda}{8} - \frac{k}{8} - \frac{1}{2} > 0; \frac{1}{2\kappa_2} - \frac{5}{8} > 0 \end{aligned} \quad (5.42)$$

Equation (5.41) can be rewritten in the simple form as

$$\dot{V} \leq -\Pi V + \psi \quad (5.43)$$

where

$$\Pi = \min \left\{ \begin{array}{l} 2\eta_2 - 5\lambda - 5k + \frac{5}{\kappa_1} - 8; \frac{\Gamma_{f_1}}{\gamma_{f_1}} - \frac{4\lambda_{f_1}}{\kappa_1}; \frac{\Gamma_{df_1}}{\gamma_{df_1}}; \frac{\Gamma_{f_2}}{\gamma_{f_2}} - \frac{4\lambda_{f_2}}{\kappa_2}; \frac{\Gamma_{g_2}}{\gamma_{g_2}}; \\ \frac{\Gamma_{G_1}}{\gamma_{G_1}} - \frac{4\lambda_{G_1}}{\kappa_2}; \frac{\Gamma_{G_2}}{\gamma_{G_2}}; \frac{7}{4\kappa_1} - \frac{\lambda}{4} - \frac{k}{4} - 1; \frac{1}{\kappa_2} - \frac{5}{4} \end{array} \right\} \quad (5.44)$$

and

$$\begin{aligned} \psi = & \frac{\Gamma_{f_1}}{2\gamma_{f_1}} W_{f_1M}^2 + \frac{\Gamma_{df_1}}{2\gamma_{df_1}} W_{df_1M}^2 + \frac{\Gamma_{f_2}}{2\gamma_{f_2}} W_{f_2M}^2 + \frac{\Gamma_{g_2}}{2\gamma_{g_2}} W_{g_2M}^2 + \frac{\Gamma_{G_1}}{2\gamma_{G_1}} W_{G_1M}^2 \\ & + \frac{\Gamma_{G_2}}{2\gamma_{G_2}} W_{G_2M}^2 + \left(\frac{\lambda}{2} + \frac{k}{2} + \frac{7}{2\kappa_1} \right) \varepsilon_{f_1M}^2 + \frac{\varepsilon_{df_1M}^2}{2} + \left(\frac{1}{2} + \frac{2}{\kappa_2} \right) \varepsilon_{f_2M}^2 \\ & + \left(\frac{1}{4} + \frac{2}{\kappa_2} \right) \varepsilon_{G_1M}^2 + \frac{1}{4} \varepsilon_{G_2M}^2 + \delta_1^2 + \frac{\delta_2^2}{2} \end{aligned} \quad (5.45)$$

From (5.45), one obtains

$$V \leq V(0)e^{-\Pi t} + \frac{\psi}{\Pi} (1 - e^{-\Pi t}) \quad (5.46)$$

Based on this, one can conclude that σ is bounded which implies that the tracking errors of the system are also bounded. Therefore, the ultimately uniformly bounded tracking performance of the system is guaranteed by using the proposed control strategy.

Hence, Theorem 5-2 is completely proven.

5.4 Numerical Simulation

5.4.1 Simulation Setup

To verify the effectiveness of the proposed control strategy, the hydraulic servo system [76] is adopted. System parameters for the simulation are given in Table 5-1

Table 5-1 System parameters of the studied EHSS.

Parameter (Unit)	Value	Parameter (Unit)	Value
J (kg·m ²)	0.2	C_0 (m ³ ·s ⁻¹ ·Pa ⁻²)	0
B (N·m·s·rad ⁻¹)	90	C_1 (m ³ ·s ⁻¹ ·Pa ⁻¹)	1.0×10^{-12}

Parameter (Unit)	Value	Parameter (Unit)	Value
$D_m (\text{m}^3 \cdot \text{rad}^{-1})$		$C_2 (\text{m}^3 \cdot \text{s}^{-1})$	1.0×10^{-12}
$\beta_e (\text{Pa})$	7×10^8	$P_s (\text{Pa})$	1.0×10^7
$k_t (\text{m}^3 \cdot \text{s}^{-1} \cdot \text{V}^{-1} \cdot \text{Pa}^{1/2})$	1.1969×10^{-8}	$V_t (\text{m}^3)$	1.16×10^{-4}
$\tau_{c0} (\text{N} \cdot \text{m} \cdot \text{s} \cdot \text{rad}^{-1})$	35	$\omega_s (\text{rad} \cdot \text{s}^{-1})$	0.01
$\tau_{s0} (\text{N} \cdot \text{m} \cdot \text{s} \cdot \text{rad}^{-1})$	40		

To illustrate the superiority of the proposed method, some controllers are employed for comparison as follows:

1) The proposed controller with the control parameters $\lambda = 1000$, $k = 150$, $\eta_1 = 1000$, and $\eta_2 = 4.1 \times 10^4$. The parameters for the first Levant's differentiator are chosen as $\varsigma_1 = 100$, $\varsigma_2 = 50$, $\varsigma_3 = 100$, and $\varsigma_4 = 100$. For the second differentiator $\xi_1 = 350$, $\xi_2 = 1.5 \cdot 10^4$, and $\xi_3 = 1.5 \cdot 10^4$ are selected. The RBF NNs with single hidden layer are designed with 51 nodes in the hidden layer and their parameters are $\gamma_{f_1} = 0.15$, $\gamma_{d_{f_1}} = 0.2$, $\gamma_{f_2} = 0.02$, $\gamma_{g_2} = 0.1$, $\gamma_{G_1} = 0.01$, $\gamma_{G_2} = 0.1$, $\Gamma_{f_1} = 10^3$, $\Gamma_{d_{f_1}} = 10^{-7}$, $\Gamma_{f_2} = 10^3$, $\Gamma_{g_2} = 10^{-7}$, $\Gamma_{G_1} = 2 \times 10^3$, and $\Gamma_{G_2} = 10^{-7}$. The disturbance observer gains are chosen as $\kappa_1 = 0.005$ and $\kappa_2 = 0.005$.

2) RBF NN-based sliding mode control without disturbance observer (RBF-SMC) in which larger controller gains are designed $\eta_1 = 1500$ and $\eta_2 = 4.1 \times 10^4$ to attenuate the effects of disturbances while avoidance of chattering phenomenon is guaranteed. The structures and parameters of RBF NNs are the same as the proposed method.

3) Extended state observer-based backstepping controller (ESO-BC) [95] with the assumption that nominal system parameters are known. The control laws are designed based on the backstepping control framework as

$$\begin{aligned}
u &= \frac{1}{g_{20}} \left(-f_{20} - \hat{d}_2 + \dot{\alpha}_2 - k_3 (x_3 - \alpha_2) \right) \\
\alpha_2 &= -f_{10} + \dot{\alpha}_1 - k_2 z_2 - \hat{d}_1 \\
\alpha_1 &= \dot{x}_{1d} - k_1 (x_1 - x_{1d})
\end{aligned} \tag{5.47}$$

where tracking errors z_1, z_2, z_3 are given by $z_1 = x_1 - x_{1d}$, $z_2 = \hat{x}_2 - \alpha_1$, $z_3 = x_3 - \alpha_2$, respectively, and the nominal dynamical functions are presented as

$$\begin{aligned}
f_{10} &= -\frac{1}{J} B_0 \hat{x}_2 - \left(\tau_{c0} + \tau_{s0} e^{\left(\frac{|\hat{x}_2|}{\omega_s} \right)} \right) \tanh(c_f \hat{x}_2) \\
f_{20} &= -\frac{4D_m^2 \beta_{e0}}{J V_{t0}} \hat{x}_2 - \frac{4\beta_{e0} J C_{20}}{V_{t0} D_m} x_3 \\
g_{20} &= \frac{4\beta_{e0} k_{t0}}{V_{t0}} \sqrt{P_s - \text{sign}(u) \frac{J}{D_m} x_3}
\end{aligned}$$

To estimate the immeasurable angular velocity of the actuator and both lumped mismatched and matched disturbances, the two ESOs are designed as follows:

$$\begin{cases} \dot{\hat{x}}_1 = \hat{x}_2 + 3\omega_{e1}(x_1 - \hat{x}_1) \\ \dot{\hat{x}}_2 = x_3 + f_{10}(\hat{x}_2) + \hat{d}_1 + 3\omega_1^2(x_1 - \hat{x}_1) \\ \dot{\hat{d}}_1 = \omega_1^3(x_1 - \hat{x}_1) \\ \dot{\hat{x}}_3 = f_{20}(\hat{x}_2, x_3) + g_{20}(x_3, u)u + 2\omega_2(x_3 - \hat{x}_3) \\ \dot{\hat{d}}_2 = \omega_2^2(x_3 - \hat{x}_3) \end{cases} \quad (5.48)$$

where $f_{10}(x_2)$, $f_{20}(x_2, x_3)$, and $g_{20}(x_3, u)$ are nominal system dynamic functions using known nominal system parameters, ω_1 and ω_2 are the observer gains, \hat{d}_1 and \hat{d}_2 are the estimates of mismatched and matched disturbances, respectively, and \hat{x}_i is the estimated value of the system state x_i . The control parameters and observer gains are chosen as $k_1 = 450$, $k_2 = 350$, and $k_3 = 350$; $\omega_1 = 1000$ and $\omega_2 = 1000$, respectively, to achieve the tracking performance as well as possible without chattering issues. In this case, the nominal system parameters which are slightly different from the actual system parameters employed to design the backstepping control law are illustrated in Table 5-2.

Table 5-2 Nominal system parameters of the EHSS for backstepping control design.

Parameter (Unit)	Value	Parameter (Unit)	Value
B_0 (N·m·s·rad ⁻¹)	80	C_{20} (m ³ ·s ⁻¹)	0
β_{e0} (Pa)	7×10^8	k_{t0} (m ³ ·s ⁻¹ ·V ⁻¹ ·Pa ^{1/2})	1.0×10^{-8}
C_{00} (m ³ ·s ⁻¹ ·Pa ⁻²)	0	V_{t0} (m ³)	1.0×10^{-4}
C_{10} (m ³ ·s ⁻¹ ·Pa ⁻¹)	1.0×10^{-12}		

4) Proportional-Integral-Derivative (PID) controller with controller gains are manually tuned to achieve a tracking performance as good as possible without chattering in the control input as $K_p = 750$, $K_I = 500$, and $K_D = 0.02$.

The time-varying sinusoidal-like mismatched and matched disturbances $d_1(t)$ and $d_2(t)$ are intentionally injected into the control system for performance examination as follows:

$$\begin{cases} d_1(t) = 1.5 \times 10^3 \sin(\pi t) \quad (\text{rad} \cdot \text{s}^{-2}) \\ d_2(t) = 10^6 \sin(\pi t) \quad (\text{rad} \cdot \text{s}^{-3}) \end{cases} \quad (5.49)$$

where the magnitudes of these disturbances are chosen based on the specifications of the EHSS.

Performance indexes in the steady-state regime including the maximum, average, and standard deviation of the tracking errors [76] are used to measure the tracking qualifications of the above controllers. These terms are given by:

- Maximal absolute tracking error

$$M_e = \max_{i=1, \dots, N} \{ |e_1(i)| \} \quad (5.50)$$

where e_1 is the output tracking error and N denotes the number of samples.

- Average tracking error

$$\mu_e = \frac{1}{N} \sum_{i=1}^N |e_1(i)| \quad (5.51)$$

- Standard deviation of the tracking errors

$$\sigma_e = \sqrt{\frac{1}{N} \sum_{i=1}^N (|e_1(i)| - \mu_e)^2} \quad (5.52)$$

5.4.2 Simulation Results

a) *Slow-Motion Reference Trajectory*

In this case, the smooth reference trajectory is chosen to evaluate the effectiveness of the proposed controller as

$$x_{1d}(t) = \frac{\pi}{8} \left(1 - \cos\left(\frac{\pi}{2}t\right) \right) (1 - e^{-t}) \text{ (rad)} \quad (5.53)$$

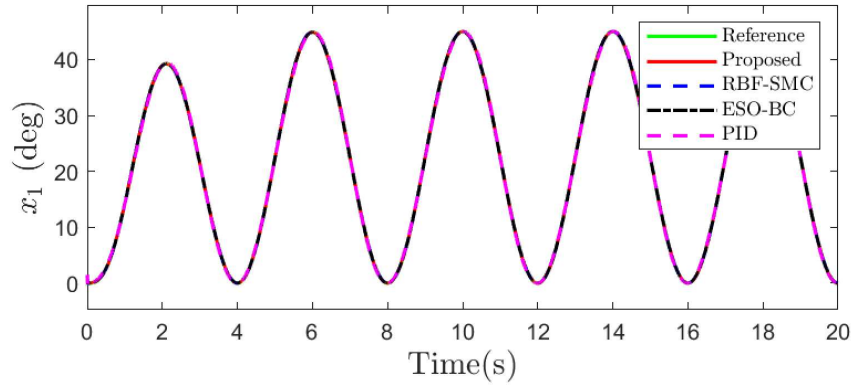


Fig. 5-2 The tracking performance of the proposed strategy compared with other control laws with slow-motion reference trajectory.

The tracking performances and tracking errors of all four controllers are depicted in Fig. 5-2 and Fig. 5-3, respectively. As shown in Fig. 5-2, all four controllers guarantee the system output tracks the desired trajectory at an acceptable level.

Nevertheless, from Fig. 5-3, it is obviously seen that the proposed controller performs better than others with the smallest tracking errors, whereas the ESO-BC controller can track the reference trajectory closer than RBF-SMC and PID controllers. For more details, the final tracking accuracies of all controllers are indicated via the three performance indexes given in Table 5-3. It is clear that, although having some robustness, the PID controller can do little with uncertainties and disturbances due to the lack of model-based compensation mechanisms. Consequently, it performs the worst tracking performance in all performance indexes (maximal value, average, and standard deviation of the tracking error are about 0.4684 degrees, 0.2169 degrees, and 0.1326 degrees, respectively). Meanwhile, with the support of ESOs (5.48), both mismatched and matched disturbances are estimated and efficiently compensated, based on that, the ESO-BC controller (maximal error of about 0.0315 degrees) achieves better tracking performance in comparison with the RBF-SMC controller (maximal error about 0.0358 degrees). It is noted that the maximal tracking error is only about 0.0148 degrees in the case of the proposed controller. The results demonstrate the effectiveness of the suggested control strategy in which the combination of DOBs and NNs is able to effectively deal with full unknown system dynamics and both mismatched and matched disturbances.

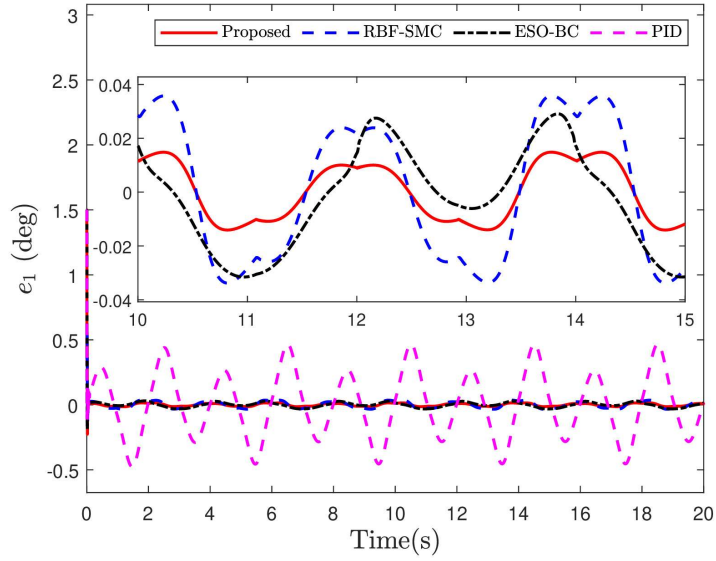


Fig. 5-3 The tracking errors of the considered four control strategies with slow-motion reference trajectory.

Table 5-3 Performance indexes in slow-motion reference trajectory of all considered controllers

Controller	M_e (degree)	μ_e (degree)	σ_e (degree)
Proposed Controller	0.0148	0.0097	0.0038
RBF-SMC Controller	0.0358	0.0233	0.0092
ESO-BC Controller	0.0315	0.0151	0.0104
PID Controller	0.4684	0.2169	0.1326

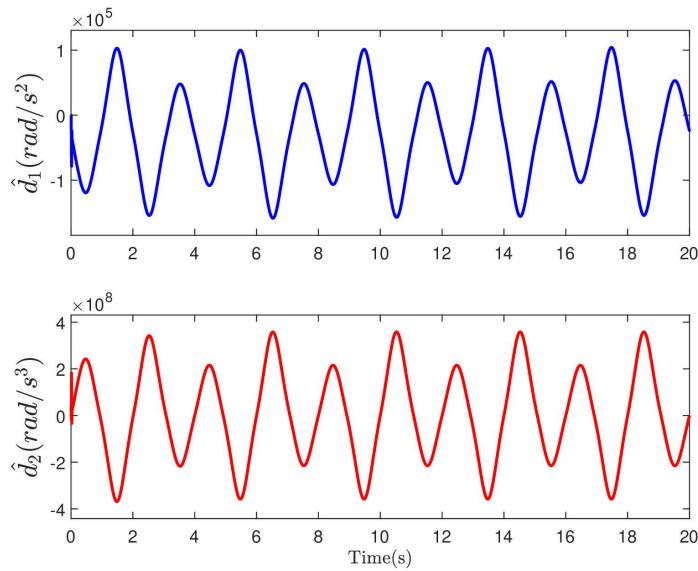


Fig. 5-4 The estimates of the mismatched and matched disturbances of the proposed method

The estimates of the mismatched and matched lumped disturbances and the weighting values of RBF NNs for approximating all unknown dynamic functions are illustrated in Fig. 5-4 and Fig. 5-5, respectively. It is noted that from Fig. 5-5, the weighting values of RBF NNs are smooth and bounded. Moreover, the estimates of both mismatched and matched disturbances have the same frequencies as the injected disturbances (5.49). However, they are not in sinusoidal shapes since the estimates of

disturbances also include the approximation errors of RBF NNs. The control inputs of all controllers are depicted in Fig. 5-6. With the same desired reference trajectory, the control input shapes of all controllers are relatively similar. The interesting thing is that the control input is generated without chattering by the proposed controller, which demonstrates the effectiveness of the combination between RBF NNs and DOBs in dealing with the problem of full model uncertainties and disturbance of the recommended control method.

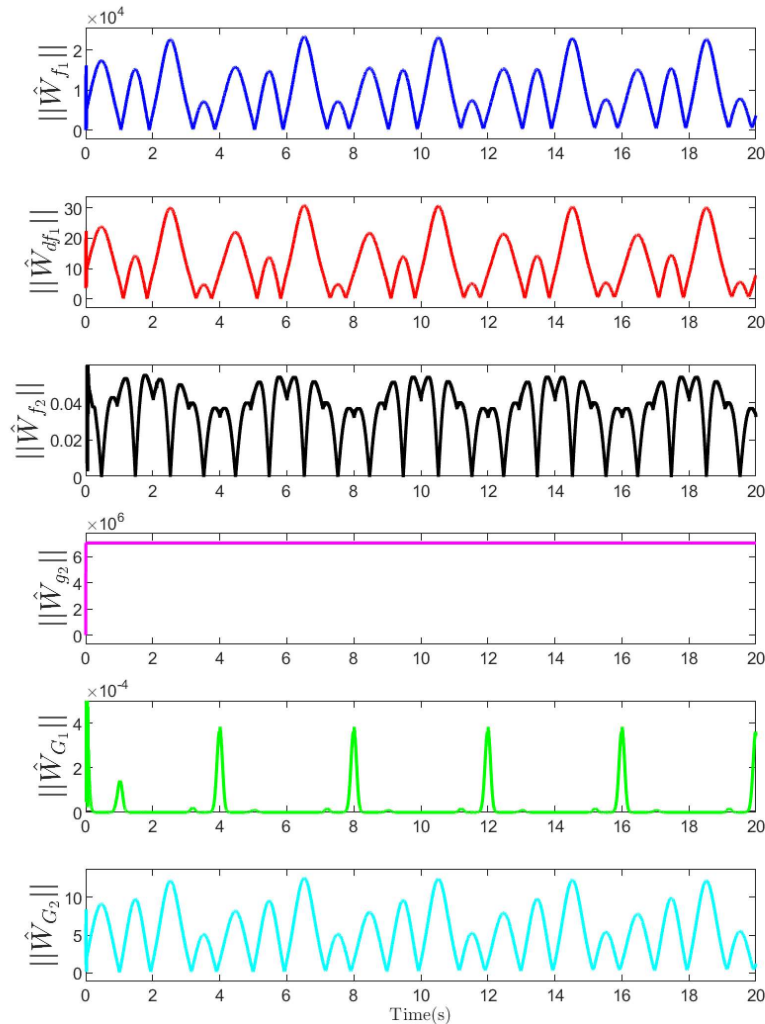


Fig. 5-5 The weighting values of RFB NNs employed of the proposed method.

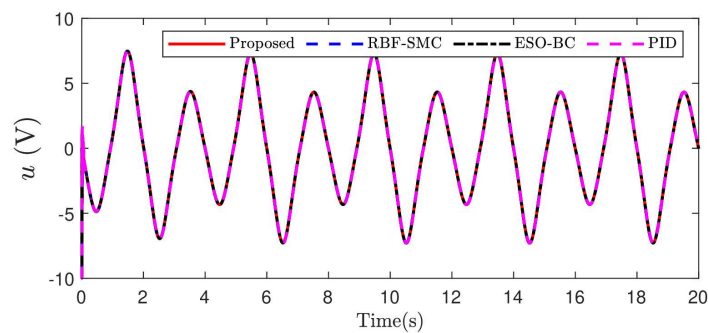


Fig. 5-6 The control signal of all controllers with slow-motion reference trajectory.

b) Fast-Motion Reference Trajectory

For further capability investigation of the suggested control algorithm, a smooth fast-motion reference trajectory is chosen as

$$x_{1d}(t) = \frac{\pi}{16}(1 - \cos(2\pi t))(1 - e^{-t}) \text{ (rad)} \quad (5.54)$$

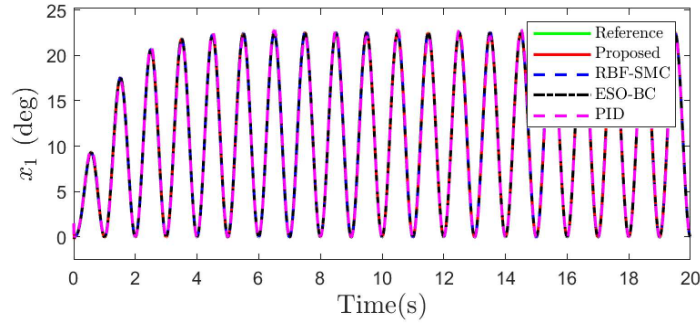


Fig. 5-7 The tracking performance of the proposed strategy compared with other control laws in fast-motion reference trajectory.

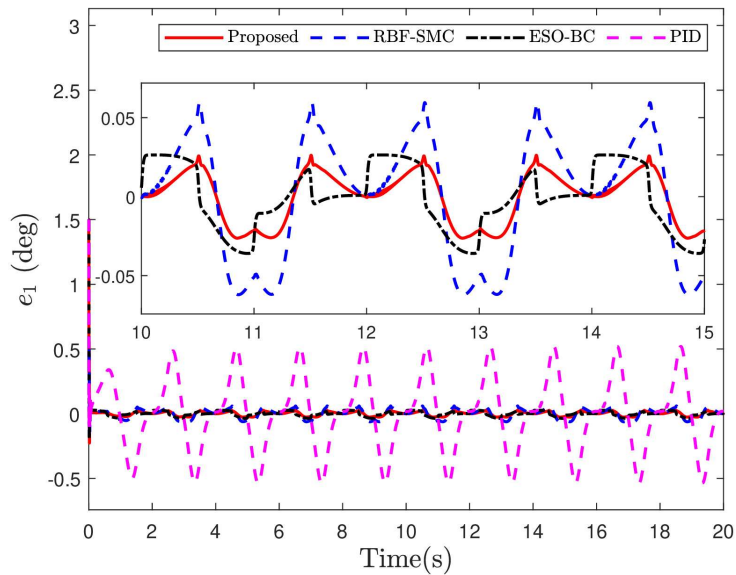


Fig. 5-8 The tracking errors of the four controllers in fast-motion reference trajectory.

The tracking characteristics of all controllers with the fast-motion reference trajectory are illustrated in Fig. 5-7. As in the above case, all controllers still follow the desired trajectory. Due to bandwidth limitations of EHSSs, the tracking errors of all control approaches depicted in Fig. 5-8 rise remarkably along with the increase in the frequency of reference trajectory. The tracking accuracies of all controllers in terms of the three performance indexes are illustrated in Table 5-4. As shown, the tracking performances of the PID controller and the RBF-SMC controller significantly degrade with the maximal final tracking errors are 0.5364 degrees and 0.0621 degrees, respectively. Meanwhile, the ESO-BC controller demonstrates robustness against uncertainties and disturbances based on the support of ESOs and known nominal system dynamics. However, it is worth noting that the proposed

controller tracks the reference trajectory more accurately than others. This once again demonstrates the effectiveness of the recommended method in dealing with full model uncertainties and disturbances.

Table 5-4 Performance indexes in fast-motion reference trajectory of all considered controllers

Controller	M_e (degree)	μ_e (degree)	σ_e (degree)
Proposed Controller	0.0148	0.0097	0.0038
RBF-SMC Controller	0.0358	0.0233	0.0092
ESO-BC Controller	0.0315	0.0151	0.0104 0
PID Controller	0.4684	0.2169	0.1326

5.5 Conclusions

In this chapter, adaptive robust control for the EHSS subject to completely unknown dynamics and disturbances based on RBF NNs and NN-based DOBs was proposed. For the first time, the combination of DOBs and RBF NNs was developed to effectively deal with both disturbances and completely unknown dynamics. In addition, the employment of the excessive switching gain of the controller was avoided; hence, the chattering issue was efficiently eliminated. The system stability was successfully proven by using the Lyapunov theory. The high-accuracy tracking performance achieved with several case studies demonstrated the effectiveness of the recommended control approach. In addition, the proposed method can be considered as a new framework dealing with control systems with limited knowledge about the system dynamics. Sophisticated control laws and experiments on a real test bench will be considered in further studies.

Chapter 6

EXTENDED SLIDING MODE OBSERVER-BASED OUTPUT FEEDBACK CONTROL FOR MOTION TRACKING OF ELECTRO- HYDROSTATIC ACTUATORS

6.1 Introduction

By means of some noteworthy features including high power density, great endurance, smooth operation, less maintenance, and precise control capability [198] compared with electric actuator-based drive systems, hydraulic actuators have become a great solution for heavy-duty industrial applications [199-201]. Being considered as one of the configurations of hydraulic systems, valve-operated actuation electro-hydraulic systems (VEHSs) or electrohydraulic servo systems (EHSSs) have some advantages, including fast response, smooth motion, and high controllability [202]. Nonetheless, there are some drawbacks of EHSSs, such as low energy efficiency because of high flow throttling loss, considerable system construction and maintenance cost, and they require more space for installation compared to the so-called pump-controlled EHSs or electro-hydrostatic actuators (EHAs) [20]. In addition, the pumping system in EHSSs must supply constant pressure to the system regardless of the working conditions, which contributes to electrical extravagance. Therefore, recently, EHAs with simple structures have been broadly adopted in various applications such as exoskeleton robots [203, 204], aerospace applications [205, 206], hydraulic robot manipulators [207], and so on [208] to avoid the aforementioned shortcomings of the EHSSs. However, the dynamic behaviors of EHAs are extremely complex and highly nonlinear. Achieving a high-accuracy tracking performance with such EHAs is a challenging control problem, particularly in the presence of modeling errors, unmodeled dynamics, and unknown external load.

To achieve a satisfactory tracking performance, numerous controllers have been introduced in the literature. It can be observed that proportional-integral-derivative (PID) controllers are the most commonly applied model-free controller in industrial applications due to their simplicity, easy implementation, and limited tuning parameters. In addition, the requirement for an accurate system model is mitigated and the stability of the closed-loop system can be guaranteed by applying this control law. However, the desired performance may not be satisfied because of the highly nonlinear factors such as complicated friction and pressure dynamics of EHAs, and unmodeled dynamics. To this end, advanced control techniques have been introduced to overcome this problem and achieve a high-accuracy tracking performance for pump-controlled EHSs. For example, in [209], an adaptive robust control using a backstepping framework was established for a pump-controlled hydraulic system. In this control scheme, a deterministic model of pump flow rate at low speeds based on experimental data was originally constructed and compensated in the controller design, and consequently, improved tracking performance was achieved. However, in practice, the parameters of the pump flow rate model can change depending on different working conditions; hence, the accuracy of this model can be reduced. To overcome this drawback, an adaptive nonlinear pump flow model [210] was formulated, and better tracking performance was obtained as a result. For further improvement of tracking accuracy, in [211], Chen Li et al. developed an adaptive robust control framework of an independent metering hydraulic system by introducing a nonlinear valve flow model. To enhance the convergence speed of the adaptation parameter, a composite learning adaptive motion following control for electro-hydraulic servo systems was constructed [212]. Nonetheless, it should be noted that there are two major disadvantages of the above-mentioned control approaches. Firstly, all system states are assumed to be directly measured, many sensors are required, and system cost and

structure complexity increase as a consequence. In addition, uncertainties are compensated by adaptive methods under the assumption that the exact model of the considered hydraulic system is available.

Disturbance and uncertainty attenuation for motion tracking problems has attracted great attention from the research community to improve the control accuracy and the robustness of the closed-loop control system of EHSs. To cope with state-dependent unstructured uncertainties, adaptive approximators based on neural network or fuzzy logic system approaches have been utilized [90, 150, 213, 214]. Nevertheless, due to the complexity of excessive tuning parameters, expert knowledge requirements, and heavy computational burden, these approaches are difficult to implement in practical systems. On the other hand, they are no longer available for state-independent uncertainties. As one of the valuable solutions to this problem, disturbance observers (DOBs) have been carefully studied and successfully applied to EHSs to lessen the adverse effects of model uncertainties and external disturbances. Specifically, in [69, 97, 215], high-gain disturbance observers (HGDOBs) were developed for estimating lumped uncertainties in an EHSS, then their estimated values were fed back into backstepping control laws to compensate for their influences on the position-tracking capability. Furthermore, a coupled DOB [70] was designed to attenuate the independent and coupled elements of external load on hydraulic actuators of multi-degree-of-freedom manipulators. Based on that, the tracking errors were constrained within a prescribed steady-state level. In addition, Hamid Razmjooei et al. developed estimation error-based DOBs to counteract uncertainties and estimation errors of state observers and guarantee finite-time tracking performance [156]. However, it is worth noting that all system states are required to be accessible to implement the above control algorithms, and this requirement may complicate the control system structure and increase the system cost as a result.

Considering the shortage of system states and negative effects of model uncertainties, inherited from the Luenberger observer [51, 52], a linear extended state observer (LESO), which was first introduced by Jingqing Han [73], can be considered a great solution. The convergence of an ESO for nonlinear systems subject to uncertainties was rigorously proven in [216]. ESO does not require an exact system model, and the burden of an offline identification process can be reduced [217]. Because of such a favorable feature, ESO-based control approaches, which are known as active disturbance rejection control (ADRC) schemes, have been widely employed in various engineering systems in recent years. However, for nonlinear systems subject to the so-called mismatched uncertainties, ESO-based control algorithms are no longer available. To this end, in [218], a generalized ESO-based control for systems with mismatched uncertainties was introduced. To improve the convergence time of the conventional ESO, a novel ESO [219, 220], employing nonlinear and/or switching terms that ensure the estimation errors converge to a neighborhood of the origin in finite time, was put forward. Although conventional ESOs have been successfully adopted in various applications in recent years, they have several disadvantages, such as the peaking phenomenon, insufficient estimation accuracy, and long convergence time. Inheriting from sliding mode observer (SMO), recently, ESMOs have been successfully implemented in several applications. For instance, in [173], an ESMO was constructed for current control of permanent magnet synchronous motor systems to estimate the stator current and lumped disturbance. Jinyong Yu et al. proposed a fault-tolerant control based on an ESMO that is introduced to estimate states and faults of descriptor stochastic systems [175]. However, as far as the authors know, the development of an ESMO for high-order pump-controlled EHSs to estimate not only immeasurable states but also modeling uncertainties has not been considered in the literature.

Inspired by the above observations, in this chapter, a novel output feedback control scheme for motion tracking of an EHA suffering from model uncertainties, unknown dynamics, and external load was presented. The main innovations of this study are summarized as follows:

1) For the first time, an ESMO based on a system model was constructed to estimate immeasurable system states, i.e., angular velocity and load pressure, and lumped matched disturbance in the pressure dynamics caused by parameter deviations and modeling errors.

2) Based on the designed ESMO, a novel output feedback robust control scheme using the backstepping control framework and dynamic surface control technique is synthesized for the motion-tracking problem of the studied EHA.

3) The stability of the ESMO and the overall closed-loop system is theoretically verified by the Lyapunov theory. Experiments on the real test bench are conducted to illustrate the practicability and advantage of the suggested controller in comparison with some reference methods under various working scenarios.

The rest of this chapter is organized as follows. In Section 2, the development of the ESMO and observer-based output feedback control approach are provided. Section 3 presents comparative experiment results of the proposed control algorithm and several reference controllers. Finally, a conclusion is given in Section 4.

6.2 Observer-Based Output Feedback Control Design

The proposed control methodology is illustrated in Fig. 6-1. In this control scheme, an ESMO is designed to estimate immeasurable states and lumped disturbance simultaneously. Based on the state estimates of the ESMO, an observer is then developed to reconstruct the lumped mismatched disturbance. To achieve desired tracking performance, an output feedback controller is designed using the backstepping control technique combined with the DSC approach, in which estimated values of immeasurable states and disturbances are fed back into the system, and consequently their influences on the system output tracking qualification are effectively attenuated.

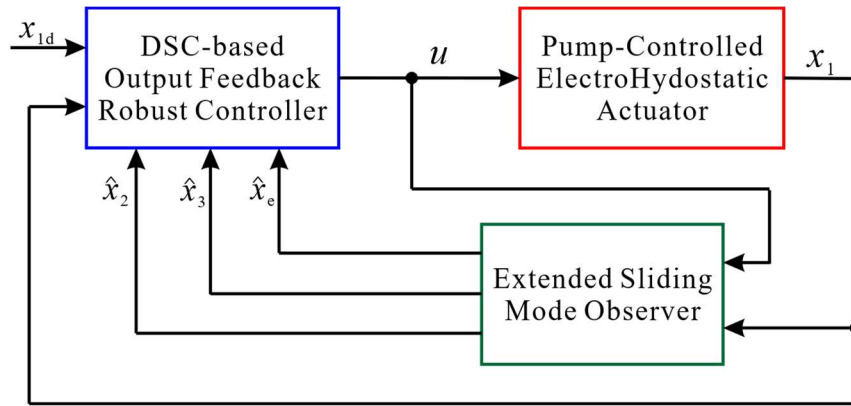


Fig. 6-1: The control structure of the proposed method.

6.2.1 Extended Sliding Mode Observer

Considering the system dynamics (2.15) by defining $x_{e1} \triangleq d_2(t)$ as an extended state, augmented system dynamics are obtained as

$$\begin{cases} \dot{x}_1 = x_2 \\ \dot{x}_2 = x_3 + f_2(x_2) + d_1(t) \\ \dot{x}_3 = g_3(x_1)u + f_3(x_2, x_3) + x_{e1} \\ \dot{x}_{e1} = h_2(t) \end{cases} \quad (6.1)$$

An extended sliding mode observer is constructed as

$$\begin{cases} v_{eq} = \eta \text{sign}(x_1 - \hat{x}_1) \\ \dot{\hat{x}}_1 = \hat{x}_2 + v_{eq} \\ \dot{\hat{x}}_2 = \hat{x}_3 + f_1(\hat{x}_2) + 3\omega v_{eq} \\ \dot{\hat{x}}_3 = f_2(\hat{\mathbf{x}}) + \mathbf{g}_2(x_1)u + \hat{x}_e + 3\omega^2 v_{eq} \\ \dot{\hat{x}}_e = \omega^3 v_{eq} \end{cases} \quad (6.2)$$

where $\eta > 0$ is the switching gain, $\omega > 0$ is the bandwidth of the observer to be selected, and $\text{sign}(\cdot)$ is the standard signum function. \hat{x}_1 , \hat{x}_2 , \hat{x}_3 , and \hat{x}_e are the estimates of x_1 , x_2 , x_3 , and x_e , respectively.

Theorem 6-1: Noting the system dynamics (6.1), by appropriately choosing the switching gain η , the proposed ESMO (6.2) guarantees that the estimation errors, i.e., $\tilde{x}_1 = x_1 - \hat{x}_1$, $\tilde{x}_2 = x_2 - \hat{x}_2$, $\tilde{x}_3 = x_3 - \hat{x}_3$, and $\tilde{x}_e = x_e - \hat{x}_e$, exponentially converge to an arbitrarily small bounded region depending on the selection of the observer bandwidth ω .

Proof of Theorem 6-1: Choose a candidate Lyapunov function:

$$V_{\tilde{x}_1} = 0.5\tilde{x}_1^2 \quad (6.3)$$

Taking the time derivative of it leads to

$$\dot{V}_{\tilde{x}_1} = \tilde{x}_1(\dot{x}_1 - \dot{\hat{x}}_1) \quad (6.4)$$

Combining with (6.1) and (6.2), (6.4) can be transformed into

$$\begin{aligned} \dot{V}_{\tilde{x}_1} &= \tilde{x}_1(\tilde{x}_2 - \eta \text{sign}(\tilde{x}_1)) \\ &\leq -(\eta - |\tilde{x}_2|)|\tilde{x}_1| = -\eta_0 \sqrt{2} V_{\tilde{x}_1}^{1/2} \end{aligned} \quad (6.5)$$

From (6.5), it can be observed that if the switching gain η is chosen such that $\eta = \eta_0 + |\tilde{x}_2(0)|$ with η_0 as a small positive constant, the estimation error \tilde{x}_1 converges to the origin in finite time and it remains at the origin thereafter.

Hence, in the sliding mode, i.e., $\tilde{x}_2 = v_{eq}$, the reduced-order dynamics of the observer (6.2) can be obtained as

$$\begin{cases} \dot{\tilde{x}}_2 = \hat{x}_3 + f_1(\hat{x}_2) + 3\omega \tilde{x}_2 \\ \dot{\tilde{x}}_3 = f_2(x_1, \hat{x}_2, \hat{x}_3) + \mathbf{g}_2(x_1)u + \hat{x}_e + 3\omega^2 \tilde{x}_2 \\ \dot{\tilde{x}}_e = \omega^3 \tilde{x}_2 \end{cases} \quad (6.6)$$

For the sake of concise expression, d_1 , d_2 , and h_2 are used for upcoming mathematical transformations instead of using $d_1(\mathbf{x}, t)$, $d_2(\mathbf{x}, t)$, and $h_2(\mathbf{x}, t)$. Noting the system dynamics (6.1) and the reduced-order dynamics (6.6) the error dynamics are derived as

$$\begin{cases} \dot{\tilde{x}}_2 = -3\omega \tilde{x}_2 + \tilde{x}_3 + \tilde{f}_1 + d_1 \\ \dot{\tilde{x}}_3 = -3\omega^2 \tilde{x}_2 + \tilde{x}_e + \tilde{f}_2 \\ \dot{\tilde{x}}_e = -\omega^3 \tilde{x}_2 + h_2 \end{cases} \quad (6.7)$$

where

$$\begin{cases} \tilde{f}_1 = f_1(x_2) - f_1(\hat{x}_2) \\ \tilde{f}_2 = f_2(x_1, x_2, x_3) - f_2(x_1, \hat{x}_2, \hat{x}_3) \end{cases} \quad (6.8)$$

Letting $\boldsymbol{\varepsilon} = [\varepsilon_1, \varepsilon_2, \varepsilon_3]^T = [\tilde{x}_2, \tilde{x}_3 / \omega, \tilde{x}_e / \omega]^T$ as the scaled estimation error vector, (6.7) can be rewritten as

$$\dot{\boldsymbol{\varepsilon}} = -\omega \mathbf{A} \boldsymbol{\varepsilon} + \mathbf{B}(\tilde{f}_1 + d_1) + \mathbf{C} \frac{\tilde{f}_2}{\omega} + \mathbf{D} \frac{h_2}{\omega^2} \quad (6.9)$$

where the matrices \mathbf{A} , \mathbf{B} , \mathbf{C} , and \mathbf{D} are defined by

$$\mathbf{A} = \begin{bmatrix} -3 & 1 & 0 \\ -3 & 0 & 1 \\ -1 & 0 & 0 \end{bmatrix}; \mathbf{B} = \begin{bmatrix} 1 \\ 0 \\ 0 \end{bmatrix}; \mathbf{C} = \begin{bmatrix} 0 \\ 1 \\ 0 \end{bmatrix}; \mathbf{D} = \begin{bmatrix} 0 \\ 0 \\ 1 \end{bmatrix} \quad (6.10)$$

Since matrix \mathbf{A} is Hurwitz, for any positive definite matrix \mathbf{Q} , there always exists a positive definite matrix \mathbf{P} satisfying the following Lyapunov function:

$$\mathbf{A}^T \mathbf{P} + \mathbf{P} \mathbf{A} = -2\mathbf{Q} \quad (6.11)$$

Selecting a candidate Lyapunov function $V_{ESMO} = \frac{1}{2} \boldsymbol{\varepsilon}^T \mathbf{P} \boldsymbol{\varepsilon}$, then taking the time derivative of it yields

$$\begin{aligned} \dot{V}_{ESMO} &= \frac{1}{2} \dot{\boldsymbol{\varepsilon}}^T \mathbf{P} \boldsymbol{\varepsilon} + \frac{1}{2} \boldsymbol{\varepsilon}^T \mathbf{P} \dot{\boldsymbol{\varepsilon}} \\ &= -\omega \boldsymbol{\varepsilon}^T \mathbf{Q} \boldsymbol{\varepsilon} + \boldsymbol{\varepsilon}^T \mathbf{P} \mathbf{B}(\tilde{f}_1 + d_1) + \boldsymbol{\varepsilon}^T \mathbf{P} \mathbf{C} \frac{\tilde{f}_2}{\omega} + \boldsymbol{\varepsilon}^T \mathbf{P} \mathbf{D} \frac{h_2}{\omega^2} \end{aligned} \quad (6.12)$$

Applying the Young's inequality, one has

$$\begin{aligned} \boldsymbol{\varepsilon}^T \mathbf{P} \mathbf{B} \tilde{f}_1 &\leq \frac{1}{2} \boldsymbol{\varepsilon}^T \boldsymbol{\varepsilon} + \frac{1}{2} \mathbf{B}^T \mathbf{P}^T \mathbf{P} \mathbf{B} \tilde{f}_1^2 \\ \boldsymbol{\varepsilon}^T \mathbf{P} \mathbf{B} d_1 &\leq \frac{1}{2} \boldsymbol{\varepsilon}^T \boldsymbol{\varepsilon} + \frac{1}{2} \mathbf{B}^T \mathbf{P}^T \mathbf{P} \mathbf{B} d_1^2 \\ \boldsymbol{\varepsilon}^T \mathbf{P} \mathbf{C} \frac{\tilde{f}_2}{\omega} &\leq \frac{1}{2} \boldsymbol{\varepsilon}^T \boldsymbol{\varepsilon} + \frac{1}{2} \mathbf{C}^T \mathbf{P}^T \mathbf{P} \mathbf{C} \frac{\tilde{f}_2^2}{\omega^2} \\ \boldsymbol{\varepsilon}^T \mathbf{P} \mathbf{D} \frac{h_2}{\omega^2} &\leq \frac{1}{2} \boldsymbol{\varepsilon}^T \boldsymbol{\varepsilon} + \frac{1}{2} \mathbf{D}^T \mathbf{P}^T \mathbf{P} \mathbf{D} \frac{h_2^2}{\omega^4} \end{aligned} \quad (6.13)$$

From Assumption 2-5 and combining with the definition of scaled estimation errors, we have

$$\begin{cases} |\tilde{f}_1| \leq \frac{C_1}{\omega} \|\boldsymbol{\varepsilon}\| \\ |\tilde{f}_2| \leq \left(\frac{C_2}{\omega} + \frac{C_3}{\omega^2} \right) \|\boldsymbol{\varepsilon}\| \end{cases} \quad (6.14)$$

where C_1 , C_2 , and C_3 are Lipschitz constants.

Hence, (6.12) is transformed into

$$\begin{aligned}\dot{V}_{ESMO} &\leq -\left(\omega\lambda_{\min}\{\mathbf{Q}\} - 2 - \frac{\lambda_1 C_1^2}{2\omega^2} - \frac{\lambda_2}{2}\left(\frac{C_2}{\omega} + \frac{C_3}{\omega^2}\right)^2\right)\boldsymbol{\varepsilon}^T \boldsymbol{\varepsilon} + \left(\frac{\lambda_2 \delta_1^2}{\omega} + \frac{\lambda_3 \gamma_2^2}{\omega^4}\right) \\ &= -\Gamma_{ESMO} V_{ESMO} + \Pi_{ESMO}\end{aligned}\quad (6.15)$$

where $\lambda_1 = \|\mathbf{PB}\|^2$, $\lambda_2 = \|\mathbf{PC}\|^2$, $\lambda_3 = \|\mathbf{PD}\|^2$ with $\|\vartheta\|$ as the Euclidean norm of ϑ , and

$$\begin{aligned}\Gamma_{ESMO} &= -\frac{1}{\lambda_{\max}\{\mathbf{P}\}}\left(\omega\lambda_{\min}\{\mathbf{Q}\} - 2 - \frac{\lambda_1 C_1^2}{2\omega^2} - \frac{\lambda_2}{2}\left(\frac{C_2}{\omega} + \frac{C_3}{\omega^2}\right)^2\right) \\ \Pi_{ESMO} &= \frac{\lambda_2 \delta_1^2}{\omega} + \frac{\lambda_3 \gamma_2^2}{\omega^4}\end{aligned}$$

where $\lambda_{\min}\{\chi\}$ and $\lambda_{\max}\{\chi\}$ denote the maximal and minimal eigenvalues of matrix χ , respectively.

According to (6.15), the estimation errors exponentially converge to the neighborhood of the origin defined by $\Pi_{ESMO} / \Gamma_{ESMO}$ when time goes to infinity. The upper bound of this region decreases if the observer bandwidth decreases and vice versa.

This completes the proof of Theorem 6-1.

Remark 6-1: To reduce the chattering in the estimated values of both unmeasured states and lumped disturbance caused by unmodeled dynamics and modeling errors, a hyperbolic tangent function is adopted to replace the discontinuous “sign” function in the design of the observer. In addition, the observer bandwidth should be meticulously selected to achieve a trade-off between accurate estimation and reducing negative effects of measurement noise.

6.2.2 Observer-Based Control Design

We define tracking errors as

$$e_1 = x_1 - x_{1d}; e_2 = \hat{x}_2 - \alpha_{1f}; e_3 = \hat{x}_3 - \alpha_{2f} \quad (6.16)$$

where x_{1d} is the reference motion trajectory, and α_{1f} and α_{2f} are filtered signals of virtual control laws α_1 and α_2 to be designed using the traditional backstepping control framework, respectively, through the following low-pass filters.

The command filters are constructed as

$$\begin{cases} T_1 \dot{\alpha}_{1f} + \alpha_{1f} = \alpha_1; \alpha_{1f}(0) = \alpha_1(0) \\ T_2 \dot{\alpha}_{2f} + \alpha_{2f} = \alpha_2; \alpha_{2f}(0) = \alpha_2(0) \end{cases} \quad (6.17)$$

where T_1 and T_2 are the time constants defining the cut-off frequencies of the designed filters.

Defining $\tilde{\alpha}_i = \alpha_{if} - \alpha_i$ with $i = 1, 2$ as the deviations between the original virtual control laws and their filtered signals, the dynamics of the filtering errors are obtained as

$$\dot{\tilde{\alpha}}_i = -\frac{1}{T_i}(\tilde{\alpha}_i + \rho_i) \quad (6.18)$$

where $\rho_i = -\dot{\alpha}_i$ is assumed to be bounded by an unknown constant, i.e., $|\rho_i| \leq \rho_{iM}$.

Remark 6-2: By applying a series of first-order low-pass filters (6.17), influences of measurement noise can be mitigated. In addition, the derivative of the filtered signals can be directly computed;

hence, the requirement of computing analytic derivations of virtual control laws at backstepping iterations is effectively relaxed.

The control laws for stabilizing the closed-loop system are designed as

$$\begin{aligned}\alpha_1 &= -k_1 e_1 + \dot{x}_{1d} - v_{eq} \\ \alpha_2 &= -k_2 e_2 - e_1 - f_1(\hat{x}_2) + \dot{\alpha}_{1f} - 3\omega v_{eq} \\ u &= \frac{1}{g_2(x_1)} (-k_3 e_3 - e_2 - f_2(x_1, \hat{x}_2, \hat{x}_3) - \hat{x}_e - 3\omega^2 v_{eq})\end{aligned}\quad (6.19)$$

Noting the system dynamics (2.15), definition of tracking errors (6.16), and synthesized control laws (6.19), the tracking error dynamics of the closed-loop system are given by

$$\begin{cases} \dot{e}_1 = -k_1 e_1 + e_2 + \tilde{\alpha}_1 \\ \dot{e}_2 = -k_2 e_2 - e_1 + e_3 + \tilde{\alpha}_2 \\ \dot{e}_3 = -k_3 e_3 - e_2 \end{cases}\quad (6.20)$$

6.2.3 Closed-Loop Stability Analysis

Theorem 6-2: Considering the system dynamics (2.15) under Assumptions 2-4, 2-5, and 2-6, an ultimately uniformly bounded (UUB) tracking performance is guaranteed by using control laws (6.19) and observer (6.2), that is, the tracking errors converge to an arbitrarily small vicinity of the origin whose upper bounds depend on the selection of control gains k_1 , k_2 , and k_3 ; observer bandwidth ω ; and time constants T_1 and T_2 as time goes to infinity.

Proof of Theorem 6-2: For analyzing the stability of the closed-loop system, a candidate Lyapunov function is chosen as

$$V_c = \frac{1}{2} \mathbf{e}^T \mathbf{e} + \frac{1}{2} \tilde{\mathbf{a}}^T \tilde{\mathbf{a}} + \frac{1}{2} \boldsymbol{\varepsilon}^T \mathbf{P} \boldsymbol{\varepsilon}\quad (6.21)$$

where $\mathbf{e} = [e_1, e_2, e_3]^T$ and $\tilde{\mathbf{a}} = [\tilde{\alpha}_1, \tilde{\alpha}_2]^T$.

Taking the time derivative of (6.21) then combining with (6.18) and (6.20), we have

$$\dot{V}_c = -k_1 e_1^2 - k_2 e_2^2 - k_3 e_3^2 - \frac{1}{T_1} \tilde{\alpha}_1^2 - \frac{1}{T_2} \tilde{\alpha}_2^2 + e_1 \tilde{\alpha}_1 + e_2 \tilde{\alpha}_2 + \alpha_1 \rho_1 + \alpha_2 \rho_2 + \dot{V}_{ESMO}\quad (6.22)$$

Applying the Young's inequality, one has

$$\begin{aligned}\dot{V}_c &\leq -\left(k_1 - \frac{1}{2}\right) e_1^2 - \left(k_2 - \frac{1}{2}\right) e_2^2 - \left(k_3 - \frac{1}{2}\right) e_3^2 \\ &\quad - \left(\frac{1}{T_1} - 1\right) \tilde{\alpha}_1^2 - \left(\frac{1}{T_2} - 1\right) \tilde{\alpha}_2^2 + \frac{\rho_{1M}^2}{2} + \frac{\rho_{2M}^2}{2} + \dot{V}_{ESMO}\end{aligned}\quad (6.23)$$

Substituting (6.15) into (6.23) leads to

$$\begin{aligned}\dot{V}_c &\leq -\mathbf{e}^T \mathbf{K} \mathbf{e} - \tilde{\mathbf{a}}^T \mathbf{T} \tilde{\mathbf{a}} - \frac{\Gamma_{ESMO}}{2} \boldsymbol{\varepsilon}^T \mathbf{P} \boldsymbol{\varepsilon} + \frac{\rho_{1M}}{2} + \frac{\rho_{2M}}{2} + \Pi_{ESMO} \\ &= -\Gamma_c V_c + \Pi_c\end{aligned}\quad (6.24)$$

where the matrices \mathbf{K} and \mathbf{T} are defined by

$$\mathbf{K} = \text{diag} \left\{ k_1 - \frac{1}{2}; k_2 - \frac{1}{2}; k_3 - \frac{1}{2} \right\}$$

$$\mathbf{T} = \text{diag} \left\{ \frac{1}{T_1} - 1; \frac{1}{T_2} - 1 \right\}$$

and

$$\Gamma_c = \min \left\{ 2\lambda_{\min} \{ \mathbf{K} \}; 2\lambda_{\min} \{ \mathbf{T} \}; \Gamma_{ESMO} \right\}$$

$$\Pi_c = \Pi_{ESMO} + \frac{\rho_{1M}^2}{2} + \frac{\rho_{2M}^2}{2}$$
(6.25)

From (6.24), it can be observed that when time goes to infinity, the Lyapunov function (6.21) converges to a region defined by Π_c / Γ_c as time goes to infinity, and consequently a UUB performance can be achieved. The upper bound of this region depends on the selection of observer bandwidth, controller gains, and time constants of the low-pass filters.

Hence, the proof of Theorem 6-2 is completed.

6.3 Experiment Validation

6.3.1 Experiment Setup

For the performance evaluation of the recommended control method, a test rig for an electro-hydrostatic actuator was built, which is illustrated in Fig. 6-2. It includes a compact hydraulic power pack, a rotary actuator, and an incremental encoder. The rotary actuator is provided by KNR company. To control the motion of the actuator, a bidirectional hydraulic pump was adopted and it is driven by a DC motor with the motor driver MD03, whose output voltage can be controlled by various types of input signals or communication. An incremental encoder E40H8-5000-3-V-5 with the resolution as 5000 pulses per revolution was installed so as to precisely observe the position of the actuator. Pilot check valves and relief valves are integrated into a center block to manipulate the oil flow into or out of the actuator and ensure that the system pressure inside the actuator does not exceed the predefined maximum pressure, respectively. In addition, a pulley system fixed to the frame of the test bed was directly attached to the actuator shaft and a load stand. Based on this, loads can be easily changed to evaluate the tracking performance of comparative controllers under different load conditions.

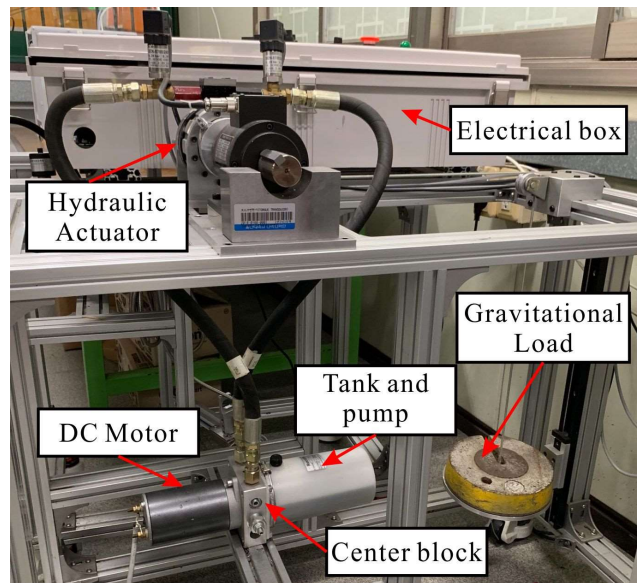


Fig. 6-2: The experimental platform of the studied electro-hydrostatic actuator.

The system parameters which were experimentally identified are given in Table 6-1. These parameters were used to design not only the main controller but also the observer. A smooth friction model is employed as $S_f(x_2) = \tanh(\tau_1 x_2) - \tanh(\tau_2 x_2)$ that is able to capture the Stribeck effect and static friction at the very low motion speed of the actuator with $\tau_1 = 100$ and $\tau_2 = 5$.

Table 6-1 The parameters of the studied EHA.

Parameter	Notation	Value	SI Unit
Viscous friction coefficient of the actuator	\bar{B}_f	50	$\text{N} \cdot \text{m} \cdot \text{rad}^{-1} \cdot \text{s}$
Coulomb friction coefficient of the actuator	\bar{A}_f	45	$\text{N} \cdot \text{m}$
Moment of inertia of the actuator	\bar{J}_A	0.15	$\text{kg} \cdot \text{m}^2$
Hydraulic actuator displacement	\bar{D}_A	5.8442×10^{-6}	$\text{m}^3 \cdot \text{rad}^{-1}$
Hydraulic pump displacement	\bar{D}_P	0.1544×10^{-7}	$\text{m}^3 \cdot \text{rad}^{-1}$
Effective bulk modulus of the hydraulic oil	$\bar{\beta}_e$	1.5×10^9	$\text{N} \cdot \text{m}^{-2}$ or Pa
Total leakage coefficient	\bar{C}_t	4.267×10^{-12}	$\text{m}^3 \cdot \text{s}^{-1} \cdot \text{Pa}^{-1}$
Initial control volume of the forward chamber	\bar{V}_{01}	1.25×10^{-5}	m^3
Initial control volume of the reverse chamber	\bar{V}_{02}	2.27×10^{-5}	m^3

To verify the effectiveness of the proposed method, the following controllers are adopted for comparison:

1) ESMOBC: The proposed controller, whose control gains are chosen as $k_1 = 80$, $k_2 = 505$, $k_3 = 30$. The time constants of the low-pass filters are $T_1 = T_2 = 0.01$ and the observer bandwidth is $\omega = 120$.

2) PID: Proportional-derivative-integral controller (PID), whose controller gains are ultimately selected as $K_p = 2.25 \times 10^3$, $K_i = 1.25 \times 10^2$, and $K_d = 11.5$. The larger gains would cause the closed-loop system to be unstable due to measurement noise and unmodeled dynamics.

3) PIDVFF [20]: Velocity feed-forward-based proportional-derivative-integral controller (PIDVFF), whose PID gains are chosen as the same as the above PID controller, and the velocity feed-forward coefficient is selected as $K_v = 1.15 \times 10^2$.

4) STW [221]: Super-twisting-based controller, whose structure is designed as

$$\begin{cases} \dot{u} = l_1 |x_1 - x_{1d}|^{1/2} \text{sign}(x_1 - x_{1d}) + v \\ \dot{v} = l_2 \text{sign}(x_1 - x_{1d}) \end{cases} \quad (6.26)$$

where $l_1 = 4.58 \times 10^2$ and $l_2 = 15$.

Remark 6-3: For a fair comparison, controller gains of the compared model-free controllers are first selected to guarantee that the closed-loop system is stable. As far as we know, the PID controller can be considered as the most popular controller in real-life applications because of its simplicity and limited tuning parameters. Hence, it can be treated as a reference controller for comparison. In addition, to improve the tracking performance by using the traditional PID controller, PIDVFF was commonly used for motion tracking problems by virtue of a feed-forward term which is proportional to the derivative of the desired trajectory. Furthermore, an STW controller was proven to be an effective control algorithm for systems subject to uncertainties and disturbances [222].

Performance indexes, including the maximum, average, and standard deviation of the tracking errors, are employed to assess the tracking accuracy of each control algorithm in the steady state. Their mathematical formulas are given as follows:

1) Maximal tracking error is defined as

$$M_e = \max_{i=1, \dots, N} \{|e_1(i)|\} \quad (6.27)$$

where N is the number of samples that are used for evaluation.

2) Average tracking error is computed as

$$\mu_e = \frac{1}{N} \sum_{i=1}^N |e_1(i)| \quad (6.28)$$

3) The standard deviation of the tracking errors is formulated as

$$\sigma_e = \sqrt{\frac{1}{N} \sum_{i=1}^N (|e_1(i)| - \mu_e)^2} \quad (6.29)$$

6.3.2 Experiment Results

a) *Slow-Motion Reference Trajectory under Light-Load Condition*

To demonstrate the performance of the proposed controller, the four considered controllers were first evaluated with the slow-motion reference trajectory that is mathematically formulated as $x_{1d}(t) = 30\sin(0.1\pi t - \pi/2) + 35(^{\circ})$ and a gravitational load as $m = 1$ kg.

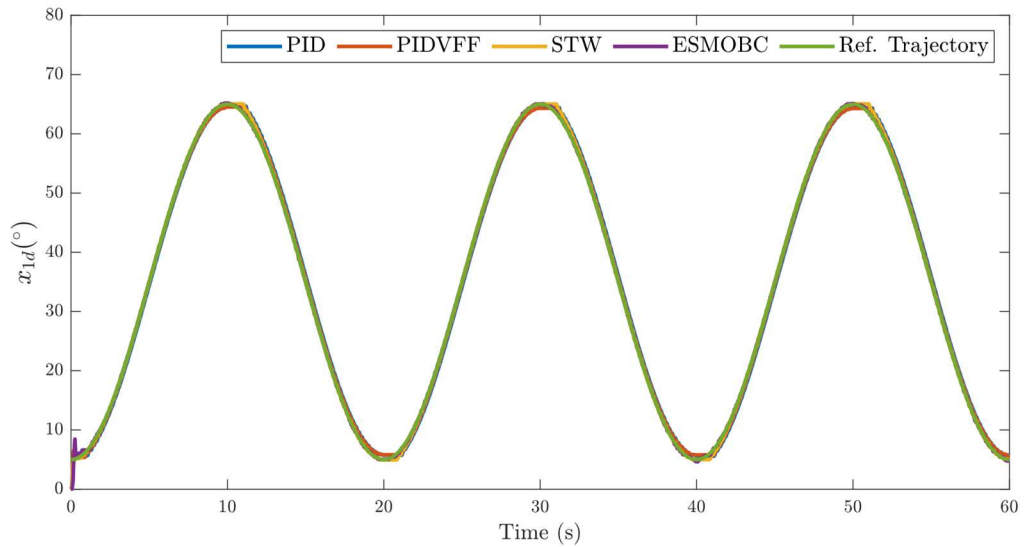


Fig. 6-3: Tracking performances of the compared controllers with the slow-motion reference trajectory and low-load condition.

The angular positions of the hydraulic actuator and desired trajectory are illustrated in Fig. 6-3. It can be seen from this figure that the proposed controller and high-gain model-free control approaches are able to guarantee that the system output tracks the reference trajectory at an acceptable level despite the nonlinearities and model uncertainties that naturally exist in the dynamics of the considered EHA. The tracking errors caused by the compared controllers are depicted in Fig. 6-4. As shown, the tracking errors significantly increase when the actuator changes the motion direction due to the friction between the vanes of the actuator and its frame and the load force applied to the actuator shaft. In the

transient time, because of the deviations between the actual states and their estimated values, the peaking value of the tracking error generated by the ESMOBC is remarkably higher than the others as a consequence. However, in the steady-state regime, it is worth noting that due to the highly nonlinear behaviors of the EHA and the lack of model compensation mechanisms, the model-free controllers generate considerably larger tracking errors compared to the ESMOBC controller.

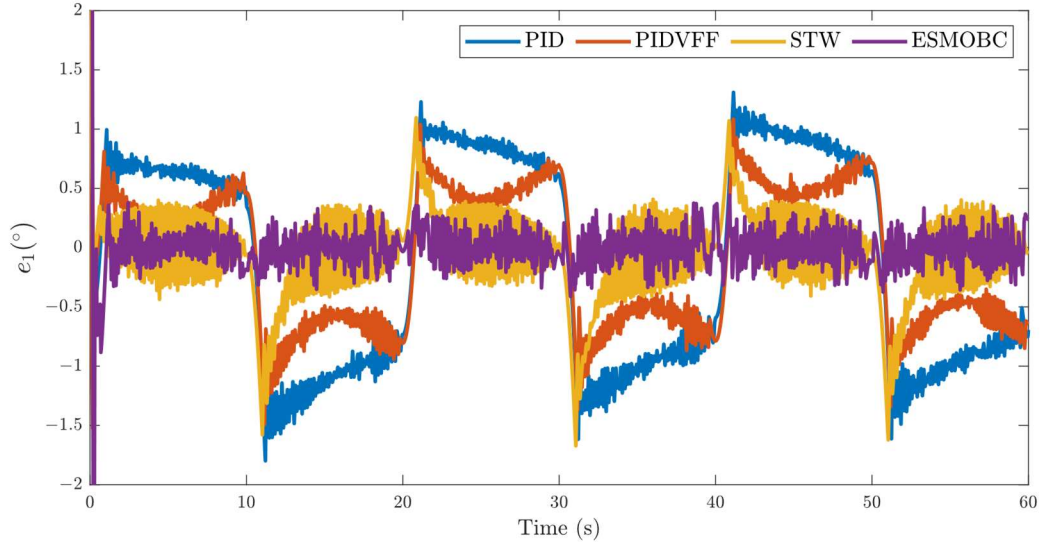


Fig. 6-4: Tracking errors of the compared controllers with the slow-motion reference trajectory and low-load condition.

To quantitatively indicate the reference-tracking capability of the compared controllers, performance indexes, including maximal tracking error, average tracking error, and standard deviation, in the steady-state regime of all four controllers are presented in Table 6-2. From this table, the PID controller exhibited the worst performance with the three indexes, with the maximal tracking error, average tracking error, and standard deviation as 1.6129° , 0.8859° , and 0.2336° , respectively. Meanwhile, by using the additional velocity feed-forward term, the tracking performance was substantially enhanced by the PIDVFF controller in all performance indexes. Compared to the traditional PID controller, the maximal tracking error, average, and standard deviation of the tracking errors were reduced to 1.3412° , 0.5819° , and 0.1639° by using the PIDVFF controller. Regarding the STW controller, the convergence speed of the tracking error can be improved by the employment of the fractional-order component and the discontinuous “sign” function. Hence, compared to PID and PIDVFF controllers, although both the maximal tracking error and standard deviation performance indexes are higher, the average tracking error obtained by the STW controller is significantly smaller (0.2721°). Nonetheless, it should be noted that with the help of compensation mechanisms by using the ESMO, the proposed method presented the best performance in terms of all performance indexes, with the maximal, average, and standard deviation of the tracking errors being 0.4426° , 0.1075° , and 0.1340° , respectively.

Table 6-2: Performance indexes in the slow-motion trajectory and low-load condition

Controller	M_e (deg)	μ_e (deg)	σ_e (deg)
PID Controller	1.6129	0.8859	0.2336
PIDVFF Controller	1.3412	0.5819	0.1639
STW Controller	1.6223	0.2721	0.2625
ESMOBC Controller	0.4426	0.1075	0.1340

b) Slow-Motion Reference Trajectory under Heavy-Load Condition

For evaluating the tracking performance of all considered controllers under the heavy-load condition, a gravitational load $m = 21\text{kg}$ is applied to the actuator with the same reference trajectory as the previous test case. The tracking errors of all controllers are displayed in Fig. 6-5 and the three performance indexes during the last cycle are presented in Table 6-3. It can be seen from Fig. 6-5, similar to the above test case, according to the inherent model compensation feature of the backstepping technique with the support of the proposed ESMO, that the ESMOBC controller still performed better, with smaller tracking errors compared to the PID, PIDVFF, and STW controllers. From Table 6-3, it is worth noting that the tracking performance indexes slightly increase in comparison with these values in the light-load condition, which indicates the robustness of all four controllers against heavy-load conditions. In particular, the absolute maximal tracking errors derived by the PID, PIDVFF, STW, and ESMOBC controllers increased by 0.1919° , 0.1588° , 0.5037° , and 0.2473° , respectively. In addition, the smaller values of the remaining performance indexes belong to the proposed control algorithm. It indicates the advantages of the proposed method compared to the model-free controllers.

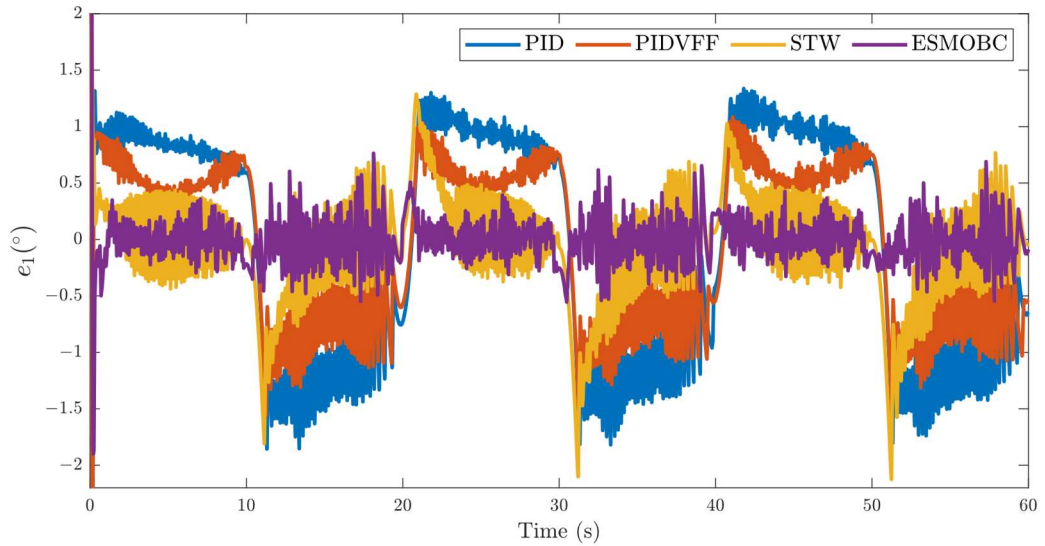


Fig. 6-5: Tracking errors of the compared controllers with the slow-motion reference trajectory and heavy-load condition.

Table 6-3: Performance indexes in the slow-motion trajectory under heavy-load condition.

Controller	M_e (deg)	μ_e (deg)	σ_e (deg)
PID Controller	1.8048	0.9508	0.3183
PIDVFF Controller	1.5000	0.6471	0.2392
STW Controller	2.1260	0.3496	0.3381
ESMOBC Controller	0.6899	0.1254	0.0978

c) Fast-Motion Reference Trajectory under Light-Load Condition

In this case study, the four considered controllers were further tested with a fast-motion reference trajectory that is analytically represented as $x_{1d}(t) = 20\sin(\pi t - \pi/2) + 25^\circ$ under the light-load condition $m = 1\text{kg}$. The tracking errors under the compared controllers are illustrated in Fig. 6-6. As shown in this figure, the tracking performances obtained by the four controllers were significantly degraded compared to the previous case studies under high-speed reference trajectory. The three

performance indexes of the controllers are presented in Table 6-4. It can be seen that, similar to the above scenarios, compared to the other control approaches, the STW controller exhibited the worst tracking performance in all three performance indexes, with the maximal, average, and standard deviation of the tracking errors in the steady state as 4.6298° , 2.6314° , and 1.4136° , respectively. For the time being, the proposed control approach achieved better performance, with the corresponding performance indexes as 1.5766° , 0.4831° , and 0.2977° compared to other controllers.

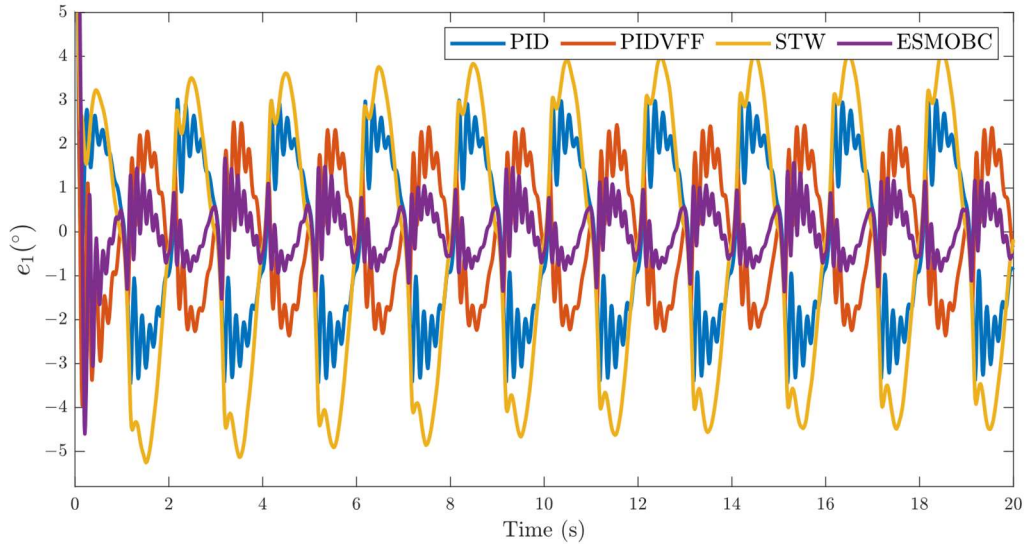


Fig. 6-6: Tracking errors of the compared controllers with the fast-motion reference trajectory and low-load condition.

Table 6-4: Tracking errors of the compared controllers with the fast-motion reference trajectory and low-load condition.

Controller	M_e (deg)	μ_e (deg)	σ_e (deg)
PID Controller	3.4388	1.7721	0.7923
PIDVFF Controller	2.4396	1.1953	0.6883
STW Controller	4.6298	2.6314	0.4136
ESMOBC Controller	1.5766	0.4831	0.2977

The estimated values of the angular speed of the actuator's shaft, load pressure-related term, and lumped disturbance in the pressure dynamics are illustrated in Fig. 6-7, Fig. 6-8, and Fig. 6-9, respectively. By using the proposed ESMO, the output feedback control based on the backstepping control technique can be realized in the absence of speed and pressure sensors. In addition, the ESMO plays an important role in reducing the system cost and improving the tracking performance of the EHA, since it is able to estimate not only immeasurable system states but also disturbance caused by parameter deviations and unmodeled dynamics.

The control input signal of the recommended control approach is presented in Fig. 6-10. As shown, a relatively smooth control input was obtained by using the ESMOBC. Due to the influence of the gravitational load, a higher control effort has to be generated when lifting the load, and vice versa. To track the sinusoidal-like reference trajectory, a periodical control input signal was constructed with the same frequency as the reference trajectory. The fluctuation of the control input in case of motion direction change compensates for the effects of complicated friction characteristics inside the actuator and guarantees a high-accuracy tracking performance.

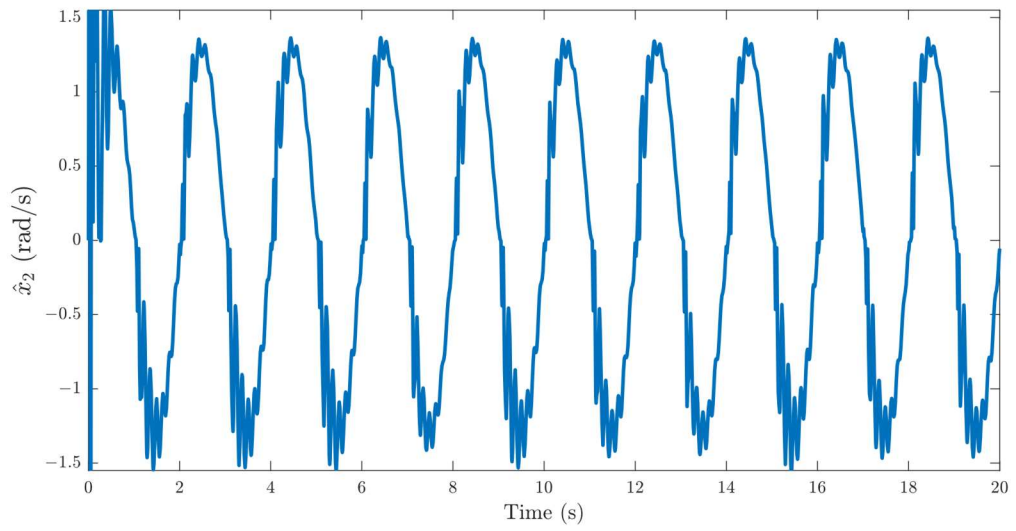


Fig. 6-7: The angular velocity estimation performance.

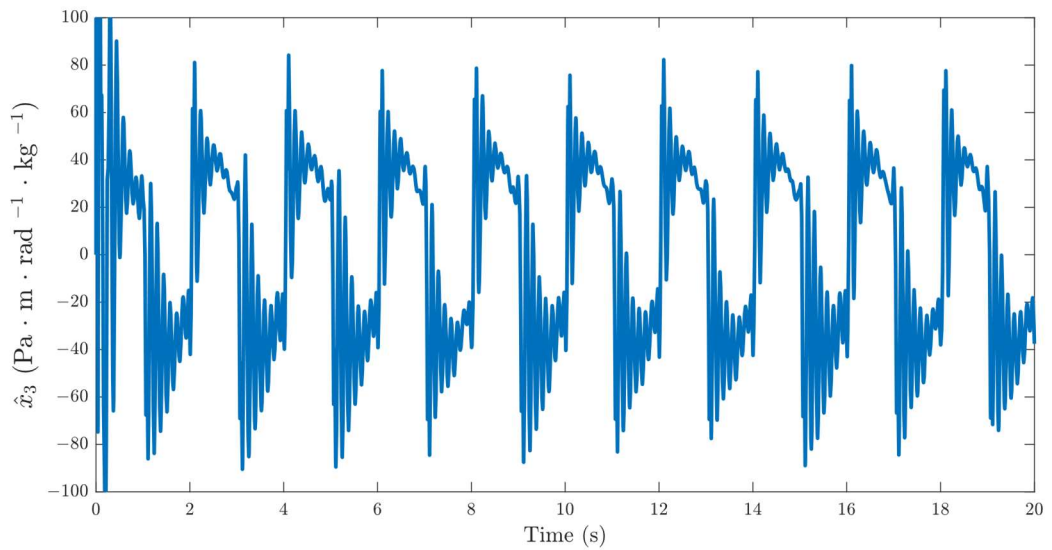


Fig. 6-8: The estimation of the load pressure-related term.

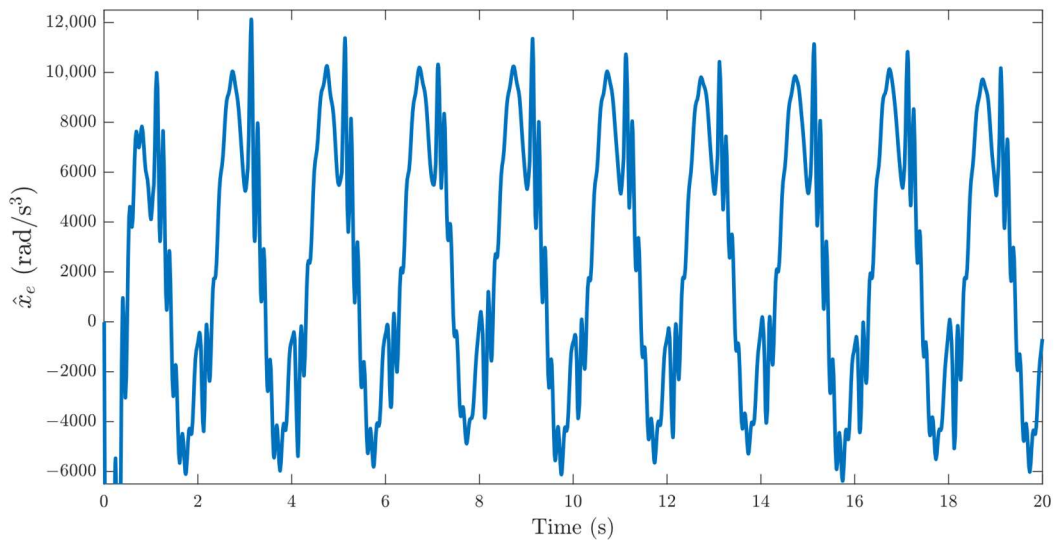


Fig. 6-9: Disturbance estimation in the fast-motion reference trajectory.

Based on the obtained experimental results in distinct working conditions, the proposed control approach was capable of achieving better tracking performance in comparison with some reference controllers. Hence, with the simple control structure, the suggested control approach provided a valuable solution to the tracking problem of the EHAs in practical applications for enhancing control accuracy. However, when designing an observer, it is essential to pick the switching gain carefully to prevent severe chattering that may arise from the selection of an excessive value. Furthermore, the observer bandwidth should be designed to make a trade-off between convergence time and the occurrence of the peaking phenomenon. Finally, advanced control algorithms will be further studied to increase the robustness and tracking performance of electro-hydrostatic actuators in future work.

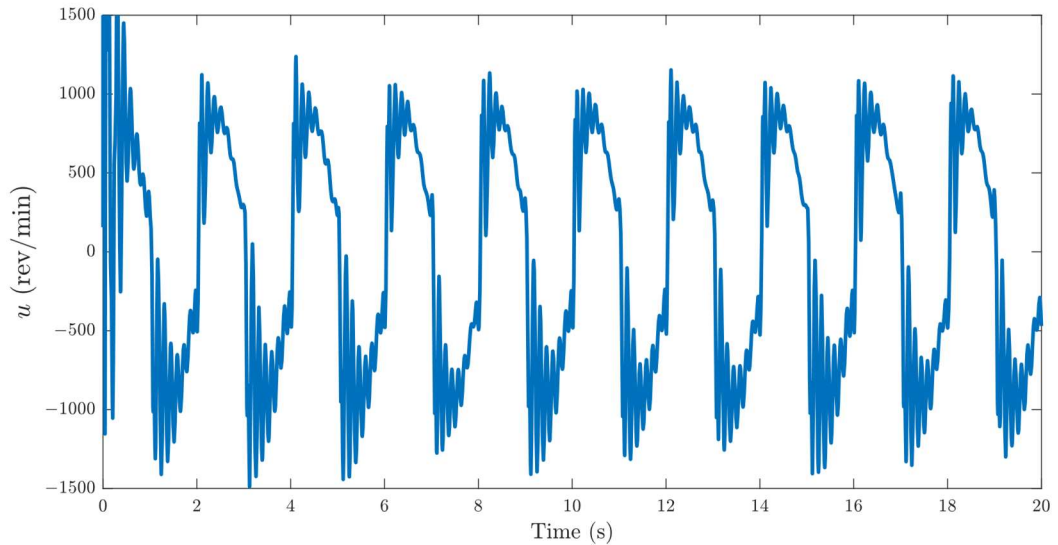


Fig. 6-10: The control input in the fast-motion reference trajectory and low-load condition.

6.4 Conclusion

This chapter presented a novel output feedback control of a pump-controlled EHA subject to model uncertainties. An ESMO was developed to estimate not only immeasurable states but also lumped-matched disturbance attributed to parametric uncertainties and unmodeled dynamics in the pressure dynamics of the actuator. A backstepping controller based on the DSC technique employing estimated values of states and lumped disturbance was designed to stabilize the closed-loop system and ensure a UUB tracking performance. Furthermore, the stability of the overall closed-loop system was rigorously demonstrated through the Lyapunov theory. Finally, experimental results under various working conditions in comparison with some reference model-free control approaches are obtained to demonstrate the superiority of the proposed method. The dynamics of the pump and electric motor system will be carefully considered in future work to improve the tracking capability of the proposed method.

OUTPUT FEEDBACK ROBUST CONTROL FOR HYDROSTATIC ACTUATORS WITH MISMATCHED UNCERTAINTIES

7.1 Introduction

Due to some excellent characteristics such as high power density, great reliability, excellent durability, and high-accuracy control capability [72, 198, 223], electro-hydraulic systems (EHSs) are broadly employed in a variety of industrial and engineering applications including construction machinery, aerospace, manufacturing, agriculture, and so on [211]. According to the utilization of the control element, EHSs are classified into two main groups, which are valve-controlled and pump-controlled EHSs. With regard to the tracking control aspect, valve-controlled EHSs can be considered as a remarkable solution for high-accuracy tracking control applications; however, they are not suitable for applications that require high energy efficiency because of throttling loss at the control valves [210]. Meanwhile, variable-speed pump-controlled hydraulic systems (VSPHSs) are able to get rid of this energy dissipation and, consequently, improve the overall system efficiency [203, 210]. Nonetheless, it is challenging to achieve high-precision motion control of the actuator owing to the high-order dynamics, highly nonlinear characteristics, uncertain nonlinearities, and external disturbances of the system dynamics.

Although the closed-loop system stability cannot be theoretically confirmed, the proportional-derivative-integral (PID) control, fuzzy control, and fuzzy PID hybrid control schemes are control methods that are favorable and widely adopted for nonlinear EHSs in various applications due to their simplicity in implementation without the requirement of a system model and the limited number of control parameters that need to be adjusted. For example, a self-tuning grey predictor fuzzy-PID controller [224] was developed for force control of a hydraulic load simulator. The obtained results showed that enhanced force regulation performance in both the transient and steady-state regimes was achieved in comparison with the conventional PID, fuzzy PID, and fixed-step grey predictor fuzzy PID. Besides, in [225], a fractional-order PID whose control gains were automatically tuned by fuzzy rules was developed to significantly improve the tracking performance of a VSPHS compared to the traditional PID controller. Additionally, how to obtain optimal PID gains is also an intriguing problem that has attracted great attention from the research community, recently. For instance, an improved particle swarm optimization (PSO)-PID was introduced in [12] to increase the convergence speed of the basic PSO algorithm. Distinct optimization algorithms such as the beetle antennae search (BAS) algorithm [226], genetic algorithm (GA) [15], improved differential evolution (IDE) [14], etc., have also been utilized to enhance the tracking performance of EHSs. Nonetheless, it is noteworthy that, due to the lack of a dynamic model and disturbance compensation mechanisms, it is challenging to attain satisfactory control performance using such model-free control approaches. Therefore, model-based control strategies including sliding mode control [227, 228], the backstepping approach [93, 109, 122], and feedback linearization control [229] can be considered as powerful tools to enhance the control performance of VSPHSs, which have been introduced in various previous studies [211, 230-232]. Among them, the backstepping control technique is the most appropriate tool to design a control strategy for high-order nonlinear systems in general and EHSs specifically based on its recursive structure. Nonetheless, this technique suffers from the problem of computational complexity as a consequence of the requirement of repetitive analytic derivative calculation of virtual control laws at each subsequent step. To overcome this obstacle, the dynamic surface control (DSC) concept [35] was developed by D. Swaroop et al. The key idea of this technique is using a set of low-pass filters for the virtual control laws to obtain their first-order derivatives. Hence, the "explosion of complexity" of the traditional backstepping is effectively avoided. However, it should be noted that the above model-

based control algorithms require information on the system states, which may not always be readily accessible in practical applications.

The utilization of state estimators that are based on the system model is the key technique to implement state feedback control algorithms for nonlinear systems in the case of lacking system state information. The first concept of a state observer was developed by Luenberger [51] to construct the missing internal states of a linear time-invariant system. Subsequently, the extended Luenberger observer [53] for nonlinear systems was introduced by M. Zeitz, in which the relationships for a state transformation into the nonlinear observer canonical form were developed. However, the Luenberger observers may not be sufficiently accurate in the presence of model uncertainties. To overcome this problem, sliding mode observers can be considered as a robust state estimator based on the equivalent theory for reconstructing unmeasurable states in the presence of model perturbation [233], which have been applied to various applications including electro-hydraulic systems [165, 234], electric motor drivers [235, 236], wind turbine systems [237, 238], and so on. However, because of the employment of the discontinuous term, the so-called “sign” function and, consequently, the chattering in the estimated values might be unavoidable. It is worth noting that the above state observers are only able to reconstruct the system states and their performance mainly depends on the accuracy of the identified system model. Then, the concept of the active disturbance rejection control (ADRC) paradigm [73], which relaxes the demand of the precise system model and requires the system order only, was introduced by J. Han. In this concept, an extended state observer (ESO) is a core component for state and disturbance estimation in the case of insufficient information on the system dynamics. Inspired by this research, several ESO-based control algorithms have been developed for numerous practical systems [76, 231, 239-243]. For instance, in [231], an ESO-based sliding mode control for an electrohydraulic actuator was constructed based on the acceleration model. In [210], B. Helian et al. proposed an adaptive robust controller for the motion control of a directly driven EHS, which is able to cope with dynamic nonlinearities and uncertainties, and improved tracking performance was accordingly achieved. Nonetheless, some sensors must be utilized to directly measure internal system states including velocity and pressure, and the system cost increases as a result. In [76], an output feedback control scheme that employs a single ESO was presented. The mechanism was able to effectively estimate and compensate for matched disturbances in a feedforward manner; however, a negligible improvement of the control performance was achieved compared to a traditional PI controller since the mismatched uncertainties were not considered. However, the implementation of the output feedback motion control for VSPHSs using ESOs to handle both mismatched and matched uncertainties is an intriguing and unexplored control problem.

Motivated by the above analysis, in this chapter, a novel output feedback robust tracking control for a pump-controlled hydraulic system in the presence of disturbances and uncertainties caused by the parameter deviations, unmodeled dynamics, and external load in a mechanical system and pressure dynamics was developed. The main contributions of this work are as follows:

- 1) For the first time, two ESOs were sophisticatedly coordinated to address the shortage of system state measurement mechanisms and the estimation of both matched and mismatched uncertainties in the studied pump-controlled hydraulic system. This combination serves as the basis for the implementation of the robust control algorithm, which merely requires the system output information.

- 2) Based on the nominal system parameters and information provided by the above ESOs, a novel output feedback robust control mechanism in which the uncertainties and disturbances estimated by the ESOs are feedforward compensated was constructed to guarantee a high-accuracy motion control performance in spite of the nonlinearities and uncertainties in the system dynamics.

3) The theoretical stability of the ESOs and overall closed-loop system was rigorously confirmed using Lyapunov's theory. Several comparative experiment results are given to verify the effectiveness and superiority of the proposed control methodology over the existing popular control algorithms under different working conditions.

The rest of this chapter is structured as follows. Section 7.2 presents the establishment of two ESOs and a control algorithm. Subsequently, Section 7.3 presents the experimental verification. Finally, a conclusion is given in Section 7.4.

7.2 Control System Design

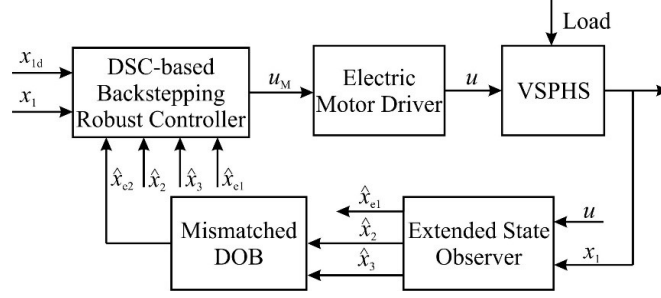


Fig. 7-1: The control structure of the proposed method

The control structure of the proposed method is illustrated in Fig. 7-1. As shown, an ESO is established to reconstruct not only the internal states, including the angular velocity and state variable relating to load pressure but also the total matched disturbances resulting from modeling errors and parametric uncertainties. It plays a crucial role in implementing the output feedback control mechanism for accurate motion tracking of the studied VSPHS. In addition, to improve the control performance, a mismatched disturbance observer that estimates the lumped mismatched disturbances produced by uncertain nonlinearities and unknown external loads, was constructed. Finally, to guarantee high-accuracy tracking performance, a DSC-based backstepping controller was designed. The DSC technique was adopted to overcome the computational burden of traditional backstepping, which requires the repetitive analytical derivative calculation of the virtual control laws. The design of the above observers and control strategy will be meticulously presented in the subsequent sections.

7.2.1 Extended State Observer Design

Considering the system dynamics (2.15) and defining $x_{e1} \triangleq d_2(t)$ as an extended state, the augmented system dynamics can be obtained as

$$\begin{cases} \dot{x}_1 = x_2 \\ \dot{x}_2 = x_3 + f_2(x_2) + d_1(t) \\ \dot{x}_3 = g_3(x_1)u + f_3(x_2, x_3) + x_{e1} \\ \dot{x}_{e1} = h_2(t) \end{cases} \quad (7.1)$$

According to this, the ESO for estimating not only the internal states x_2 and x_3 , but also the lumped matched disturbance is constructed as follows:

$$\begin{cases} \dot{\hat{x}}_1 = \hat{x}_2 + 4\omega_1 \tilde{x}_1 \\ \dot{\hat{x}}_2 = \hat{x}_3 + f_2(\hat{x}_2) + 6\omega_1^2 \tilde{x}_1 \\ \dot{\hat{x}}_3 = g_3(x_1)u + f_3(\hat{x}_2, \hat{x}_3) + \hat{x}_{e1} + 4\omega_1^3 \tilde{x}_1 \\ \dot{\hat{x}}_{e1} = \omega_1^4 \tilde{x}_1 \end{cases} \quad (7.2)$$

where \tilde{x}_1 denotes the error between the measured and estimated values of the system output, i.e., $\tilde{x}_1 = x_1 - \hat{x}_1$; \hat{x}_2 , \hat{x}_3 , and \hat{x}_{e1} are the estimates of x_2 , x_3 , and x_{e1} , respectively; ω_1 signifies the bandwidth of the observer (7.2).

Combining (7.1) and (7.2), the error dynamics of the observer are derived as

$$\begin{cases} \dot{\tilde{x}}_1 = -4\omega_1\tilde{x}_1 + \tilde{x}_2 \\ \dot{\tilde{x}}_2 = -6\omega_1^2\tilde{x}_1 + \tilde{x}_3 + \tilde{f}_2(x_2, \hat{x}_2) + d_1(t) \\ \dot{\tilde{x}}_3 = -4\omega_1^3\tilde{x}_1 + \tilde{x}_{e1} + \tilde{f}_3(x_2, x_3, \hat{x}_2, \hat{x}_3) \\ \dot{\tilde{x}}_{e1} = -\omega_1^4\tilde{x}_1 + h_2(t) \end{cases} \quad (7.3)$$

where \tilde{x}_2 , \tilde{x}_3 , and \tilde{x}_{e1} are the estimation errors of x_2 , x_3 , and x_{e1} , respectively, i.e., $\tilde{x}_2 = x_2 - \hat{x}_2$, $\tilde{x}_3 = x_3 - \hat{x}_3$, and $\tilde{x}_{e1} = x_{e1} - \hat{x}_{e1}$. Error functions $\tilde{f}_2(x_2, \hat{x}_2)$ and $\tilde{f}_3(x_2, x_3, \hat{x}_2, \hat{x}_3)$ are given by

$$\begin{aligned} \tilde{f}_2(x_2, \hat{x}_2) &= f_2(x_2) - f_2(\hat{x}_2) \\ \tilde{f}_3(x_2, x_3, \hat{x}_2, \hat{x}_3) &= f_3(x_2, x_3) - f_3(\hat{x}_2, \hat{x}_3) \end{aligned} \quad (7.4)$$

According to Assumption 7.2, one obtains

$$\begin{aligned} |\tilde{f}_2(x_2, \hat{x}_2)| &\leq L_{f_2} |\tilde{x}_2| \\ |\tilde{f}_3(x_2, x_3, \hat{x}_2, \hat{x}_3)| &\leq L_{f_{31}} |\tilde{x}_2| + L_{f_{32}} |\tilde{x}_3| \end{aligned} \quad (7.5)$$

where L_{f_2} , $L_{f_{31}}$, and $L_{f_{32}}$ are known Lipschitz constants.

Let $\boldsymbol{\varepsilon} = [\varepsilon_1, \varepsilon_2, \varepsilon_3, \varepsilon_4]^T = [\tilde{x}_1, \tilde{x}_2 / \omega_1, \tilde{x}_3 / \omega_1^2, \tilde{x}_{e1} / \omega_1^3]^T$ denote the scaled estimation error vector, then the error dynamics (7.3) can be transformed into

$$\dot{\boldsymbol{\varepsilon}} = \omega_1 \mathbf{A}_1 \boldsymbol{\varepsilon} + \mathbf{B}_1 \frac{\tilde{f}_2(x_2, \hat{x}_2) + d_1(t)}{\omega_1} + \mathbf{C}_1 \frac{\tilde{f}_3(x_2, x_3, \hat{x}_2, \hat{x}_3)}{\omega_1^2} + \mathbf{D}_1 \frac{h_2(t)}{\omega_1^3} \quad (7.6)$$

where the matrices \mathbf{A}_1 , \mathbf{B}_1 , \mathbf{C}_1 , and \mathbf{D}_1 are given by

$$\mathbf{A}_1 = \begin{bmatrix} -4 & 1 & 0 & 0 \\ -6 & 0 & 1 & 0 \\ -4 & 0 & 0 & 1 \\ -1 & 0 & 0 & 0 \end{bmatrix}; \mathbf{B}_1 = \begin{bmatrix} 0 \\ 1 \\ 0 \\ 0 \end{bmatrix}; \mathbf{C}_1 = \begin{bmatrix} 0 \\ 0 \\ 1 \\ 0 \end{bmatrix}; \mathbf{D}_1 = \begin{bmatrix} 0 \\ 0 \\ 0 \\ 1 \end{bmatrix} \quad (7.7)$$

Since the matrix \mathbf{A}_1 is negative definite, for an arbitrary symmetric positive definite \mathbf{Q}_1 , there always exists a symmetric positive definite \mathbf{P}_1 satisfying the following Lyapunov equation:

$$\mathbf{A}_1^T \mathbf{P}_1 + \mathbf{P}_1 \mathbf{A}_1 = -\mathbf{Q}_1 \quad (7.8)$$

Theorem 7-1: Considering the system dynamics (2.15) and the observer (7.2), the estimation errors converge to an arbitrarily small bounded region whose bound depends on the selection of the observer bandwidth ω_1 when time goes to infinity.

Proof of Theorem 7-1: Consider the following candidate Lyapunov function:

$$V_\varepsilon = \boldsymbol{\varepsilon}^T \mathbf{P}_1 \boldsymbol{\varepsilon} \quad (7.9)$$

Taking the derivative of it and combining with (7.6) yield

$$\begin{aligned}
\dot{V}_\varepsilon &= \dot{\boldsymbol{\varepsilon}}^T \mathbf{P}_1 \boldsymbol{\varepsilon} + \boldsymbol{\varepsilon}^T \mathbf{P}_1 \dot{\boldsymbol{\varepsilon}} \\
&= -\omega_1 \boldsymbol{\varepsilon}^T \mathbf{Q}_1 \boldsymbol{\varepsilon} + 2\boldsymbol{\varepsilon}^T \mathbf{P}_1 \mathbf{B}_1 \frac{\tilde{f}_2(x_2, \hat{x}_2) + d_1(t)}{\omega_1} + 2\boldsymbol{\varepsilon}^T \mathbf{P}_1 \mathbf{C}_1 \frac{\tilde{f}_3(x_2, x_3, \hat{x}_2, \hat{x}_3)}{\omega_1^2} + 2\boldsymbol{\varepsilon}^T \mathbf{P}_1 \mathbf{D}_1 \frac{h_2(t)}{\omega_1^3} \\
&\leq -\omega_1 \boldsymbol{\varepsilon}^T \mathbf{Q}_1 \boldsymbol{\varepsilon} + 2\boldsymbol{\varepsilon}^T \mathbf{P}_1 \mathbf{B}_1 \frac{L_{f2} |\tilde{x}_2| + |d_1(t)|}{\omega_1} + 2\boldsymbol{\varepsilon}^T \mathbf{P}_1 \mathbf{C}_1 \frac{L_{f31} |\tilde{x}_2| + L_{f32} |\tilde{x}_3|}{\omega_1^2} + 2\boldsymbol{\varepsilon}^T \mathbf{P}_1 \mathbf{D}_1 \frac{|h_2(t)|}{\omega_1^3}
\end{aligned} \tag{7.10}$$

Applying Young's inequality leads to

$$\begin{aligned}
\dot{V}_\varepsilon &\leq -\left(\omega_1 \lambda_{\min} \{ \mathbf{Q}_1 \} - 4 - \frac{\mathbf{B}_1^T \mathbf{P}_1^T \mathbf{P}_1 \mathbf{B}_1 L_{f2}^2}{\omega_1^2} - \mathbf{C}_1^T \mathbf{P}_1^T \mathbf{P}_1 \mathbf{C}_1 \frac{(L_{f31}^2 + L_{f32}^2)}{\omega_1^4} \right) \|\boldsymbol{\varepsilon}\|^2 \\
&\quad + \mathbf{B}_1^T \mathbf{P}_1^T \mathbf{P}_1 \mathbf{B}_1 \frac{d_1^2(t)}{\omega_1^2} + \mathbf{D}_1^T \mathbf{P}_1^T \mathbf{P}_1 \mathbf{D}_1 \frac{h_2^2(t)}{\omega_1^6} \\
&\leq -\left(\omega_1 \lambda_{\min} \{ \mathbf{Q}_1 \} - 4 - \frac{\mathbf{B}_1^T \mathbf{P}_1^T \mathbf{P}_1 \mathbf{B}_1 L_{f2}^2}{\omega_1^2} - \mathbf{C}_1^T \mathbf{P}_1^T \mathbf{P}_1 \mathbf{C}_1 \frac{(L_{f31}^2 + L_{f32}^2)}{\omega_1^4} \right) \|\boldsymbol{\varepsilon}\|^2 \\
&\quad + \mathbf{B}_1^T \mathbf{P}_1^T \mathbf{P}_1 \mathbf{B}_1 \frac{\bar{d}_1^2}{\omega_1^2} + \mathbf{D}_1^T \mathbf{P}_1^T \mathbf{P}_1 \mathbf{D}_1 \frac{\bar{h}_2^2}{\omega_1^6}
\end{aligned} \tag{7.11}$$

where $\lambda_{\min} \{ \mathbf{X} \}$ and $\lambda_{\max} \{ \mathbf{X} \}$ are the maximal and minimal eigenvalues of the matrix \mathbf{X} .

According to (7.9), one attains

$$\lambda_{\min} \{ \mathbf{P} \} \|\boldsymbol{\varepsilon}\|^2 \leq V_\varepsilon \leq \lambda_{\max} \{ \mathbf{P} \} \|\boldsymbol{\varepsilon}\|^2 \tag{7.12}$$

Based on this, (7.11) can be rewritten as

$$\dot{V}_\varepsilon \leq -\Gamma_\varepsilon V_\varepsilon + \Pi_\varepsilon \tag{7.13}$$

where

$$\begin{aligned}
\Gamma_\varepsilon &= \frac{1}{\lambda_{\max} \{ \mathbf{P}_1 \}} \left(\omega_1 \lambda_{\min} \{ \mathbf{Q}_1 \} - 4 - \frac{\mathbf{B}_1^T \mathbf{P}_1^T \mathbf{P}_1 \mathbf{B}_1 L_{f2}^2}{\omega_1^2} - \mathbf{C}_1^T \mathbf{P}_1^T \mathbf{P}_1 \mathbf{C}_1 \frac{(L_{f31}^2 + L_{f32}^2)}{\omega_1^4} \right) \\
\Pi_\varepsilon &= \mathbf{B}_1^T \mathbf{P}_1^T \mathbf{P}_1 \mathbf{B}_1 \frac{\bar{d}_1^2}{\omega_1^2} + \mathbf{D}_1^T \mathbf{P}_1^T \mathbf{P}_1 \mathbf{D}_1 \frac{\bar{h}_2^2}{\omega_1^6}
\end{aligned} \tag{7.14}$$

According to (7.13) and (7.14), it can be seen that the estimation errors are constrained in a region whose bound depends on the selection of the observer bandwidth ω_1 , which is defined by $\Pi_\varepsilon / \Gamma_\varepsilon$ when time goes to infinity.

This completes the proof of Theorem 7-1.

7.2.2 Mismatched Disturbance Observer

It can be seen from the above section that only lumped matched disturbance was estimated. The system performance may seriously deteriorate owing to the inherent existence of mismatched uncertainties caused by modeling errors and external load in the velocity dynamics.

Consider the velocity dynamics of the actuator:

$$\dot{x}_2 = x_3 + f_2(x_2) + d_1(t) \tag{7.15}$$

Let $x_{e2} = d_1(t)$ denote the extended state, (7.15) can be transformed into

$$\begin{cases} \dot{x}_2 = x_3 + f_2(x_2) + x_{e2} \\ \dot{x}_{e2} = h_1(t) \end{cases} \quad (7.16)$$

According to Theorem 7-1, the immeasurable system state x_2 and x_3 can be exactly estimated with arbitrarily small estimation errors; hence, the second derivatives of these estimation errors are also bounded by unknown positive constants. Their estimates were employed to the establish disturbance observer, whose dynamics are given as

$$\begin{cases} \dot{z}_2 = \hat{x}_3 + f_2(\hat{x}_2) + \hat{x}_{e2} + 2\omega_2(\hat{x}_2 - z_2) \\ \dot{\hat{x}}_{e2} = \omega_2^2(\hat{x}_2 - z_2) \end{cases} \quad (7.17)$$

where z_2 and \hat{x}_{e2} are the estimated values of \hat{x}_2 and x_{e2} ; ω_2 is the observer gain to be designed.

In accordance with (7.16) and (7.17), the error dynamics can be obtained as

$$\begin{cases} \dot{\tilde{z}}_2 = -2\omega_2\tilde{z}_2 + \tilde{x}_{e2} + \tilde{x}_3 + \tilde{f}_2(x_2, \hat{x}_2) + \ddot{\tilde{x}}_2 \\ \dot{\tilde{x}}_{e2} = -\omega_2^2\tilde{z}_2 + h_1(t) \end{cases} \quad (7.18)$$

Defining the scaled estimation error vector $\boldsymbol{\eta} = [\eta_1, \eta_2]^T = [\tilde{z}_2, \tilde{x}_{e2}]^T$, the error dynamics (7.18) can be rewritten as

$$\dot{\boldsymbol{\eta}} = \omega_2 \mathbf{A}_2 \boldsymbol{\eta} + \mathbf{B}_2 \frac{\tilde{x}_3 + \tilde{f}_2(x_2, \hat{x}_2) + \ddot{\tilde{x}}_2}{\omega_2} + \mathbf{C}_2 \frac{h_1(t)}{\omega_2^2} \quad (7.19)$$

where the matrices \mathbf{A}_2 , \mathbf{B}_2 , and \mathbf{C}_2 are given by

$$\mathbf{A}_2 = \begin{bmatrix} -2 & 1 \\ -1 & 0 \end{bmatrix}; \mathbf{B}_2 = \begin{bmatrix} 1 \\ 0 \end{bmatrix}; \mathbf{C}_2 = \begin{bmatrix} 0 \\ 1 \end{bmatrix} \quad (7.20)$$

Since the matrix \mathbf{A}_2 is Hurwitz, for a symmetric positive definite \mathbf{Q}_2 , there exists a symmetric positive definite \mathbf{P}_2 satisfying the following Lyapunov equation:

$$\mathbf{A}_2^T \mathbf{P}_2 + \mathbf{P}_2 \mathbf{A}_2 = -\mathbf{Q}_2 \quad (7.21)$$

Theorem 7-2: Consider the system dynamics (7.16); the observer (7.17) is capable of exactly estimating the lumped mismatched uncertainty $d_1(t)$ with a small estimation error, whose value decreases if the observer bandwidth increases.

Proof of Theorem 7-2: A candidate Lyapunov function was chosen as $V_\eta = \boldsymbol{\eta}^T \mathbf{P}_2 \boldsymbol{\eta}$. Taking the time derivative of it and combining it with (7.19) and (7.21) yield

$$\dot{V}_\eta = -\omega_2 \boldsymbol{\eta}^T \mathbf{Q}_2 \boldsymbol{\eta} + 2\boldsymbol{\eta}^T \mathbf{P}_2 \mathbf{B}_2 \frac{\tilde{x}_3 + \tilde{f}_2(x_2, \hat{x}_2) + \ddot{\tilde{x}}_2}{\omega_2} + 2\boldsymbol{\eta}^T \mathbf{P}_2 \mathbf{C}_2 \frac{h_1(t)}{\omega_2^2} \quad (7.22)$$

Applying Young's inequality leads to

$$\begin{aligned} V_\eta &\leq -(\omega_2 \lambda_{\min} \{\mathbf{Q}_2\} - 3) \|\boldsymbol{\eta}\|^2 + \mathbf{B}_2^T \mathbf{P}_2^T \mathbf{P}_2 \mathbf{B}_2 \frac{\tilde{x}_3^2 + L_{f_2} \tilde{x}_2^2 + |\ddot{\tilde{x}}_2|_{\max}}{\omega_2^2} + \mathbf{C}_2^T \mathbf{P}_2^T \mathbf{P}_2 \mathbf{C}_2 \frac{\bar{h}_1^2}{\omega_2^4} \\ &= -\Gamma_\eta V_\eta + \Pi_\eta \end{aligned} \quad (7.23)$$

where

$$\Gamma_\eta = \frac{\lambda_{\min}\{\mathbf{Q}_2\} - 3}{\lambda_{\max}\{\mathbf{P}_2\}}; \Pi_\eta = \mathbf{B}_2^T \mathbf{P}_2^T \mathbf{P}_2 \mathbf{B}_2 \frac{\tilde{x}_3^2 + L_{f_2} \tilde{x}_2^2 + |\ddot{\tilde{x}}_2|_{\max}}{\omega_2^2} + \mathbf{C}_2^T \mathbf{P}_2^T \mathbf{P}_2 \mathbf{C}_2 \frac{\bar{h}_1^2}{\omega_2^4} \quad (7.24)$$

According to Theorem 7-1, Assumption 2-6, and (7.23), the estimation error \tilde{x}_{e2} reaches a small region whose boundary decreases if the observer gain ω_2 increases and vice visa.

Hence, Theorem 7-2 is completely verified.

7.2.3 Observer-based Control Strategy Design

Based on the states and disturbances estimation, a backstepping controller was synthesized to guarantee the high-accuracy tracking performance of the closed-loop system as follows:

Reconsider the original system dynamics:

$$\begin{cases} \dot{x}_1 = x_2 \\ \dot{x}_2 = x_3 + f_2(x_2) + d_1(t) \\ \dot{x}_3 = g_3(x_1)u + f_3(x_2, x_3) + d_2(t) \end{cases} \quad (7.25)$$

The system output tracking error is defined as $e_1 = x_1 - x_{1d}$. To ensure that the system output tracks the desired trajectory, the virtual control law is synthesized as

$$\alpha_1 = \dot{x}_{1d} - k_1 e_1 \quad (7.26)$$

The dynamic surface control approach was adopted to avoid repeatedly differentiating α_1 by using a first-order filter as

$$\tau_1 \dot{\alpha}_{1f} + \alpha_{1f} = \alpha_1; \alpha_{1f}(0) = \alpha_1(0) \quad (7.27)$$

where τ_1 is a positive constant and α_{1f} denotes the filtered signal of α_1 .

According to this, the dynamic surface function is the error between the filtered signal α_{1f} and the virtual control law (7.26) in this step, that is $\rho_1 = \alpha_{1f} - \alpha_1$, and the first-order derivative of the filtered control law is given as

$$\dot{\alpha}_{1f} = -\frac{\rho_1}{\tau_1} \quad (7.28)$$

Following the structure of the applied first-order filter (7.26) and (7.27), the error dynamics can be determined as

$$\dot{\rho}_1 = -\frac{\rho_1}{\tau_1} + \epsilon_1 \quad (7.29)$$

where $\epsilon_1 = -\dot{\alpha}_1$ is continuous and bounded, and its maximum value is defined as ϵ_{1M} .

A candidate Lyapunov function was selected as $V_1 = e_1^2 / 2$. Taking the derivative of it and combining it with (7.25), one obtains

$$\dot{V}_1 = -k_1 e_1^2 + e_1 e_2 + \rho_1 e_1 \quad (7.30)$$

where $e_2 = x_2 - \alpha_{1f}$.

Applying Young's inequality yields

$$\begin{aligned}\dot{V}_1 &\leq -k_1 e_1^2 + e_1 e_2 + \frac{1}{2} \rho_1^2 + \frac{1}{2} e_1^2 \\ &= -\left(k_1 - \frac{1}{2}\right) e_1^2 + \frac{1}{2} \rho_1^2 + e_1 e_2\end{aligned}\quad (7.31)$$

From the definition of e_2 , we have

$$\begin{aligned}\dot{e}_2 &= \dot{x}_2 - \dot{\alpha}_{1f} \\ &= x_3 + f_2 + d_1 - \dot{\alpha}_{1f}\end{aligned}\quad (7.32)$$

Choose a candidate Lyapunov function as

$$V_2 = V_1 + \frac{1}{2} e_2^2 + \frac{1}{2} \rho_1^2 \quad (7.33)$$

Differentiating (7.33), then combining with (7.29) and (7.32), one obtains

$$\begin{aligned}\dot{V}_2 &= \dot{V}_1 + e_2 \dot{e}_2 + \rho_1 \dot{\rho}_1 \\ &= \dot{V}_1 + e_2 (\rho_2 + \alpha_2 + e_3 + f_2 + d_1 - \dot{\alpha}_{1f}) + \rho_1 \left(-\frac{\rho_1}{\tau_1} + \epsilon_1\right)\end{aligned}\quad (7.34)$$

where $e_3 = x_3 - \alpha_{2f}$ is the virtual tracking error of the subsequent step; the dynamic surface function of this step $\rho_2 = \alpha_{2f} - \alpha_2$ with α_{2f} as the filtered signal through a first-order filter of virtual control law α_2 , which is formulated as

$$\tau_2 \dot{\alpha}_{2f} + \alpha_{1f} = \alpha_2; \alpha_{2f}(0) = \alpha_2(0) \quad (7.35)$$

where τ_2 is a small positive constant to be designed.

The dynamics of the dynamic surface function is given by

$$\dot{\rho}_2 = -\frac{\rho_2}{\tau_2} + \epsilon_2 \quad (7.36)$$

where $\epsilon_2 = -\dot{\alpha}_2$ is also continuous and upper bounded by $\epsilon_{2M} > 0$.

Since the angular velocity and lumped mismatched disturbance are immeasurable, the estimates of these terms were utilized; according to (7.34), the virtual control law is designed as

$$\alpha_2 = -f_2(\hat{x}_2) - \hat{x}_{e2} + \dot{\alpha}_{1f} - k_2 e_2 - e_1 \quad (7.37)$$

where k_2 is a non-negative constant to be selected.

Substituting (7.31) and (7.36) into (7.34), then applying Young's inequality, we have

$$\begin{aligned}\dot{V}_2 &\leq -\left(k_1 - \frac{1}{2}\right) e_1^2 + \frac{1}{2} \rho_1^2 + e_1 e_2 - k_2 e_2^2 - e_1 e_2 + e_2 \rho_2 + e_2 e_3 + e_2 \tilde{f}_2 + e_2 \tilde{x}_{e2} + \rho_1 \left(-\frac{\rho_1}{\tau_1} + \epsilon_1\right) \\ &\leq -\left(k_1 - \frac{1}{2}\right) e_1^2 - \left(k_2 - \frac{3}{2}\right) e_2^2 - \left(\frac{1}{\tau_1} - \frac{1}{2a} \epsilon_{1M}^2 - \frac{1}{2}\right) \rho_1^2 + e_2 e_3 + \frac{1}{2} \tilde{f}_2^2 + \frac{1}{2} \tilde{x}_{e2}^2 + \frac{1}{2} \rho_2^2 + \frac{a}{2}\end{aligned}\quad (7.38)$$

where a is a positive constant, $\tilde{f}_2 = f(x_2) - f(\hat{x}_2)$, and $e_3 = x_3 - \alpha_{2f}$.

According to the definition of the virtual tracking error e_3 , one obtains

$$\begin{aligned}\dot{e}_3 &= \dot{x}_3 - \dot{\alpha}_{2f} \\ &= g_3(x_1)u + f_3(x_2, x_3) + d_2 - \dot{\alpha}_{2f}\end{aligned}\quad (7.39)$$

A candidate Lyapunov function is selected as

$$V_3 = V_2 + \frac{1}{2}e_3^2 + \frac{1}{2}\rho_2^2 \quad (7.40)$$

Taking the derivative of it, then combining with (7.36) and (7.39) yield

$$\dot{V}_3 = \dot{V}_2 + e_3(g_3u + f_3 + d_2 - \dot{\alpha}_{2f}) + \rho_2\left(-\frac{\rho_2}{\tau_2} + \epsilon_2\right) \quad (7.41)$$

The actual control law is constructed as

$$u = \frac{1}{g_3}\left(-\hat{f}_3 - \hat{x}_{e1} + \dot{\alpha}_{2f} - k_3e_3 - e_2\right) \quad (7.42)$$

where $k_3 > 0$ is to be chosen and $\hat{f}_3 = f_3(\hat{x}_2, \hat{x}_3)$.

According to (7.41) and (7.42) then applying Young's inequality, one obtains

$$\begin{aligned}\dot{V}_3 &= \dot{V}_2 + e_3(\tilde{f}_3 + \tilde{x}_{e1} - k_3e_3 - e_2) + \rho_2\left(-\frac{\rho_2}{\tau_2} + \epsilon_2\right) \\ &\leq \dot{V}_2 - (k_3 - 1)e_3^2 - \left(\frac{1}{\tau_2} - \frac{1}{2a}\epsilon_{2M}^2\right)\rho_2^2 - e_2e_3 + \frac{1}{2}\tilde{f}_3^2 + \frac{1}{2}\tilde{x}_{e1}^2 + \frac{a}{2}\end{aligned}\quad (7.43)$$

Substituting (7.38) into (7.43) leads to

$$\begin{aligned}\dot{V}_3 &\leq -\left(k_1 - \frac{1}{2}\right)e_1^2 - \left(k_2 - \frac{3}{2}\right)e_2^2 - \left(\frac{1}{\tau_1} - \frac{1}{2a}\epsilon_{1M}^2 - \frac{1}{2}\right)\rho_2^2 \\ &\quad - (k_3 - 1)e_3^2 - \left(\frac{1}{\tau_2} - \frac{1}{2a}\epsilon_{2M}^2\right)\rho_2^2 + \frac{1}{2}\tilde{f}_2^2 + \frac{1}{2}\tilde{f}_3^2 + \frac{1}{2}\tilde{x}_{e1}^2 + \frac{1}{2}\tilde{x}_{e2}^2 + a\end{aligned}\quad (7.44)$$

The inequality (7.44) can be rewritten as

$$\dot{V}_3 \leq -\Gamma V_3 + \Pi \quad (7.45)$$

where Γ and Π are determined as

$$\begin{aligned}\Gamma &= \min\left\{2k_1 - 1; 2k_3 - 2; 2k_3 - 2; \frac{2}{\tau_1} - \frac{\epsilon_{1M}^2}{a} - 1; \frac{2}{\tau_2} - \frac{\epsilon_{2M}^2}{a}\right\} \\ \Pi &= \frac{\tilde{f}_2^2}{2} + \frac{\tilde{f}_3^2}{2} + \frac{\tilde{x}_{e1}^2}{2} + \frac{\tilde{x}_{e2}^2}{2} + a\end{aligned}\quad (7.46)$$

Based on Theorems 7.1 and 7.2, and (7.45), by using the control laws (7.26), (7.37), and (7.42), a bounded tracking performance of the closed-loop system is guaranteed. The output tracking error reduces as the controller gains k_1 , k_2 , and k_3 increase and vice versa.

Remark 7-1. The time constants of the low-pass filters (7.27) and (7.35) should be selected sufficiently small to guarantee not only the closed-loop system dynamics, but also the small errors between the virtual control laws and their filtered signals, and consequently, the control performance can be significantly improved. Although only bounded stability can be achieved, the employment of

the DSC technique effectively avoids the analytic derivative calculation of the virtual control laws in the conventional backstepping control framework; hence, the computational complexity can be substantially reduced.

7.3 Experiment Verification

7.3.1 Experiment Setup

The real apparatus that is used to study the control problem and verify the advantage of the suggested control strategy is shown in Fig. 7-2. As shown, it consisted of a compact hydraulic power unit, a vane rotary actuator, two pressure transmitters, and an encoder. The hydraulic power pack manufactured by Bosch Rexroth includes a bidirectional gear pump that is driven by a DC motor. To control the speed of the DC motor, a medium-power motor driver MD-03 was provided by Robot Electronics company. Besides, to measure the pressure of the actuator, two pressure sensors of Model KOBOLD SEN-8700/2A095 were adopted. In addition, an encoder E40H8-5000-3-V-5 made by Autonics company was employed to measure the angular position of the actuator.

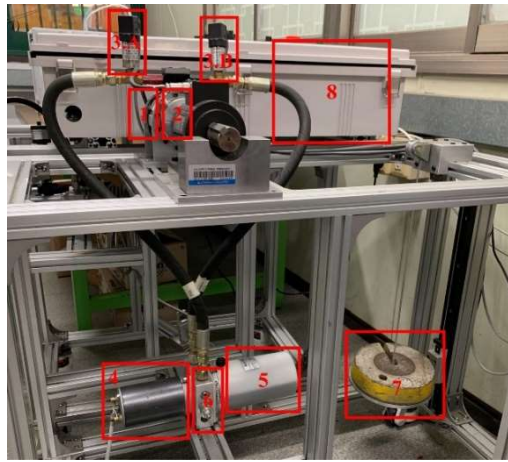


Fig. 7-2. The experimental platform of the studied pump-controlled electro-hydraulic system.

- (1) Hydraulic rotary actuator with an encoder rigidly connected to the actuator shaft; (2) drum; (3.A, 3.B) pressure transmitters; (4) DC motor; (5) hydraulic tank with a pump inside; (6) center block; (7) gravitational load; (8) electric control box.

The nominal system parameters of the real VSPHS are listed in Table 7-1, which were used to design the observers and control laws of the proposed control method.

Table 7-1. The nominal parameter of the studied VSPHS

Parameter	Notation	Value	SI Unit
Viscous friction coefficient of the actuator	\bar{B}_f	50	$\text{N} \cdot \text{m} \cdot \text{rad}^{-1} \cdot \text{s}$
Coulomb friction coefficient of the actuator	\bar{A}_f	45	$\text{N} \cdot \text{m}$
Moment of inertia of the actuator	\bar{J}_A	0.15	$\text{kg} \cdot \text{m}^2$
Hydraulic actuator displacement	\bar{D}_A	5.8442×10^{-6}	$\text{m}^3 \cdot \text{rad}^{-1}$
Hydraulic pump displacement	\bar{D}_P	0.1544×10^{-7}	$\text{m}^3 \cdot \text{rad}^{-1}$
Effective bulk modulus of the hydraulic oil	$\bar{\beta}_e$	1.5×10^9	$\text{N} \cdot \text{m}^{-2}$ or Pa
Total leakage coefficient	\bar{C}_t	4.267×10^{-12}	$\text{m}^3 \cdot \text{s}^{-1} \cdot \text{Pa}^{-1}$
Initial control volume of the forward chamber	\bar{V}_{01}	1.25×10^{-5}	m^3
Initial control volume of the reverse chamber	\bar{V}_{02}	2.27×10^{-5}	m^3

To demonstrate the advantage of the recommended control approach, the following controllers were compared:

1) DESO-OFRC: The proposed controller whose control gains were chosen as $k_1 = 80$, $k_2 = 15$, $k_3 = 30$. In addition, the bandwidths of the observers (7.2) and (7.17) were $\omega_1 = 50$ and $\omega_2 = 50$, respectively.

2) SESO-OFRC: The output feedback control using a single ESO, which has a similar structure to the proposed method. The parameters of the controller were also selected the same as the above controller with the observer bandwidth $\omega = 50$.

3) VF-PID: The proportional-integral-derivative controller with the velocity feedforward mechanism is mathematically presented as

$$u = K_P e(t) + K_I \int_0^t e(\tau) d\tau + K_D \frac{de(t)}{dt} + K_V \dot{x}_{1d}(t) \quad (7.47)$$

where $e(t) = x_{1d}(t) - x_1(t)$ and $\dot{x}_{1d}(t)$ is the first derivative of the desired trajectory.

As far as we know, the PID is the most-popular control algorithm that is adopted in industrial applications due to the simple implementation and limited tuning parameters. In particular, it does not require the system model, and only the position of the actuator is required; hence, it can be treated as the reference controller for comparison. The parameters of the VF-PID controller were meticulously manually tuned to achieve an acceptable tracking performance and guarantee the system stability as $K_P = 3.5 \times 10^4$, $K_I = 3.5 \times 10^3$, $K_D = 5 \times 10^2$, and $K_V = 2 \times 10^3$. The selection of bigger parameters would cause the closed-loop system to be unstable.

To measure the effectiveness of each control approach, two performance indexes [76, 97] including the maximum and standard deviation of the tracking errors were employed. These indexes are defined as follows:

(i) The maximal absolute value of the tracking errors is given by

$$M_e = \max_{i=1, \dots, N} \{|e_1(i)|\} \quad (7.48)$$

(ii) The standard deviation performance index is defined as

$$\sigma_e = \sqrt{\frac{1}{N} \sum_{i=1}^N [\mu_e - e_1(i)]^2} \quad (7.49)$$

where μ_e denotes the average tracking error, which is calculated as $\mu_e = \frac{1}{N} \sum_{i=1}^N |e_1(i)|$.

7.3.2 Experiment Results

a) Case study 1

Firstly, a slow-motion desired trajectory was employed to evaluate the reference-following capability of the three considered controllers, which is mathematically presented as

$x_{1d}(t) = 5 + 30(1 - \cos(0.1\pi t))(1 - \exp(-t))^\circ$, with a load of 10 kg.

The tracking performance of the proposed control method in comparison with those of other controllers is demonstrated in Fig. 7-3 and Fig. 7-4. As shown in Fig. 7-3, all controllers guarantee that the system outputs of the hydraulic actuator are able to follow the reference trajectory. Fig. 7-4 indicates the tracking accuracy of each controller. The peaks of the tracking errors happen when the motion direction changes because of the external load and the friction inside the hydraulic actuator. From this figure, it can be seen that the maximal tracking errors of the VF-PID controller and SESO-OFRBC controller were slightly different with the tracking errors as 1.0033° and 0.9717° in the steady state, as shown in Table 7-2, respectively. Meanwhile, the DESO-OFRBC control approach outperformed the other controllers, and the maximal tracking error was reduced almost down to 0.8354° since the effect of uncertainties and external load in the velocity dynamics was effectively compensated by using the dual ESOs compared to the single ESO employed in the SESO-OFRBC control scheme.

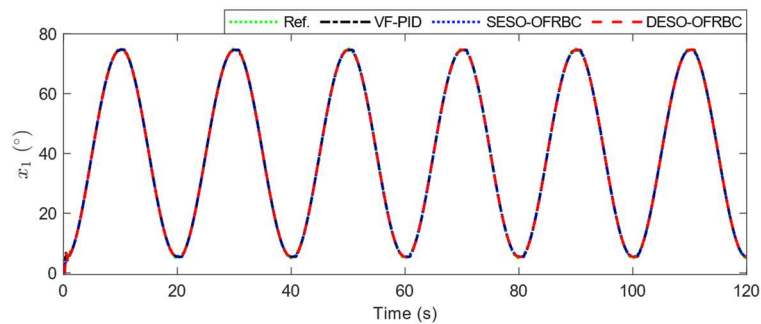


Fig. 7-3. The output tracking performances of the three controllers under the slow-motion reference trajectory.

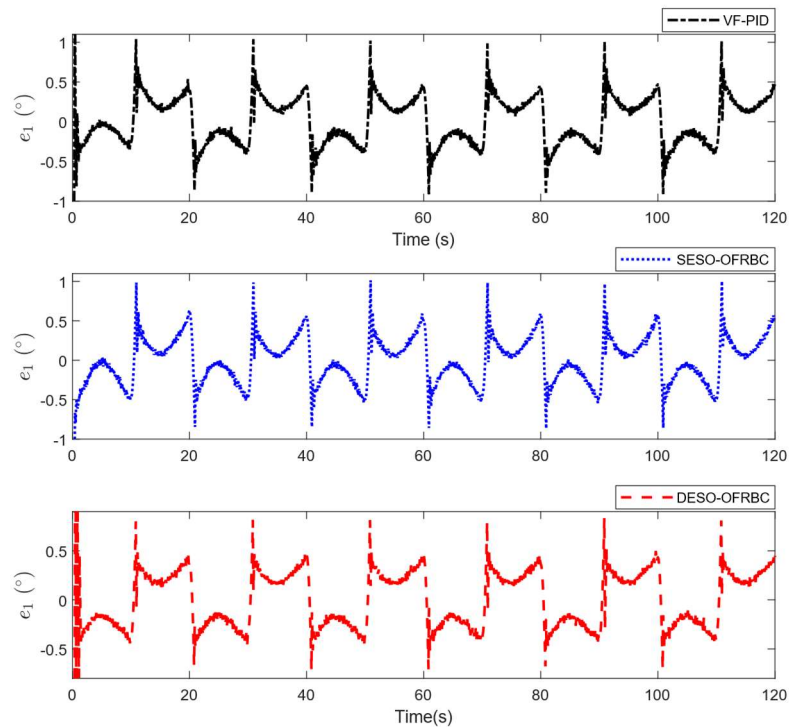


Fig. 7-4 The output tracking errors of the three controllers under the slow-motion reference trajectory.

Table 7-2. Performance indexes in the slow-motion reference trajectory case.

Controller	M_e (degree)	σ_e (degree)
VF-PID Controller	1.0033	0.1329
SESO-OFRBC Controller	0.9717	0.1615
DESO-OFRBC Controller	0.8354	0.0960

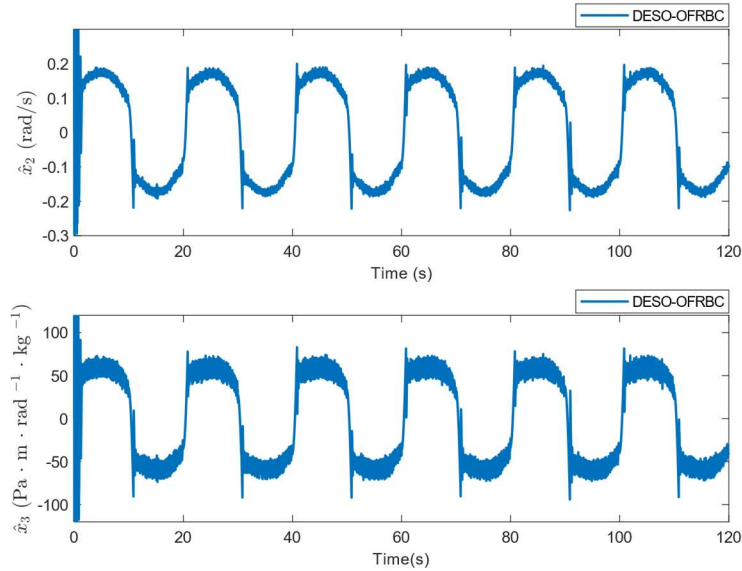


Fig. 7-5. The estimates of the angular velocity and load-pressure-related term under the proposed controller.

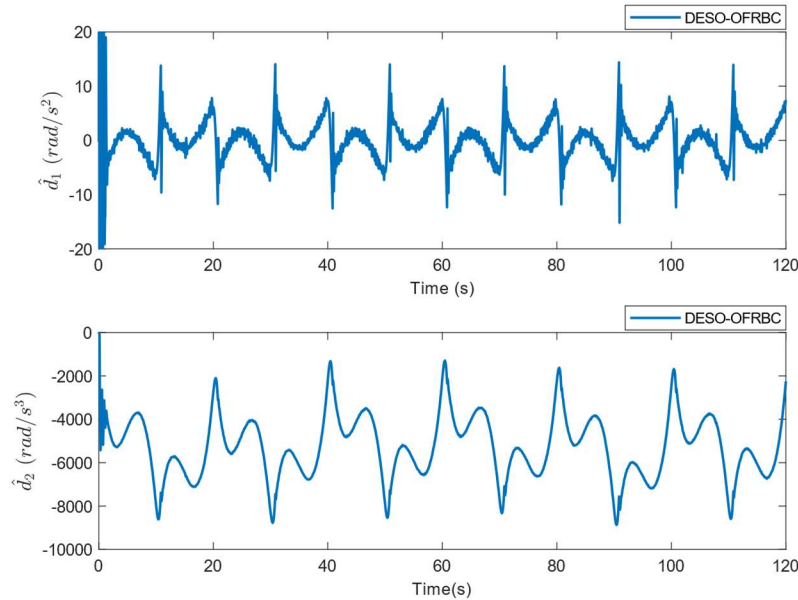


Fig. 7-6. The estimates of lumped mismatched and matched uncertainties under the proposed controller.

The estimations of the angular velocity, load-pressure-related term, and lumped mismatched and matched disturbances are depicted in Fig. 7-5 and Fig. 7-6, respectively. According to these estimates, state feedback control can be realized. In the DESO-OFRBC control structure, the lumped mismatched and matched disturbances caused by parametric uncertainties, unmodeled dynamics, and external

disturbances were estimated based on the system output only and then compensated, resulting in better tracking performance being achieved compared to the two remaining control methods.

b) Case study 2

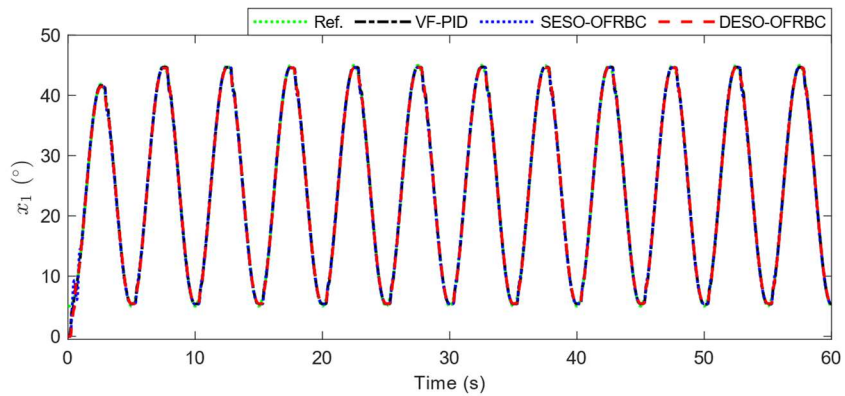


Fig. 7-7. The output tracking performances of the three controllers under the faster motion reference trajectory.

For further examination of the tracking performance of the three controllers, a four-times faster reference trajectory was adopted as $x_{1d}(t) = 5 + 20(1 - \cos(0.4\pi t))(1 - \exp(-t))^\circ$, and the load was 15 kg.

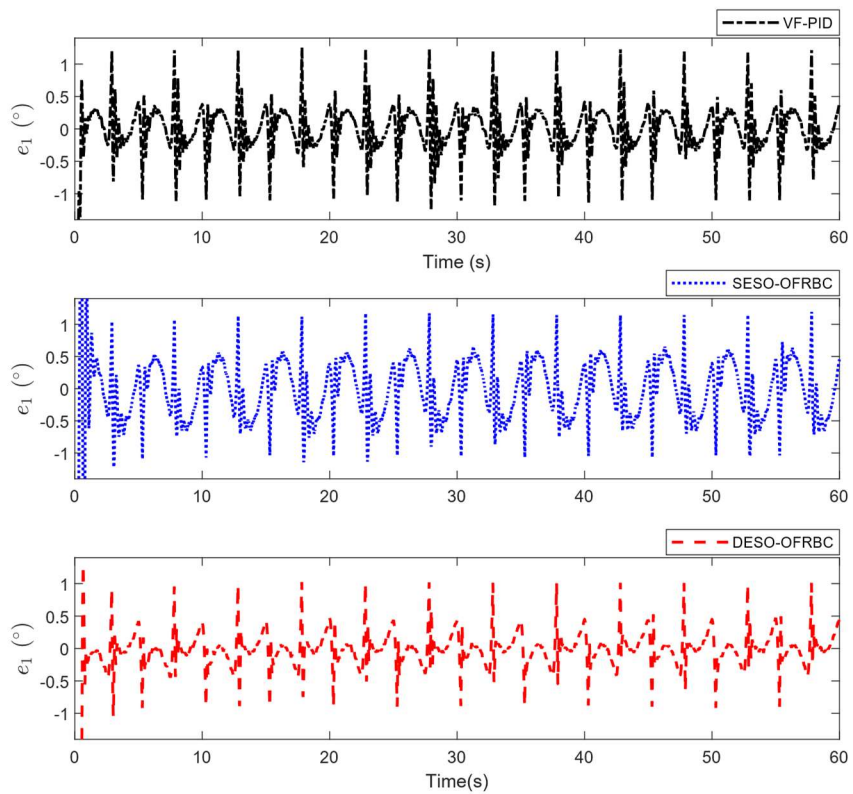


Fig. 7-8. The output tracking errors of the three controllers under the faster motion reference trajectory.

The tracking performances of the three controllers are presented in Fig. 7-7. As shown, similar to the above case study, all comparative controllers were able to ensure that the system output could follow the reference trajectory in the presence of the model uncertainty and external load.

In addition, the tracking capabilities of the three controllers are explicitly illustrated in Fig. 7-8. Under the faster reference trajectory and heavier load, the tracking errors achieved by these controllers considerably increased. The two performance indexes in this case are presented in Table 7-3. Due to the lack of nonlinear model dynamics and disturbance compensation mechanisms, the absolute maximal tracking error in the steady state obtained by the VF-PID controller went up to 1.2260° . Meanwhile, this performance index attained by the SESO-OFRC controller was 1.1438° . It should be noted that the smallest tracking error was achieved by the DESO-OFRC controller (1.0134°).

Table 7-3. Performance indexes in the faster motion reference trajectory case.

Controller	M_e (degree)	σ_e (degree)
VF-PID Controller	1.0033	0.1329
SESO-OFRC Controller	0.9717	0.1615
DESO-OFRC Controller	0.8354	0.0960

7.4 Conclusions

This chapter presented a novel active disturbance rejection control for position tracking of a variable-speed pump-controlled hydraulic system. To cope with the shortage of system state information and the online estimate of the lumped matched disturbance, a linear ESO was adopted with a single tuning parameter. In addition, to alleviate the effect of the lumped mismatched disturbance originating from the parametric uncertainties, unmodeled dynamics, and external load on the mechanical dynamics, a mismatched disturbance observer was constructed. According to this, an observer-based approach was established by using the backstepping control technique. Moreover, to avoid the computational burden of the conventional backstepping concept, the dynamic surface control was integrated. Furthermore, the stability of not only the observers but also the closed-loop system was verified by using the Lyapunov theory. Finally, several experiments were carried out on the real VSPHS to demonstrate the effectiveness of the recommended method in comparison with some reference methods. Two case studies were considered, and the results showed that smaller maximal absolute tracking errors were achieved by the suggested controller (0.8534° in the slow-motion case and 1.0134° in the faster-motion case) compared to these values obtained by the SESO-OFRC controller (0.9717° and 1.1438° , respectively) and VF-PID controller (1.0033° and 1.2260° , respectively). Some advanced estimation and control techniques for improving the tracking performance of VSPHSs will be investigated in future work.

Chapter 8

CONCLUSIONS AND FUTURE WORKS

8.1 Conclusions

This thesis introduces several control approaches for improving the motion-tracking performance of electro-hydraulic systems suffering from model uncertainties and external disturbances. In these control schemes, observers play an important role in dealing with the nonexistence of sufficient measurement mechanisms, and uncertainties and disturbances attenuation. Meanwhile, nominal controllers are designed based on backstepping and sliding mode control techniques. Finally, the unknown terms in control laws are compensated by their estimated values in order to achieve the desired performance. The main contributions of the dissertation are summarized as follows:

- To minimize the influence of both matched and mismatched disturbances on the reference-following capability of EHSs, disturbance observers that have a simple structure and easy implementation, have been developed. The angular velocity of the actuator has been attained by employing a second-order Levant's differentiator. Based on that, a state feedback controller has been designed by using the conventional backstepping control technique, in which both matched and mismatched disturbances have been sufficiently compensated.
- The concept of ADRC was first introduced by Han [73]. It was proposed to deal with the shortage of exact system models and developed based on ESOs that are able to estimate not only immeasurable states but also disturbances. However, peaking phenomena is the major disadvantage of ESOs and it may cause system instability when using high observer gains. Based on the sliding mode theory and to avoid this demerit of the standard ESO design, ESMOs have been successfully investigated and applied to control applications of EHSs. The obtained results showed that better estimation performance by ESMOs was achieved compared to the ESOs with a similar level of observer gains, and consequently, more accurate tracking control was attained.
- Additionally, tracking control of an EHS subject to completely unknown dynamics has been studied in this thesis. As far as we know, system identification is a challenging task when designing a controller for a mechanical system. In some sense, the model of complex systems cannot be obtained by using fundamental knowledge. To reduce this burden, adaptive NN-based control for tracking the problem of EHSs has been explored in this thesis. Multiple NNs have been adopted to approximate dynamical functions. The imperfections of NN-based approximations and the adverse impacts of external disturbances have been treated by DOBs. Finally, the control algorithm has been synthesized by employing SMC theory.
- Finally, an output feedback control for a pump-controlled electro-hydrostatic actuator that has been utilized in various practical applications, has been also investigated in this thesis. The lack of system states and both mismatched and matched disturbances is solved by using dual ESOs. The DSC approach has been employed to avoid the "explosion of complexity" of the standard backstepping control due to the repeated differentiation of virtual control law at each backstepping iteration.

8.2 Future works

It should be noted that although improved performance was achieved by employing the developed control algorithms, for further improvements in motion tracking control of EHSs, some practical problems should be carefully considered in future works as follows:

- The relationship between input saturation and prescribed performance should be pointed out clearly. Since the control input is saturated in case of rapidly changing reference trajectories that exceed the kinematic and dynamic constraints of real-life EHSs. In this scenario, predetermined performance indexes cannot be assured and the tracking performance will deteriorate as a result.
- In EHSs, the dead-zone characteristics of servo valves and motor drives in pumping systems naturally exist and they should be meticulously considered to enhance the overall control accuracy. In fact, the dead-zone is time-varying depending on system working conditions. Effective techniques of compensation for the dead-zone should be investigated
- In recent decades, finite-time estimation for nonlinear systems has become one of the interesting research directions. Nevertheless, strong assumptions that are not always satisfied in practical conditions were made to achieve finite-time criterion. Therefore, obtaining finite-time estimation when some strong assumptions are relaxed, is also one of the research gaps that need to be discovered in future works.
- Complex systems are constructed from multiple actuators to realize distinct tasks, hence, developing control algorithms for such systems is necessary. In heavy-duty applications, electro-hydraulic actuators whose dynamics are high-order and highly nonlinear, are widely used. Therefore, control of these systems becomes more challenging than electrical counterparts and requires further consideration.
- In practical systems, the working conditions of sensors and actuators cannot always be guaranteed. In case of sensor and/or failure, the system performance is not able to remain and this problem may even cause unexpected consequences that are harmful to operators and overall controlled systems. Assurance of acceptable performance and safety conditions for operators in a specific period of time requires the development of sophisticated control algorithms that are able to take sensor and actuator faults into account simultaneously.
- The selection of control gains during the design stage of controllers is an ad hoc and painstaking process. How to choose optimal gains for constructed controllers is still a big research question that demands a great effort from the research community. Hence, optimal control methods should also be considered in future research.

Published papers

A. International Journal

1. **M. H. Nguyen**, H. V. Dao, and K. K. Ahn, "Active Disturbance Rejection Control for Position Tracking of Electro-Hydraulic Servo Systems under Modeling Uncertainty and External Load," *Actuators*, vol. 10, no. 2, doi: 10.3390/act10020020.
2. **M. H. Nguyen** and K. K. Ahn, "A Novel Trajectory Adjustment Mechanism-Based Prescribed Performance Tracking Control for Electro-Hydraulic Systems Subject to Disturbances and Modeling Uncertainties," *Applied Sciences*, vol. 12, no. 12, doi: 10.3390/app12126034.
3. **M. H. Nguyen** and K. K. Ahn, "An Improved Voltage Regulation Performance of Floating Interleaved Boost Converters for Fuel Cell Applications Subject to Input Variation and Load Change," *Applied Sciences*, vol. 12, no. 22, doi: 10.3390/app122211501.
4. **M. H. Nguyen**, H. V. Dao, and K. K. Ahn, "Adaptive Robust Position Control of Electro-Hydraulic Servo Systems with Large Uncertainties and Disturbances," *Applied Sciences*, vol. 12, no. 2, doi: 10.3390/app12020794.
5. **M. H. Nguyen** and K. K. Ahn, "Output Feedback Robust Tracking Control for a Variable-Speed Pump-Controlled Hydraulic System Subject to Mismatched Uncertainties," *Mathematics*, vol. 11, no. 8, doi: 10.3390/math11081783.
6. **M. H. Nguyen**, H. V. Dao, and K. K. Ahn, "Extended sliding mode observer-based high-accuracy motion control for uncertain electro-hydraulic systems," *International Journal of Robust and Nonlinear Control*, <https://doi.org/10.1002/rnc.6421> vol. 33, no. 2, pp. 1351-1370, 2023/01/25 2023, doi: <https://doi.org/10.1002/rnc.6421>.
7. H.-A. Trinh, H. V. A. Truong, T. C. Do, **M. H. Nguyen**, V. D. Phan, and K. K. Ahn, "Optimization-based energy management strategies for hybrid construction machinery: A review," *Energy Reports*, vol. 8, pp. 6035-6057, 2022/11/01/ 2022, doi: <https://doi.org/10.1016/j.egyr.2022.04.050>.
8. H. V. A. Truong, **M. H. Nguyen**, D. T. Tran, and K. K. Ahn, "A novel adaptive neural network-based time-delayed estimation control for nonlinear systems subject to disturbances and unknown dynamics," *ISA Transactions*, vol. 142, pp. 214-227, 2023/11/01/ 2023, doi: <https://doi.org/10.1016/j.isatra.2023.07.032>.
9. **M. H. Nguyen** and K. K. Ahn, "Extended Sliding Mode Observer-Based Output Feedback Control for Motion Tracking of Electro-Hydrostatic Actuators," *Mathematics*, vol. 11, no. 20, doi: 10.3390/math11204324.
10. H. V. Dao, **M. H. Nguyen**, and K. K. Ahn, "Nonlinear Functional Observer Design for Robot Manipulators," *Mathematics*, vol. 11, no. 19, doi: 10.3390/math11194033.

B. International Conference

1. **M. H. Nguyen**, H. V. Dao and K. K. Ahn, "Nonlinear robust control for electro-hydraulic servo systems with largely unknown model dynamics and disturbances," 2021 24th International Conference on Mechatronics Technology (ICMT), Singapore, 2021, pp. 1-6, doi: 10.1109/ICMT53429.2021.9687105.
2. D. T. Tran, H. N. Tong, M. P. Tran, T. B. Ha, **M.H. Nguyen** and K. K. Ahn, "Extended State Observer Based Sliding Mode Control For 6 DOF Manipulator With Lumped Uncertainties," 2022

25th International Conference on Mechatronics Technology (ICMT), Kaohsiung, Taiwan, 2022, pp. 1-6, doi: 10.1109/ICMT56556.2022.9997714.

3. **M. H. Nguyen**, J. H. Ahn, and K. K. Ahn, "A Novel Finite-time Continuous Exact First-order Differentiator," in 2023 International Conference on System Science and Engineering (ICSSE), 27-28 July 2023 2023, pp. 170-173, doi: 10.1109/ICSSE58758.2023.10227219.

4. D. T. Tran; T. N. Nguyen; X. T. Nguyen; D. M. Nguyen; Q. T. Truong; H. A. Trinh; **M. H. Nguyen**; K. K. Ahn, "Practical Sliding Mode Control with Time Delay Estimation for a 4-DOF Parallel Manipulator with Variant Payload," in 2023 26th International Conference on Mechatronics Technology (ICMT), 18-21 Oct. 2023 2023, pp. 1-5, doi: 10.1109/ICMT59920.2023.10373626.

References

- [1] A. Melander, A. Delic, A. Björkblad, P. Juntunen, L. Samek, and L. Vadillo, "Modelling of electro hydraulic free and die forming of sheet steels," *International Journal of Material Forming*, vol. 6, no. 2, pp. 223-231, 2013/06/01 2013, doi: 10.1007/s12289-011-1080-5.
- [2] L. Li, H. Huang, F. Zhao, J. W. Sutherland, and Z. Liu, "An Energy-Saving Method by Balancing the Load of Operations for Hydraulic Press," *IEEE/ASME Transactions on Mechatronics*, vol. 22, no. 6, pp. 2673-2683, 2017, doi: 10.1109/TMECH.2017.2759228.
- [3] H. Roozbahani, M. Alizadeh, A. Ahomäki, and H. Handroos, "Coordinate-based control for a materials handling equipment utilizing real-time simulation," *Automation in Construction*, vol. 122, p. 103483, 2021/02/01/ 2021, doi: <https://doi.org/10.1016/j.autcon.2020.103483>.
- [4] S. Jaiswal, L. Pyrhönen, and A. Mikkola, "Computationally Efficient Coupling of Multibody Dynamics and Hydraulic Actuators in Simulating Hydraulic Machinery," *IEEE/ASME Transactions on Mechatronics*, vol. 28, no. 3, pp. 1291-1302, 2023, doi: 10.1109/TMECH.2022.3225711.
- [5] P. Egli and M. Hutter, "A General Approach for the Automation of Hydraulic Excavator Arms Using Reinforcement Learning," *IEEE Robotics and Automation Letters*, vol. 7, no. 2, pp. 5679-5686, 2022, doi: 10.1109/LRA.2022.3152865.
- [6] A. C. Bertolino, A. De Martin, G. Jacazio, and M. Sorli, "A Case Study on the Detection and Prognosis of Internal Leakages in Electro-Hydraulic Flight Control Actuators," *Actuators*, vol. 10, no. 9, doi: 10.3390/act10090215.
- [7] A. De Martin, A. Dellacasa, G. Jacazio, and M. Sorli, "High-Fidelity Model of Electro-Hydraulic Actuators for Primary Flight Control Systems," 2018. [Online]. Available: <https://doi.org/10.1115/FPMC2018-8917>.
- [8] H. Feng *et al.*, "A new adaptive sliding mode controller based on the RBF neural network for an electro-hydraulic servo system," *ISA Transactions*, vol. 129, pp. 472-484, 2022/10/01/ 2022, doi: <https://doi.org/10.1016/j.isatra.2021.12.044>.
- [9] G. Yang and J. Yao, "Multilayer neuroadaptive force control of electro-hydraulic load simulators with uncertainty rejection," *Applied Soft Computing*, vol. 130, p. 109672, 2022/11/01/ 2022, doi: <https://doi.org/10.1016/j.asoc.2022.109672>.
- [10] M. Y. Coskun and M. İtik, "Intelligent PID control of an industrial electro-hydraulic system," *ISA Transactions*, 2023/04/12/ 2023, doi: <https://doi.org/10.1016/j.isatra.2023.04.005>.
- [11] A. Tony Thomas, R. Parameshwaran, S. Sathiyavathi, and A. Vimala Starbino, "Improved Position Tracking Performance of Electro Hydraulic Actuator Using PID and Sliding Mode Controller," *IETE Journal of Research*, vol. 68, no. 3, pp. 1683-1695, 2022/05/04 2022, doi: 10.1080/03772063.2019.1664341.
- [12] H. Feng, W. Ma, C. Yin, and D. Cao, "Trajectory control of electro-hydraulic position servo system using improved PSO-PID controller," *Automation in Construction*, vol. 127, p. 103722, 2021/07/01/ 2021, doi: <https://doi.org/10.1016/j.autcon.2021.103722>.
- [13] T. C. Do, D. T. Tran, T. Q. Dinh, and K. K. Ahn, "Tracking Control for an Electro-Hydraulic Rotary Actuator Using Fractional Order Fuzzy PID Controller," *Electronics*, vol. 9, no. 6, doi: 10.3390/electronics9060926.
- [14] W. Ma, S. Ma, W. Qiao, D. Cao, and C. Yin, "Research on PID Controller of Excavator Electro-Hydraulic System Based on Improved Differential Evolution," *Machines*, vol. 11, no. 2, doi: 10.3390/machines11020143.
- [15] F. Cao, "PID controller optimized by genetic algorithm for direct-drive servo system," *Neural Computing and Applications*, vol. 32, no. 1, pp. 23-30, 2020/01/01 2020, doi: 10.1007/s00521-018-3739-z.

- [16] J. Pongfai, X. Su, H. Zhang, and W. Assawinchaichote, "A novel optimal PID controller autotuning design based on the SLP algorithm," *Expert Systems*, <https://doi.org/10.1111/exsy.12489> vol. 37, no. 2, p. e12489, 2020/04/01 2020, doi: <https://doi.org/10.1111/exsy.12489>.
- [17] G. Wrat, M. Bholra, P. Ranjan, S. K. Mishra, and J. Das, "Energy saving and Fuzzy-PID position control of electro-hydraulic system by leakage compensation through proportional flow control valve," *ISA Transactions*, vol. 101, pp. 269-280, 2020/06/01/ 2020, doi: <https://doi.org/10.1016/j.isatra.2020.01.003>.
- [18] J. Pongfai, X. Su, H. Zhang, and W. Assawinchaichote, "PID Controller Autotuning Design by a Deterministic Q-SLP Algorithm," *IEEE Access*, vol. 8, pp. 50010-50021, 2020, doi: 10.1109/ACCESS.2020.2979810.
- [19] P. Shah and S. Agashe, "Review of fractional PID controller," *Mechatronics*, vol. 38, pp. 29-41, 2016/09/01/ 2016, doi: <https://doi.org/10.1016/j.mechatronics.2016.06.005>.
- [20] M. H. Nguyen and K. K. Ahn, "Output Feedback Robust Tracking Control for a Variable-Speed Pump-Controlled Hydraulic System Subject to Mismatched Uncertainties," *Mathematics*, vol. 11, no. 8, doi: 10.3390/math11081783.
- [21] V. D. Phan, C. P. Vo, H. V. Dao, and K. K. Ahn, "Actuator Fault-Tolerant Control for an Electro-Hydraulic Actuator Using Time Delay Estimation and Feedback Linearization," *IEEE Access*, vol. 9, pp. 107111-107123, 2021, doi: 10.1109/ACCESS.2021.3101038.
- [22] J. Seo, R. Venugopal, and J.-P. Kenné, "Feedback linearization based control of a rotational hydraulic drive," *Control Engineering Practice*, vol. 15, no. 12, pp. 1495-1507, 2007/12/01/ 2007, doi: <https://doi.org/10.1016/j.conengprac.2007.02.009>.
- [23] X. Yuan, Z. Chen, Y. Yuan, Y. Huang, X. Li, and W. Li, "Sliding mode controller of hydraulic generator regulating system based on the input/output feedback linearization method," *Mathematics and Computers in Simulation*, vol. 119, pp. 18-34, 2016/01/01/ 2016, doi: <https://doi.org/10.1016/j.matcom.2015.08.020>.
- [24] H. A. Mintsa, R. Venugopal, J. P. Kenne, and C. Belleau, "Feedback Linearization-Based Position Control of an Electrohydraulic Servo System With Supply Pressure Uncertainty," *IEEE Transactions on Control Systems Technology*, vol. 20, no. 4, pp. 1092-1099, 2012, doi: 10.1109/TCST.2011.2158101.
- [25] Y. Liu and H. Handroos, "Technical note Sliding mode control for a class of hydraulic position servo," *Mechatronics*, vol. 9, no. 1, pp. 111-123, 1999/02/01/ 1999, doi: [https://doi.org/10.1016/S0957-4158\(98\)00044-0](https://doi.org/10.1016/S0957-4158(98)00044-0).
- [26] C. Guan and S. Pan, "Adaptive sliding mode control of electro-hydraulic system with nonlinear unknown parameters," *Control Engineering Practice*, vol. 16, no. 11, pp. 1275-1284, 2008/11/01/ 2008, doi: <https://doi.org/10.1016/j.conengprac.2008.02.002>.
- [27] J. Kim, M. Jin, W. Choi, and J. Lee, "Discrete time delay control for hydraulic excavator motion control with terminal sliding mode control," *Mechatronics*, vol. 60, pp. 15-25, 2019/06/01/ 2019, doi: <https://doi.org/10.1016/j.mechatronics.2019.04.008>.
- [28] H. Komurcugil, S. Biricik, S. Bayhan, and Z. Zhang, "Sliding Mode Control: Overview of Its Applications in Power Converters," *IEEE Industrial Electronics Magazine*, vol. 15, no. 1, pp. 40-49, 2021, doi: 10.1109/MIE.2020.2986165.
- [29] S. J. Gambhire, D. R. Kishore, P. S. Londhe, and S. N. Pawar, "Review of sliding mode based control techniques for control system applications," *International Journal of Dynamics and Control*, vol. 9, no. 1, pp. 363-378, 2021/03/01 2021, doi: 10.1007/s40435-020-00638-7.
- [30] W. Gu, J. Yao, Z. Yao, and J. Zheng, "Robust Adaptive Control of Hydraulic System With Input Saturation and Valve Dead-Zone," *IEEE Access*, vol. 6, pp. 53521-53532, 2018, doi: 10.1109/ACCESS.2018.2871069.

- [31] X. Li, J. Yao, and C. Zhou, "Output feedback adaptive robust control of hydraulic actuator with friction and model uncertainty compensation," *Journal of the Franklin Institute*, vol. 354, no. 13, pp. 5328-5349, 2017/09/01/ 2017, doi: <https://doi.org/10.1016/j.jfranklin.2017.06.020>.
- [32] S. Chen *et al.*, "Adaptive Robust Cascade Force Control of 1-DOF Hydraulic Exoskeleton for Human Performance Augmentation," *IEEE/ASME Transactions on Mechatronics*, vol. 22, no. 2, pp. 589-600, 2017, doi: 10.1109/TMECH.2016.2614987.
- [33] X. Hao, I. Salhi, S. Laghrouche, Y. Ait-Amirat, and A. Djerdir, "Backstepping Supertwisting Control of Four-Phase Interleaved Boost Converter for PEM Fuel Cell," *IEEE Transactions on Power Electronics*, vol. 37, no. 7, pp. 7858-7870, 2022, doi: 10.1109/TPEL.2022.3149099.
- [34] H. K. Khalil, *Nonlinear systems*. (in English), 2002.
- [35] D. Swaroop, J. K. Hedrick, P. P. Yip, and J. C. Gerdes, "Dynamic surface control for a class of nonlinear systems," *IEEE Transactions on Automatic Control*, vol. 45, no. 10, pp. 1893-1899, 2000, doi: 10.1109/TAC.2000.880994.
- [36] D. Swaroop, J. C. Gerdes, P. P. Yip, and J. K. Hedrick, "Dynamic surface control of nonlinear systems," in *Proceedings of the 1997 American Control Conference (Cat. No.97CH36041)*, 6-6 June 1997 1997, vol. 5, pp. 3028-3034 vol.5, doi: 10.1109/ACC.1997.612013.
- [37] J. A. Farrell, M. Polycarpou, M. Sharma, and W. Dong, "Command Filtered Backstepping," *IEEE Transactions on Automatic Control*, vol. 54, no. 6, pp. 1391-1395, 2009, doi: 10.1109/TAC.2009.2015562.
- [38] W. Dong, J. A. Farrell, M. M. Polycarpou, V. Djapic, and M. Sharma, "Command Filtered Adaptive Backstepping," *IEEE Transactions on Control Systems Technology*, vol. 20, no. 3, pp. 566-580, 2012, doi: 10.1109/TCST.2011.2121907.
- [39] Z. J. Yang, K. Miyazaki, S. Kanae, and K. Wada, "Robust position control of a magnetic levitation system via dynamic surface control technique," *IEEE Transactions on Industrial Electronics*, vol. 51, no. 1, pp. 26-34, 2004, doi: 10.1109/TIE.2003.822095.
- [40] D. Wang and H. Jie, "Neural network-based adaptive dynamic surface control for a class of uncertain nonlinear systems in strict-feedback form," *IEEE Transactions on Neural Networks*, vol. 16, no. 1, pp. 195-202, 2005, doi: 10.1109/TNN.2004.839354.
- [41] Z. Peng, D. Wang, Z. Chen, X. Hu, and W. Lan, "Adaptive Dynamic Surface Control for Formations of Autonomous Surface Vehicles With Uncertain Dynamics," *IEEE Transactions on Control Systems Technology*, vol. 21, no. 2, pp. 513-520, 2013, doi: 10.1109/TCST.2011.2181513.
- [42] D.-J. Li, "Adaptive output feedback control of uncertain nonlinear chaotic systems based on dynamic surface control technique," *Nonlinear Dynamics*, vol. 68, no. 1, pp. 235-243, 2012/04/01 2012, doi: 10.1007/s11071-011-0222-0.
- [43] W. Chenliang and L. Yan, "Adaptive dynamic surface control for linear multivariable systems," *Automatica*, vol. 46, no. 10, pp. 1703-1711, 2010/10/01/ 2010, doi: <https://doi.org/10.1016/j.automatica.2010.06.020>.
- [44] Y. Pan, H. Wang, X. Li, and H. Yu, "Adaptive Command-Filtered Backstepping Control of Robot Arms With Compliant Actuators," *IEEE Transactions on Control Systems Technology*, vol. 26, no. 3, pp. 1149-1156, 2018, doi: 10.1109/TCST.2017.2695600.
- [45] Q. Shen and P. Shi, "Distributed command filtered backstepping consensus tracking control of nonlinear multiple-agent systems in strict-feedback form," *Automatica*, vol. 53, pp. 120-124, 2015/03/01/ 2015, doi: <https://doi.org/10.1016/j.automatica.2014.12.046>.
- [46] K. Liu and R. Wang, "Antisaturation Command Filtered Backstepping Control-Based Disturbance Rejection for a Quadrotor UAV," *IEEE Transactions on Circuits and Systems II: Express Briefs*, vol. 68, no. 12, pp. 3577-3581, 2021, doi: 10.1109/TCSII.2021.3069967.
- [47] G. Cui, J. Yu, and Q. G. Wang, "Finite-Time Adaptive Fuzzy Control for MIMO Nonlinear Systems With Input Saturation via Improved Command-Filtered Backstepping," *IEEE*

Transactions on Systems, Man, and Cybernetics: Systems, vol. 52, no. 2, pp. 980-989, 2022, doi: 10.1109/TSMC.2020.3010642.

- [48] G. Besançon, *Nonlinear observers and applications*. Springer, 2007.
- [49] G. Ellis, *Observers in control systems: a practical guide*. Elsevier, 2002.
- [50] D. G. Luenberger, "Observing the State of a Linear System," *IEEE Transactions on Military Electronics*, vol. 8, no. 2, pp. 74-80, 1964, doi: 10.1109/TME.1964.4323124.
- [51] D. Luenberger, "An introduction to observers," *IEEE Transactions on Automatic Control*, vol. 16, no. 6, pp. 596-602, 1971, doi: 10.1109/TAC.1971.1099826.
- [52] D. Luenberger, "Observers for multivariable systems," *IEEE Transactions on Automatic Control*, vol. 11, no. 2, pp. 190-197, 1966, doi: 10.1109/TAC.1966.1098323.
- [53] M. Zeitz, "The extended Luenberger observer for nonlinear systems," *Systems & Control Letters*, vol. 9, no. 2, pp. 149-156, 1987/08/01/ 1987, doi: [https://doi.org/10.1016/0167-6911\(87\)90021-1](https://doi.org/10.1016/0167-6911(87)90021-1).
- [54] H. W. Sorenson, "Kalman filtering: theory and application," (*No Title*), 1985.
- [55] M. Sepasi and F. Sassani, "On-line fault diagnosis of hydraulic systems using Unscented Kalman Filter," *International Journal of Control, Automation and Systems*, vol. 8, no. 1, pp. 149-156, 2010/02/01 2010, doi: 10.1007/s12555-010-0119-6.
- [56] K. K. Ahn and D. Q. Truong, "Online tuning fuzzy PID controller using robust extended Kalman filter," *Journal of Process Control*, vol. 19, no. 6, pp. 1011-1023, 2009/06/01/ 2009, doi: <https://doi.org/10.1016/j.jprocont.2009.01.005>.
- [57] S. Raghavan and J. K. Hedrick, "Observer design for a class of nonlinear systems," *International Journal of Control*, vol. 59, no. 2, pp. 515-528, 1994/02/01 1994, doi: 10.1080/00207179408923090.
- [58] V. I. Utkin, *Sliding modes in control and optimization*. Springer Science & Business Media, 2013.
- [59] C. Edwards, S. K. Spurgeon, and R. J. Patton, "Sliding mode observers for fault detection and isolation," *Automatica*, vol. 36, no. 4, pp. 541-553, 2000/04/01/ 2000, doi: [https://doi.org/10.1016/S0005-1098\(99\)00177-6](https://doi.org/10.1016/S0005-1098(99)00177-6).
- [60] X. Yi and M. Saif, "Sliding mode observer for nonlinear uncertain systems," *IEEE Transactions on Automatic Control*, vol. 46, no. 12, pp. 2012-2017, 2001, doi: 10.1109/9.975511.
- [61] K. Veluvolu, Y. Soh, and W. Cao, "Robust discrete-time nonlinear sliding mode state estimation of uncertain nonlinear systems," *International Journal of Robust and Nonlinear Control: IFAC-Affiliated Journal*, vol. 17, no. 9, pp. 803-828, 2007.
- [62] C. Wen-Hua, "Disturbance observer based control for nonlinear systems," *IEEE/ASME Transactions on Mechatronics*, vol. 9, no. 4, pp. 706-710, 2004, doi: 10.1109/TMECH.2004.839034.
- [63] K. Ohishi, "Torque-speed regulation of DC motor based on load torque estimation," *Proc. IEEEJ IPEC, Tokyo, Japan, 1983-3*, vol. 2, pp. 1209-1216, 1983.
- [64] W.-H. Chen, D. J. Ballance, P. J. Gawthrop, and J. O'Reilly, "A nonlinear disturbance observer for robotic manipulators," *IEEE Transactions on industrial Electronics*, vol. 47, no. 4, pp. 932-938, 2000.
- [65] N. Gu, D. Wang, Z. Peng, J. Wang, and Q.-L. Han, "Disturbance observers and extended state observers for marine vehicles: A survey," *Control Engineering Practice*, vol. 123, p. 105158, 2022.
- [66] S. Komada, M. Ishida, K. Ohnishi, and T. Hori, "Disturbance observer-based motion control of direct drive motors," *IEEE Transactions on Energy Conversion*, vol. 6, no. 3, pp. 553-559, 1991.

- [67] W. Zhao, S. Jiao, Q. Chen, D. Xu, and J. Ji, "Sensorless control of a linear permanent-magnet motor based on an improved disturbance observer," *IEEE Transactions on Industrial Electronics*, vol. 65, no. 12, pp. 9291-9300, 2018.
- [68] K. Guo, J. Wei, J. Fang, R. Feng, and X. Wang, "Position tracking control of electro-hydraulic single-rod actuator based on an extended disturbance observer," *Mechatronics*, vol. 27, pp. 47-56, 2015.
- [69] D. Won, W. Kim, D. Shin, and C. C. Chung, "High-gain disturbance observer-based backstepping control with output tracking error constraint for electro-hydraulic systems," *IEEE transactions on control systems technology*, vol. 23, no. 2, pp. 787-795, 2014.
- [70] Q. Guo, J.-m. Yin, T. Yu, and D. Jiang, "Coupled-disturbance-observer-based position tracking control for a cascade electro-hydraulic system," *ISA transactions*, vol. 68, pp. 367-380, 2017.
- [71] E. Sariyildiz, R. Oboe, and K. Ohnishi, "Disturbance Observer-Based Robust Control and Its Applications: 35th Anniversary Overview," *IEEE Transactions on Industrial Electronics*, vol. 67, no. 3, pp. 2042-2053, 2020, doi: 10.1109/TIE.2019.2903752.
- [72] M. H. Nguyen, H. V. Dao, and K. K. Ahn, "Active Disturbance Rejection Control for Position Tracking of Electro-Hydraulic Servo Systems under Modeling Uncertainty and External Load," *Actuators*, vol. 10, no. 2, doi: 10.3390/act10020020.
- [73] J. Han, "From PID to Active Disturbance Rejection Control," *IEEE Transactions on Industrial Electronics*, vol. 56, no. 3, pp. 900-906, 2009, doi: 10.1109/TIE.2008.2011621.
- [74] J. Liu, S. Vazquez, L. Wu, A. Marquez, H. Gao, and L. G. Franquelo, "Extended state observer-based sliding-mode control for three-phase power converters," *IEEE Transactions on Industrial Electronics*, vol. 64, no. 1, pp. 22-31, 2016.
- [75] J. Yao, Z. Jiao, and D. Ma, "Adaptive robust control of DC motors with extended state observer," *IEEE transactions on industrial electronics*, vol. 61, no. 7, pp. 3630-3637, 2013.
- [76] J. Yao, Z. Jiao, and D. Ma, "Extended-state-observer-based output feedback nonlinear robust control of hydraulic systems with backstepping," *IEEE Transactions on Industrial electronics*, vol. 61, no. 11, pp. 6285-6293, 2014.
- [77] S. E. Talole, J. P. Kolhe, and S. B. Phadke, "Extended-state-observer-based control of flexible-joint system with experimental validation," *IEEE Transactions on Industrial Electronics*, vol. 57, no. 4, pp. 1411-1419, 2009.
- [78] H. Guang-Bin, P. Saratchandran, and N. Sundararajan, "A generalized growing and pruning RBF (GGAP-RBF) neural network for function approximation," *IEEE Transactions on Neural Networks*, vol. 16, no. 1, pp. 57-67, 2005, doi: 10.1109/TNN.2004.836241.
- [79] D. Shang, X. Li, M. Yin, and F. Li, "Dynamic modeling and RBF neural network compensation control for space flexible manipulator with an underactuated hand," *Chinese Journal of Aeronautics*, vol. 37, no. 3, pp. 417-439, 2024/03/01/ 2024, doi: <https://doi.org/10.1016/j.cja.2023.08.003>.
- [80] Y. Ge, J. Zhou, W. Deng, J. Yao, and L. Xie, "Neural network robust control of a 3-DOF hydraulic manipulator with asymptotic tracking," *Asian Journal of Control*, <https://doi.org/10.1002/asjc.2867> vol. n/a, no. n/a, 2022/06/10 2022, doi: <https://doi.org/10.1002/asjc.2867>.
- [81] W. Deng, H. Zhou, J. Zhou, and J. Yao, "Neural Network-Based Adaptive Asymptotic Prescribed Performance Tracking Control of Hydraulic Manipulators," *IEEE Transactions on Systems, Man, and Cybernetics: Systems*, pp. 1-11, 2022, doi: 10.1109/TSMC.2022.3178626.
- [82] Y. Zhang, D. Kim, Y. Zhao, and J. Lee, "PD Control of a Manipulator with Gravity and Inertia Compensation Using an RBF Neural Network," *International Journal of Control, Automation and Systems*, vol. 18, no. 12, pp. 3083-3092, 2020/12/01 2020, doi: 10.1007/s12555-019-0482-x.

- [83] W. He, A. O. David, Z. Yin, and C. Sun, "Neural Network Control of a Robotic Manipulator With Input Deadzone and Output Constraint," *IEEE Transactions on Systems, Man, and Cybernetics: Systems*, vol. 46, no. 6, pp. 759-770, 2016, doi: 10.1109/TSMC.2015.2466194.
- [84] D. Zhang, C. Wang, Y. Wei, and L. Yang, "Analysis of motion interference characteristics of underwater vehicles salvo based on the RBF Neural Network," *Ocean Engineering*, vol. 277, p. 114254, 2023/06/01/ 2023, doi: <https://doi.org/10.1016/j.oceaneng.2023.114254>.
- [85] Y. J. Liu, Q. Zeng, L. Liu, and S. Tong, "An Adaptive Neural Network Controller for Active Suspension Systems With Hydraulic Actuator," *IEEE Transactions on Systems, Man, and Cybernetics: Systems*, vol. 50, no. 12, pp. 5351-5360, 2020, doi: 10.1109/TSMC.2018.2875187.
- [86] R. Ding, C. Ding, Y. Xu, W. Liu, and X. Yang, "Neural network-based robust integral error sign control for servo motor systems with enhanced disturbance rejection performance," *ISA Transactions*, vol. 129, pp. 580-591, 2022/10/01/ 2022, doi: <https://doi.org/10.1016/j.isatra.2021.12.026>.
- [87] R. Ding, C. Ding, Y. Xu, and X. Yang, "Neural-network-based adaptive robust precision motion control of linear motors with asymptotic tracking performance," *Nonlinear Dynamics*, vol. 108, no. 2, pp. 1339-1356, 2022/04/01 2022, doi: 10.1007/s11071-022-07258-0.
- [88] Y. Yang, Y. Li, X. Liu, and D. Huang, "Adaptive neural network control for a hydraulic knee exoskeleton with valve deadband and output constraint based on nonlinear disturbance observer," *Neurocomputing*, vol. 473, pp. 14-23, 2022/02/07/ 2022, doi: <https://doi.org/10.1016/j.neucom.2021.12.010>.
- [89] W. Yang, F. Meng, S. Meng, S. Man, and A. Pang, "Tracking Control of Magnetic Levitation System Using Model-Free RBF Neural Network Design," *IEEE Access*, vol. 8, pp. 204563-204572, 2020, doi: 10.1109/ACCESS.2020.3037352.
- [90] Z. Yao, J. Yao, and W. Sun, "Adaptive RISE Control of Hydraulic Systems With Multilayer Neural-Networks," *IEEE Transactions on Industrial Electronics*, vol. 66, no. 11, pp. 8638-8647, 2019, doi: 10.1109/TIE.2018.2886773.
- [91] M. H. Nguyen and K. K. Ahn, "A Novel Trajectory Adjustment Mechanism-Based Prescribed Performance Tracking Control for Electro-Hydraulic Systems Subject to Disturbances and Modeling Uncertainties," *Applied Sciences*, vol. 12, no. 12, 2022, doi: 10.3390/app12126034.
- [92] H. E. Merritt, "Hydraulic control systems, 1967," *J. Wiley*, 1967.
- [93] W. Deng, J. Yao, Y. Wang, X. Yang, and J. Chen, "Output feedback backstepping control of hydraulic actuators with valve dynamics compensation," *Mechanical Systems and Signal Processing*, vol. 158, p. 107769, 2021, doi: 10.1016/j.ymssp.2021.107769.
- [94] W. Deng and J. Yao, "Extended-State-Observer-Based Adaptive Control of Electrohydraulic Servomechanisms Without Velocity Measurement," *IEEE/ASME Transactions on Mechatronics*, vol. 25, no. 3, pp. 1151-1161, 2020, doi: 10.1109/TMECH.2019.2959297.
- [95] J. Yao and W. Deng, "Active Disturbance Rejection Adaptive Control of Hydraulic Servo Systems," *IEEE Transactions on Industrial Electronics*, vol. 64, no. 10, pp. 8023-8032, 2017, doi: 10.1109/TIE.2017.2694382.
- [96] S. Yu, X. Yu, B. Shirinzadeh, and Z. Man, "Continuous finite-time control for robotic manipulators with terminal sliding mode," *Automatica*, vol. 41, no. 11, pp. 1957-1964, 2005/11/01/ 2005, doi: <https://doi.org/10.1016/j.automatica.2005.07.001>.
- [97] M. H. Nguyen, H. V. Dao, and K. K. Ahn, "Active Disturbance Rejection Control for Position Tracking of Electro-Hydraulic Servo Systems under Modeling Uncertainty and External Load," in *Actuators*, 2021, vol. 10, no. 2: Multidisciplinary Digital Publishing Institute, p. 20.
- [98] M. Krstic and H. Deng, *Stabilization of nonlinear uncertain systems*. Springer, 1998.
- [99] B. Yang and W. Lin, "Homogeneous observers, iterative design, and global stabilization of high-order nonlinear systems by smooth output feedback," *IEEE Transactions on Automatic Control*, vol. 49, no. 7, pp. 1069-1080, 2004.

- [100] C. Luo, J. Yao, F. Chen, L. Li, and Q. Xu, "Adaptive Repetitive Control of Hydraulic Load Simulator With RISE Feedback," *IEEE Access*, vol. 5, pp. 23901-23911, 2017, doi: 10.1109/ACCESS.2017.2762665.
- [101] J. Koivumäki and J. Mattila, "Stability-Guaranteed Impedance Control of Hydraulic Robotic Manipulators," *IEEE/ASME Transactions on Mechatronics*, vol. 22, no. 2, pp. 601-612, 2017, doi: 10.1109/TMECH.2016.2618912.
- [102] T. X. Dinh, T. D. Thien, T. H. V. Anh, and K. K. Ahn, "Disturbance Observer Based Finite Time Trajectory Tracking Control for a 3 DOF Hydraulic Manipulator Including Actuator Dynamics," *IEEE Access*, vol. 6, pp. 36798-36809, 2018, doi: 10.1109/ACCESS.2018.2848240.
- [103] H. V. Truong, D. T. Tran, X. D. To, K. K. Ahn, and M. Jin, "Adaptive Fuzzy Backstepping Sliding Mode Control for a 3-DOF Hydraulic Manipulator with Nonlinear Disturbance Observer for Large Payload Variation," *Applied Sciences*, vol. 9, no. 16, 2019, doi: 10.3390/app9163290.
- [104] H.-V.-A. Truong, D.-T. Tran, and K. K. Ahn, "A Neural Network Based Sliding Mode Control for Tracking Performance with Parameters Variation of a 3-DOF Manipulator," *Applied Sciences*, vol. 9, no. 10, doi: 10.3390/app9102023.
- [105] T. Trần, A. Truong, and K. K. Ahn, "Adaptive Backstepping Sliding Mode Control Based RBFNN for a Hydraulic Manipulator Including Actuator Dynamics," *Applied Sciences*, vol. 9, p. 1265, 03/26 2019, doi: 10.3390/app9061265.
- [106] S. Bongain and M. Jamett, "Electrohydraulic Active Suspension Fuzzy-Neural Based Control System," *IEEE Latin America Transactions*, vol. 16, no. 9, pp. 2454-2459, 2018, doi: 10.1109/TLA.2018.8789568.
- [107] H. Pan and W. Sun, "Nonlinear Output Feedback Finite-Time Control for Vehicle Active Suspension Systems," *IEEE Transactions on Industrial Informatics*, vol. 15, no. 4, pp. 2073-2082, 2019, doi: 10.1109/TII.2018.2866518.
- [108] C. Sun, J. Fang, J. Wei, and B. Hu, "Nonlinear Motion Control of a Hydraulic Press Based on an Extended Disturbance Observer," *IEEE Access*, vol. 6, pp. 18502-18510, 2018, doi: 10.1109/ACCESS.2018.2813317.
- [109] Q. Guo, Y. Zhang, B. G. Celler, and S. W. Su, "Backstepping Control of Electro-Hydraulic System Based on Extended-State-Observer With Plant Dynamics Largely Unknown," *IEEE Transactions on Industrial Electronics*, vol. 63, no. 11, pp. 6909-6920, 2016, doi: 10.1109/TIE.2016.2585080.
- [110] J.-h. Kwon, T.-h. Kim, J. Jang, and i.-y. Lee, *Feedback Linearization Control of a Hydraulic Servo System*. 2006, pp. 455-460.
- [111] B. Ayalew and K. W. Jablolkow, "Partial feedback linearising force-tracking control: implementation and testing in electrohydraulic actuation," *IET Control Theory & Applications*, vol. 1, no. 3, pp. 689-698. [Online]. Available: https://digital-library.theiet.org/content/journals/10.1049/iet-cta_20060186
- [112] H. A. Mintsa, R. Venugopal, J. Kenne, and C. Belleau, "Feedback Linearization-Based Position Control of an Electrohydraulic Servo System With Supply Pressure Uncertainty," *IEEE Transactions on Control Systems Technology*, vol. 20, no. 4, pp. 1092-1099, 2012, doi: 10.1109/TCST.2011.2158101.
- [113] A. A. Kabanov, "Feedback Linearization of Nonlinear Singularly Perturbed Systems with State-dependent Coefficients," *International Journal of Control, Automation and Systems*, vol. 18, no. 7, pp. 1743-1750, 2020/07/01 2020, doi: 10.1007/s12555-019-0357-1.
- [114] L. Hung-Ching and L. Wen-Chen, "Robust controller with disturbance rejection for hydraulic servo systems," *IEEE Transactions on Industrial Electronics*, vol. 40, no. 1, pp. 157-162, 1993, doi: 10.1109/41.184833.

- [115] J. Yao, Z. Jiao, D. Ma, and L. Yan, "High-Accuracy Tracking Control of Hydraulic Rotary Actuators With Modeling Uncertainties," *IEEE/ASME Transactions on Mechatronics*, vol. 19, no. 2, pp. 633-641, 2014, doi: 10.1109/TMECH.2013.2252360.
- [116] J. Baek, M. Jin, and S. Han, "A New Adaptive Sliding Mode Control Scheme for Application to Robot Manipulators," *IEEE Transactions on Industrial Electronics*, vol. 63, pp. 1-1, 06/01 2016, doi: 10.1109/TIE.2016.2522386.
- [117] V. Utkin and H. Lee, "CHATTERING PROBLEM IN SLIDING MODE CONTROL SYSTEMS," *IFAC Proceedings Volumes*, vol. 39, no. 5, p. 1, 2006/01/01/ 2006, doi: <https://doi.org/10.3182/20060607-3-IT-3902.00003>.
- [118] H.-M. Chen, J.-C. Renn, and J.-P. Su, "Sliding mode control with varying boundary layers for an electro-hydraulic position servo system," *The International Journal of Advanced Manufacturing Technology*, vol. 26, no. 1, pp. 117-123, 2005/07/01 2005, doi: 10.1007/s00170-004-2145-0.
- [119] M. A. Ghazy, "Variable structure control for electrohydraulic position servo system," in *IECON'01. 27th Annual Conference of the IEEE Industrial Electronics Society (Cat. No.37243)*, 29 Nov.-2 Dec. 2001 2001, vol. 3, pp. 2194-2198 vol.3, doi: 10.1109/IECON.2001.975634.
- [120] J. J. Rath, M. Defoort, H. R. Karimi, and K. C. Veluvolu, "Output Feedback Active Suspension Control With Higher Order Terminal Sliding Mode," *IEEE Transactions on Industrial Electronics*, vol. 64, no. 2, pp. 1392-1403, 2017, doi: 10.1109/TIE.2016.2611587.
- [121] S. Alvarez-Rodríguez, G. Flores, and N. A. Ochoa, "Variable Gains Sliding Mode Control," *International Journal of Control, Automation and Systems*, vol. 17, no. 3, pp. 555-564, 2019/03/01 2019, doi: 10.1007/s12555-018-0095-9.
- [122] K. K. Ahn, D. N. C. Nam, and M. Jin, "Adaptive Backstepping Control of an Electrohydraulic Actuator," *IEEE/ASME Transactions on Mechatronics*, vol. 19, no. 3, pp. 987-995, 2014, doi: 10.1109/TMECH.2013.2265312.
- [123] J. Yao, W. Deng, and Z. Jiao, "RISE-Based Adaptive Control of Hydraulic Systems With Asymptotic Tracking," *IEEE Transactions on Automation Science and Engineering*, vol. 14, no. 3, pp. 1524-1531, 2017, doi: 10.1109/TASE.2015.2434393.
- [124] G. Yang and J. Yao, "Nonlinear adaptive output feedback robust control of hydraulic actuators with largely unknown modeling uncertainties," *Applied Mathematical Modelling*, vol. 79, pp. 824-842, 2020/03/01/ 2020, doi: <https://doi.org/10.1016/j.apm.2019.10.062>.
- [125] L. Feng and H. Yan, "Nonlinear Adaptive Robust Control of the Electro-Hydraulic Servo System," *Applied Sciences*, vol. 10, no. 13, p. 4494, 2020. [Online]. Available: <https://www.mdpi.com/2076-3417/10/13/4494>.
- [126] W. Chen, J. Yang, L. Guo, and S. Li, "Disturbance-Observer-Based Control and Related Methods—An Overview," *IEEE Transactions on Industrial Electronics*, vol. 63, no. 2, pp. 1083-1095, 2016, doi: 10.1109/TIE.2015.2478397.
- [127] D. Won, W. Kim, D. Shin, and C. C. Chung, "High-Gain Disturbance Observer-Based Backstepping Control With Output Tracking Error Constraint for Electro-Hydraulic Systems," *IEEE Transactions on Control Systems Technology*, vol. 23, no. 2, pp. 787-795, 2015, doi: 10.1109/TCST.2014.2325895.
- [128] G. Xu, N. Lu, and G. Lv, "High-Gain Observer-Based Sliding Mode Force Control for the Single-Rod Electrohydraulic Servo Actuator," *IEEE Access*, vol. 7, pp. 161849-161857, 2019, doi: 10.1109/ACCESS.2019.2951696.
- [129] W. Jie, Z. Yudong, B. Yulong, H. H. Kim, and M. C. Lee, "Trajectory Tracking Control Using Fractional-Order Terminal Sliding Mode Control With Sliding Perturbation Observer for a 7-DOF Robot Manipulator," *IEEE/ASME Transactions on Mechatronics*, vol. 25, no. 4, pp. 1886-1893, 2020, doi: 10.1109/TMECH.2020.2992676.

- [130] D. Deepika, S. Narayan, and S. Kaur, "Robust finite time integral sliding mode tracker for nth-order non-affine non-linear system with uncertainty and disturbance estimator," *Mathematics and Computers in Simulation*, vol. 156, pp. 364-376, 2019/02/01/ 2019, doi: <https://doi.org/10.1016/j.matcom.2018.09.006>.
- [131] Z. Tian, Z. Lyu, J. Yuan, and C. Wang, "UDE-based sliding mode control of DC-DC power converters with uncertainties," *Control Engineering Practice*, vol. 83, pp. 116-128, 2019/02/01/ 2019, doi: <https://doi.org/10.1016/j.conengprac.2018.10.019>.
- [132] G. Palli, S. Strano, and M. Terzo, "Sliding-mode observers for state and disturbance estimation in electro-hydraulic systems," *Control Engineering Practice*, vol. 74, pp. 58-70, 2018/05/01/ 2018, doi: <https://doi.org/10.1016/j.conengprac.2018.02.007>.
- [133] G. Flores, V. González-Huitron, and A. E. Rodríguez-Mata, "Output Feedback Control for a Quadrotor Aircraft Using an Adaptive High Gain Observer," *International Journal of Control, Automation and Systems*, vol. 18, no. 6, pp. 1474-1486, 2020/06/01 2020, doi: 10.1007/s12555-019-0944-6.
- [134] D. X. Ba, T. Q. Dinh, J. Bae, and K. K. Ahn, "An Effective Disturbance-Observer-Based Nonlinear Controller for a Pump-Controlled Hydraulic System," *IEEE/ASME Transactions on Mechatronics*, vol. 25, no. 1, pp. 32-43, 2020, doi: 10.1109/TMECH.2019.2946871.
- [135] M. Du, D. Zhao, T. Ni, L. Ma, and S. Du, "Output Feedback Control for Active Suspension Electro-Hydraulic Actuator Systems With a Novel Sampled-Data Nonlinear Extended State Observer," *IEEE Access*, vol. 8, pp. 128741-128756, 2020, doi: 10.1109/ACCESS.2020.3008734.
- [136] X. Zhou, Y. Shi, L. Li, R. Yu, and L. Zhao, "A High Precision Compound Control Scheme Based on Non-singular Terminal Sliding Mode and Extended State Observer for an Aerial Inertially Stabilized Platform," *International Journal of Control, Automation and Systems*, vol. 18, no. 6, pp. 1498-1509, 2020/06/01 2020, doi: 10.1007/s12555-019-0250-y.
- [137] J. Liu, W. Gai, J. Zhang, and Y. Li, "Nonlinear Adaptive Backstepping with ESO for the Quadrotor Trajectory Tracking Control in the Multiple Disturbances," *International Journal of Control, Automation and Systems*, vol. 17, no. 11, pp. 2754-2768, 2019/11/01 2019, doi: 10.1007/s12555-018-0909-9.
- [138] S. Zhang, S. Li, and F. Dai, "Integral Sliding Mode Backstepping Control of an Asymmetric Electro-Hydrostatic Actuator Based on Extended State Observer," *Proceedings*, vol. 64, no. 1, doi: 10.3390/IeCAT2020-08495.
- [139] A. Levant, "Higher-order sliding modes, differentiation and output-feedback control," *International Journal of Control*, vol. 76, no. 9-10, pp. 924-941, 2003/01/01 2003, doi: 10.1080/0020717031000099029.
- [140] E. Cruz-Zavala and J. A. Moreno, "Levant's Arbitrary-Order Exact Differentiator: A Lyapunov Approach," *IEEE Transactions on Automatic Control*, vol. 64, no. 7, pp. 3034-3039, 2019, doi: 10.1109/TAC.2018.2874721.
- [141] A. Levant, "Robust exact differentiation via sliding mode technique**This paper was recommended for publication in final form by Associate Editor Hassan Khalil under the direction of Editor Tamer Basar," *Automatica*, vol. 34, no. 3, pp. 379-384, 1998/03/01/ 1998, doi: [https://doi.org/10.1016/S0005-1098\(97\)00209-4](https://doi.org/10.1016/S0005-1098(97)00209-4).
- [142] Q.-c. Zhong, A. Kuperman, and R. Stobart, "Design of UDe based controllers from their tw degree of freedom nature," *International Journal of Robust and Nonlinear Control*, vol. 21, pp. 1994-2008, 2011.
- [143] W. Lee, S. Yoo, S. Nam, K. Kim, and W. K. Chung, "Passivity-Based Robust Compliance Control of Electro-Hydraulic Robot Manipulators With Joint Angle Limit," *IEEE Robotics and Automation Letters*, vol. 5, no. 2, pp. 3190-3197, 2020, doi: 10.1109/LRA.2020.2975724.
- [144] H. V. Dao and K. K. Ahn, "Extended Sliding Mode Observer-Based Admittance Control for Hydraulic Robots," *IEEE Robotics and Automation Letters*, vol. 7, no. 2, pp. 3992-3999, 2022, doi: 10.1109/LRA.2022.3147244.

- [145] F. Zhang, J. Zhang, M. Cheng, and B. Xu, "A Flow-Limited Rate Control Scheme for the Master-Slave Hydraulic Manipulator," *IEEE Transactions on Industrial Electronics*, vol. 69, no. 5, pp. 4988-4998, 2022, doi: 10.1109/TIE.2021.3084175.
- [146] W. Sun, H. Pan, and H. Gao, "Filter-Based Adaptive Vibration Control for Active Vehicle Suspensions With Electrohydraulic Actuators," *IEEE Transactions on Vehicular Technology*, vol. 65, no. 6, pp. 4619-4626, 2016, doi: 10.1109/TVT.2015.2437455.
- [147] S. Lee, P. Y. Li, and F. Eskilsson, "Energetically Passive Multi-Degree-of-Freedom Hydraulic Human Power Amplifier With Assistive Dynamics," *IEEE Transactions on Control Systems Technology*, vol. 28, no. 4, pp. 1296-1308, 2020, doi: 10.1109/TCST.2019.2909724.
- [148] Y. Yamamoto *et al.*, "A Sliding-Mode Set-Point Position Controller for Hydraulic Excavators," *IEEE Access*, vol. 9, pp. 153735-153749, 2021, doi: 10.1109/ACCESS.2021.3128215.
- [149] Z. Xu, G. Qi, Q. Liu, and J. Yao, "ESO-based adaptive full state constraint control of uncertain systems and its application to hydraulic servo systems," *Mechanical Systems and Signal Processing*, vol. 167, p. 108560, 2022/03/15/ 2022, doi: <https://doi.org/10.1016/j.ymssp.2021.108560>.
- [150] M. H. Nguyen, H. V. Dao, and K. K. Ahn, "Adaptive Robust Position Control of Electro-Hydraulic Servo Systems with Large Uncertainties and Disturbances," *Applied Sciences*, vol. 12, no. 2, 2022, doi: 10.3390/app12020794.
- [151] Q. Guo and Z. Chen, "Neural adaptive control of single-rod electrohydraulic system with lumped uncertainty," *Mechanical Systems and Signal Processing*, vol. 146, p. 106869, 2021/01/01/ 2021, doi: <https://doi.org/10.1016/j.ymssp.2020.106869>.
- [152] S. Yin, P. Shi, and H. Yang, "Adaptive Fuzzy Control of Strict-Feedback Nonlinear Time-Delay Systems With Unmodeled Dynamics," *IEEE Transactions on Cybernetics*, vol. 46, no. 8, pp. 1926-1938, 2016, doi: 10.1109/TCYB.2015.2457894.
- [153] Y.-J. Liu and S. Tong, "Adaptive fuzzy control for a class of unknown nonlinear dynamical systems," *Fuzzy Sets and Systems*, vol. 263, pp. 49-70, 2015/03/15/ 2015, doi: <https://doi.org/10.1016/j.fss.2014.08.008>.
- [154] J. Wei, Q. Zhang, M. Li, and W. Shi, "High-performance motion control of the hydraulic press based on an extended fuzzy disturbance observer," *Proceedings of the Institution of Mechanical Engineers, Part I: Journal of Systems and Control Engineering*, vol. 230, no. 9, pp. 1044-1061, 2016/10/01 2016, doi: 10.1177/0959651816662562.
- [155] J. Na, Y. Li, Y. Huang, G. Gao, and Q. Chen, "Output Feedback Control of Uncertain Hydraulic Servo Systems," *IEEE Transactions on Industrial Electronics*, vol. 67, no. 1, pp. 490-500, 2020, doi: 10.1109/TIE.2019.2897545.
- [156] H. Razmjooei, G. Palli, and M. Nazari, "Disturbance observer-based nonlinear feedback control for position tracking of electro-hydraulic systems in a finite time," *European Journal of Control*, p. 100659, 2022/05/20/ 2022, doi: <https://doi.org/10.1016/j.ejcon.2022.100659>.
- [157] J. Han, "Control theory: Is it a theory of model or control?," *Systems Science and Mathematical Sciences*, vol. 9, no. 4, pp. 328-335, 1989.
- [158] J. Han, "Nonlinear State Error Feedback Control Law-NLSEF," 1995.
- [159] J. Han, "Extended state observer for a kind of uncertain systems," *Control and Decision*, vol. 10, no. 1, p. 85, 1995.
- [160] H. Razmjooei, G. Palli, and E. Abdi, "Continuous finite-time extended state observer design for electro-hydraulic systems," *Journal of the Franklin Institute*, vol. 359, no. 10, pp. 5036-5055, 2022/07/01/ 2022, doi: <https://doi.org/10.1016/j.jfranklin.2022.04.030>.
- [161] H. Razmjooei, G. Palli, E. Abdi, S. Strano, and M. Terzo, "Finite-time continuous extended state observers: design and experimental validation on electro-hydraulic systems☆," *Mechatronics*, vol. 85, p. 102812, 2022/08/01/ 2022, doi: <https://doi.org/10.1016/j.mechatronics.2022.102812>.

- [162] C. Edwards and S. Spurgeon, "Sliding mode control : theory and applications," 1998.
- [163] S. K. Spurgeon, "Sliding mode observers: a survey," *Intern. J. Syst. Sci.*, vol. 39, no. 8, pp. 751–764, 2008, doi: 10.1080/00207720701847638.
- [164] S. Drakunov and V. Utkin, "Sliding mode observers. Tutorial," in *Proceedings of 1995 34th IEEE Conference on Decision and Control*, 13-15 Dec. 1995 1995, vol. 4, pp. 3376-3378 vol.4, doi: 10.1109/CDC.1995.479009.
- [165] G. Palli, S. Strano, and M. Terzo, "A novel adaptive-gain technique for high-order sliding-mode observers with application to electro-hydraulic systems," *Mechanical Systems and Signal Processing*, vol. 144, p. 106875, 2020/10/01/ 2020, doi: <https://doi.org/10.1016/j.ymssp.2020.106875>.
- [166] Y. Lu, "Sliding-Mode Disturbance Observer With Switching-Gain Adaptation and Its Application to Optical Disk Drives," *IEEE Transactions on Industrial Electronics*, vol. 56, no. 9, pp. 3743-3750, 2009, doi: 10.1109/TIE.2009.2025719.
- [167] B. Wang, Z. Dong, Y. Yu, G. Wang, and D. Xu, "Static-Errorless Deadbeat Predictive Current Control Using Second-Order Sliding-Mode Disturbance Observer for Induction Machine Drives," *IEEE Transactions on Power Electronics*, vol. 33, no. 3, pp. 2395-2403, 2018, doi: 10.1109/TPEL.2017.2694019.
- [168] H. Rabiee, M. Ataei, and M. Ekramian, "Continuous nonsingular terminal sliding mode control based on adaptive sliding mode disturbance observer for uncertain nonlinear systems," *Automatica*, vol. 109, p. 108515, 2019/11/01/ 2019, doi: <https://doi.org/10.1016/j.automatica.2019.108515>.
- [169] J. Sun, J. Yi, Z. Pu, and X. Tan, "Fixed-Time Sliding Mode Disturbance Observer-Based Nonsmooth Backstepping Control for Hypersonic Vehicles," *IEEE Transactions on Systems, Man, and Cybernetics: Systems*, vol. 50, no. 11, pp. 4377-4386, 2020, doi: 10.1109/TSMC.2018.2847706.
- [170] S. Jeong and D. Chwa, "Sliding-Mode-Disturbance-Observer-Based Robust Tracking Control for Omnidirectional Mobile Robots With Kinematic and Dynamic Uncertainties," *IEEE/ASME Transactions on Mechatronics*, vol. 26, no. 2, pp. 741-752, 2021, doi: 10.1109/TMECH.2020.2998506.
- [171] F. Wang and L. He, "FPGA-Based Predictive Speed Control for PMSM System Using Integral Sliding-Mode Disturbance Observer," *IEEE Transactions on Industrial Electronics*, vol. 68, no. 2, pp. 972-981, 2021, doi: 10.1109/TIE.2020.2969107.
- [172] J. Zhang, P. Shi, and W. Lin, "Extended sliding mode observer based control for Markovian jump linear systems with disturbances," *Automatica*, vol. 70, pp. 140-147, 2016/08/01/ 2016, doi: <https://doi.org/10.1016/j.automatica.2016.03.020>.
- [173] D. Ke, F. Wang, L. He, and Z. Li, "Predictive Current Control for PMSM Systems Using Extended Sliding Mode Observer With Hurwitz-Based Power Reaching Law," *IEEE Transactions on Power Electronics*, vol. 36, no. 6, pp. 7223-7232, 2021, doi: 10.1109/TPEL.2020.3043489.
- [174] C. Yang, B. Song, Y. Xie, and X. Tang, "Online Parallel Estimation of Mechanical Parameters for PMSM Drives via a Network of Interconnected Extended Sliding-Mode Observers," *IEEE Transactions on Power Electronics*, vol. 36, no. 10, pp. 11818-11834, 2021, doi: 10.1109/TPEL.2021.3067328.
- [175] J. Yu, Y. Sun, W. Lin, and Z. Li, "Fault-tolerant control for descriptor stochastic systems with extended sliding mode observer approach," *IET Control Theory & Applications*, <https://doi.org/10.1049/iet-cta.2016.0282> vol. 11, no. 8, pp. 1079-1087, 2017/05/01 2017, doi: <https://doi.org/10.1049/iet-cta.2016.0282>.
- [176] H. Yi, M. Liu, and H. Li, "Satellites Autonomous Navigation With an Extended State and Disturbance Sliding Mode Observer Method," *IEEE Access*, vol. 7, pp. 112693-112702, 2019, doi: 10.1109/ACCESS.2019.2930354.

- [177] X. Zhou and X. Li, "Trajectory tracking control for electro-optical tracking system based on fractional-order sliding mode controller with super-twisting extended state observer," *ISA Transactions*, vol. 117, pp. 85-95, 2021/11/01/ 2021, doi: <https://doi.org/10.1016/j.isatra.2021.01.062>.
- [178] M. H. Nguyen, H. V. Dao, and K. K. Ahn, "Active Disturbance Rejection Control for Position Tracking of Electro-Hydraulic Servo Systems under Modeling Uncertainty and External Load," *Actuators*, vol. 10, no. 2, 2021, doi: 10.3390/act10020020.
- [179] H. V. Truong, H. A. Trinh, and K. K. Ahn, "Safety Operation of n-DOF Serial Hydraulic Manipulator in Constrained Motion with Consideration of Contact-Loss Fault," *Applied Sciences*, vol. 10, no. 22, doi: 10.3390/app10228107.
- [180] K. Choi *et al.*, "Experimental Study on the Dynamic Characteristics of Hydro-Pneumatic Semi-Active Suspensions for Agricultural Tractor Cabins," *Applied Sciences*, vol. 10, no. 24, doi: 10.3390/app10248992.
- [181] J. Das, S. K. Mishra, R. Saha, S. Mookherjee, and D. Sanyal, "Nonlinear modeling and PID control through experimental characterization for an electrohydraulic actuation system: system characterization with validation," *Journal of the Brazilian Society of Mechanical Sciences and Engineering*, vol. 39, no. 4, pp. 1177-1187, 2017/04/01 2017, doi: 10.1007/s40430-016-0634-3.
- [182] G. Sun, L. Wu, Z. Kuang, Z. Ma, and J. Liu, "Practical tracking control of linear motor via fractional-order sliding mode," *Automatica*, vol. 94, pp. 221-235, 2018/08/01/ 2018, doi: <https://doi.org/10.1016/j.automatica.2018.02.011>.
- [183] Y. Ma, D. Li, Y. Li, and L. Yang, "A Novel Discrete Compound Integral Terminal Sliding Mode Control With Disturbance Compensation For PMSM Speed System," *IEEE/ASME Transactions on Mechatronics*, vol. 27, no. 1, pp. 549-560, 2022, doi: 10.1109/TMECH.2021.3068192.
- [184] Y. Ma and Y. Li, "Active Disturbance Compensation Based Robust Control for Speed Regulation System of Permanent Magnet Synchronous Motor," *Applied Sciences*, vol. 10, no. 2, 2020, doi: 10.3390/app10020709.
- [185] V. Utkin, "Variable structure systems with sliding modes," *IEEE Transactions on Automatic Control*, vol. 22, no. 2, pp. 212-222, 1977, doi: 10.1109/TAC.1977.1101446.
- [186] M. Jelali and A. Kroll, *Hydraulic servo-systems: modelling, identification and control*. Springer Science & Business Media, 2012.
- [187] L. V. Truong, S. D. Huang, V. T. Yen, and P. V. Cuong, "Adaptive Trajectory Neural Network Tracking Control for Industrial Robot Manipulators with Deadzone Robust Compensator," *International Journal of Control, Automation and Systems*, vol. 18, no. 9, pp. 2423-2434, 2020/09/01 2020, doi: 10.1007/s12555-019-0513-7.
- [188] Z. Chen, F. Huang, W. Sun, J. Gu, and B. Yao, "RBF-Neural-Network-Based Adaptive Robust Control for Nonlinear Bilateral Teleoperation Manipulators With Uncertainty and Time Delay," *IEEE/ASME Transactions on Mechatronics*, vol. 25, no. 2, pp. 906-918, 2020, doi: 10.1109/TMECH.2019.2962081.
- [189] T. Li, S. Duan, J. Liu, L. Wang, and T. Huang, "A Spintronic Memristor-Based Neural Network With Radial Basis Function for Robotic Manipulator Control Implementation," *IEEE Transactions on Systems, Man, and Cybernetics: Systems*, vol. 46, no. 4, pp. 582-588, 2016, doi: 10.1109/TSMC.2015.2453138.
- [190] X. Li, W. Fu, L. Liu, and Y. Wang, "Adaptive Dynamic Surface Control for Aircraft With Multiple Disturbances Based on Radial Basis Network," *IEEE Access*, vol. 8, pp. 57709-57721, 2020, doi: 10.1109/ACCESS.2020.2982495.
- [191] W. Ruan, Q. Dong, X. Zhang, and Z. Li, "Friction Compensation Control of Electromechanical Actuator Based on Neural Network Adaptive Sliding Mode," *Sensors*, vol. 21, no. 4, 2021, doi: 10.3390/s21041508.

- [192] R. Fan and Y. Li, "An Adaptive Fuzzy Trajectory Tracking Control via Improved Cerebellar Model Articulation Controller for Electro-Hydraulic Shovel," *IEEE/ASME Transactions on Mechatronics*, vol. 26, no. 6, pp. 2870-2880, 2021, doi: 10.1109/TMECH.2021.3094284.
- [193] C. Wang, Z. Zhang, H. Wang, B. Zhao, and L. Quan, "Disturbance observer-based output feedback control of hydraulic servo system considering mismatched uncertainties and internal pressure dynamics stability," *IET Control Theory & Applications*, vol. 14, no. 8, pp. 1046-1056, 2020, doi: 10.1049/iet-cta.2019.0346.
- [194] B. Wang, N. Zhang, and H. Ji, "Study on Precise Displacement Control of a Miniature Hydraulic System via RBF-DOB," *IEEE Access*, vol. 6, pp. 69162-69171, 2018, doi: 10.1109/ACCESS.2018.2879716.
- [195] Y. Cheng, B. Xu, Z. Lian, Z. Shi, and P. Shi, "Adaptive Learning Control of Switched Strict-Feedback Nonlinear Systems With Dead Zone Using NN and DOB," *IEEE Transactions on Neural Networks and Learning Systems*, pp. 1-10, 2021, doi: 10.1109/TNNLS.2021.3106781.
- [196] J. Park and I. W. Sandberg, "Approximation and Radial-Basis-Function Networks," *Neural Computation*, vol. 5, no. 2, pp. 305-316, 1993, doi: 10.1162/neco.1993.5.2.305.
- [197] M. J. Orr, "Introduction to radial basis function networks," ed: Technical Report, center for cognitive science, University of Edinburgh ..., 1996.
- [198] M. H. Nguyen and K. K. Ahn, "A Novel Trajectory Adjustment Mechanism-Based Prescribed Performance Tracking Control for Electro-Hydraulic Systems Subject to Disturbances and Modeling Uncertainties," *Applied Sciences*, vol. 12, no. 12, doi: 10.3390/app12126034.
- [199] T. Qin, Y. Li, L. Quan, and L. Yang, "An Adaptive Robust Impedance Control Considering Energy-Saving of Hydraulic Excavator Boom and Stick Systems," *IEEE/ASME Transactions on Mechatronics*, vol. 27, no. 4, pp. 1928-1936, 2022, doi: 10.1109/TMECH.2022.3173991.
- [200] M.-H. Chiang, "A novel pitch control system for a wind turbine driven by a variable-speed pump-controlled hydraulic servo system," *Mechatronics*, vol. 21, no. 4, pp. 753-761, 2011/06/01/ 2011, doi: <https://doi.org/10.1016/j.mechatronics.2011.01.003>.
- [201] H. Hänninen, T. Minav, and M. Pietola, "Replacing a Constant Pressure Valve Controlled System With a Pump Controlled System," 2016. [Online]. Available: <https://doi.org/10.1115/FPMC2016-1777>.
- [202] M. H. Nguyen, H. V. Dao, and K. K. Ahn, "Extended sliding mode observer-based high-accuracy motion control for uncertain electro-hydraulic systems," *International Journal of Robust and Nonlinear Control*, <https://doi.org/10.1002/rnc.6421> vol. n/a, no. n/a, 2022/10/17 2022, doi: <https://doi.org/10.1002/rnc.6421>.
- [203] M. Sun, X. Ouyang, J. Mattila, Z. Chen, H. Yang, and H. Liu, "Lightweight Electrohydrostatic Actuator Drive Solution for Exoskeleton Robots," *IEEE/ASME Transactions on Mechatronics*, vol. 27, no. 6, pp. 4631-4642, 2022, doi: 10.1109/TMECH.2022.3153706.
- [204] K. Staman, A. J. Veale, and H. v. d. Kooij, "Design, Control and Evaluation of the Electro-Hydrostatic Actuator, PREHydrA, for Gait Restoration Exoskeleton Technology," *IEEE Transactions on Medical Robotics and Bionics*, vol. 3, no. 1, pp. 156-165, 2021, doi: 10.1109/TMRB.2020.3048224.
- [205] Y. Shang *et al.*, "A Novel Electro Hydrostatic Actuator System With Energy Recovery Module for More Electric Aircraft," *IEEE Transactions on Industrial Electronics*, vol. 67, no. 4, pp. 2991-2999, 2020, doi: 10.1109/TIE.2019.2905834.
- [206] J. Zhang, Y. Li, B. Xu, M. Pan, and Q. Chao, "Experimental study of an insert and its influence on churning losses in a high-speed electro-hydrostatic actuator pump of an aircraft," *Chinese Journal of Aeronautics*, vol. 32, no. 8, pp. 2028-2036, 2019/08/01/ 2019, doi: <https://doi.org/10.1016/j.cja.2018.10.003>.
- [207] T. Zhu, H. Xie, and H. Yang, "Design and tracking control of an electro-hydrostatic actuator for a disc cutter replacement manipulator," *Automation in Construction*, vol. 142, p. 104480, 2022/10/01/ 2022, doi: <https://doi.org/10.1016/j.autcon.2022.104480>.

- [208] F. Tessari, R. Galluzzi, A. Tonoli, N. Amati, L. De Michieli, and M. Laffranchi, "Knee prosthesis powered by a fully integrated and highly back-drivable electro-hydrostatic actuator," *Mechatronics*, vol. 91, p. 102972, 2023/05/01/ 2023, doi: <https://doi.org/10.1016/j.mechatronics.2023.102972>.
- [209] B. Helian, Z. Chen, and B. Yao, "Precision Motion Control of a Servomotor-Pump Direct-Drive Electrohydraulic System With a Nonlinear Pump Flow Mapping," *IEEE Transactions on Industrial Electronics*, vol. 67, no. 10, pp. 8638-8648, 2020, doi: 10.1109/TIE.2019.2947803.
- [210] B. Helian, Z. Chen, B. Yao, L. Lyu, and C. Li, "Accurate Motion Control of a Direct-Drive Hydraulic System With an Adaptive Nonlinear Pump Flow Compensation," *IEEE/ASME Transactions on Mechatronics*, vol. 26, no. 5, pp. 2593-2603, 2021, doi: 10.1109/TMECH.2020.3043576.
- [211] C. Li, L. Lyu, B. Helian, Z. Chen, and B. Yao, "Precision Motion Control of an Independent Metering Hydraulic System With Nonlinear Flow Modeling and Compensation," *IEEE Transactions on Industrial Electronics*, vol. 69, no. 7, pp. 7088-7098, 2022, doi: 10.1109/TIE.2021.3102434.
- [212] K. Guo, M. Li, W. Shi, and Y. Pan, "Adaptive Tracking Control of Hydraulic Systems With Improved Parameter Convergence," *IEEE Transactions on Industrial Electronics*, vol. 69, no. 7, pp. 7140-7150, 2022, doi: 10.1109/TIE.2021.3101006.
- [213] S. Huang and K. K. Tan, "Intelligent Friction Modeling and Compensation Using Neural Network Approximations," *IEEE Transactions on Industrial Electronics*, vol. 59, no. 8, pp. 3342-3349, 2012, doi: 10.1109/TIE.2011.2160509.
- [214] H. Feng *et al.*, "A new adaptive sliding mode controller based on the RBF neural network for an electro-hydraulic servo system," *ISA Transactions*, 2022/01/10/ 2022, doi: <https://doi.org/10.1016/j.isatra.2021.12.044>.
- [215] D. Won and W. Kim, "Disturbance observer based backstepping for position control of electro-hydraulic systems," *International Journal of Control, Automation and Systems*, vol. 13, no. 2, pp. 488-493, 2015/04/01 2015, doi: 10.1007/s12555-013-0396-y.
- [216] B.-Z. Guo and Z.-l. Zhao, "On the convergence of an extended state observer for nonlinear systems with uncertainty," *Systems & Control Letters*, vol. 60, no. 6, pp. 420-430, 2011/06/01/ 2011, doi: <https://doi.org/10.1016/j.sysconle.2011.03.008>.
- [217] M. Ran, J. Li, and L. Xie, "A new extended state observer for uncertain nonlinear systems," *Automatica*, vol. 131, p. 109772, 2021/09/01/ 2021, doi: <https://doi.org/10.1016/j.automatica.2021.109772>.
- [218] S. Li, J. Yang, W. H. Chen, and X. Chen, "Generalized Extended State Observer Based Control for Systems With Mismatched Uncertainties," *IEEE Transactions on Industrial Electronics*, vol. 59, no. 12, pp. 4792-4802, 2012, doi: 10.1109/TIE.2011.2182011.
- [219] S. Xiong, W. Wang, X. Liu, Z. Chen, and S. Wang, "A novel extended state observer," *ISA Transactions*, vol. 58, pp. 309-317, 2015/09/01/ 2015, doi: <https://doi.org/10.1016/j.isatra.2015.07.012>.
- [220] W. Weiwen and G. Zhiqiang, "A comparison study of advanced state observer design techniques," in *Proceedings of the 2003 American Control Conference, 2003.*, 4-6 June 2003 2003, vol. 6, pp. 4754-4759 vol.6, doi: 10.1109/ACC.2003.1242474.
- [221] J. Rivera, L. Garcia, C. Mora, J. J. Raygoza, and S. Ortega, "Super-twisting sliding mode in motion control systems," *Sliding mode control*, vol. 1, pp. 237-254, 2011.
- [222] V. Utkin, "On Convergence Time and Disturbance Rejection of Super-Twisting Control," *IEEE Transactions on Automatic Control*, vol. 58, no. 8, pp. 2013-2017, 2013, doi: 10.1109/TAC.2013.2251812.
- [223] M. H. Nguyen, H. V. Dao, and K. K. Ahn, "Extended sliding mode observer-based high-accuracy motion control for uncertain electro-hydraulic systems," *International Journal of*

- Robust and Nonlinear Control*, <https://doi.org/10.1002/rnc.6421> vol. 33, no. 2, pp. 1351-1370, 2023/01/25 2023, doi: <https://doi.org/10.1002/rnc.6421>.
- [224] D. Q. Truong and K. K. Ahn, "Force control for hydraulic load simulator using self-tuning grey predictor – fuzzy PID," *Mechatronics*, vol. 19, no. 2, pp. 233-246, 2009/03/01/ 2009, doi: <https://doi.org/10.1016/j.mechatronics.2008.07.007>.
- [225] T. C. Do, D. T. Tran, T. Q. Dinh, and K. K. Ahn, "Tracking Control for an Electro-Hydraulic Rotary Actuator Using Fractional Order Fuzzy PID Controller," *Electronics*, vol. 9, no. 6, 2020, doi: 10.3390/electronics9060926.
- [226] Y. Fan, J. Shao, and G. Sun, "Optimized PID Controller Based on Beetle Antennae Search Algorithm for Electro-Hydraulic Position Servo Control System," *Sensors*, vol. 19, no. 12, doi: 10.3390/s19122727.
- [227] G. Chen *et al.*, "Research on Feedback-Linearized Sliding Mode Control of Direct-Drive Volume Control Electro-Hydraulic Servo System," *Processes*, vol. 9, no. 9, doi: 10.3390/pr9091676.
- [228] F. E. Alsaadi, A. Yasami, H. Alsubaie, A. Alotaibi, and H. Jahanshahi, "Control of a Hydraulic Generator Regulating System Using Chebyshev-Neural-Network-Based Non-Singular Fast Terminal Sliding Mode Method," *Mathematics*, vol. 11, no. 1, doi: 10.3390/math11010168.
- [229] Q. Guo *et al.*, "Synchronous control for multiple electrohydraulic actuators with feedback linearization," *Mechanical Systems and Signal Processing*, vol. 178, p. 109280, 2022/10/01/ 2022, doi: <https://doi.org/10.1016/j.ymssp.2022.109280>.
- [230] B. Helian, Z. Chen, and B. Yao, "Constrained Motion Control of an Electro-hydraulic Actuator under Multiple Time-varying Constraints," *IEEE Transactions on Industrial Informatics*, pp. 1-11, 2023, doi: 10.1109/TII.2023.3249760.
- [231] D.-T. Tran, T.-C. Do, and K.-K. Ahn, "Extended High Gain Observer-Based Sliding Mode Control for an Electro-hydraulic System with a Variant Payload," *International Journal of Precision Engineering and Manufacturing*, vol. 20, no. 12, pp. 2089-2100, 2019/12/01 2019, doi: 10.1007/s12541-019-00256-0.
- [232] N. M. Tri, D. X. Ba, and K. K. Ahn, "A Gain-Adaptive Intelligent Nonlinear Control for an Electrohydraulic Rotary Actuator," *International Journal of Precision Engineering and Manufacturing*, vol. 19, no. 5, pp. 665-673, 2018/05/01 2018, doi: 10.1007/s12541-018-0080-5.
- [233] S. K. Spurgeon, "Sliding mode observers: a survey," *International Journal of Systems Science*, vol. 39, no. 8, pp. 751-764, 2008/08/01 2008, doi: 10.1080/00207720701847638.
- [234] S. Li, Q. Guo, Y. Yan, and Y. Shi, "Terminal sliding mode observer based–asymptotic tracking control of electro-hydraulic systems with lumped uncertainties," *Transactions of the Institute of Measurement and Control*, vol. 45, no. 1, pp. 17-26, 2023/01/01 2022, doi: 10.1177/01423312221105136.
- [235] R. A. McCann, M. S. Islam, and I. Husain, "Application of a sliding-mode observer for position and speed estimation in switched reluctance motor drives," *IEEE Transactions on Industry Applications*, vol. 37, no. 1, pp. 51-58, 2001, doi: 10.1109/28.903126.
- [236] W. Xu, S. Qu, L. Zhao, and H. Zhang, "An Improved Adaptive Sliding Mode Observer for Middle- and High-Speed Rotor Tracking," *IEEE Transactions on Power Electronics*, vol. 36, no. 1, pp. 1043-1053, 2021, doi: 10.1109/TPEL.2020.3000785.
- [237] M. Rahnavard, M. Ayati, and M. R. H. Yazdi, "Robust actuator and sensor fault reconstruction of wind turbine using modified sliding mode observer," *Transactions of the Institute of Measurement and Control*, vol. 41, no. 6, pp. 1504-1518, 2019/04/01 2018, doi: 10.1177/0142331218754620.
- [238] H. Habibi, I. Howard, S. Simani, and A. Fekih, "Decoupling Adaptive Sliding Mode Observer Design for Wind Turbines Subject to Simultaneous Faults in Sensors and Actuators,"

- IEEE/CAA Journal of Automatica Sinica*, vol. 8, no. 4, pp. 837-847, 2021, doi: 10.1109/JAS.2021.1003931.
- [239] Z. Xu, W. Deng, H. Shen, and J. Yao, "Extended-State-Observer-Based Adaptive Prescribed Performance Control for Hydraulic Systems With Full-State Constraints," *IEEE/ASME Transactions on Mechatronics*, vol. 27, no. 6, pp. 5615-5625, 2022, doi: 10.1109/TMECH.2022.3186390.
- [240] Z. Chen, Q. Guo, T. Li, Y. Yan, and D. Jiang, "Gait Prediction and Variable Admittance Control for Lower Limb Exoskeleton With Measurement Delay and Extended-State-Observer," *IEEE Transactions on Neural Networks and Learning Systems*, pp. 1-14, 2022, doi: 10.1109/TNNLS.2022.3152255.
- [241] J. Wang, D. Huang, S. Fang, Y. Wang, and W. Xu, "Model Predictive Control for ARC Motors Using Extended State Observer and Iterative Learning Methods," *IEEE Transactions on Energy Conversion*, vol. 37, no. 3, pp. 2217-2226, 2022, doi: 10.1109/TEC.2022.3159834.
- [242] J. Yue, L. Liu, Z. Peng, D. Wang, and T. Li, "Data-driven adaptive extended state observer design for autonomous surface vehicles with unknown input gains based on concurrent learning," *Neurocomputing*, vol. 467, pp. 337-347, 2022/01/07/ 2022, doi: <https://doi.org/10.1016/j.neucom.2021.09.062>.
- [243] L. Sun, G. Li, and F. You, "Combined internal resistance and state-of-charge estimation of lithium-ion battery based on extended state observer," *Renewable and Sustainable Energy Reviews*, vol. 131, p. 109994, 2020/10/01/ 2020, doi: <https://doi.org/10.1016/j.rser.2020.109994>.